Thioketone and Pyrazole based Luminescent Boron Compounds: Synthesis, Characterization and Photophysical Properties of Poly(indazaboles)

By

MURALI A C

CHEM11201704020

National Institute of Science Education and Research,
Bhubaneshwar, Odisha-752050

A thesis submitted to the

Board of Studies in Chemical Sciences

In partial fulfillment of requirements

for the Degree of

DOCTOR OF PHILOSOPHY

of

HOMI BHABHA NATIONAL INSTITUTE

December, 2023

Homi Bhabha National Institute[1]

Recommendations of the Viva Voce Committee

As members of the Viva Voce Committee, we certify that we have read the dissertation prepared by **Murali A C** entitled **"Thioketone and Pyrazole based Luminescent Boron Compounds: Synthesis, Characterization and Photophysical Properties of Poly(indazaboles)"** and recommend that it may be accepted as fulfilling the thesis requirement for the award of Degree of Doctor of Philosophy.

Chairman: Prof. A. Srinivasan		Date: 19/12/2023
Guide: Dr. V. Krishnan		Date: 19/12/2023
Co-Guide (if any): -		Date: -
Examiner: Prof. S. Natarajan		Date: 19/12/2023
Member 1- Dr. S. Peruncheralathan		Date: 19/12/2023
Member 2- Dr. Bidraha Bagh		Date: 19/12/2023
Member 3- Dr. Snehasis Chowdhuri (IIT-Bhubaneswar)		Date: 19/12/2023

Final approval and acceptance of this thesis is contingent upon the candidate'ssubmission of the final copies of the thesis to HBNI.
We hereby certify that we have read this thesis prepared under my/ourdirection and recommend that it may be accepted as fulfilling the thesis requirement.

Date: 19/12/2023

(Prof. V. Krishnan)

Place: Bhubaneswar **Co-guide (if any)** **Guide**

[1] This page is to be included only for final submission after successful completion of viva voce.

STATEMENT BY AUTHOR

This dissertation has been submitted in partial fulfillment of requirements for an advanced degree at Homi Bhabha National Institute (HBNI) and is deposited in the Library to be made available to borrowers under rules of the HBNI.

Brief quotations from this dissertation are allowable without special permission, provided that accurate acknowledgement of source is made. Requests for permission for extended quotation from or reproduction of this manuscript in whole or in part may be granted by the Competent Authority of HBNI when in his or her judgment the proposed use of the material is in the interests of scholarship. In all other instances, however, permission must be obtained from the author.

Murali A C

DECLARATION

I, hereby declare that the investigation presented in the thesis has been carried out by me. The work is original and has not been submitted earlier as a whole or in part for a degree / diploma at this or any other Institution / University.

Murali A C

List of Publications arising from the thesis

Journal (# Pertaining to thesis)

1. #**Murali, A. C.;** Nayak, P.; Nayak, S.; Das, S.; Senanayak, S. P.; Venkatasubbaiah, K. *Angew. Chem., Int. Ed.* **2023,** *62,* e202216871.
2. #**Murali, A. C.;** Nayak, P.; Panda, R.; Das, R.; Venkatasubbaiah, K. *ACS Appl. Opt. Mater.* **2023,** *1,* 1033-1042.
3. #**Murali, A. C.;** Pratakshya, P.; Patel, P.; Nayak, P.; Peruncheralathan, S.; Venkatasubbaiah, K. *New. J. Chem.* **2023,** *47*, 17835 – 17842.
4. **Murali, A. C.;**† Nayak, P.;† Venkatasubbaiah, K. *Dalton Trans.* **2022,** *51,* 5751-5771. (†Contributed equally, Review)
5. Nayak, P.; **Murali, A. C.;** Rao Velpuri, V.; Chandrasekhar, V.; Venkatasubbaiah, K. *Adv. Synth. Catal.* **2023,** *365,* 230-237.
6. Nayak, P.; **Murali, A. C.;** Pal, P. K.; Priyakumar, U. D.; Chandrasekhar, V.; Venkatasubbaiah, K. *Inorg. Chem.* **2022,** *61,* 14511-14516.
7. Nayak, P.; **Murali, A. C.;** Chandrasekhar, V.; Venkatasubbaiah, K. *Mater. Adv.* **2022,** *3*, 5893-5899.
8. Sa, S.; Ponniah, J. S.; Biswal, P.; Sathesh, V.; **Murali, A. C.;** Venkatasubbaiah, K. *Eur. J. Inorg. Chem.* **2022,** *25*, e202200283.
9. Sa, S.; Sathesh, V.; **Murali, A. C.;** Nayak, P.; Venkatasubbaiah, K. *J. Organomet. Chem.* **2021,** *950*, 121977.
10. Sa, S.; **Murali, A. C.;** Nayak, P.; Venkatasubbaiah, K. *Chem. Commun.* **2021,** *57*, 10170-10173.
11. Vanga, M.; Sa, S.; Kumari, A.; **Murali, A. C.;** Nayak, P.; Das, R.; Venkatasubbaiah, K. *Dalton Trans.* **2020,** *49*, 7737-7746.

12. Chinta, R. V. R. N.; Aradhyula, B. P. R.; **Murali, A. C.;** Venkatasubbaiah, K. *J. Organomet. Chem.* **2019,** *891*, 20-27.

Chapters in books and lectures notes

1. **Murali, A. C.;** Venkatasubbaiah, K. *Developments in Inorganic Chemistry,* **2022,** *2,* 59-153. (Elsevier Publication, Book Chapter)

Conferences

1. Poster Presentation in International Conference on "Main Group Molecule to Material – II, 2021 organized by school of Chemical Sciences, NISER Bhubaneswar, India (December 13 - 15, 2021)

2. Poster Presentation in 27th CRSI-National Symposium Chemistry held at the Novotel Hotel, Kolkata, organized by IISER Kolkata and CRSI India (September 26 - 29, 2021)

3. Poster Presentation in International Conference on "Main Group Molecule to Material – III, 2023 organized by IIT Hyderabad, University of Hyderabad, India (December 9 - 11, 2023). **Awarded best poster by American Chemical Society.**

Murali A C

Dedicated

To

All the first graduate students in their family

ACKNOWLEDGEMENTS

I would like to express my deepest gratitude to my thesis advisor, **Dr. V. Krishnan**, for his unwavering support, guidance, and priceless insights throughout the entire research process. This thesis would not have been possible without his expertise and mentorship. I also wants say my sincere thanks to my doctoral committee members - **Prof. A. Srinivasan (Chairman), Dr. S. Peruncheralathan, Dr. Bidraha Bagh, Dr. Snehasis Chowdhuri** (IIT Bhubaneswar).

My sincere thanks also go to **Prof. Hirendra Nath Ghosh** (Director), **Prof. Sudhakar Panda** (Former Director), NISER for giving such a big laboratory facilities to my research work.

It is my privilege to thank **Dr. Sharanappa Nembenna** (Chairperson of School of Chemical Sciences), and other faculty members of SCS. I must also express my gratitude to **Prof. A. Srinivasan, Prof. C. Gunanathan, Dr. V. Krishnan, Dr. S. Peruncheralathan, Dr. Bidraha Bagh, Dr. Moloy Sarkar, Dr. U. Louderaj** who taught me in the coursework during my Ph.D. program. I would like to express my extended thanks to **Dr. Arun Kumar, Dr. Priyanka Pandey** (Scientific Officer), and all the technicians of School of Chemical Sciences.

I am also thankful to **National Institute of Science Education and Research (NISER), on OCC of HBNI, Bhubaneswar, Odisha-752050** for the financial support, excellent resources and research facilities. Their support allowed me to focus on my research and complete my work.

I would like to convey my sincere acknowledgement to my The American College Professors **Dr. Dorothy Sheela, Dr. Helen Ratna Monica, Dr. B. Krithika Rani, Dr. K. Kartik** who taught chemistry and motivated me towards research.

I am also thank full to **Dr. U. P. Senthil Kumar** former vice president, Orchid Pharmaceutical, **Dr. A. Aravind** and other seniors who gave me the opportunity to learn the experiments in organic chemistry which is helpful in my research work.

I express my warm thanks to all my past and present lab mates **Dr. Shreenibasa, Dr. Prakash, Dr. Priyabrata, Dr. Samser, Mr. Susanth, Ms. Sasmita, Ms. Swetapadma, Ms. Anusmita, Ms. Husna, Ms. Shyamali, Mr. Ashish, Mr. Pabitra, Mr. Rohith, Mr. Sunil**, especially, **Dr. Prakash Nayak, Dr. Shreenibasa sa** who helped and supported for my research work. I am also thankful to my 13PGC friends **Siva Subramani, Mukesh Singh, Jothi Murugan, Ramesh, Prem Kumar, Eswar, Thenmozhi, Abinaya, Dhanapriya** and also my school friends for their encouragement and support. I pleasure to express my thanks to NISER friends **Sanjay** and **Aswini** for cheer up me in all my toughest situations.

Last but not least, I would like to express my sincere gratitude to beloved my dear parents **Mr. Anna Ramamoorthy Chandrasekar** and **Mrs. Anna Chandrasekar Ramila** for bringing me into this world as well as for their unwavering support, unwavering motivation, love, affection, and endless encouragement throughout this journey. Above all, I thank the almighty for giving this most unforgettable journey.

--- Murali A C

CONTENTS

SYNOPSIS

This thesis has been organized into four chapters, and the content of the chapters are briefly discussed below.

Chapter 1: Introduction

Chapter 1, deals with a brief introduction to luminescent boron compounds. Luminescent boron compounds are classified into two major category, namely, (a) tri-coordinated boron compounds, and (b) tetra-coordinated boron compounds. The boron center in tri-coordinated compounds has vacant p_z orbital, the presence of vacant p_z orbital on the boron centre triggers π-electron acceptor's tendency, which makes the molecules significantly delocalized when conjugated with organic π-aromatic system. The presence of a vacant p_z orbital makes the molecules highly reactive towards nucleophiles such as water, which breaks the conjugation of the molecule. Hence they are sensitive towards moisture. Compared with tri-coordinated boron compounds, tetra-coordinated boron compounds show high stability due to coordinative saturation.

Considerable effort has been taken by different research groups for the synthesis of tetra-coordinated boron compounds which have been widely used in various fields like photo-responsive materials, OLEDs, OFETs, sensors, biological imaging materials etc.,[1] A brief overview of different types of fluorescent tetra-coordinated boron complexes are presented in this chapter.

Chapter 2: This chapter is divided into four parts

Chapter 2A: Synthesis of Bis(pentafluorophenyl)boron and Diphenylboron Thioketonates: Study Their Optical, and Electrochemical Properties

Among the various four-coordinated boron containing luminescent materials, boron-β-diketonates have been explored as multiphoton materials, semiconductors, photochromic

materials, polymers, and sensors due to their high molar absorption co-efficient, and high quantum yields.[2] A little modification of boron-β-diketonates results a huge variation in the optical properties. Hence, various methodologies were followed to fine-tune the optical properties of boron-β-diketonates.[3] The optical properties of the boron-β-diketonates were tuned by using different methodology, such as a) by altering the R groups on the 1,3-positions of diketonates, b) by altering the substituents on the 'boron' center, and c) by substituting oxygen of the diketonates with other hetero atoms.

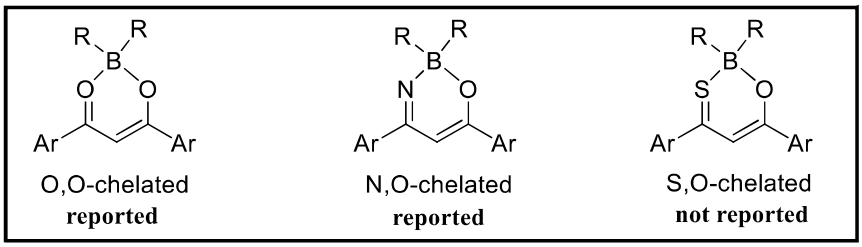

This chapter describes the synthesis of monothio-β-diketonate based O,S-chelated bis(pentafluorophenyl)boron and diphenylboron compounds with varying substituents on the peripheral site of one of the aromatic ring of the monothio-β-diketonates. The characterization, optical and electrochemical properties of these materials are presented in this chapter.

Chapter 2B: Far Red/Near infrared emissive Boron-thioketonates: Synthesis, Optical, Electrochemical, and Charge Transport Properties

In this chapter, we described a series of donor substituted (-NMe_2, -NPh_2, -OMe) monothio-β-diketonate based O,S-chelated four-coordinated boron compounds. All the boron compounds are well characterized with multi-nuclear NMR spectroscopy analysis, and X-ray diffraction analysis. The optical, electrochemical, and sensing behavior of these compounds are discussed. Moreover, the semi-conducting as well as single-component photo-detector properties of these materials are presented in this chapter.

Chapter 2C: Red Emitting TPE-based Boron-thioketonates: Synthesis, Optical, Electrochemical, Cyanide ion sensing and Their NLO Properties

In this chapter, we discussed the synthesis, optical, and electrochemical properties of tetraphenyl-ethylene (TPE) and dimethylaniline (DMA) monothio-β-diketonate based O,S-chelated four-coordinated boron compounds. All the tetraphenyl-ethylene based boron compounds showed aggregation-induced enhanced emission (AIEE). The non-linear optical properties and cyanide ion sensing capabilities of these materials are also presented in this chapter

Chapter 2D: Carbazole-based Boron-thioketonates: Synthesis, Optical, Electrochemical and TADF Properties

In this chapter, we discusses the synthesis, optical, and electrochemical properties of the carbazole and anisole substituted boron monothio-β-diketonates. Further, carbazole substituted boron-thioketonates showed thermally activated delayed fluorescence. These results are presented in this part of the chapter 2.

Chapter 3: Synthesis, Structural, Optical Properties of N,O Chelated Pyrazolyl Anchored Bis(pentafluorophenyl) Boron Complexes

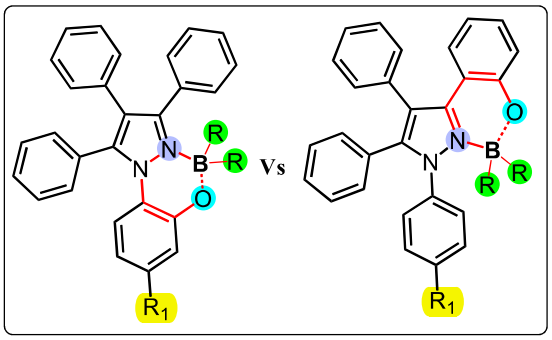

This chapter describes the synthesis of a series of pyrazole-based N,O-chelated boron compounds with different donor substituents. All the synthesized pyrazole boron compounds are well characterized with multinuclear NMR techniques and X-ray

diffraction analysis. The photophysical properties of these boron molecules are well documented. The propeller nature of all pyrazole molecules was examined for the AIEE properties. Moreover, picric acid sensing capabilities of these materials are also presented in this chapter.

Chapter 4: Synthesis and optical properties of Indazaboles and their polymers

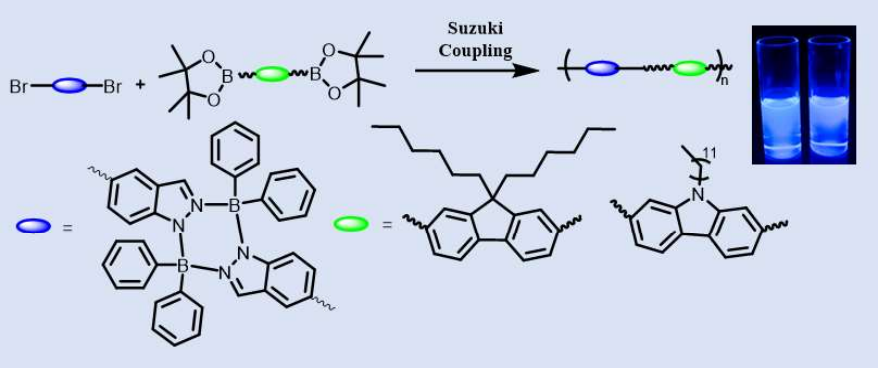

In this chapter, we described the synthesis of N,N-chelated indazole fused organo-boron π-extended monomers and main chain polymers. All the synthesized monomers and polymers are well characterized with multinuclear NMR techniques. The optical properties of these monomers and polymers were discussed. DFT calculation of the π-extended monomers is also documented.

References:

1. Murali, A. C.; Nayak, P.; Venkatasubbaiah, K. Recent advances in the synthesis of luminescent tetra-coordinated boron compounds. *Dalton Trans.* **2022,** *51*, 5751-5771.
2. Chen, P.-Z.; Niu, L.-Y.; Chen, Y.-Z.; Yang, Q.-Z. Difluoroboron β-diketonate dyes: Spectroscopic properties and applications. *Coord. Chem. Rev.* **2017,** *350*, 196-216.

3. Gon, M.; Tanaka, K.; Chujo, Y. Concept of Excitation-Driven Boron Complexes and Their Applications for Functional Luminescent Materials. *Bull. Chem. Soc. Jpn.* **2018,** *92*, 7-18.

List of figures

List of tables

List of schemes

List of abbreviations

^{1}H NMR	Proton nuclear magnetic resonance
^{13}C NMR	Carbon-13 nuclear magnetic resonance
^{19}F NMR	Fluorine-19 nuclear magnetic resonance
^{11}B NMR	Boron-11 nuclear magnetic resonance
^{1}H-^{1}H COSY	Proton-proton correlated spectroscopy
UV-Vis	Ultraviolet-visible
PL	Photoluminescence
NIR	Near infrared
MLCT	Metal ligand charge transfer
ESI	Electrospray ionization
HRMS	High-resolution mass spectrometry
PXRD	Powder X-ray diffraction
XRD	X-ray diffraction
TGA	Thermogravimetric analysis
DFT	Density functional theory
IRF	Instrument response function
ICT	Intramolecular charge transfer
CV	Cyclic voltammetry
XRD	X-ray diffraction
TLC	Thin layer chromatography
GOOF	Goodness of fit
LED	Light emitting diode
OLEDs	Organic light emitting diodes

OFETs	Organic field effect transistors
POLEDs	Plastic organic light emitting diodes
TADF	Thermally activated delayed fluorescence
RTP	Room temperature phosphorescence
BODIPY	Boron dipyrromethene
BOPHY	Bis(difluoroboron)1,2-bis((pyrrol-2-yl)methylene) hydrazine
HOMO	Highest occupied molecular orbital
LUMO	Lowest unoccupied molecular orbital
eV	Electron volt
OA	Open aperture
CA	Closed aperture
TPA	Two photon absorption
EL	Electroluminescence
ACQ	Aggregation caused quenching
AIE	Aggregation induced emission
AIEE	Aggregation induced enhanced emission
TICT	Twisted intramolecular charge transfer
RIR	Restriction of intramolecular rotation
ppm	Parts per million
CH_2Cl_2	Dichloromethane
$CHCl_3$	Chloroform
MeOH	Methanol
EtOH	Ethanol
THF	Tetrahydrofuran
DMF	Dimethylformamide

$CDCl_3$	Deuterated chloroform
DMSO-d_6	Deuterated dimethyl sulphoxide
Acetone-d_6	Deuterated acetone
Acetonitrile-d3	Deuterated acetonitrile
AcOH	Acetic acid
TFA	Trifluoroacetic acid
Na_2CO_3	Sodium carbonate
K_2CO_3	Potassium carbonate
CaH_2	Calcium hydride
$AlCl_3$	Aluminium trichloride
TBACl	Tetrabutylammonium chloride
TBABr	Tetrabutylammonium bromide
TBAF	Tetrabutylammonium fluoride
TBACN	Tetrabutylammonium cyanide
TBAOAc	Tetrabutylammonium acetate
$TBANO_3$	Tetrabutylammonium nitrate
$TBAHSO_4$	Tetrabutylammonium hydrogen sulphate
$TBAPF_6$	Tetrabutylammonium hexafluoro phosphate
Bu_4NPF_6	Tetrabutylammonium hexafluorophosphate
NBS	N-bromosuccinimide
NaH	Sodium hydride
$Pd(dppf)Cl_2$	[1,1'-bis(diphenylphosphino)ferrocene]dichloropalladium(II)
$B(C_6F_5)_3$	Tris(pentafluorophenyl)borane
$Pd(PPh_3)_4$	Tetrakis(triphenylphosphine)palladium(0)
TPE	1,1,2,2-Tetraphenylethylene

MTDKH	1,3-monothio-β-diketone
MTDKB	Boron 1,3-monothio-β-diketonate
ITO	Indium tin oxide
PEDOT	Poly[3,4-ethylene dioxythiophene]
PSS	Poly[styrenesulfonate]
SCLC	Space charge limited current
FWHM	Full width at half maximum
PMMA	Poly(methyl methacrylate)
MCP	Multi-channel plate
DMA	N,N-dimethyl aniline
NLO	Nonlinear optics
2,4-DNB	2,4-dinitobenzene
2,4-DNP	2,4-dinitrophenol
2,4-DNT	2,4-dinitrotoluene

CHAPTER 1

INTRODUCTION

1.1 Introduction of luminescent boron compounds

1.1.1 Tri-coordinate boron compounds

1.1.2 Tetra-coordinate boron compounds

1.1.2.1. O,O-chelated boron compounds

1.1.2.2 N,O-chelate boron compounds

1.1.2.3 N,N- chelate boron compounds

1.1.2.3A. Pyrazabole fused N,N-chelated system

1.3 References

Boron compounds and their classifications: Synthesis, structure and applications:

A literature survey

1.1. Luminescent boron compounds:

Organic luminescent compounds are crucial in various fields such as sensing, bioimaging, biolabeling, and organic light-emitting diodes (OLEDs).[1-16] Organoboron complexes are extended family members of organic luminescent materials and have shown excellent photophysical properties. Organic luminophores containing boron can be divided into two types: tri-coordinated and tetra-coordinated boron compounds (**Figure 1.1**).

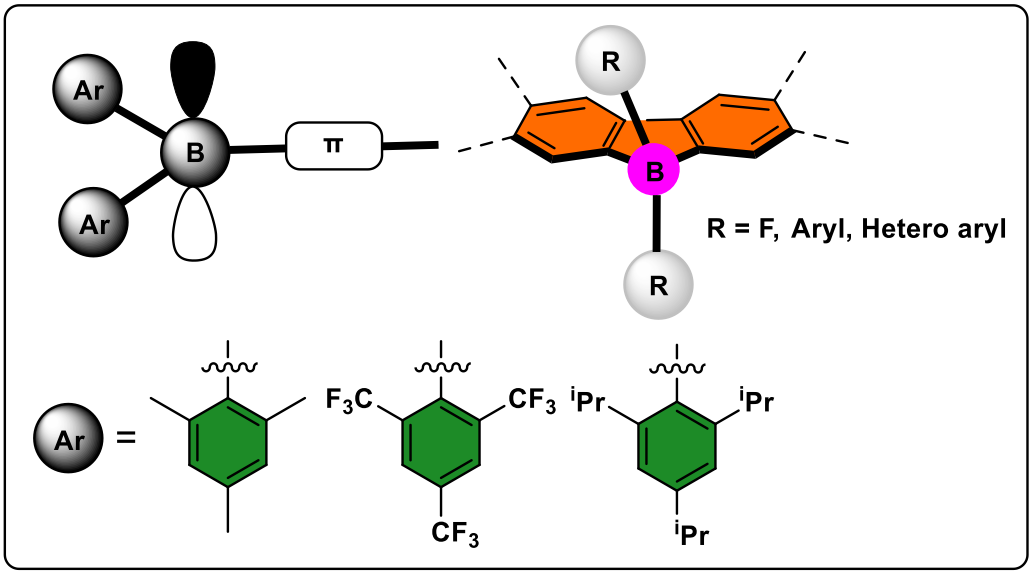

Figure 1.1: Diagrammatic illustration of compounds containing tri- and tetra-coordinates of boron (left and right, respectively).

1.1.1. Tri-coordinated boron compounds:

In tri-coordinated boron compounds, the boron centre has sp^2 hybridization and one vacant p_z orbital. The presence of vacant p_z orbital on the boron centre triggers the strong π-electron acceptor's tendency, which makes the molecules significantly delocalized when conjugated with an adjacent organic π-aromatic or aliphatic system. The presence vacant p_z orbital makes the compound highly reactive towards nucleophiles such as water,

which breaks the conjugation of the molecule. Bulky aryl groups such as tripyl (2,4,6-triisopropylphenyl), mesityl (2,4,6-trimethlphenyl), and fluoromesityl (2,4,6-tris(trifluoromethyl)phenyl) help to protect the boron center from the incoming nucleophile and prevent from π-π interaction in the solid state. Hence, bulky aryl group substituted boron compounds are moisture and thermally stable. Moreover, Lewis acidic nature of the boron centre helps for the selective sensing of small anions like fluoride and cyanide anions.[17, 18] Other than sensing, tri-coordinated boron compounds have been used in OLEDs, nonlinear optics, as fluorescent emitters, and fluorescent indicators in bioimaging.[19-21]

1.1.2. Tetra-coordinated boron compounds:

Neutral bases like amines, phosphines, sulfides etc., coordinate with tri-coordinated boron compounds and result in the formation of tetracoordinate boron compounds. The coordinative saturation of the boron center in the tetra-coordinate compounds increase the stability and rigidity of these compounds.[22] Efforts have been made by various research groups to synthesize different tetra-coordinated boron compounds and utilize them in various fields like photoresponsive materials, OLEDs, OFETs, sensors, biological imaging materials etc.,[23] Four types of tetra-coordinate boron compounds can be distinguished according on their chelation, namely, (a) N,N-chelated boron compounds (b) N,O-chelated boron compounds (c) N,C-chelated boron compounds (d) O,O-chelated boron compounds. In this chapter, I will present some of the recent literature related to O,O-chelated, N,O-chelated and N,N-chelated boron compounds.

1.1.2.1. O,O-chelated boron compounds:

BF_2bdks is one of the classes of highly luminous boron compounds with excellent photophysical properties. Morgan and Tunstall reported the first member of the BF_2bdks family in 1924, but it was not widely recognized until recently. The various derivatives of β-diketones can be readily accessible by the Claisen condensation between the ester and a carbonyl derivatives. The photophysical properties of BF_2bdks are decided by the nature of their substitution at R and R' (**Figure 1.2**). If aliphatic groups are present in both R and R' positions, they are non-fluorescent in the visible region due to the lack of molecular conjugation but when aryl groups occupy the R and R' it becomes emissive and can be tunable from visible to near-infrared (NIR) by modulating structural characteristics of ligands. In contrast to the most widely reported BODIPY dyes, most BF_2bdks compounds exhibit high emissions in the solid state.

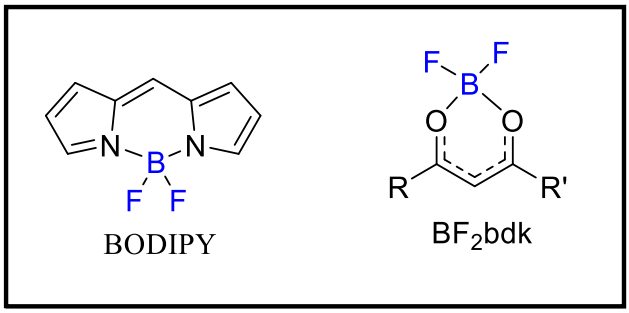

Figure 1.2: Structure of BODIPY and BF_2bdk core

The solid-state emission properties of BF_2bdks are associated with the intrinsic molecular components and molecular packing with multiple intermolecular interactions like hydrogen bonding, π-π stacking, and dipole-dipole interactions. The emission spectra of solid-state emitters vary significantly due to changes in the molecule conformation and packing modes. As a result, BF_2bdks show room temperature phosphorescence (RTP) and have mechanochromic properties.[24]

Representative synthetic steps for β-diketone (bdks) ligands and BF_2bdks complexes are shown in the **Scheme 1.1.** The alternative route for the Claisen condensation reaction to get β-diketone is also shown in **Scheme 1.1** Claisen-Schmidt condensation between benzaldehyde derivatives and acetophenone derivatives gives conjugated enone, which is reacted with bromine to obtain the addition product. The reaction of the brominated product with sodium methoxide followed by acid hydrolysis affords the required β-diketone.[25, 26]

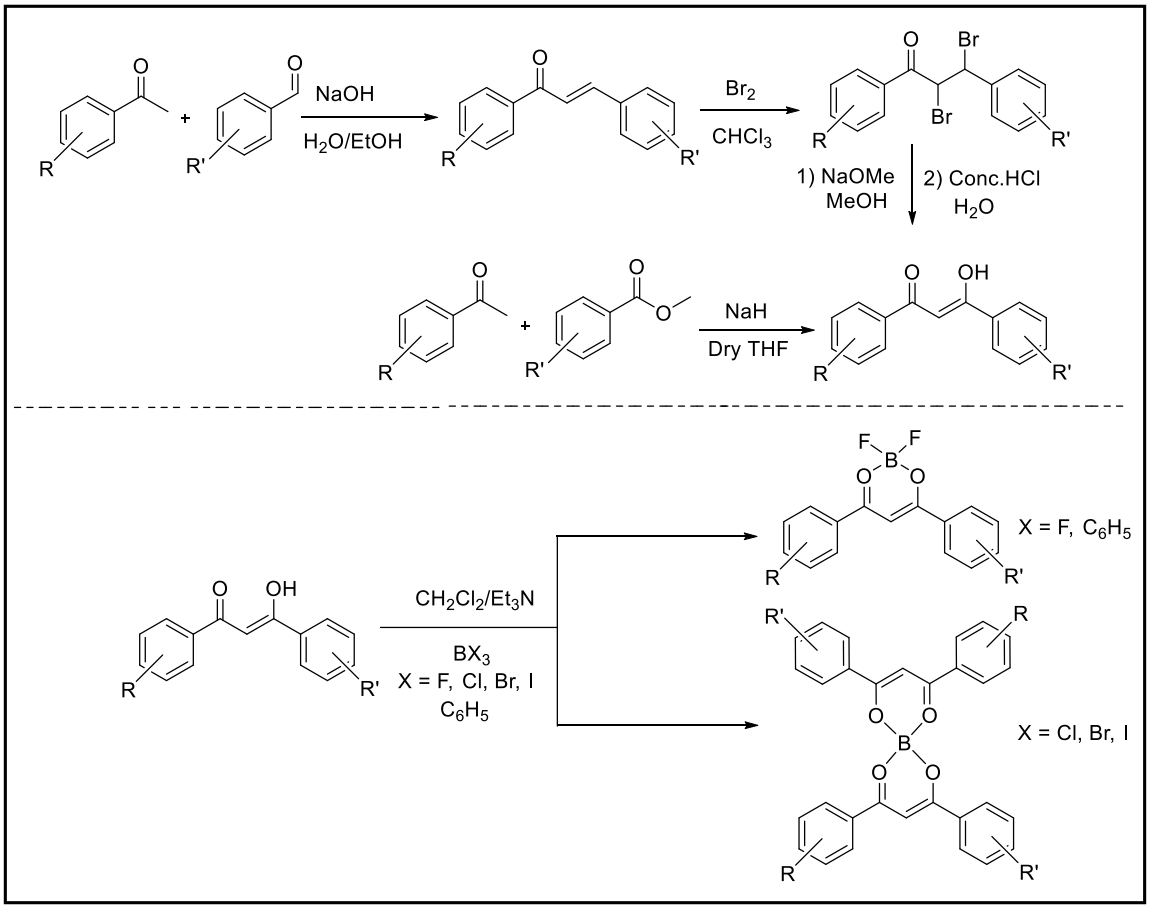

Scheme 1.1. Synthesis of β-diketones ligands and boron compounds

BF_2bdks were synthesized by the treatment of β-diketone ligand and trifluoro boron etherate in presence of triethyl amine or diisopropylethylamine in the dry non-carbonyl solvents (dichloromethane or THF). Variety of boron-bearing reagents are available for

the synthesis of a variety of boron compounds. In addition to BF_3, other regents are also available like BPh_3, BCl_3, BBr_3, and BI_3. According to the leaving group ability of the halogen atom, β-diketones form either monomeric or dimeric boron complexes. BF_3 and BPh_3 react with β-diketone to give exclusively monomeric BF_2bdks and BPh_2bdks while BBr_3 and BI_3 gives bis coordinated boron complexes.[27]

Fraser and co-workers reported numerous BF_2bdks and, made efforts to show the use of boron compounds in various fields. They reported stimuli-responsive materials and the effect of the amine ring size (**1-4**). BF_2bdks showed interesting properties like aggregation-induced enhanced emission (AIEE), solvatochromism, mechanochromism, viscochromism, oxygen sensors, TADF emitters, room temperature phosphorescence, etc.,[28-30]

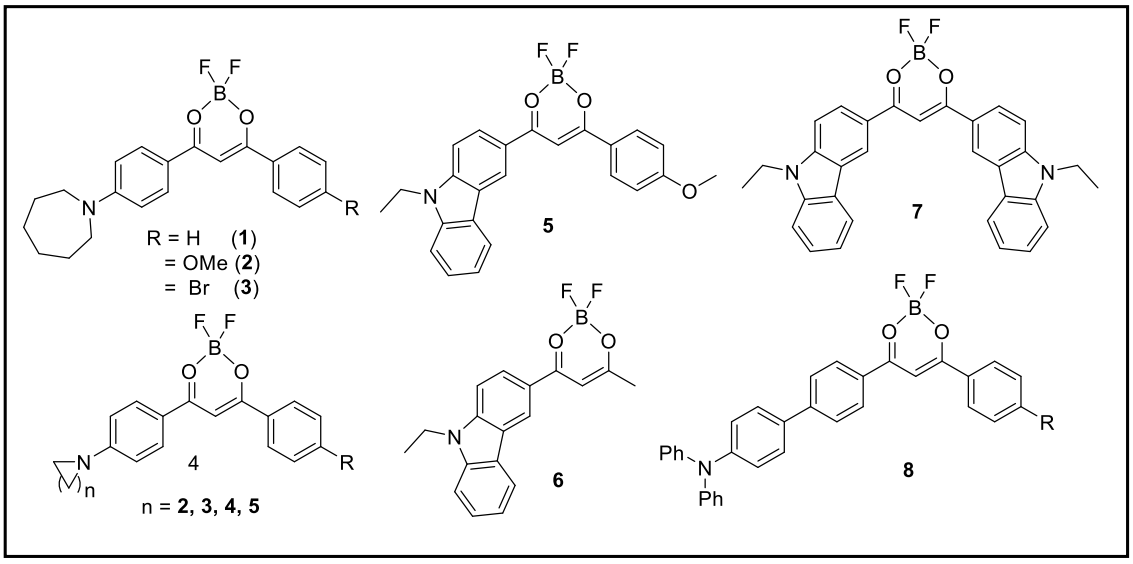

Figure 1.3: Structure of O,O-chelated tetra-coordinated boron compounds (**1-8**)

[31]Yang and co-workers reported carbazole substituted BF_2bdks (**5-7**) and investigated their two-photon excited fluorescence in the solution state and reported mechanochromic behavior by grinding, heating, and exposing to solvent vapor. Carbazole substituted BF_2bdks (**7**) were used to explore the crystallization process of organic microcrystalline

materials and for its optical waveguide ability with low optical loss.[32, 33] Triphenylamine substituted BF_2bdks (**8**) displayed solid-state emission and thermally activated delayed fluorescence and showed different colors of emission in the crystalline and amorphous states. The red emission in the amorphous state and orange emission in the crystalline state of these compounds can be reversibly tuned by grinding and fuming processes. Moreover, these compounds displayed thermally activated delayed fluorescence (TADF) in amorphous medium but not in the crystalline medium due to the different ΔE_{ST} values in the respective states.

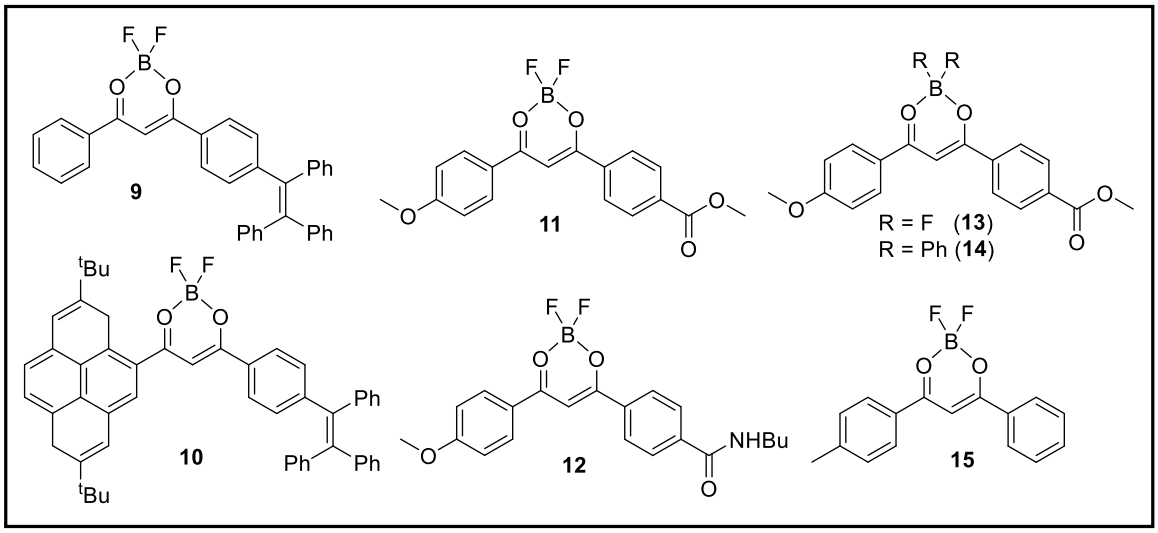

Figure 1.4: Structure of O,O-chelated tetra-coordinated boron compounds (**9-15**)

In general, tetraphenylethylene substituted BF_2bdks showed aggregation-induced emission, and some molecules displayed mechanochromic properties.[34-39] Tetraphenylene-phenyl-BF_2bdks (**9**) showed four emissive colors such as green, yellow, orange, and red in four different polymorphs. Moreover, compound **9** exhibited reversible emission behaviour in response to external stimuli like grinding, heating, and pressure.[38] The attachment of pyrene and tetraphenylene-phenyl units in BF_2bdks (**10**) displayed high torsional molecular conformation. Furthermore, compound (**10**) exhibited reversible mechanochromic behavior.[36] A series of aromatic BF_2bdks with carbonyl substitution (**11-15**) were reported. The varying number of exciton traps in amorphous and crystalline

states is responsible for the mechanochromic properties which are proved by experimental and theoretical studies.[40, 41] Moreover, the nature of the substituent on boron (**13-14**) plays an important role in the observed optical and mechanofluorochromic properties. The -BF_2 anchored compounds showed mechanochromic properties while the -BPh_2 anchored compounds did not display any changes in fluorescence over grinding.[42] By attaching oxygen-bridged electron donor groups, Zhang and co-workers reported heavy atom-free BF_2bdks (**16-18**) that displayed triplet quantum yield. These molecules displayed triplet quantum yield through a combination of intersystem crossing and transition angular momentum.[43] A series of BF_2bdks (**19-21**) with alkyl and alkoxy-substituted compounds were synthesized and used as thermometers i.e. at different temperatures, it showed a change in fluorescence from green to orange.[44, 45]

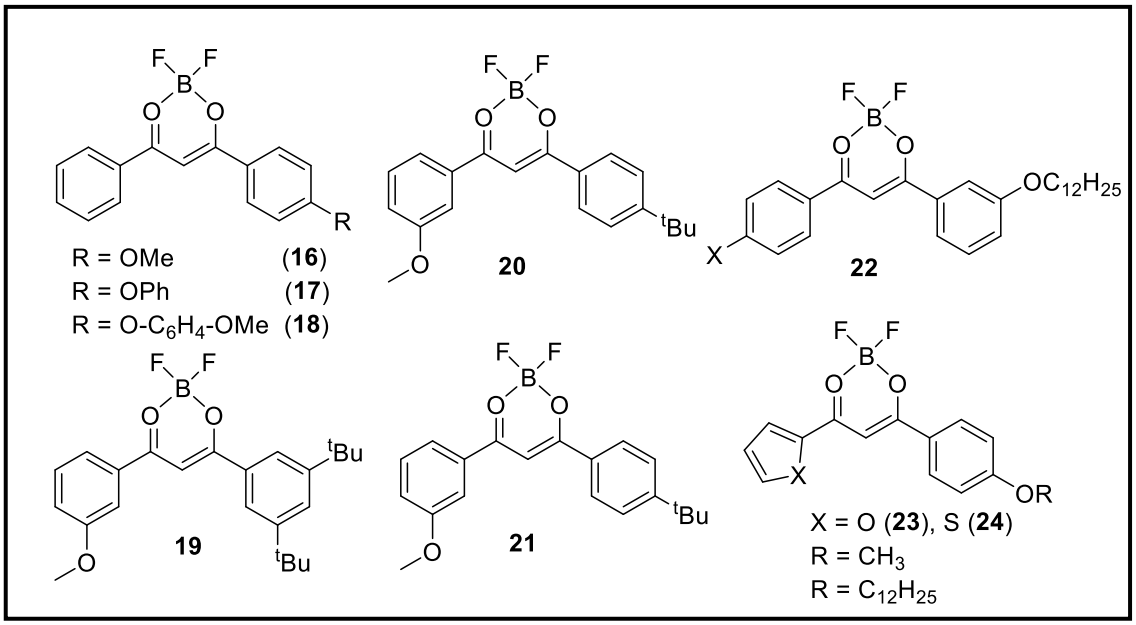

Figure 1.5: Structure of O,O-chelated tetra-coordinated boron compounds (**16-24**)

Detection of oxygen is very important because it is very essential in life. Fraser and co-workers reported meta-alkoxy substituted BF_2bdks. These compounds showed intramolecular charge transfer (ICT) from the oxygen of the meta-alkoxy group to boron and halide in the excited state process. Oxygen calibrations of those meta-alkoxy BF_2bdks

(**22**) reveals stronger phosphorescence and better oxygen sensing than para-alkoxy BF_2bdks.[46] The effect of thiophene and furan-substituted BF_2bdks (**23-24**) was also studied. The optical properties of these BF_2bdks with mixed heteroaryl, methoxy-aryl substituted compounds showed mechanochromic and thermal responsive properties.[47]

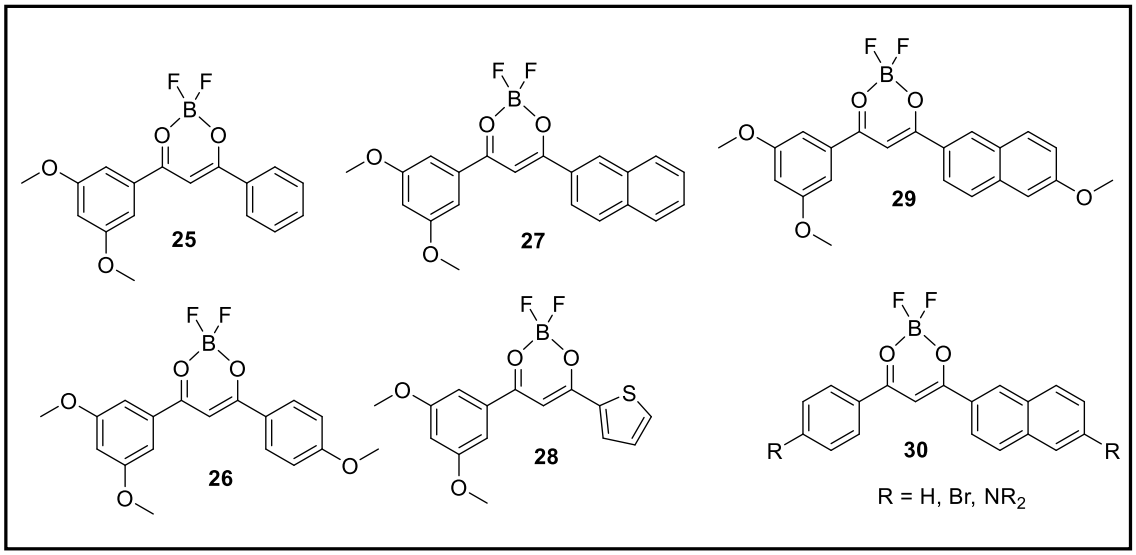

Figure 1.6: Structure of O,O-chelated tetra-coordinated boron compounds (**25-30**)

BF_2bdks with methoxy substituted aromatic groups on one side and different aryl groups on the other side were reported by Fraser and co-workers. These compounds (**25-30**) blended with polylactide showed phosphorescence and act as oxygen sensors.[48, 49] By substituting -Br on phenyl, naphthyl, or both, the fluorescence and phosphorescence ratio and room temperature phosphorescence lifetime of compound **30** was tuned by taking advantage of the heavy atom effect[50]

Sasabe and co-workers reported the OLED properties of BF_2bdks (**31**) along with a carbazole derivative which form exciplex to give orange luminescence with an external quantum efficiency (η_{ext}) of 10 %.[51] A nopinone-based BF_2bdks (**32-35**) was synthesized and studied for its AIE and electroluminescence properties. The compound (R = OCH_3)

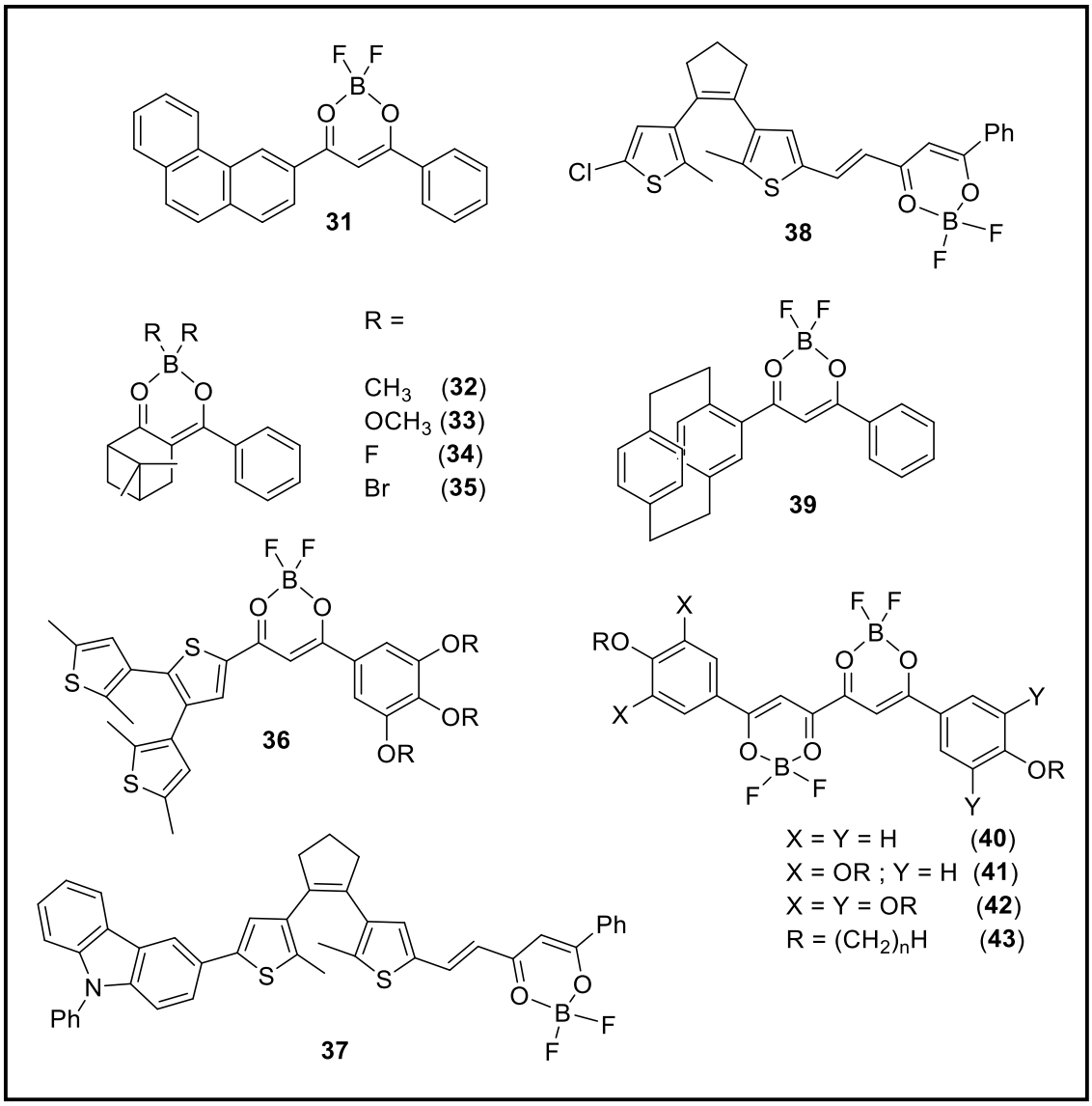

Figure 1.7: Structure of O,O-chelated tetra-coordinated boron compounds (**31-43**)

displayed a luminescence efficacy of 7.49 lm W^{-1}.[52] BF_2bdks having dithienyl ethene were synthesized and studied for their photo-responsive behavior by different groups.[53-58] Compound (**36**) and compound (**37**) are reported by [53]Yam and [54]Li groups. Dithienylethene (**38**) bearing chloro on one side and BF_2bdks on the other side was reported by [59]Li group and were utilized as a blue/red light triggered optical switches. [2.2] paracyclophane-based BF_2bdks (**39**) was reported by [60]Hiroshi Ikeda and co-workers and explored as a solvafluorochromic materials. This boron complex showed a larger stoke shift by excited-state intramolecular charge transfer. [61]Lai and co-workers

reported bis-BF_2bdks (**40-43**), synthesized from substituted tetraketonates, and investigated phase transition and mesomorphic properties.

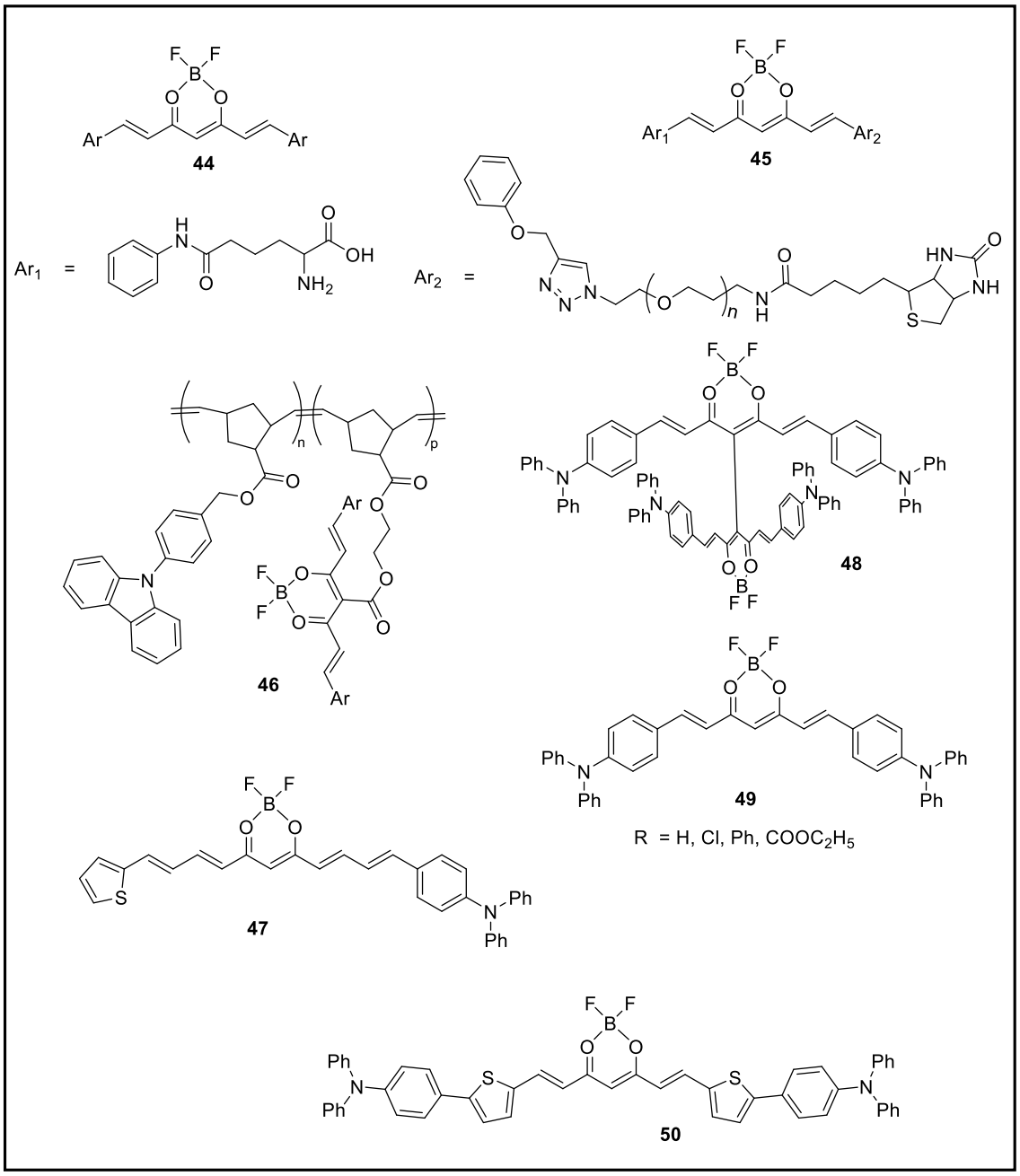

Figure 1.8: Structure of O,O-chelated tetra-coordinated boron compounds **(44-50)**

β-diketonates units having one or more extended π-conjugation are known as curcuminoids. Due to the extended conjugation, curcuminoid-BF_2bdks shows strong absorption and emission in the visible and NIR region depending on the substitution.[62, 63] The effect of aryl group substitution on Curcuminoid BF_2-bdks (**44**) was reported by

Canard and co-workers.[64] Hudson and Guo groups developed derivatives of the curcuminoid boron materials for near-infrared emission. The Guo group discovered a molecule (**45**) having Glu-DFB-biotin unit which can differentiate hepatic cancer cells.[65] Similarly, Hudson group developed curcuminoid-BF_2bdks (**46**) having polymer chains for fluorescence labeling of SK-BR_3 human breast cancer cells.[66] Curcuminoid-BF_2bdks having triphenylamine as an end group (R = H, Cl, Ph) was reported and showed better chemical and thermal stability. It was used as an organic solar cell which showed a power conversion efficiency of up to 4.14%.[67] Guo and co-workers reported triphenylamine and thiophene substituted curcuminoid-BF_2bdks (**47**) and were used to sense vapoury acids and amines.[68] Adachi and co-workers reported near-infrared (NIR) emissive materials with curcuminoid-BF_2bdks. Compound (**49**) with triphenylamine showed near-infrared TADF properties[69] and dimeric compound (**48**) displayed NIR TADF emission,[70] and an OLED external quantum efficiency of 5.1%. Compound (**48**) also showed a high quantum yield at near-infrared region and amplified spontaneous emission.[71]

1.1.2.2 N,O-chelated boron compounds:

Numerous N,O- chelated B-N coordinated boron compounds have been reported so far. Among them, imine nitrogen-coordinated compounds were reported by different research groups, and studied their optical properties in detail.[72-82] The compound having imine framework (**51**) was reported by Chujo and co-workers which showed color-changing mechanochromic and aggregation-induced emission properties. The emission color of the compound changed from red to orange on grinding. The mechanochromism properties were analyzed with the crystal structure and powder XRD pattern. DSC analysis revealed that the origin of the mechanochromism properties was from the phase transition between crystalline and amorphous. The observed mechanochromism can be reversed on heating

and cooling as well.[74] Compounds (**52**) and (**53**) reported by Dai and Yang groups displayed AIE and mechanochromic properties, respectively. Compound (**53**) having the amine functionality was responsive to external stimuli like grinding and acid/base vapors. Compound (**54**) and (**55**) reported by Thilagar group, also displayed mechanochromic properties.[83] The imino derivatives (**54-57**) of B-N coordinated compounds displayed phosphorescence with lifetime values from 18-46 ms.

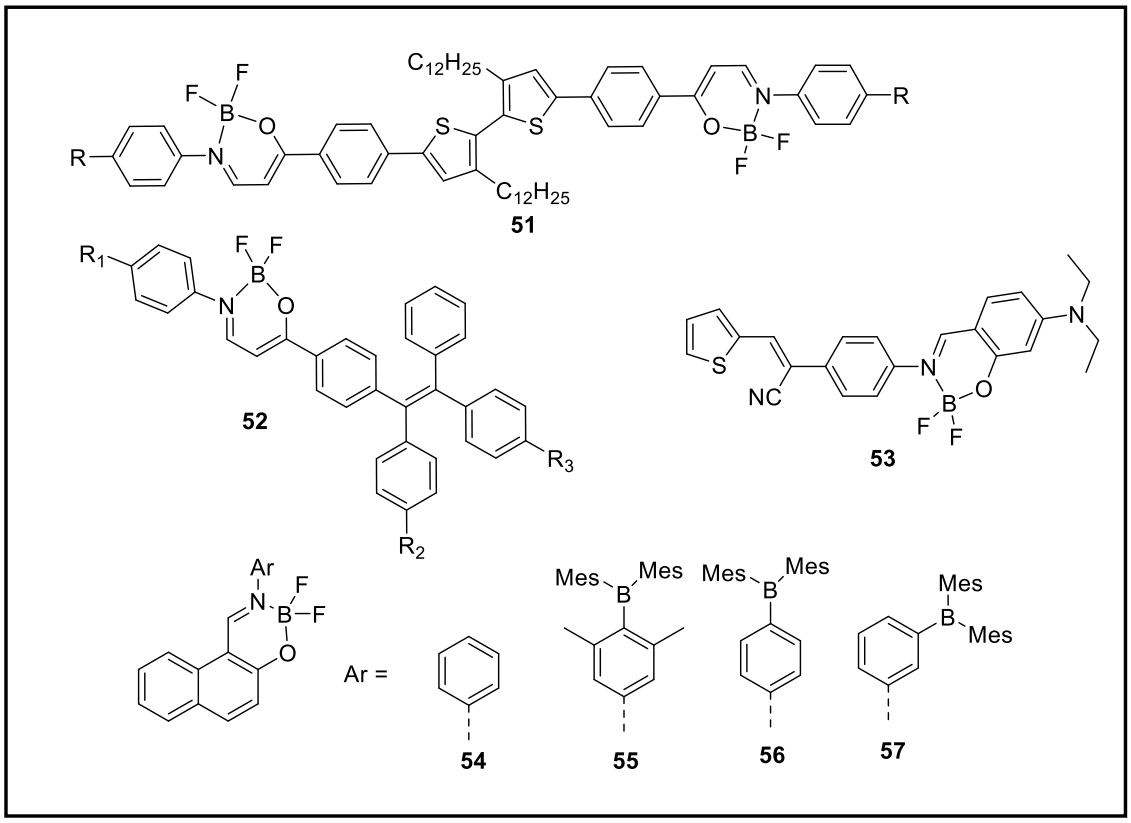

Figure 1.9: Structure of N,O-chelated tetra-coordinated boron compounds (**51-57**)

Different heterocycles-based N,O-chelated tetra coordinated boron compounds have been reported by different groups and studied their optical properties. Lu and co-workers reported boron compounds (**58-62**).[84, 85] Compound (**58**) showed two types of crystals, i.e.; a yellow crystal (Y-crystal) and a green crystal (G-crystal). Those crystals showed different emission values, the yellow crystal which emits at 518 nm was grown in THF and green crystal emits at 495 nm was grown in CH_2Cl_2/pet-ether mixture. Both Y- and

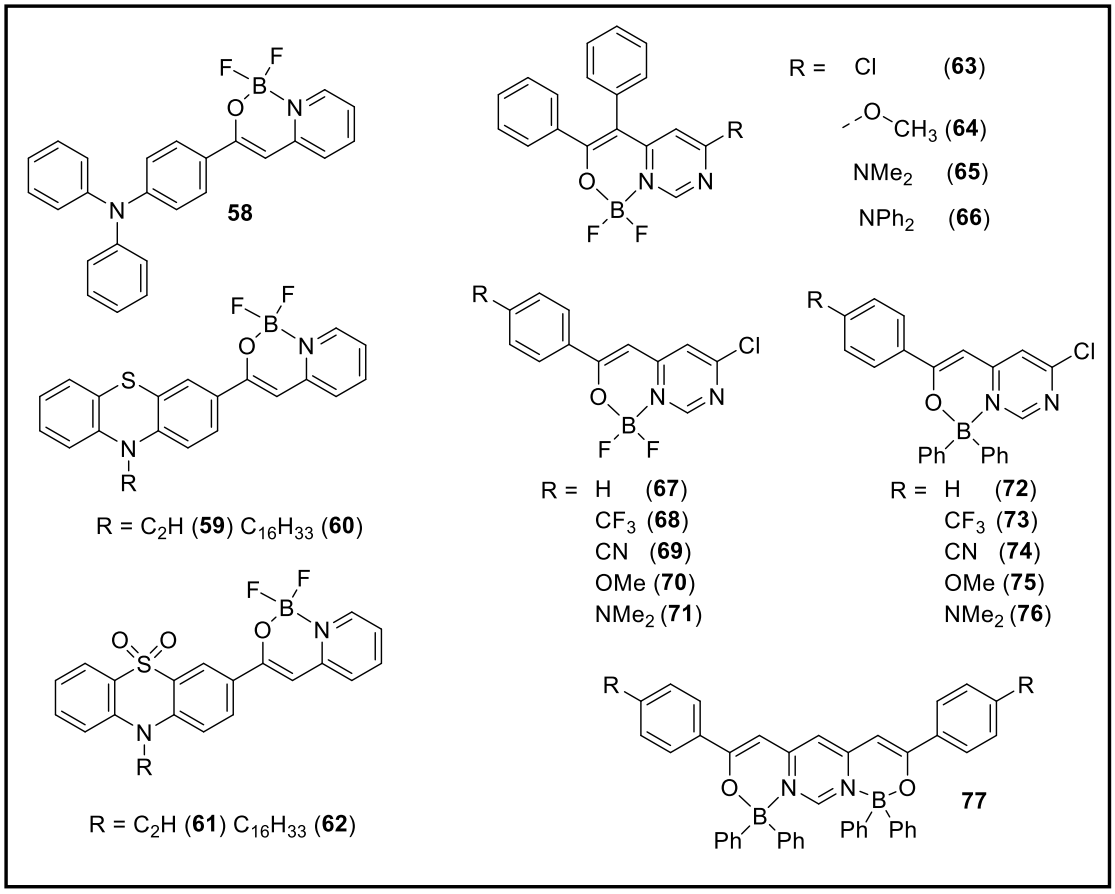

Figure 1.10: Structure of N,O-chelated tetra-coordinated boron compounds (**58-77**)

G-crystals displayed mechanochromism properties. After grinding, the Y-crystal and G-crystal displayed yellow emission at 533 nm which attained initial crystal states on fuming with CH_2Cl_2 or heating. The confirmation of mechanochromism was analyzed by PXRD. Compounds (**59**) and (**60**) displayed strong emissions due to strong intramolecular charge transfer whereas compounds (**61**) and (**62**) displayed weak emissions due to lack of intra-molecular charge transfer. Moreover, compound (**61**) displayed a multi-color response to mechanical force because of the disturbances of π-aggregates in the solid states. The compound (**63-66**) displayed weak emission in the solution state and strong emission in the solid state. Upon further analysis it was found that they displayed AIE in the THF/H_2O system. On increasing the percentage of water, the emission intensity gradually increases. X-ray analysis of the compound showed that the weak interaction in

the crystal packing might be responsible for the aggregation-induced emission properties. Further, compound (**66**) possessing -NPh_2 group displayed mechanochromism properties on grinding and changed the fluorescence colors from green to yellow-green. Matsui and co-workers reported pyrimidine-based tetra coordinated -BF_2 and -BPh_2 compounds **(67-76)** (Figure 1.10) and studied the effect of various electron-donating and withdrawing substitutions on the solution and solid-state emission.[86, 87]

In solid-state, electron-withdrawing (-CF_3 and -CN) substituents showed higher emission and better quantum yield than the solution state. The same group reported a dimer of pyrimidine (**77**) with different substituents on phenyl rings. On further investigation of pyrimidine-based boron derivatives, they found these derivatives to be AIE active.

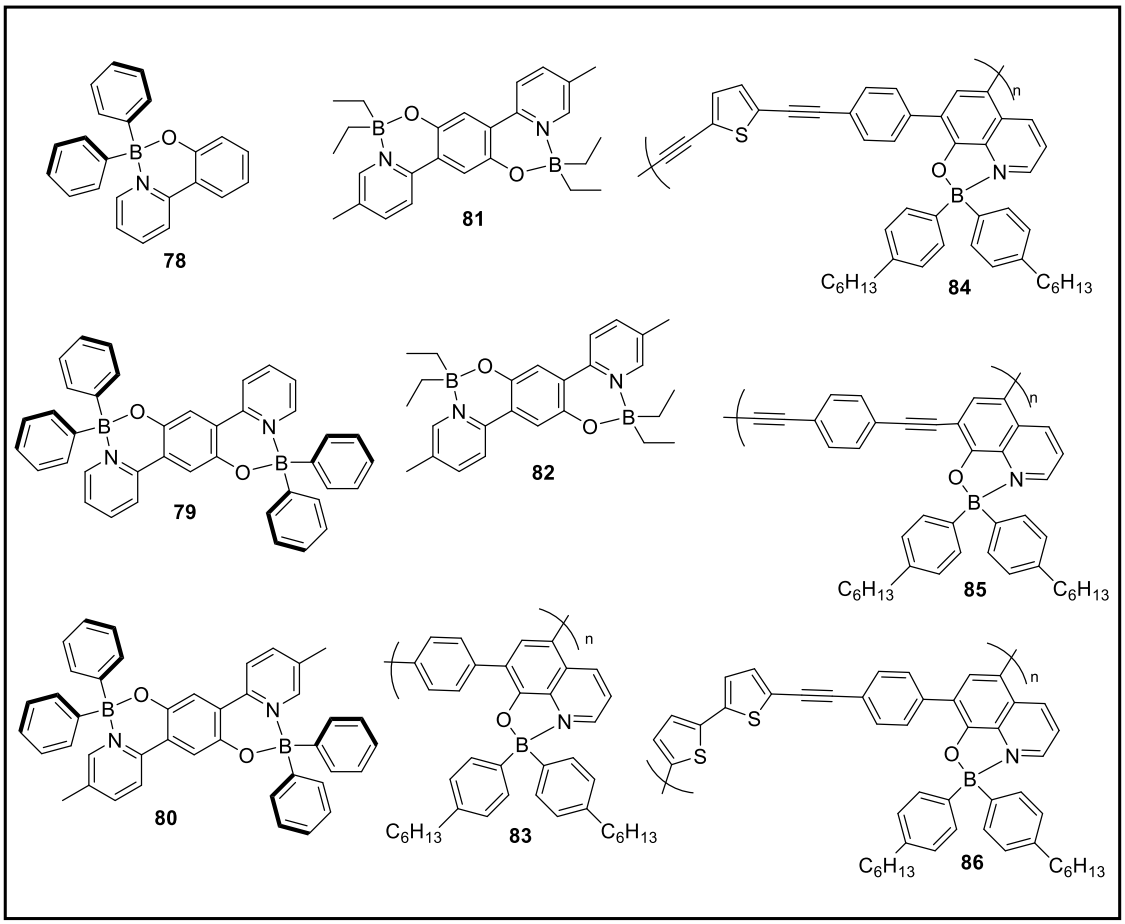

Figure 1.11: Structure of N,O-chelated tetra-coordinated boron compounds (**78-86**)

Do and co-workers reported a compound (**78**) and used it as a hole-blocking material for phosphorescent organic light emitting diodes (POLEDs). It displayed a low turn-on voltage of 3.2V, power efficiency of 6.12 (Im/W), external quantum efficiency of 4.42%, and, luminance efficiency of 20.06 (cd/A).[88] Ma and Co-worker reported a series of tetra-coordinated diboron ladder type π-conjugated compounds (**79-82**) and analyzed the optical, electrochemical, and thermal properties. Among them, compounds (**79-80**) displayed high thermal stability, moderated quantum yields, and stable redox species during the reduction, which make them prospective OLED device candidates.[89] Fang and co-workers reported hydroxyquinoline-based N,O-chelated boron polymers (**83-86**). These polymers were used to recognize volatile small molecules.[90]

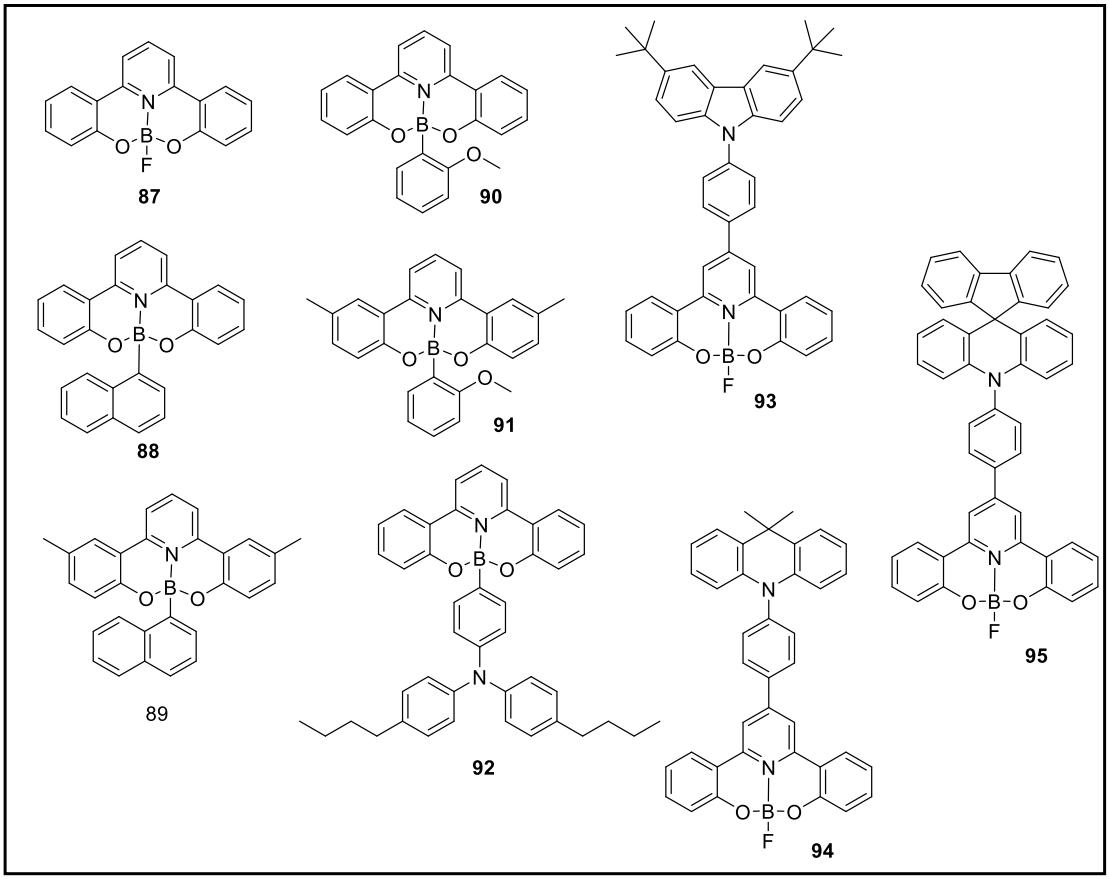

Figure 1.12: Structure of N,O-chelated tetra-coordinated boron compounds (**87-95**)

Yue Wang and co-workers reported a series of mixed phenol-pyridyl boron complexes (**87-93**) as promising candidates for electroluminescent materials. These compounds displayed good thermal stability with high T_g and T_m values. They displayed bright blue color fluorescence in the solution and in the solid state. These boron materials were utilized in white and blue electroluminescent devices.[91, 92] Tetra-coordinated boron compounds made up of tridentate 2,2'-(pyridine-2,6-diyl)diphenolate fused with carbazole or 10H-spiro[acridine-9,9'-fluorene] or 9,9-dimethyl-9,10-dihydroacridine (**94-95**) were reported recently.[93] These molecules possessed thermally activated delayed fluorescence (TADF) properties. Depending on the donor functionality, these boron molecules exhibited a wide range of emissions from blue to yellow region with larger stokes shift of 2746 cm^{-1}. Further, these boron compound OLED devices showed high performances with a current efficiency of 58.4 Im W^{-1} and external quantum efficiency of 18%.

The various imidazole derivatives of tetra-coordinated boron compounds (**96-99**) were studied for their application in OLEDs.[94, 95] Our group also reported a series of imidazole-based tetra-coordinated boron compounds (**100-102**).[96-98] The photophysical properties were fine-tuned by changing the aryl groups on the imidazole moiety. These boron compounds exhibited larger stokes shifts and moderate quantum yields. Compounds (**103-109**) were used to fabricate the electroluminescent devices and suggested that they are capable of transporting electrons. Further, compounds (**108-109**) possessing the N,N-dimethyl/diphenylamine group displayed the selective detection of picric acid. The detection of picric acid was determined with fluorescence and NMR spectroscopy. ^{1}H-NMR studies of the compound revealed that the proton abstraction of picric acid by the amine group along with weak intermolecular interactions was the reason for the selectivity.

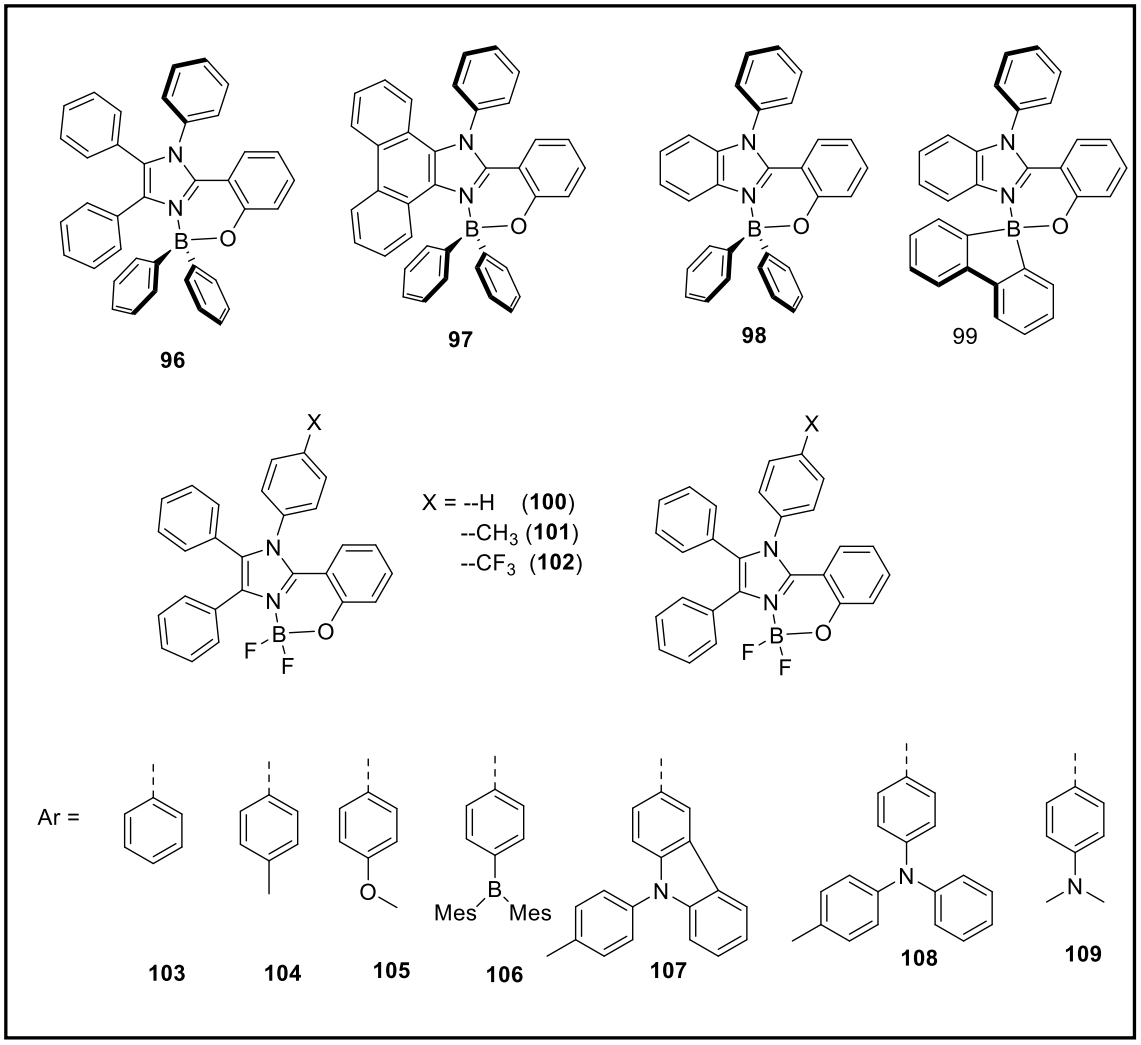

Figure 1.13: Structure of N,O-chelated tetra-coordinated boron compounds (**96-109**)

The various heterocycles containing B-N coordinated tetra coordinated boron compounds were reported by different groups. Among them, compounds (**110-112**) displayed aggregation-induced emission and reversible mechanochromism properties.[99, 100] High electron affinity and steric hindrance effect due to the cyano group resulted in twisted conformations which helped in gaining AIE and mechanochromic properties. Interestingly, compound (**110**) did not display any of AIE and mechanochromism properties due to the lack of -CN group. From the result, it was concluded that the cyano group plays an important role in displaying AIE and mechanochromic behavior. Lu group reported *tert*-butylcarbazole units which were connected to D-π-A type N,O-chelated boron compounds (**113-118**).[101] The reported boron compounds displayed self-assembly,

mechanochromism, and sensing properties. Especially, compound (**113**) displayed easy self-assembly to form gels in different organic solvents and the titration experiments confirmed that compound (**113**) showed high performance for the detection of TFA.

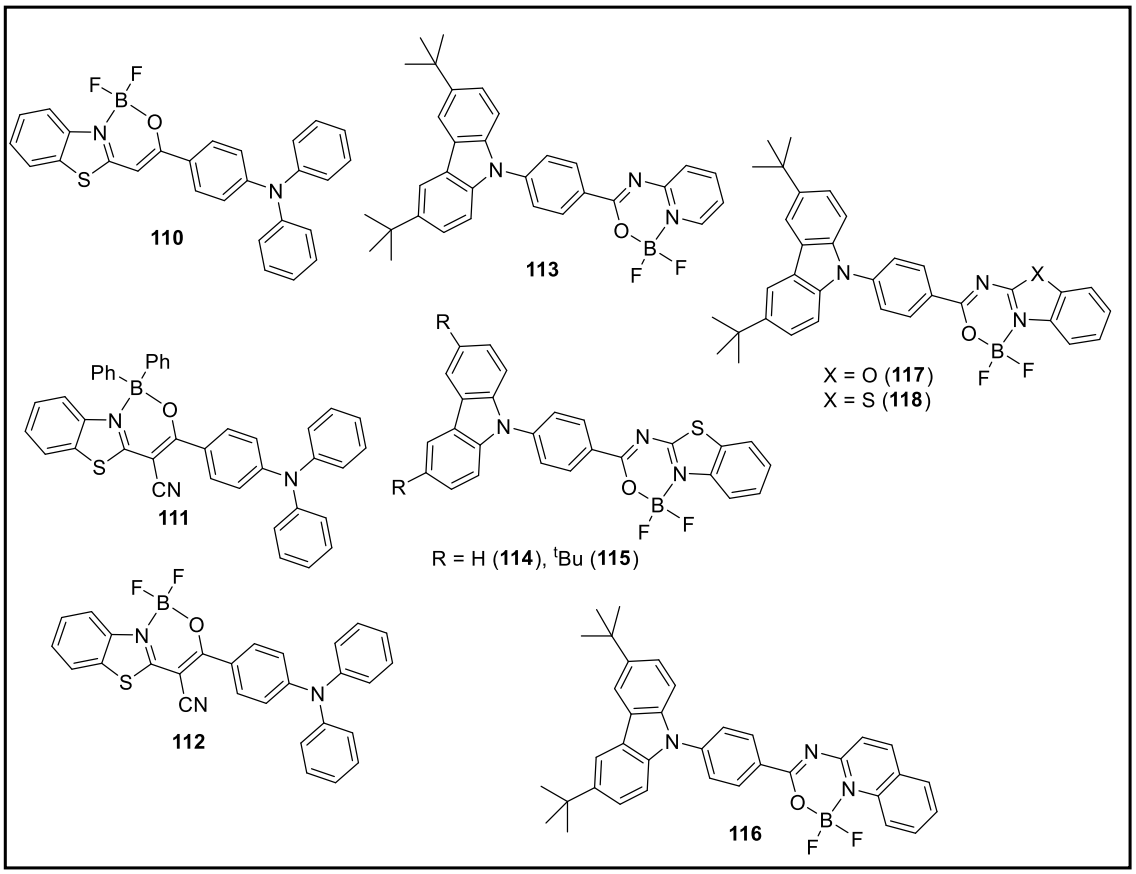

Figure 1.14: Structure of N,O chelated tetra-coordinated boron compounds (**110-118**)

Kang and co-workers reported a series of N,O-chelated oxazolyl phenolate boron compounds, by changing the electron-withdrawing and donating groups on the para position of the phenoxide group (**119-125**) and fine-tuned the electronic structures and optical properties. Particularly, electron-donating -NPh_2 group substituted compound (**125**) displayed a bipolar character due to strong intramolecular charge transfer and, it showed higher quantum yield in toluene. It has been utilized in electroluminescent devices, it displayed maximum brightness of 2905 cd/m^2 at 13 V, current efficiency (CE_{max}) of 1.63 cd/A at 6 mA/cm^2, and turn-on voltage (V_{on}) of 4.3 V.[102] Hongyu Zhang

and co-workers reported two boron molecules (**126, 127**) with efficient red and deep red solid-state emission properties. Boron compound (**127**) was more redshifted over compound (**126**) due to the heavy atom effect of sulphur (S). These compounds also displayed good stability, high fluorescence efficiency, and high carrier mobility for electroluminescent devices. Compound (**126**) displayed a turn-on voltage (V_{on}) of 2.5 V, PEmax of 0.53 lm/W, and, compound (**127**) displayed a turn-on voltage (V_{on}) of 3.0 V, PEmax of 0.46 lm/W.[103]

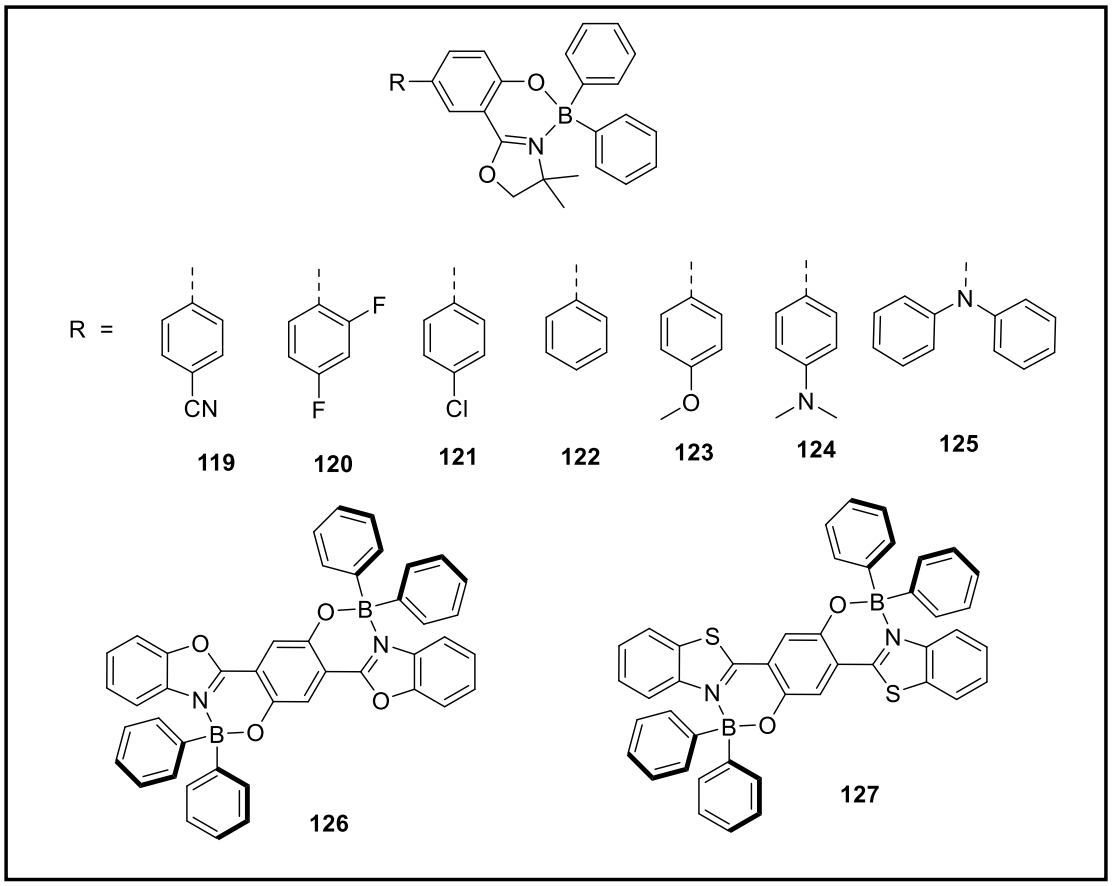

Figure 1.15: Structure of N,O-chelated tetra-coordinated boron compounds (**119-127**)

1.1.2.3. N,N-chelated boron compounds:

The boron dipyrromethene (BODIPY) compounds are well-known and highly explored N,N-chelate boron compounds. One of the two pyrrole nitrogen atoms can establish a covalent link with the boron centre, and the other nitrogen can form a coordinate covalent

bond by contributing a single pair of electrons to the boron atom's empty pz orbital. (**Figure 1.16**). BODIPY displayed a wide variety of applications in various fields due to their large extinction coefficients, high quantum yield in the solution state, tunable optical properties and possessed good photostability. However, the BODIPY compounds are poorly emissive in the solid state, which reduces some of their optoelectronic applications. So far, lot of reviews and articles were reported describing the applications of BODIPY compounds in various research fields.[104-114] Other than BODIPY derivatives, some other N,N-chelated boron compounds were reported which is discussed below.

Ziegler and Jiao group reported bis(difluoroboron)1,2-bis((pyrrol-2-yl)methylene) hydrazine (BOPHY) compounds which displayed moderate optical properties (**128, 129**).[115] [116] Shen and co-workers reported five and six-membered ring formation involving boron atoms using hydrazine-Schiff base linked bis pyrrole.[117] Six membered ring compound (**130**) that displayed efficient solid-state emission due to the weak intermolecular interactions and high Stokes shift, whereas, the five-membered ring compound (**131**) displayed strong intermolecular interactions and small Stokes shift which results in weak solid-state emission *via* the self-quenching process. Zhang and co-workers reported compound (**132**) possessing two iodine atoms and were used for the preparation of new triplet photosensitizers. Nanosecond time-resolved transient absorption spectra of compound (**132**) displayed a long-lived triplet excited state lifetime of 177.2 μs.[118] Gomes and co-workers reported pyrrolyl type of boron compounds (**133, 134**) and investigated their applications in OLEDs.[119-122] Chou and co-workers reported pyridyl pyrrolide-based boron complexes (**135-137**), which displayed efficient thermally activated delayed fluorescence properties and, investigated their application in organic light emitting diodes.[123]

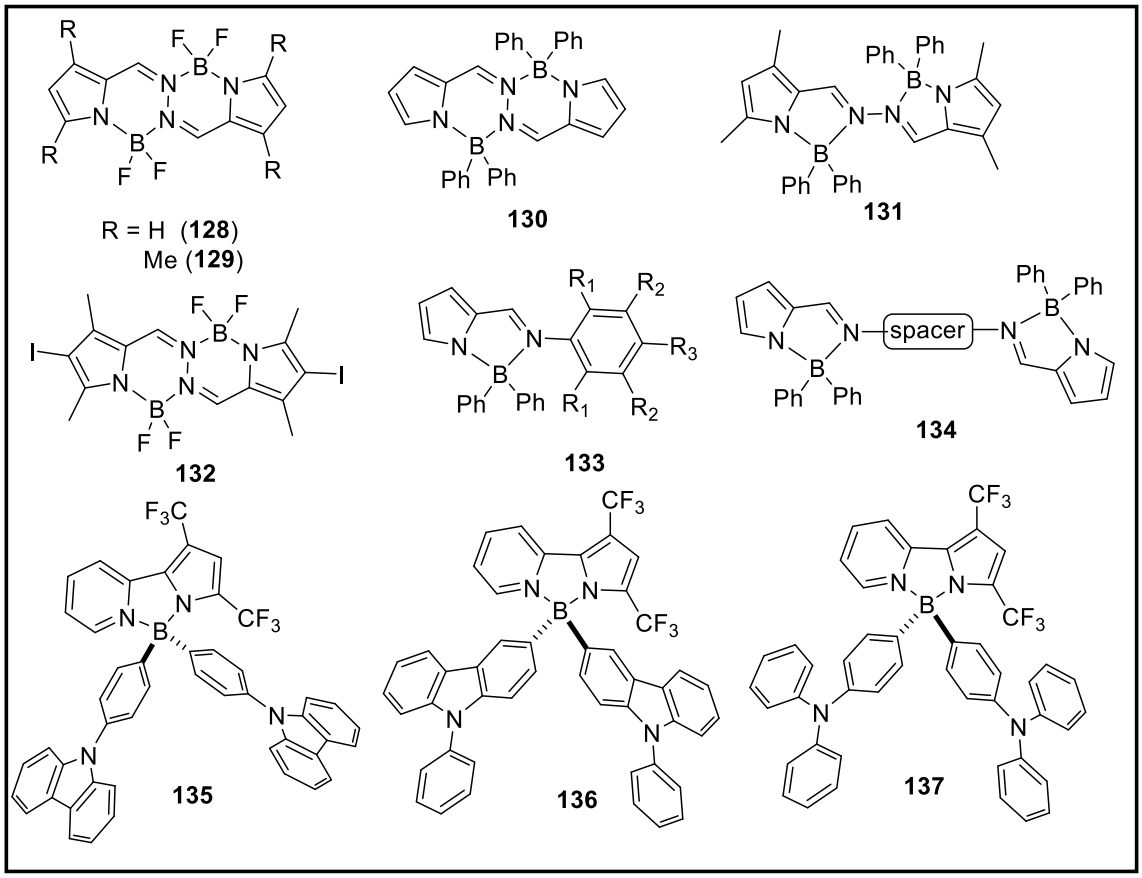

Figure 1.16: Structure of N,N-chelated tetra-coordinated boron compounds (**128-137**)

[124]Wang and co-workers reported 2-(2'-pyridyl)indole chelated boron compound (**138**) that displayed good air stability, and melting point of >250 °C. The optical and electroluminescence properties of the 2-(2'-Pyridyl)indole chelated boron compounds (**139-146**) were described by C-H replacement of the indole ring to electronegative substituents, or nitrogen atom, or the increase of conjugation to ligand system.[125, 126] Chen and co-workers reported 2-pyridyl pyrrolide boron complexes (**147-149**) that displayed good air stability in the solution state and, displayed strong emission peak at 490 nm, 510 nm, 575 nm. Moreover, compound (**149**) was fabricated as an electroluminescent device to produces red-orange emission at 580 nm, turn-on voltage (V_{on}) of 8.0 V, and external quantum yield of 0.5%.[127]

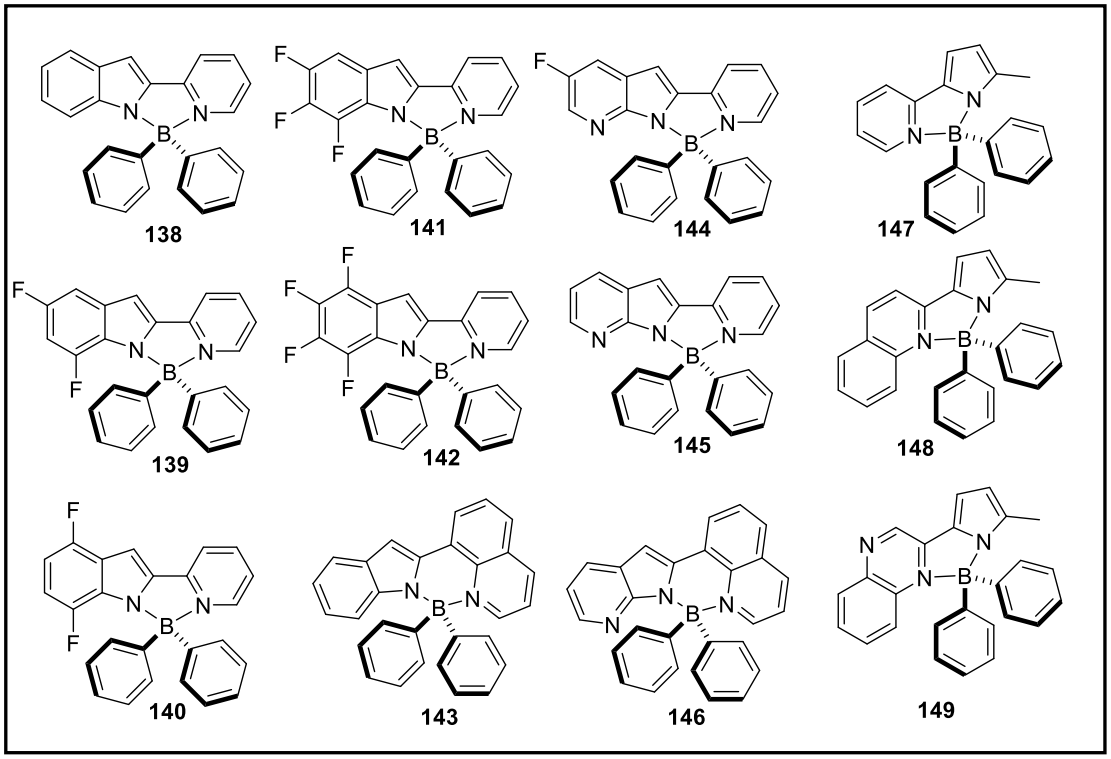

Figure 1.17: Structure of N,N-chelated tetra-coordinated boron compounds (**138-149**)

Chen and co-workers reported 2(2-quinolyl)naphtho[b] imidazole-based boron complexes (**150, 151**) and, used them as electroluminescent device.[128, 129] They displayed bright yellow fluorescence with emission maxima at 540 nm. Recently, boron-formazan dyes have been attracted due to their interesting optical properties. Gilroy and co-workers reported a variety of amine-substituted (**152-156**) tetra-coordinated formazanate-boron compounds and utilized in variety of applications.[130-135] Further, formazanate-boron compounds bridged *via* an alkyne group with N-annulated perylene diimide (**156**) were used to make organic photovoltaics.

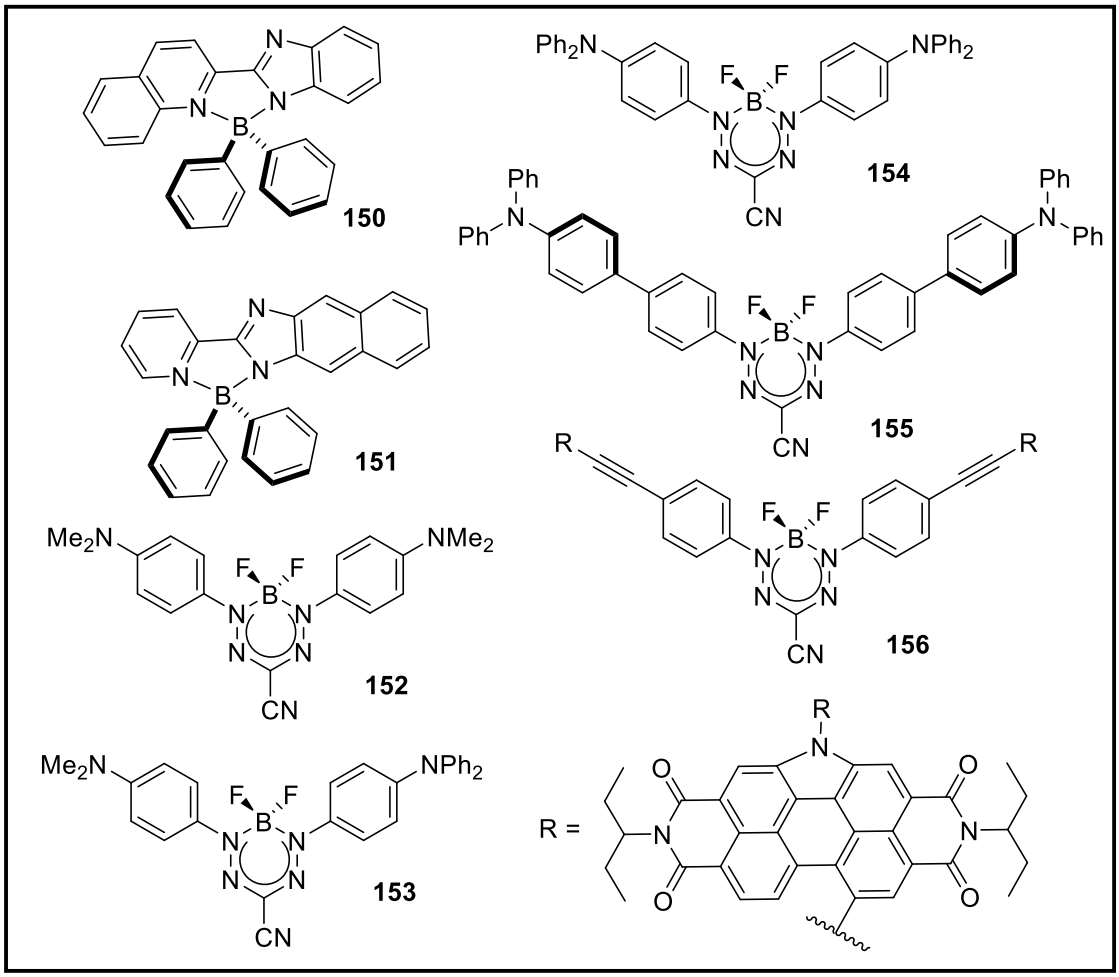

Figure 1.18: Structure of N,N-chelated tetra-coordinated boron compounds (**150-156**)

1.1.2.3A. Pyrazole fused N,N-chelated system:

Similar to N,N chelated boron system, two boron-centered N,N fused tetra-coordinated compounds namely pyrazaboles have also been reported. Pyrazabole are interesting B-N coordinated six-membered fused compounds gained considerable attention, since the pioneering work of Trofimenko.[136] [137] The importance of pyrazaboles were further explored by Trofimenko, Niedenzu, and Wagner.[138-140] Rajneesh Misra and co-workers reported different combinations of donor and acceptor pyrazabole compounds (**Figure 1.20**), and studied their properties and applications. In 2013, they reported ferrocenyl substituted pyrazabole molecules (**157-162**) and studied their multiphoton absorption properties.[141] In the same year various aryl-substituted pyrazabole molecules attached

with acetylenic linkages (**163-167**) were reported. Those compounds displayed good stability towards high temperatures and, displayed high quantum yield.[142] In 2014, ferrocenyl-substituted pyrazabole compounds were reported with their detailed crystal structures, optical, and electrochemical properties, and DFT calculations.[143]

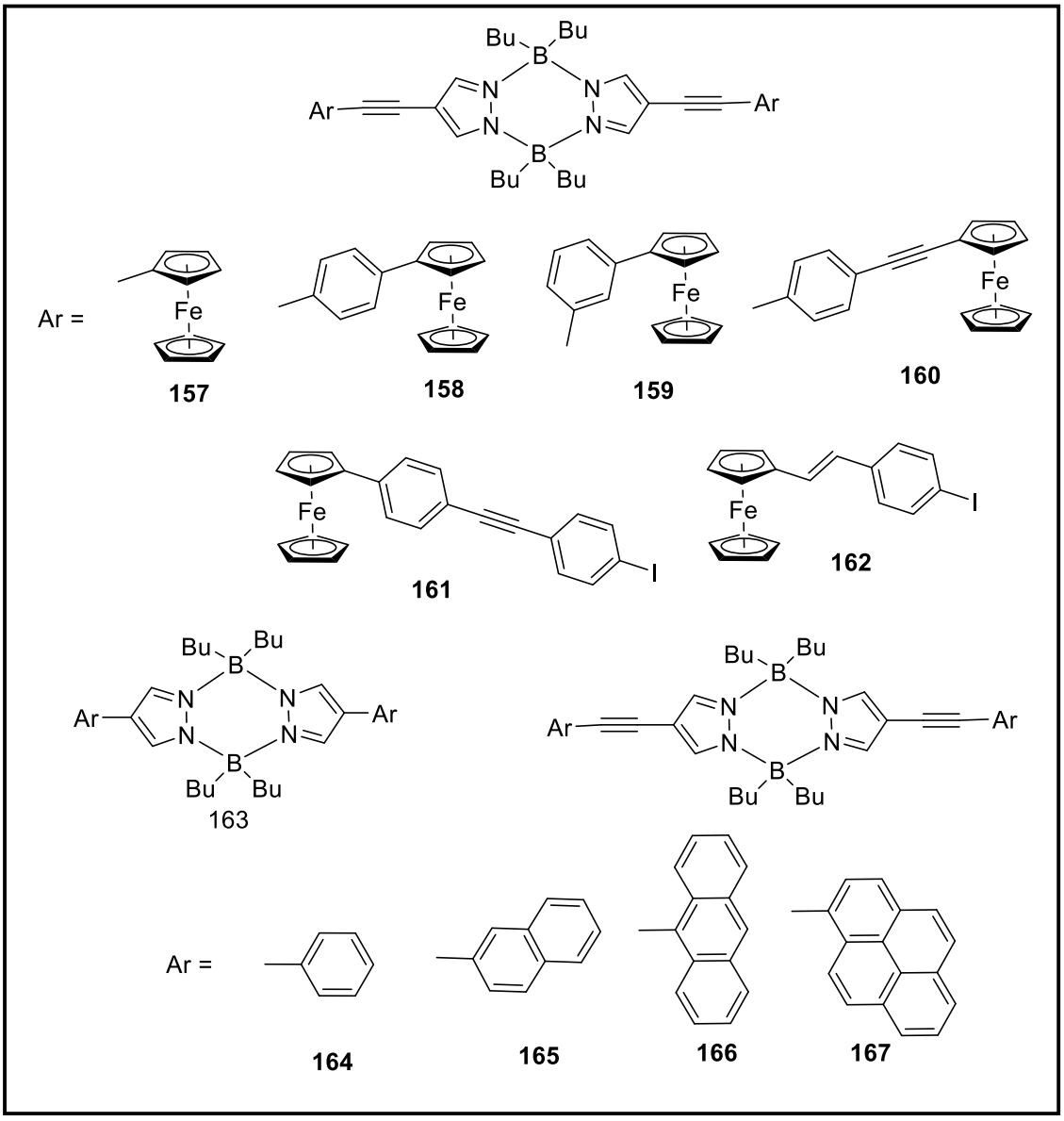

Figure 1.19: Structure of fused N,N tetra-coordinated boron compounds (**157-167**)

In 2015, TPE (tetraphenylethene) substituted pyrazabole compound was reported (**168**), and its aggregation-induced emission, and mechanochromic properties was studied.[144] In the same year tri- and tetra-coordinated boron containing pyrazabole compound (**169**)

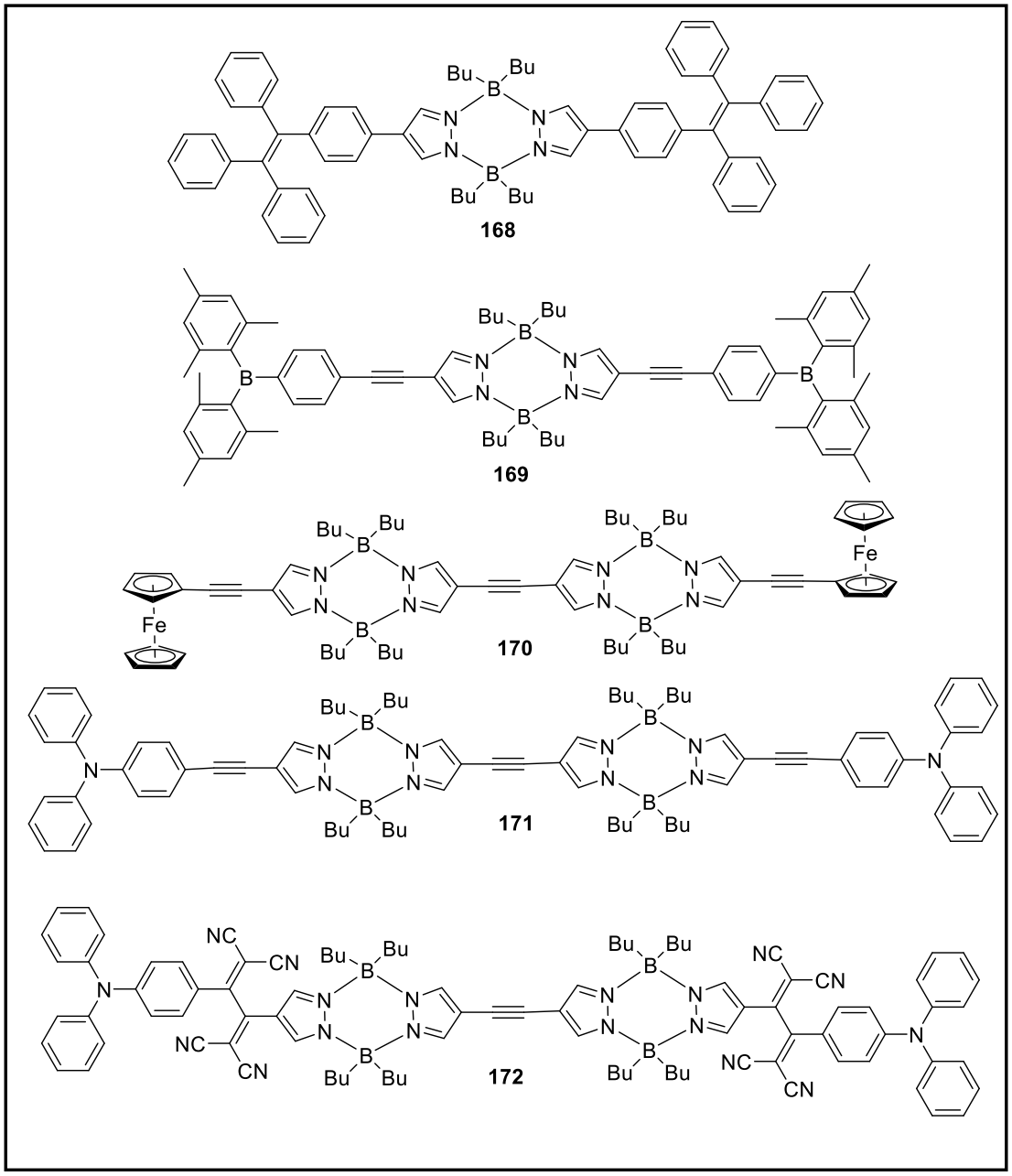

Figure 1.20: Structure of fused N,N tetra-coordinated boron compounds (**168-172**)

which showed colorimetric and fluorimetric detection of F^- and CN^- ions was reported.[145] In 2017, ferrocene and triphenylamine substituted monomeric, dimeric pyrazabole compounds (**170-172**) were reported, and their optical, electrochemical, and thermal properties were investigated.[146] Further, tetracyanobutadiene bridged pyrazabole (**172**) was reported in the same year and the effect of photonic and electrochemical properties were studied.[147]

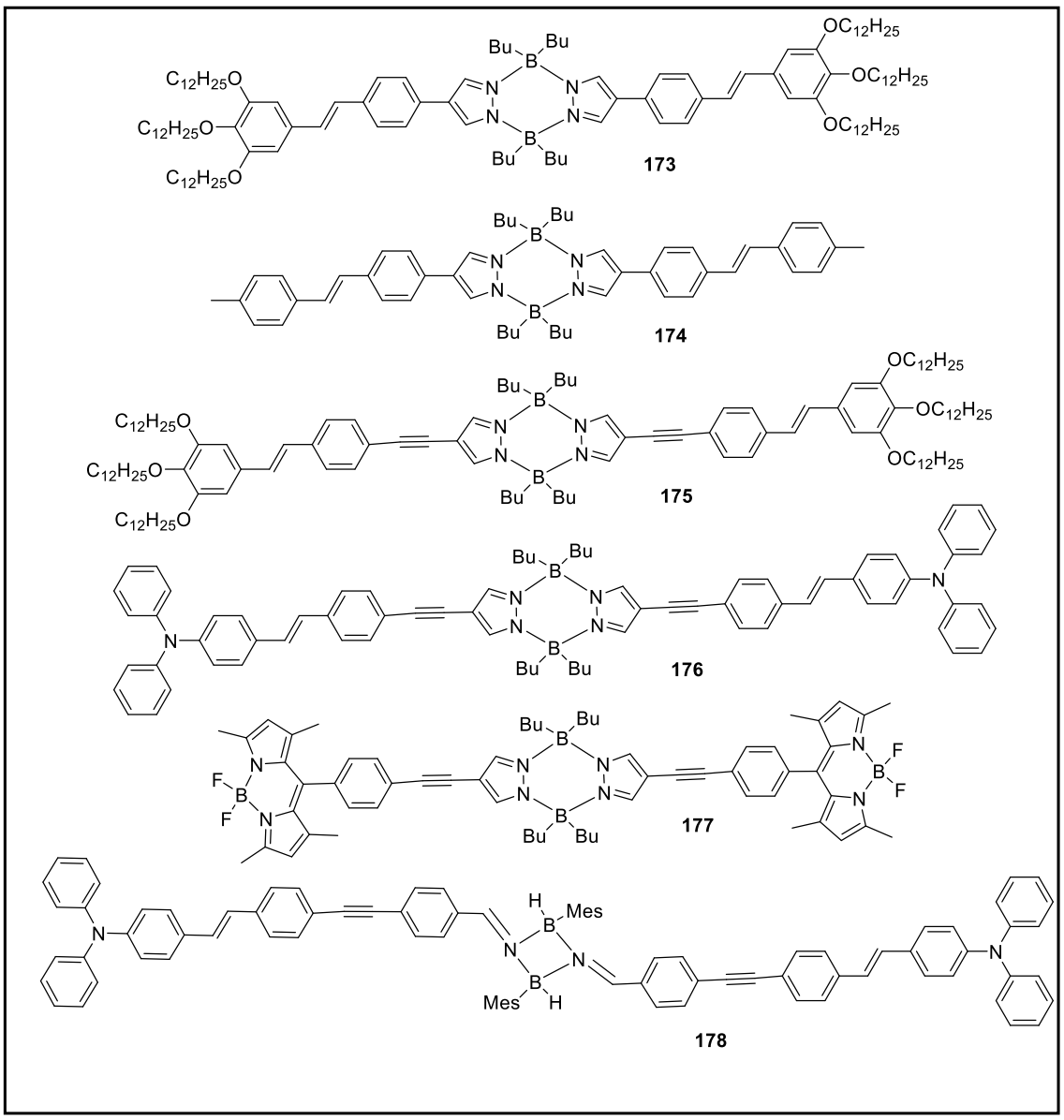

Figure 1.21: Structure of fused N,N tetra-coordinated boron compounds (**173-178**)

In 2009, Jean-Francois and co-workers reported different ethylene and acetylene-bridged pyrazabole molecules (**173-178**).[148] They fixed pyrazabole as a central core of the molecules and varied the conjugative length and position of the end groups (-OR, -NPh_2, BODIPY) and these compounds were screened for one and two-photon absorption studies.

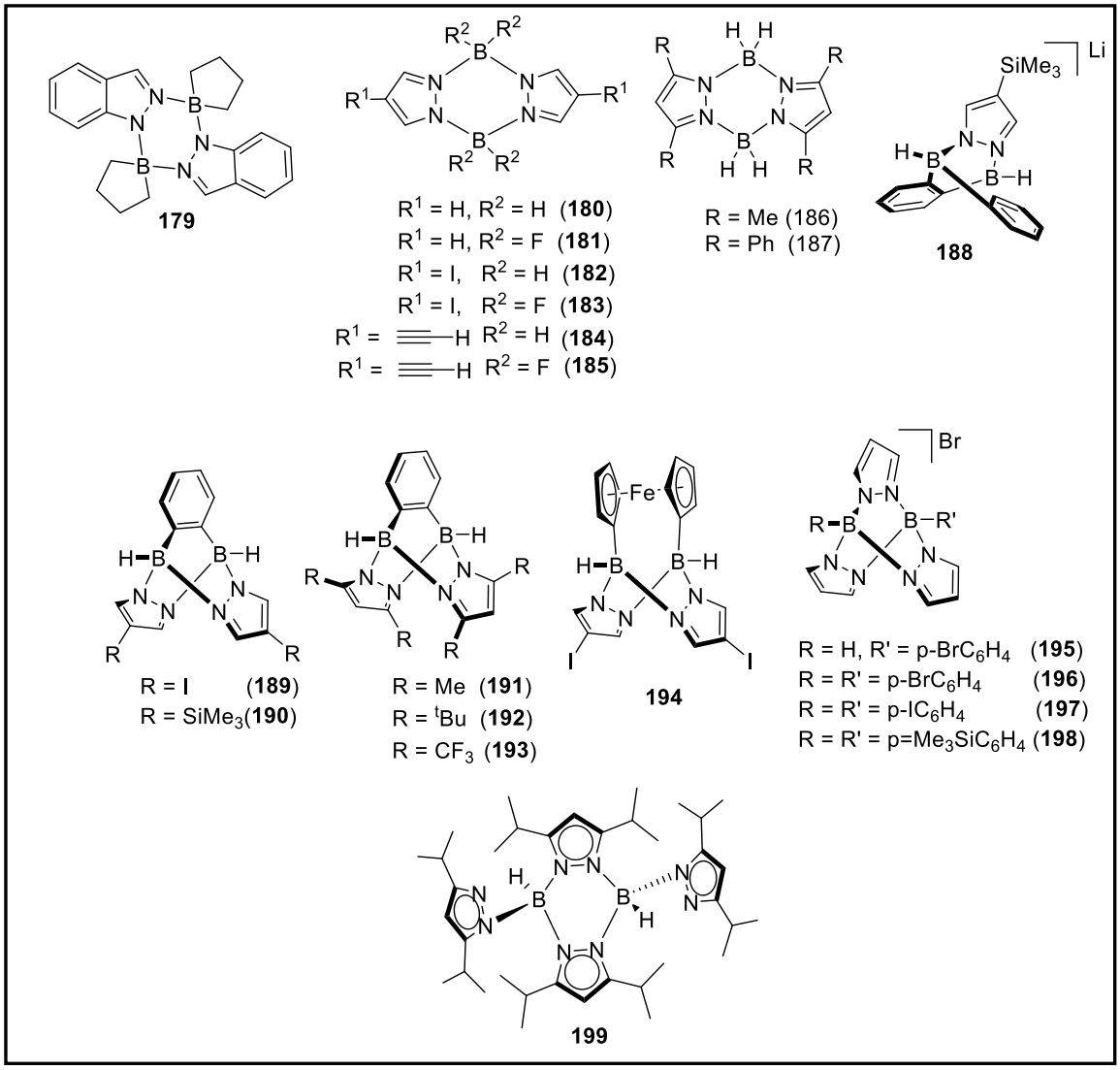

Figure 1.22: Structure of fused N,N tetra-coordinated boron compounds (**179-199**)

In 2010, Wolfgang Milius and co-workers reported the synthesis of indazabole (**179**).[149] They found the formation of two isomers of indazabole molecule at different conditions and, was confirmed by NMR spectroscopy. From the crystal structure it was found that the B_2N_4 ring formed a distorted boat conformation. In 2008, Elguero and co-workers reported iodo and ethynyl substituted new BH_2 and BF_2-pyrazabole (**180-185**) and found that molecular structures and packing arrangements depend on the substituents.[150] In 2014, Lalevee and co-workers reported a new class of N-heterocycle-boryl radicals from pyrazabole moieties (**186-187**).[151] They exhibited a low bond dissociation energy and excellent properties based on hydrogen transfer. The reactivity of the molecules has been

studied with the addition of alkynes, alkenes, O_2, iodonium salts, and alkyl halides and showed application for radical polymerization and radical dehalogenation reactions. In 2014, Wagner and co-workers reported pyrazabole-based B-N analogs of triptycene molecules (**188-198**) and studied the thermal stability and reactivity of the molecules[152]. Edelmann and co-workers prepared sterically crowded pyrazabole ligand (**199**) as well as europium (II) mono(scorpionate) complex that was structurally confirmed by X-ray crystallography.[153]

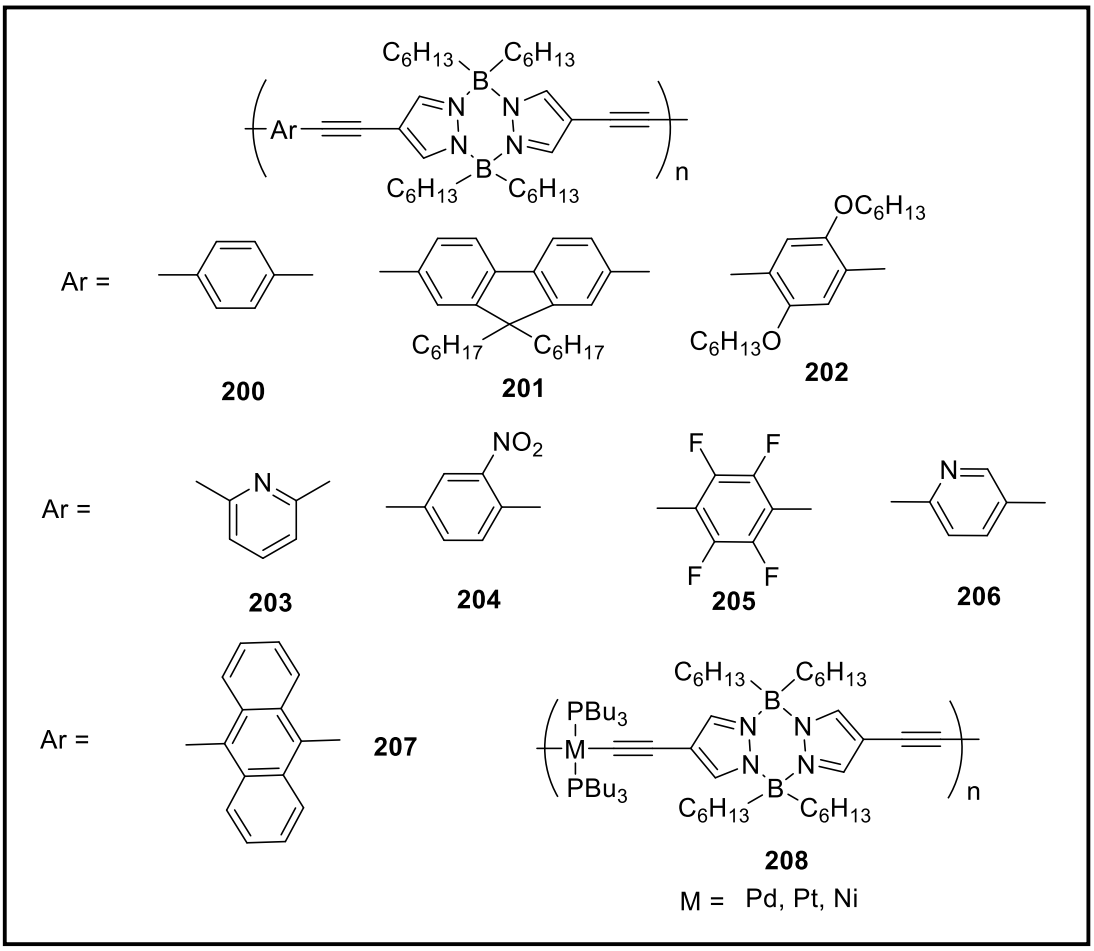

Figure 1.23: Structure of fused N,N tetra-coordinated boron polymers (**200-208**)

In 2003 and 2005, Chujo and co-workers reported polymeric pyrazabole compounds (**Figure 1.23**) with electron-withdrawing groups on the main chain of the pyrazabole that were synthesized by Heck-Sonagashira coupling reaction (**200-207**).[154, 155] They

investigated the optical properties of the polymers by UV-visible and fluorescence spectroscopy. The synthesized polymers displayed a high number average molecular weight. In 2006, they reported various transition metals (Ni, Pt, Pd) incorporated poly-pyrazaboles (**208**).[156] The Ni and Pt-based polypyrazaboles displayed MLCT transitions in the UV absorption, whereas Pd-based Polypyrazabole did not show UV absorption.

1.3. References:

1. Entwistle, C. D.; Marder, T. B. *Angew. Chem. Int. Ed.* **2002,** *41*, 2927-2931.
2. Yamaguchi, S.; Wakamiya, A. *Pure Appl. Chem.* **2006,** *78*, 1413-1424.
3. Hudnall, T. W.; Chiu, C.-W.; Gabbaï, F. P. *Acc. Chem. Res.* **2009,** *42*, 388-397.
4. Jäkle, F. *Chem. Rev.* **2010,** *110*, 3985-4022.
5. Galbraith, E.; James, T. D. *Chem. Soc. Rev.* **2010,** *39*, 3831-3842.
6. Wade, C. R.; Broomsgrove, A. E. J.; Aldridge, S.; Gabbaï, F. P. *Chem. Rev.* **2010,** *110*, 3958-3984.
7. Cheng, F.; Jäkle, F. *Polym. Chem.* **2011,** *2*, 2122-2132.
8. Rao, Y.-L.; Wang, S. *Inorg. Chem.* **2011,** *50*, 12263-12274.
9. Li, D.; Zhang, H.; Wang, Y. *Chem. Soc. Rev.* **2013,** *42*, 8416-8433.
10. Baranin, S.; Zavarzin, I. *Russ. Chem. Bull.* **2017,** *66*, 1398-1418.
11. Chen, P.-Z.; Niu, L.-Y.; Chen, Y.-Z.; Yang, Q.-Z. *Coord. Chem. Rev.* **2017,** *350*, 196-216.
12. DeRosa, C. A.; Fraser, C. L., *Tetracoordinate Boron Materials for Biological Imaging*. Hoboken, NJ: John Wiley & Sons Ltd: 2017.
13. Shah, S.; Marandi, P.; Neelakandan, P. *Front. Chem.* **2021**, 724.
14. Murali, A. C.; Nayak, P.; Venkatasubbaiah, K. *Dalton Trans.* **2022,** *51*, 5751-5771.

15. Shi, J.; Ran, Z.; Peng, F. *Dyes Pigm.* **2022,** *204*, 110383.

16. Taniguchi, T. *Chem. Eur. J.* **2022,** *28*, e202104333.

17. Jaekle, F. *Coord. Chem. Rev.* **2006,** *250*, 1107-1121.

18. Wade, C. R.; Broomsgrove, A. E. J.; Aldridge, S.; Gabbai, F. P. *Chem. Rev.* **2010,** *110*, 3958-3984.

19. Entwistle, C. D.; Marder, T. B. *Chem. Mater.* **2004,** *16*, 4574-4585.

20. Hudson, Z. M.; Wang, S. *Acc. Chem. Res.* **2009,** *42*, 1584-1596.

21. Ji, L.; Griesbeck, S.; Marder, T. B. *Chem. Sci.* **2017,** *8*, 846-863.

22. Taniguchi, T. *Chem. - Eur. J.* **2022,** *28*, e202104333.

23. Murali, A. C.; Nayak, P.; Venkatasubbaiah, K. *Dalton Trans.* **2022,** *51*, 5751-5771.

24. Chen, P.-Z.; Niu, L.-Y.; Chen, Y.-Z.; Yang, Q.-Z. *Coord. Chem. Rev.* **2017,** *350*, 196-216.

25. Cogné-Laage, E.; Allemand, J.-F.; Ruel, O.; Baudin, J.-B.; Croquette, V.; Blanchard-Desce, M.; Jullien, L. *Chem. Eur. J.* **2004,** *10*, 1445-1455.

26. Lanoë, P.-H.; Mettra, B.; Liao, Y. Y.; Calin, N.; D'Aléo, A.; Namikawa, T.; Kamada, K.; Fages, F.; Monnereau, C.; Andraud, C. *ChemPhysChem.* **2016,** *17*, 2128-2136.

27. Zhang, X.; Zhang, G. *Anal. Methods* **2012,** *4*, 2641-2643.

28. Wang, F.; De Rosa, C. A.; Daly, M. L.; Song, D.; Sabat, M.; Fraser, C. L. *Mater. Chem. Front.* **2017,** *1*, 1866-1874.

29. Gon, M.; Tanaka, K.; Chujo, Y. *Bull. Chem. Soc. Jpn.* **2018,** *92*, 7-18.

30. Massue, J.; Jacquemin, D.; Ulrich, G.*Organics* [Online], 2021, p. 365-375.

31. Chen, P.-Z.; Wang, J.-X.; Niu, L.-Y.; Chen, Y.-Z.; Yang, Q.-Z. *J. Mater. Chem. C* **2017,** *5*, 12538-12546.

32. Chen, P.-Z.; Zhang, H.; Niu, L.-Y.; Zhang, Y.; Chen, Y.-Z.; Fu, H.-B.; Yang, Q.-Z. *Adv. Funct. Mater.* **2017,** *27*, 1700332.

33. Chen, P.-Z.; Niu, L.-Y.; Zhang, H.; Chen, Y.-Z.; Yang, Q.-Z. *Mater. Chem. Front.* **2018,** *2*, 1323-1327.

34. Gao, H.; Xu, D.; Wang, Y.; Wang, Y.; Liu, X.; Han, A.; Zhang, C. *Dyes Pigm.* **2018,** *150*, 59-66.

35. Liu, W.; Wang, Y.; Ge, G.; Ma, L.; Ren, L.; Zhang, Y. *Dyes Pigm.* **2019,** *171*, 107704.

36. Sun, T.; Zhao, F.; Xi, G.; Gong, J.; Sun, M.; Dong, C.; Qiu, J. *RSC Adv.* **2019,** *9*, 19641-19647.

37. Zhang, L.; Ma, L.-L.; Wang, X.; Zhao, X.-Y. *J. Lumin.* **2019,** *214*, 116560.

38. Zhu, J.-Y.; Li, C.-X.; Chen, P.-Z.; Ma, Z.; Zou, B.; Niu, L.-Y.; Cui, G.; Yang, Q.-Z. *Mater. Chem. Front.* **2020,** *4*, 176-181.

39. Yang, H.; Zhang, W.; Lu, X.; Liu, W.; Wang, Y.; Li, H.; Yang, Y. *Dyes Pigm.* **2021,** *192*, 109396.

40. Louis, M.; Brosseau, A.; Guillot, R.; Ito, F.; Allain, C.; Métivier, R. *J. Phys. Chem. C* **2017,** *121*, 15897-15907.

41. Wilbraham, L.; Louis, M.; Alberga, D.; Brosseau, A.; Guillot, R.; Ito, F.; Labat, F.; Métivier, R.; Allain, C.; Ciofini, I. *Adv. Mater.* **2018,** *30*, 1800817.

42. Louis, M.; Guillot, R.; Métivier, R.; Allain, C. *Photochem. Photobiol. Sci.* **2018,** *17*, 822-828.

43. Huang, W.; Zhang, X.; Chen, B.; Miao, H.; Trindle, C. O.; Wang, Y.; Luo, Y.; Zhang, G. *Chem. commun.* **2019,** *55*, 67-70.

44. Wang, J.-X.; Yu, Y.-S.; Niu, L.-Y.; Zou, B.; Wang, K.; Yang, Q.-Z. *Chem. commun.* **2020,** *56*, 6269-6272.

45. Wang, J.-X.; Zhang, T.-S.; Zhu, X.; Li, C.-X.; Dong, L.; Cui, G.; Yang, Q.-Z. *J. Phys. Chem. A* **2020,** *124*, 10082-10089.

46. Daly, M. L.; Kerr, C.; DeRosa, C. A.; Fraser, C. L. *ACS Appl. Mater. Interfaces* **2017,** *9*, 32008-32017.

47. Morris, W. A.; Butler, T.; Kolpaczynska, M.; Fraser, C. L. *Mater. Chem. Front.* **2017,** *1*, 158-166.

48. DeRosa, C. A.; Daly, M. L.; Kerr, C.; Fraser, C. L. *ChemPhotoChem* **2019,** *3*, 31-36.

49. DeRosa, C. A.; Hiroto, S.; Fraser, C. L. *J. Phys. Chem. C* **2019,** *123*, 20488-20496.

50. Liu, T.; Zhang, G.; Evans, R. E.; Trindle, C. O.; Altun, Z.; DeRosa, C. A.; Wang, F.; Zhuang, M.; Fraser, C. L. *Chem. Eur. J.* **2018,** *24*, 1859-1869.

51. Sasabe, H.; Sasaki, K.; Mamiya, M.; Suwa, Y.; Watanabe, T.; Onuma, N.; Nakao, K.; Yamaji, M.; Kido, J. *Chem. Asian J.* **2017,** *12*, 2299-2303.

52. Jiang, Q.; Zhang, M.; Wang, Z.; Song, J.; Yang, Y.; Li, W.; Gu, W.; Xu, X.; Xu, H.; Wang, S. *RSC Adv.* **2018,** *8*, 30055-30060.

53. Wong, C.-L.; Poon, C.-T.; Yam, V. W.-W. *Organometallics* **2017,** *36*, 2661-2669.

54. Li, Z.; Pei, Y.; Wang, Y.; Lu, Z.; Dai, Y.; Duan, Y.; Ma, Y.; Guo, H. *J. Org. Chem.* **2019,** *84*, 13364-13373.

55. Li, Z.; Wang, Y.; Li, M.; Chen, H.; Xie, Y.; Li, P.; Guo, H.; Ya, H. *Dyes Pigm.* **2019,** *162*, 339-347.

56. Li, Z.; Hu, Y.-J.; Zhang, K.; Zhang, Y.; Hu, Q.-Q.; Zhang, X.-J.; Zhang, X.-K.; Zhu, Y.-P. *Dyes Pigm.* **2020,** *182*, 108686.

57. Li, Z.; Pei, Y.; Hou, S.; Dai, Y.; Liu, D.; Zhu, J.; Zhu, Y.-P.; Liu, X. *Dyes Pigm.* **2020,** *179*, 108419.

58. Li, Z.; Gao, X.; Hu, X.; Zhang, X.; Jia, C.; Liu, C.; Shen, L.; Zhu, H.; Cui, M.; Lu, Z.; Guo, H. *Dyes Pigm.* **2021,** *192*, 109422.

59. Lu, Z.; Yang, W.; Bai, Y.; Wang, M.; Li, Z.; Yang, Y.; Feng, X.; Zhu, Y.; Yang, X.; Li, Z. *J. Chem. Res.* **2021,** *45*, 411-416.

60. Tanaka, M.; Muraoka, S.; Matsui, Y.; Ohta, E.; Sakai, A.; Ogaki, T.; Yoshimoto, Y.; Mizuno, K.; Ikeda, H. *ChemPhotoChem* **2017,** *1*, 188-197.

61. Chen, Y.-W.; Lin, Y.-C.; Kuo, H.-M.; Lai, C. K. *J. Mater. Chem. C* **2017,** *5*, 5465-5477.

62. Polishchuk, V.; Stanko, M.; Kulinich, A.; Shandura, M. *Eur. J. Org. Chem.* **2018,** *2018*, 240-246.

63. Polishchuk, V.; Kulinich, A.; Rusanov, E.; Shandura, M. *J. Org. Chem.* **2021,** *86*, 5227-5233.

64. Canard, G.; Ponce-Vargas, M.; Jacquemin, D.; Le Guennic, B.; Felouat, A.; Rivoal, M.; Zaborova, E.; D'Aléo, A.; Fages, F. *RSC Adv.* **2017,** *7*, 10132-10142.

65. Bai, B.; Yan, C.; Zhang, Y.; Guo, Z.; Zhu, W.-H. *Chem. commun.* **2018,** *54*, 12393-12396.

66. Paisley, N. R.; Halldorson, S. V.; Tran, M. V.; Gupta, R.; Kamal, S.; Algar, W. R.; Hudson, Z. M. *Angew. Chem. Int. Ed.* **2021,** *60*, 18630-18638.

67. Archet, F.; Yao, D.; Chambon, S.; Abbas, M.; D'Aléo, A.; Canard, G.; Ponce-Vargas, M.; Zaborova, E.; Le Guennic, B.; Wantz, G.; Fages, F. *ACS Energy Lett.* **2017,** *2*, 1303-1307.

68. Li, Z.; Song, Y.; Lu, Z.; Li, Z.; Li, R.; Li, Y.; Hou, S.; Zhu, Y.-P.; Guo, H. *Dyes Pigm.* **2020,** *179*, 108406.

69. Kim, D.-H.; D'Aléo, A.; Chen, X.-K.; Sandanayaka, A. D. S.; Yao, D.; Zhao, L.; Komino, T.; Zaborova, E.; Canard, G.; Tsuchiya, Y.; Choi, E.; Wu, J. W.; Fages, F.; Brédas, J.-L.; Ribierre, J.-C.; Adachi, C. *Nat. Photon.* **2018,** *12*, 98-104.

70. Ye, H.; Kim, D. H.; Chen, X.; Sandanayaka, A. S. D.; Kim, J. U.; Zaborova, E.; Canard, G.; Tsuchiya, Y.; Choi, E. Y.; Wu, J. W.; Fages, F.; Bredas, J.-L.; D'Aléo, A.; Ribierre, J.-C.; Adachi, C. *Chem. Mater.* **2018,** *30*, 6702-6710.

71. Aoki, R.; Komatsu, R.; Goushi, K.; Mamada, M.; Ko, S. Y.; Wu, J. W.; Placide, V.; D'Aléo, A.; Adachi, C. *Adv. Opt. Mater.* **2021,** *9*, 2001947.

72. Wesela-Bauman, G.; Urban, M.; Luliński, S.; Serwatowski, J.; Woźniak, K. *Org. Biomol. Chem.* **2015,** *13*, 3268-3279.

73. Yang, Z.; Jiang, B.; Hao, W.-J.; Zhou, P.; Tu, S.-J.; Li, G. *Chem. commun.* **2015,** *51*, 1267-1270.

74. Yoshii, R.; Suenaga, K.; Tanaka, K.; Chujo, Y. *Chem. Eur. J.* **2015,** *21*, 7231-7237.

75. Wong, C.-L.; Poon, C.-T.; Yam, V. W.-W. *Chem. Eur. J.* **2016,** *22*, 12931-12940.

76. Fang, W.; Zhang, Y.; Zhang, G.; Kong, L.; Yang, L.; Yang, J. *CrystEngComm* **2017,** *19*, 1294-1303.

77. Ibarra-Rodríguez, M.; Muñoz-Flores, B. M.; Dias, H. V. R.; Sánchez, M.; Gomez-Treviño, A.; Santillan, R.; Farfán, N.; Jiménez-Pérez, V. M. *J. Org. Chem.* **2017,** *82*, 2375-2385.

78. Urban, M.; Durka, K.; Jankowski, P.; Serwatowski, J.; Luliński, S. *J. Org. Chem.* **2017,** *82*, 8234-8241.

79. Zhang, P.; Liu, W.; Niu, G.; Xiao, H.; Wang, M.; Ge, J.; Wu, J.; Zhang, H.; Li, Y.; Wang, P. *J. Org. Chem.* **2017,** *82*, 3456-3462.

80. Chen, S.; Qiu, R.; Yu, Q.; zhang, X.; Wei, M.; Dai, Z. *Tetrahedron Lett.* **2018,** *59*, 2671-2678.

81. Lugovik, K. I.; Eltyshev, A. K.; Suntsova, P. O.; Smoluk, L. T.; Belousova, A. V.; Ulitko, M. V.; Minin, A. S.; Slepukhin, P. A.; Benassi, E.; Belskaya, N. P. *Org. Biomol. Chem.* **2018,** *16*, 5150-5162.

82. Xing, J.; Jia, J. *Tetrahedron Lett.* **2021,** *78*, 153275.

83. Nandi, R. P.; Sudhakar, P.; Kalluvettukuzhy, N. K.; Thilagar, P. *Chem. Eur. J.* **2020,** *26*, 16306-16317.

84. Zhang, Z.; Wu, Z.; Sun, J.; Yao, B.; Zhang, G.; Xue, P.; Lu, R. *J. Mater. Chem. C* **2015,** *3*, 4921-4932.

85. Zhang, Z.; Wu, Z.; Sun, J.; Yao, B.; Xue, P.; Lu, R. *J. Mater. Chem. C* **2016,** *4*, 2854-2861.

86. Kubota, Y.; Kasatani, K.; Takai, H.; Funabiki, K.; Matsui, M. *Dalton Trans.* **2015,** *44*, 3326-3341.

87. Kubota, Y.; Kasatani, K.; Niwa, T.; Sato, H.; Funabiki, K.; Matsui, M. *Chem. - Eur. J.* **2016,** *22*, 1816-1824.

88. Kim, N. G.; Shin, C. H.; Lee, M. H.; Do, Y. *J. Organomet. Chem.* **2009,** *694*, 1922-1928.

89. Zhang, Z.; Bi, H.; Zhang, Y.; Yao, D.; Gao, H.; Fan, Y.; Zhang, H.; Wang, Y.; Wang, Y.; Chen, Z.; Ma, D. *Inorg. Chem.* **2009,** *48*, 7230-7236.

90. Qi, Y.; Xu, W.; Kang, R.; Ding, N.; Wang, Y.; He, G.; Fang, Y. *Chem. Sci.* **2018,** *9*, 1892-1901.

91. Li, Y.; Liu, Y.; Bu, W.; Guo, J.; Wang, Y. *Chem. commun.* **2000**, 1551-1552.

92. Zhang, H.; Huo, C.; Ye, K.; Zhang, P.; Tian, W.; Wang, Y. *Inorg. Chem.* **2006,** *45*, 2788-2794.

93. Li, P.; Chan, H.; Lai, S. L.; Ng, M.; Chan, M. Y.; Yam, V. W. W. *Angew. Chem. Int. Ed.* **2019,** *131*, 9186-9192.

94. Zhang, Z.; Zhang, H.; Jiao, C.; Ye, K.; Zhang, H.; Zhang, J.; Wang, Y. *Inorg. Chem.* **2015,** *54*, 2652-2659.

95. Zhang, Z.; Zhang, Z.; Zhang, H.; Wang, Y. *Dalton Trans.* **2018,** *47*, 127-134.

96. Mukundam, V.; Dhanunjayarao, K.; Chuang, C.-N.; Kang, D.-Y.; Leung, M.-k.; Hsieh, K.-H.; Venkatasubbaiah, K. *Dalton Trans.* **2015,** *44*, 10228-10236.

97. Dhanunjayarao, K.; Mukundam, V.; Venkatasubbaiah, K. *Inorg. Chem.* **2016,** *55*, 11153-11159.

98. Mukundam, V.; Dhanunjayarao, K.; Samal, S.; Venkatasubbaiah, K. *Asian J. Org. Chem.* **2017,** *6*, 1054-1062.

99. Zhou, L.; Xu, D.; Gao, H.; Han, A.; Yang, Y.; Zhang, C.; Liu, X.; Zhao, F. *RSC Adv.* **2016,** *6*, 69560-69568.

100. Potopnyk, M. A.; Volyniuk, D.; Luboradzki, R.; Lazauskas, A.; Grazulevicius, J. V. *Eur. J. Org. Chem.* **2021,** *2021*, 2772-2781.

101. Song, Y.; Sun, J.; Sun, M.; Simalou, O.; Gao, H.; Peng, J.; Shu, Y.; Zhai, L.; Lu, R. *Opt. Mater.* **2021,** *115*, 111006.

102. Son, H.-J.; Han, W.-S.; Wee, K.-R.; Chun, J.-Y.; Choi, K.-B.; Han, S. J.; Kwon, S.-N.; Ko, J.; Lee, C.; Kang, S. O. *Eur. J. Inorg. Chem.* **2009,** *2009*, 1503-1513.

103. Li, D.; Wang, K.; Huang, S.; Qu, S.; Liu, X.; Zhu, Q.; Zhang, H.; Wang, Y. *J. Mater. Chem.* **2011,** *21*, 15298-15304.

104. Delgado, D.; Abonia, R. *Arabian J. Chem.* **2022,** *15*, 103528.

105. Gapare, R. L.; Thompson, A. *Chem. commun.* **2022,** *58*, 7351-7359.

106. Gupta, G.; Sun, Y.; Das, A.; Stang, P. J.; Yeon Lee, C. *Coord. Chem. Rev.* **2022,** *452*, 214308.

107. Li, F.-Z.; Wu, Z.; Lin, C.; Wang, Q.; Kuang, G.-C. *Results Chem.* **2022,** *4*, 100384.

108. Liu, X.; Yu, B.; Shen, Y.; Cong, H. *Coord. Chem. Rev.* **2022,** *468*, 214609.

109. Porcu, P.; Gonzalez-Mendez, I.; Sorroza-Martinez, K.; Estrada-Montano, A. S.; Cuetara-Guadarrama, F.; Vonlanthen, M.; Rivera, E. *Dyes Pigm.* **2022,** *207*, 110713.

110. Rana, P.; Singh, N.; Majumdar, P.; Prakash Singh, S. *Coord. Chem. Rev.* **2022,** *470*, 214698.

111. Raveendran, A. V.; Sankeerthana, P. A.; Jayaraj, A.; Chinna Ayya Swamy, P. *Results Chem.* **2022,** *4*, 100297.

112. Wang, J.; Yu, C.; Hao, E.; Jiao, L. *Coord. Chem. Rev.* **2022,** *470*, 214709.

113. Wang, L.; Xiong, Z.; Ran, X.; Tang, H.; Cao, D. *Dyes Pigm.* **2022,** *198*, 110040.

114. Wang, Y.; Zhang, D.; Xiong, K.; Shang, R.; Jiang, X.-D. *Chin. Chem. Lett.* **2022,** *33*, 115-122.

115. Tamgho, I.-S.; Hasheminasab, A.; Engle, J. T.; Nemykin, V. N.; Ziegler, C. J. *J. Am. Chem. Soc.* **2014,** *136*, 5623-5626.

116. Yu, C.; Jiao, L.; Zhang, P.; Feng, Z.; Cheng, C.; Wei, Y.; Mu, X.; Hao, E. *Org. Lett.* **2014,** *16*, 3048-3051.

117. Gai, L.; Xu, J.; Wu, Y.; Lu, H.; Shen, Z. *New J. Chem.* **2016,** *40*, 5752-5757.

118. Zhang, C.; Zhao, J. *J. Mater. Chem. C* **2016,** *4*, 1623-1632.

119. Suresh, D.; Lopes, P. S.; Ferreira, B.; Figueira, C. A.; Gomes, C. S. B.; Gomes, P. T.; Di Paolo, R. E.; Maçanita, A. L.; Duarte, M. T.; Charas, A.; Morgado, J.; Calhorda, M. J. *Chem. Eur. J.* **2014,** *20*, 4126-4140.

120. Suresh, D.; Ferreira, B.; Lopes, P. S.; Gomes, C. S. B.; Krishnamoorthy, P.; Charas, A.; Vila-Viçosa, D.; Morgado, J.; Calhorda, M. J.; Maçanita, A. L.; Gomes, P. T. *Dalton Trans.* **2016,** *45*, 15603-15620.

121. Krishnamoorthy, P.; Ferreira, B.; Gomes, C. S. B.; Vila-Viçosa, D.; Charas, A.; Morgado, J.; Calhorda, M. J.; Maçanita, A. L.; Gomes, P. T. *Dyes Pigm.* **2017,** *140*, 520-532.

122. Rodrigues, A. I.; Krishnamoorthy, P.; Gomes, C. S. B.; Carmona, N.; Di Paolo, R. E.; Pander, P.; Pina, J.; Sérgio Seixas de Melo, J.; Dias, F. B.; Calhorda, M. J.; Maçanita, A. L.; Morgado, J.; Gomes, P. T. *Dalton Trans.* **2020,** *49*, 10185-10202.

123. Shiu, Y.-J.; Cheng, Y.-C.; Tsai, W.-L.; Wu, C.-C.; Chao, C.-T.; Lu, C.-W.; Chi, Y.; Chen, Y.-T.; Liu, S.-H.; Chou, P.-T. *Angew. Chem. Int. Ed.* **2016,** *55*, 3017-3021.

124. Liu, S.-F.; Wu, Q.; Schmider, H. L.; Aziz, H.; Hu, N.-X.; Popović, Z.; Wang, S. *J. Am. Chem. Soc.* **2000,** *122*, 3671-3678.

125. Liu, Q.; Mudadu, M. S.; Schmider, H.; Thummel, R.; Tao, Y.; Wang, S. *Organometallics* **2002,** *21*, 4743-4749.

126. Liu, Q. D.; Mudadu, M. S.; Thummel, R.; Tao, Y.; Wang, S. *Adv. Funct. Mater.* **2005,** *15*, 143-154.

127. Chen, H. Y.; Chi, Y.; Liu, C. S.; Yu, J. K.; Cheng, Y. M.; Chen, K. S.; Chou, P. T.; Peng, S. M.; Lee, G. H.; Carty, A. J.; Yeh, S. J.; Chen, C. T. *Adv. Funct. Mater.* **2005,** *15*, 567-574.

128. Chen, T.-R.; Chien, R.-H.; Jan, M.-S.; Yeh, A.; Chen, J.-D. *J. Organomet. Chem.* **2006,** *691*, 799-804.

129. Chen, T.-R.; Chien, R.-H.; Yeh, A.; Chen, J.-D. *J. Organomet. Chem.* **2006,** *691*, 1998-2004.

130. Dhindsa, J. S.; Maar, R. R.; Barbon, S. M.; Olivia Avilés, M.; Powell, Z. K.; Lagugné-Labarthet, F.; Gilroy, J. B. *Chem. commun.* **2018,** *54*, 6899-6902.

131. Cappello, D.; Therien, D. A. B.; Staroverov, V. N.; Lagugné-Labarthet, F.; Gilroy, J. B. *Chem. Eur. J.* **2019,** *25*, 5994-6006.

132. Maar, R. R.; Hoffman, N. A.; Staroverov, V. N.; Gilroy, J. B. *Chem. Eur. J.* **2019,** *25*, 11015-11019.

133. Cappello, D.; Maar, R. R.; Staroverov, V. N.; Gilroy, J. B. *Chem. Eur. J.* **2020,** *26*, 5522-5529.

134. Buguis, F. L.; Maar, R. R.; Staroverov, V. N.; Gilroy, J. B. *Chem. Eur. J.* **2021,** *27*, 2854-2860.

135. Dhindsa, J. S.; Buguis, F. L.; Anghel, M.; Gilroy, J. B. *J. Org. Chem.* **2021,** *86*, 12064-12074.

136. Trofimenko, S. *J. Am. Chem. Soc.* **1967,** *89*, 3165-3170.

137. Nieto, C. I.; Sanz, D.; Claramunt, R. M.; Alkorta, I.; Elguero, J. *Coord. Chem. Rev.* **2022,** *473*, 214812.

138. Jäkle, F.; Priermeier, T.; Wagner, M. *Organometallics* **1996,** *15*, 2033-2040.

139. Layton, W.; Niedenzu, K.; Niedenzu, P.; Trofimenko, S. *Inorg. Chem.* **1985,** *24*, 1454-1457.

140. Niedenzu, K.; Trofimenko, S., Pyrazole derivatives of boron. In *Structural Chemistry of Boron and Silicon*, Springer: 2005; pp 1-37.

141. Jadhav, T.; Maragani, R.; Misra, R.; Sreeramulu, V.; Rao, D. N.; Mobin, S. M. *Dalton Trans.* **2013,** *42*, 4340-4342.

142. Misra, R.; Jadhav, T.; Mobin, S. M. *Dalton Trans.* **2013,** *42*, 16614-16620.

143. Misra, R.; Jadhav, T.; Mobin, S. M. *Dalton Trans.* **2014,** *43*, 2013-2022.

144. Jadhav, T.; Dhokale, B.; patil, Y.; Misra, R. *RSC Adv.* **2015,** *5*, 68187-68191.

145. Misra, R.; Jadhav, T.; Dhokale, B.; Mobin, S. M. *Dalton Trans.* **2015,** *44*, 16052-16060.

146. Patil, Y.; Jadhav, T.; Dhokale, B.; Butenschön, H.; Misra, R. *ChemistrySelect* **2017,** *2*, 415-420.

147. Patil, Y.; Misra, R. *J. Organomet. Chem.* **2017,** *840*, 23-29.

148. Hayek, A.; Bolze, F.; Bourgogne, C.; Baldeck, P. L.; Didier, P.; Arntz, Y.; Mély, Y.; Nicoud, J.-F. *Inorg. Chem.* **2009,** *48*, 9112-9119.

149. Wrackmeyer, B.; Shahid, K.; Kempe, R.; Döring, C.; Milius, W. *Appl. Organomet. Chem.* **2010,** *24*, 398-401.

150. Cavero, E.; Giménez, R.; Uriel, S.; Beltrán, E.; Serrano, J. L.; Alkorta, I.; Elguero, J. *Cryst. Growth Des.* **2008,** *8*, 838-847.

151. Tehfe, M.-A.; Schweizer, S.; Chany, A.-C.; Ysacco, C.; Clément, J.-L.; Gigmes, D.; Morlet-Savary, F.; Fouassier, J.-P.; Neuburger, M.; Tschamber, T.; Blanchard, N.; Lalevée, J. *Chem. Eur. J.* **2014,** *20*, 5054-5063.

152. Seven, Ö.; Popp, S.; Bolte, M.; Lerner, H.-W.; Wagner, M. *Dalton Trans.* **2014,** *43*, 8241-8253.

153. Liebing, P.; Kuhling, M.; Takats, J.; Hilfert, L.; Edelmann, F. T. *Acta Crystallogr. E: Crystallogr. Commun.* **2017,** *73*, 1921-1925.

154. Matsumoto, F.; Chujo, Y. *Macromolecules* **2003,** *36*, 5516-5519.

155. Matsumoto, F.; Nagata, Y.; Chujo, Y. *Polym. Bull.* **2005,** *53*, 155-160.

156. Matsumoto, F.; Chujo, Y. **2006,** *78*, 1407-1411.

CHAPTER 2A

Synthesis of Bis(pentafluorophenyl)boron and Diphenylboron-β-Thioketonates and study their Optical, and Electrochemical properties

2A.1 Introduction

Four coordinated boron-containing luminescence materials have attracted considerable attention in various fields such as organic light-emitting diodes, organic field-effect transistors, photovoltaics, and sensors.[1-6] Among the various four-coordinated boron-containing luminescence materials, boron-β-diketonates have been well explored as multiphoton materials,[7] semiconductors,[8] photochromic materials,[9] polymers,[10] and sensors [5, 6, 11] due to their high molar absorption co-efficient,[12] and high quantum yields.[13] A little modification of boron-β-diketonates results a huge variation in the optical properties. Hence, various methodologies were followed to fine-tune the optical properties of boron-β-diketonates.[14] Among them, changing the heteroatom of the β-diketonates of one oxygen or two oxygen into another heteroatom. For instance Chujo[15, 16] and Gardinier[17] groups reported boron-β-ketoiminate and/or diiminates, and studied their optical behaviours. Recently, our group explored the synthesis of monothio-β-diketonate boron compounds,[18, 19] and studied their semiconducting behavior, and non-linear optical properties. Here, we report the synthesis of bis(pentafluorophenyl) and diphenyl boron complexes of monothio-β-diketonates and their optical and electrochemical properties.

2A.2 Results and discussion

2A.2.1 Synthesis and characterization

The boron monothio-β-diketonates **5-12** were synthesized by refluxing $B(C_6F_5)_3$ or BPh_3 with respective ligands **1-4** in dry toluene at 110 ^oC (**Scheme 2A.1**). The ligands **1-4** were synthesized by Claisen-ester condensation with NaH in DMF, a similar protocol as reported in the literature.[19] All the synthesized ligands (**1-4**) and the boron compounds (**5-12**) were characterized by multinuclear NMR techniques, X-ray studies (in case of **5-9**),

and HRMS analysis. The ^{1}H-NMR analysis of ligands **1-4** shows down fielded enolic proton resonating at 15-16 ppm. This enolic proton peak gets disappeared in **5-12** due to the boron chelation with ligand.

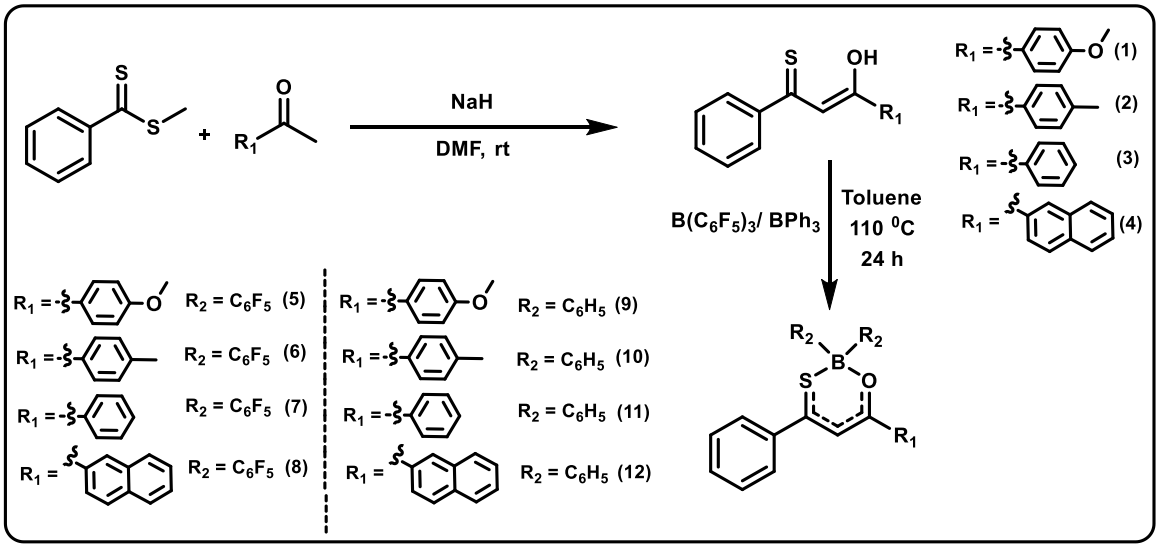

Scheme 2A.1: Synthetic routes for bis(pentafluorophenyl)boron and diphenylboron compounds **5-12**.

All the bis(pentafluorophenyl)boron compounds **5-8** showed a signal of ^{11}B{^{1}H} resonating at ~1-2 ppm, and diphenylboron compounds **9-12** resonating at ~6-7 ppm, confirming the four coordinated nature of the boron centre. The ^{19}F{^{1}H} NMR spectra of compounds **5-8** showed three sets of peaks resonating from ~ -134.0 to -163.0 ppm, due to the three different environments (ortho, meta, para) of fluorine atoms associated with -$B(C_6F_5)_2$.

Single crystals of boron compounds **5-9** (**Figure 2A.1**) for X-ray analysis were grown by slow evaporation of the respective compounds from a mixture of solvents (**5-8** from CH_2Cl_2/*n*-hexane mixture; **9** from $CHCl_3$/*n*-hexane mixture). Boron compound **5** was crystallized in the C2/c space group and, **6-9** were crystallized in P-1 space group. Selected bong lengths and bond angles were depicted in **Table 2A.1 – 2A.2** (**Table 2A.3, 2A.4** for optimized DFT structure). The observed B-S and B-O bond lengths for

bis(pentafluorophenyl)boron compounds **5-8** are significantly shorter than the diphenylboron compound **9** (see **Table 2A.1**); which indicates that electron-withdrawing pentafluorophenyl group plays a key role for this bond distance. The B-S and B-O bond lengths of the DFT optimized structures showed a similar trends and the values are slightly longer than the experimental values. The observed S-B-O bond angle of compounds **9** (104.8 (1), 104.6 (DFT optimized)) is significantly narrower than compounds **5-8** (see **Table 2A.1 - 2A.4**). Among all the boron compounds, compound **5** showed a pronounced deviation of boron atom (0.386 Å) from the C_3SOB plane.

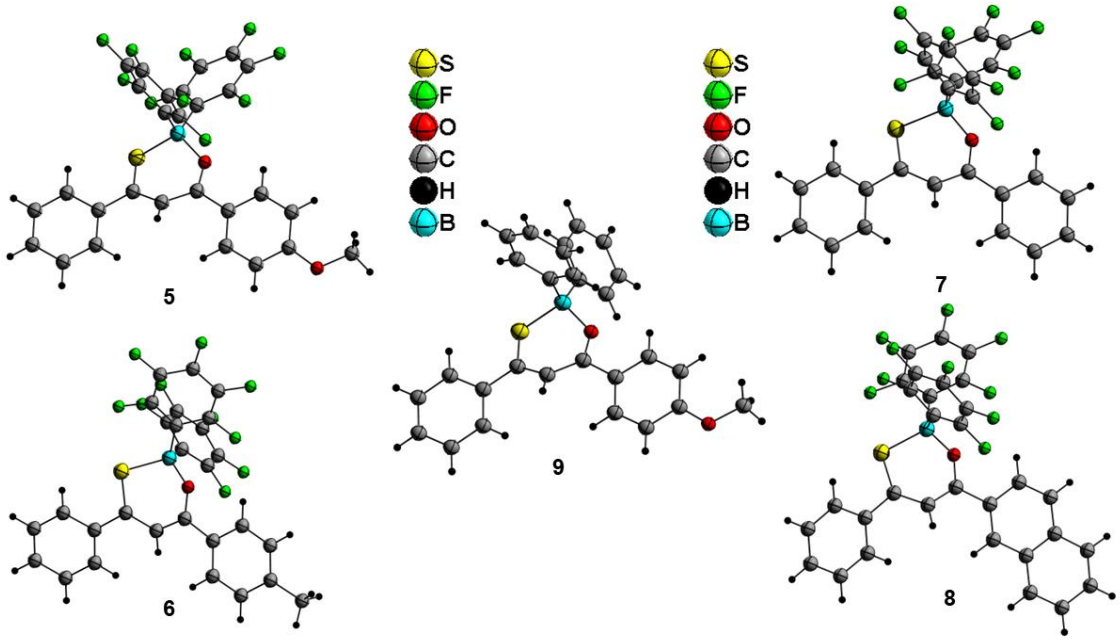

Figure 2A.1. Molecular structure of compounds **5-9** with ball and stick model (Diamond view).

Table 2A.1 Comparison of bond lengths, bond angles, and other structural data for compounds 5-7.

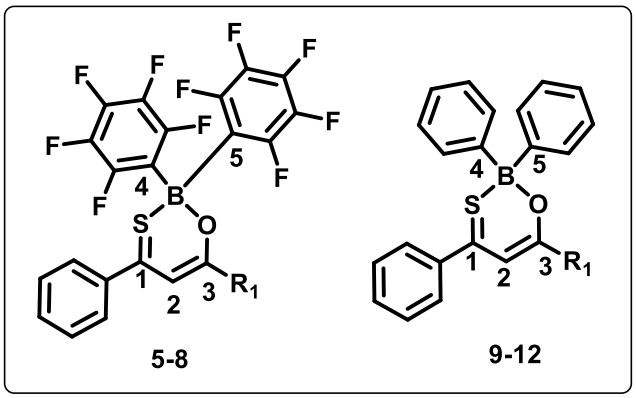

	5	6	7
S-C1 (Å)	1.732 (2)	1.710 (2)	1.704 (2)
O-C3 (Å)	1.298 (3)	1.293 (2)	1.304 (3)
B-S (Å)	1.943 (3)	1.950 (2)	1.953 (2)
B-O (Å)	1.494 (3)	1.487 (3)	1.487 (3)
B-C4 (Å)	1.629 (3)	1.621 (3)	1.633 (3)
B-C5 (Å)	1.632 (3)	1.644 (3)	1.629 (3)
C1-C2 (Å)	1.382 (3)	1.391 (3)	1.378 (4)
C2-C3 (Å)	1.403 (3)	1.395 (3)	1.393 (4)
S-B-O (deg)	105.72 (2)	106.26 (2)	107.10 (2)
S-B-C4 (deg)	109.02 (2)	112.46 (2)	108.39 (2)
O-B-C5 (deg)	106.65 (2)	113.47 (2)	105.49 (2)
C4-B-C5 (deg)	108.92 (2)	110.05 (2)	111.84 (2)
C1-C2-C3 (deg)	123.7 (2)	124.16 (2)	124.1 (2)
Deviation of B from C_3SOB plane (Å)	0.386	0.338	0.312

Table 2A.2 Comparison of bond lengths, bond angles, and other structural data for compounds 8-9.

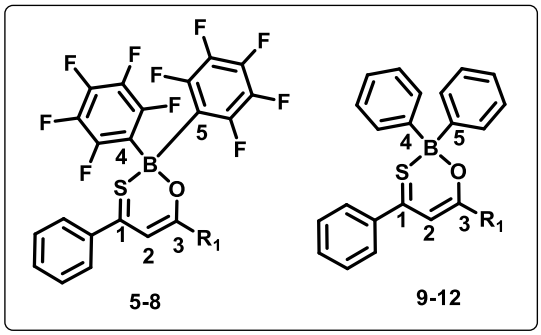

	8	9
S-C1 (Å)	1.704 (4)	1.709 (19)
O-C3 (Å)	1.299 (4)	1.301 (2)
B-S (Å)	1.962 (4)	1.986 (2)
B-O (Å)	1.496 (4)	1.515 (2)
B-C4 (Å)	1.633 (5)	1.605 (3)
B-C5 (Å)	1.620 (5)	1.603 (3)
C1-C2 (Å)	1.377 (5)	1.385 (3)
C2-C3 (Å)	1.397 (5)	1.400 (3)
S-B-O (deg)	107.1 (2)	104.8 (1)
S-B-C4 (deg)	108.6 (2)	110.23 (1)
O-B-C5 (deg)	105.7 (3)	108.51 (5)
C4-B-C5 (deg)	109.4 (3)	116.63 (2)
C1-C2-C3 (deg)	123.1 (3)	125.17 (2)
Deviation of B from C_3SOB plane (Å)	0.319	0.353

Table 2A.3 Comparison of bond lengths, bond angles, and other structural data for compounds 5-8 (DFT optimized).

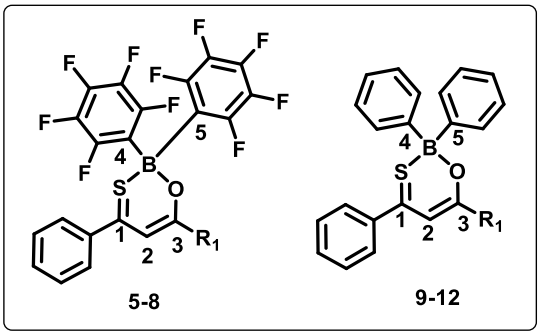

	5	6	7	8
S-C1 (Å)	1.729	1.726	1.724	1.726
O-C3 (Å)	1.307	1.305	1.304	1.304
B-S (Å)	1.971	1.973	1.973	1.972
B-O (Å)	1.497	1.498	1.499	1.499
B-C4 (Å)	1.644	1.643	1.642	1.643
B-C5 (Å)	1.627	1.627	1.626	1.627
C1-C2 (Å)	1.389	1.392	1.394	1.392
C2-C3 (Å)	1.412	1.408	1.406	1.407
S-B-O (deg)	105.28	105.25	105.30	105.35
S-B-C4 (deg)	115.18	115.14	115.18	115.22
O-B-C5 (deg)	110.35	110.38	110.44	110.42
C4-B-C5 (deg)	110.69	110.80	110.90	110.89
C1-C2-C3 (deg)	124.0	123.91	123.88	123.89
Deviation of B from C_3SOB plane (Å)	0.347	0.344	0.340	0.342

Table 2A.4 Comparison of bond lengths, bond angles, and other structural data for compounds 9-12 (DFT optimized).

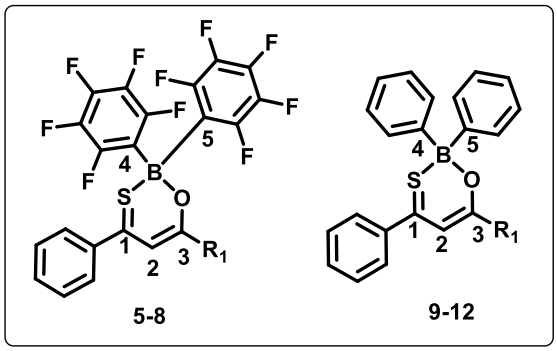

	9	10	11	12
S-C1 (Å)	1.729	1.726	1.724	1.726
O-C3 (Å)	1.303	1.302	1.301	1.301
B-S (Å)	2.007	2.010	2.010	2.010
B-O (Å)	1.517	1.518	1.518	1.519
B-C4 (Å)	1.617	1.616	1.616	1.616
B-C5 (Å)	1.612	1.612	1.612	1.612
C1-C2 (Å)	1.390	1.393	1.395	1.394
C2-C3 (Å)	1.413	1.410	1.408	1.409
S-B-O (deg)	104.59	104.49	104.42	104.47
S-B-C4 (deg)	110.58	110.40	110.36	110.41
O-B-C5 (deg)	108.12	108.08	108.14	108.10
C4-B-C5 (deg)	116.00	116.27	116.30	116.28
C1-C2-C3 (deg)	124.66	124.57	124.50	124.49
Deviation of B from C_3SOB plane (Å)	0.343	0.340	0.340	0.341

Table 2A.5 Crystal data and structure refinement for compounds 5-7.

	5	6	7
Empirical formula	$C_{28}H_{13}BF_{10}O_2S$	$C_{28}H_{13}BF_{10}OS$	$C_{27}H_{11}BF_{10}OS$
Formula weight	614.25	598.25	584.23
Temperature/K	295.3(4)	297.40(10)	297.08(10)
Crystal system	triclinic	triclinic	triclinic
Space group	P-1	P-1	P-1
a/Å	9.0220(2)	9.11940(10)	9.4574(3)

b/Å	11.8488(4)	12.2038(2)	11.1192(3)
c/Å	14.8280(4)	12.9806(2)	12.5265(3)
α/°	72.289(2)	113.767(2)	72.436(2)
β/°	81.414(2)	104.427(2)	70.979(3)
γ/°	75.568(2)	94.3510(10)	76.072(3)
Volume/Å^3	1457.69(7)	1254.84(4)	1172.39(6)
Z	2	2	2
ρ_{calc}g/cm^3	1.399	1.583	1.655
μ/mm^{-1}	1.801	2.043	2.172
F(000)	616.0	600.0	584.0
Crystal size/mm^3	0.15 × 0.14 × 0.12	0.24 × 0.23 × 0.21	0.15 × 0.12 × 0.11
Radiation	CuKα (λ = 1.54184)	CuKα (λ = 1.54184)	CuKα (λ = 1.54184)
2Θ range for data collection/°	8.024 to 151.592	7.818 to 152.894	7.696 to 153.49
Index ranges	-11 ≤ h ≤ 8, -14 ≤ k ≤ 14, -18 ≤ l ≤ 17	-11 ≤ h ≤ 11, -9 ≤ k ≤ 15, -16 ≤ l ≤ 16	-11 ≤ h ≤ 10, -13 ≤ k ≤ 14, -15 ≤ l ≤ 15
Reflections collected	21317	18768	15750
Independent reflections	5900 [R_{int} = 0.0572, R_{sigma} = 0.0302]	5125 [R_{int} = 0.0492, R_{sigma} = 0.0325]	4759 [R_{int} = 0.0556, R_{sigma} = 0.0278]
Data/restraints/parameters	5900/0/380	5125/0/371	4759/0/361
Goodness-of-fit on F^2	1.044	1.051	1.115
Final R indexes [I>=2σ (I)]	R_1 = 0.0750, wR_2 = 0.2235	R_1 = 0.0514, wR_2 = 0.1510	R_1 = 0.0518, wR_2 = 0.1496
Final R indexes [all data]	R_1 = 0.0782, wR_2 = 0.2282	R_1 = 0.0563, wR_2 = 0.1546	R_1 = 0.0554, wR_2 = 0.1520
Largest diff. peak/hole / e Å^{-3}	0.73/-0.54	0.27/-0.37	0.37/-0.30

Table 2A.6 Crystal data and structure refinement for compound 8 and 9.

	8	**9**
Empirical formula	$C_{31}H_{13}BF_{10}OS$	$C_{28}H_{23}BO_2S$
Formula weight	634.28	434.33
Temperature/K	109(13)	293(2)
Crystal system	triclinic	monoclinic
Space group	P-1	C2/c
a/Å	8.9743(4)	24.1468(5)
b/Å	11.7030(4)	12.5924(2)
c/Å	15.0237(4)	18.0515(4)
α/°	74.848(3)	90
β/°	82.963(3)	111.701(3)
γ/°	71.503(4)	90
Volume/Å^3	1443.00(10)	5099.8(2)
Z	2	8

ρ_{calc}g/cm^3	1.460	1.131
μ/mm^{-1}	1.814	1.279
F(000)	636.0	1824.0
Crystal size/mm^3	0.14 × 0.12 × 0.11	0.14 × 0.12 × 0.11
Radiation	CuKα (λ = 1.54184)	CuKα (λ = 1.54184)
2Θ range for data collection/°	8.198 to 152.024	8.79 to 150.838
Index ranges	-11 ≤ h ≤ 11, -14 ≤ k ≤ 14, -18 ≤ l ≤ 14	-23 ≤ h ≤ 30, -15 ≤ k ≤ 15, -21 ≤ l ≤ 22
Reflections collected	19128	18668
Independent reflections	5833 [R_{int} = 0.0991, R_{sigma} = 0.0570]	5054 [R_{int} = 0.0760, R_{sigma} = 0.0387]
Data/restraints/parameters	5833/0/397	5054/0/290
Goodness-of-fit on F^2	1.096	1.050
Final R indexes [I>=2σ (I)]	R_1 = 0.0893, wR_2 = 0.2742	R_1 = 0.0582, wR_2 = 0.1699
Final R indexes [all data]	R_1 = 0.0978, wR_2 = 0.2816	R_1 = 0.0638, wR_2 = 0.1749
Largest diff. peak/hole / e Å^{-3}	0.65/-0.84	0.46/-0.32

2A.2.2 Optical properties

Table 2A.7 Photophysical and Electrochemical data of compounds 5-12 at 298K

Compounds	**Solvent**	**λ_{abs}[a] /nm (ε x 10^4/M^{-1} cm^{-1})**	**λ_{ems}[b] (nm)**	**Stokes Shift (cm^{-1})**	**ϕ_F[c] (%)**	**τ[d] (ns)**
5	Toluene	356(1.3), 461(2.6)	538	3104	-	-
	THF	355(1.5), 461(3.0)	533	2930	-	-
	CH_2Cl_2	353(1.5), 458(3.0)	534	3108	0.12	0.23
	CH_3CN	351(1.8), 457(3.4)	542	3431	-	-
	Solid	-	564	-	-	-
6	Toluene	347(1.7), 451(2.1)	568	4567	-	-
	THF	347(1.9), 450(2.2)	553	4139	-	-
	CH_2Cl_2	345(1.8), 448(2.2)	551	4173	0.11	0.41
	CH_3CN	344(1.9), 446(2.3)	521	3228	-	-
	Solid	-	554	-	-	-
7	Toluene	346(1.6), 448(1.7)	569	4747	-	-
	THF	346(1.8), 446(1.8)	560	4564	-	-

	CH_2Cl_2	344(1.9), 445(1.9)	557	4518	0.10	0.59
	CH_3CN	341(1.9), 442(1.9)	551	4476	-	-
	Solid	-	614	-	-	-
8	Toluene	349(1.5), 465(2.3)	555	3487	-	-
	THF	350(2.0), 466(2.8)	537	2838	-	-
	CH_2Cl_2	348(1.8), 463(2.7)	549	3384	0.14	0.35
	CH_3CN	346(2.1), 462(3.0)	531	2813	-	-
	Solid	-	617	-	-	-
9	Toluene	348(1.5), 468(1.8)	-	-	-	-
	THF	347(1.7), 464(2.0)	-	-	-	-
	CH_2Cl_2	346(1.6), 465(2.1)	-	-	-	-
	CH_3CN	341(1.4), 457(1.8)	-	-	-	-
10	Toluene	335(1.5), 463(1.6)	-	-	-	-
	THF	335(1.7), 455(1.2)	-	-	-	-
	CH_2Cl_2	336(1.7), 455(1.3)	-	-	-	-
	CH_3CN	332(1.6), 432(1.3)	-	-	-	-
11	Toluene	333(1.5), 461(1.0)	-	-	-	-
	THF	332(1.5), 419(1.1)	-	-	-	-
	CH_2Cl_2	334(1.5), 455(1.0)	-	-	-	-
	CH_3CN	329(1.4), 413(1.4)	-	-	-	-
12	Toluene	339(1.7), 472(1.6)	-	-	-	-
	THF	336(1.7), 447(1.5)	-	-	-	-
	CH_2Cl_2	337(1.6), 467(1.6)	-	-	-	-
	CH_3CN	334(1.5), 431(1.6)	-	-	-	-

[a]Absorption maximum (concentration = 3.5 x 10^{-5} M), [b]Excited at λ_{max}, [c]Relative quantum yield using integrating sphere module, [d]Emission lifetime.

The photophysical properties of compounds **5-12** (**Table 2A.7**) were studied in different non-polar and polar solvents such as toluene, tetrahydrofuran (THF), dichloromethane (DCM), acetonitrile (ACN), and the ligands **1-4** (**Figure 2A.2**) were recorded in dichloromethane. The absorption spectra of ligands **1-4** displayed a strong absorption in the range of 320 – 430 nm. Similarly, the absorption spectra of all the eight boron

compounds showed molar absorption extinction coefficients ranging from 13000 – 34000 $M^{-1}.cm^{-1}$, which corresponds to the typical π-π* transition (**Figure 2A.3**). All the boron compounds **5-12** showed two strong absorption bands in the range of 330 – 480 nm which is similar to the ligands **1-4** absorption spectra.

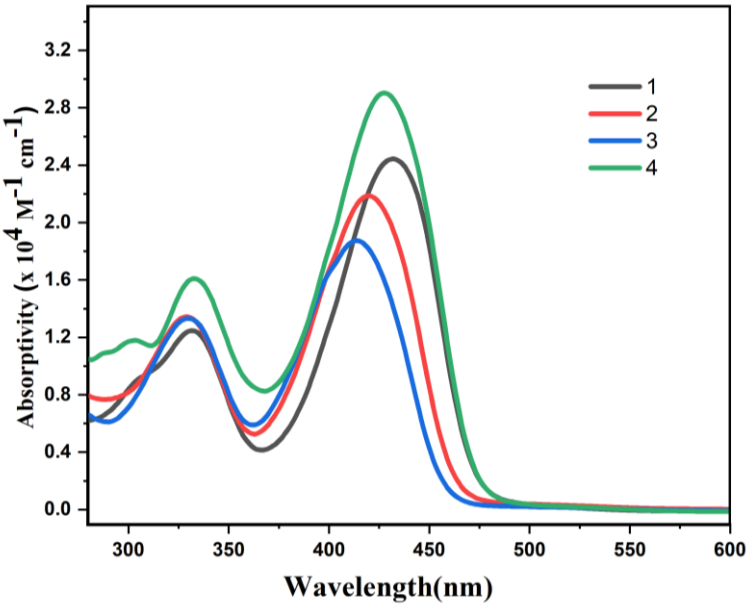

Figure 2A.2: Absorption spectra of ligands **1-4** (3.5 x 10^{-5} M) in dichloromethane.

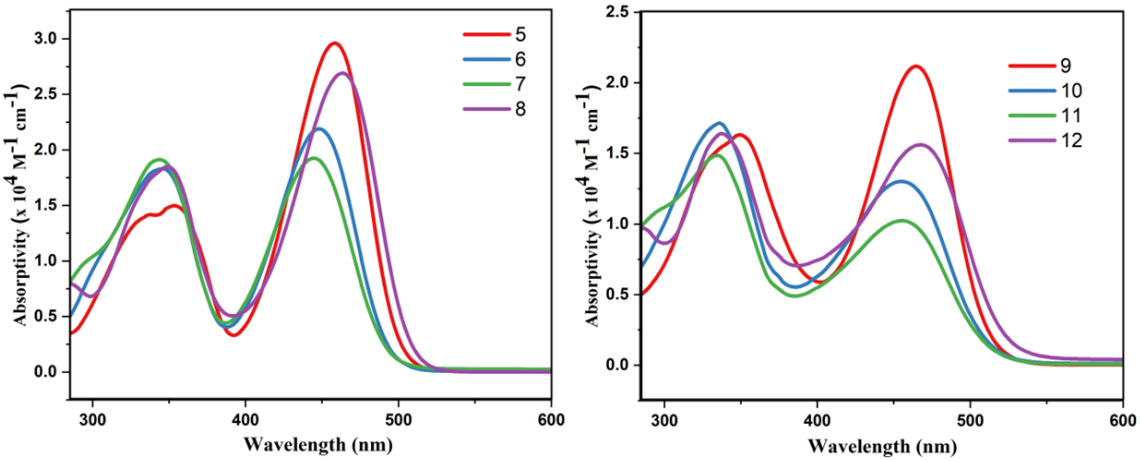

Figure 2A.3: Absorption spectra of boron compounds **5-12** (3.5 x 10^{-5} M) in dichloromethane.

The absorption maxima of **5, 6,** and **8** are red-shifted as compared to **7;** and **9, 10, 12** are also red-shifted as compared to **11** owing to the electron donating nature of -OCH_3 and -

CH_3 present in **5, 6, 9** and **10** and extended conjugation observed in **8** and **12.** Compounds **9-12** showed positive solvatochromism, however compounds **5-8,** did not exhibit any solvatochromism. These result suggest that sulfur and boron bonding in compounds **9-12** is weaker (phenyl on boron center) over compounds **5-8** (-pentafluorophenyl phenyl on boron center)**,** hence the absorption maxima changes with varying the solvent polarity in **9-12.** The photoluminescence (PL) of **5-12** were recorded by exciting shorter energy band maxima of the respective compounds (**Figure 2A.4**). The absolute fluorescence quantum yields of **5-8** ranges from 0.10 to 0.14 in dichloromethane at room temperature. However, compounds **9-12** showed almost negligible fluorescence emission (≤ 0.01), which suggest that substituents on the boron atom (C_6H_5 vs C_6F_5) plays an important role for the observed fluorescence. The PL decay of the boron compounds **5-8** showed average lifetime values in the range of 0.2 – 0.6 ns in CH_2Cl_2. The solid state PL spectra of boron compounds **5-8** were displayed emission from 554 – 617 nm (**Figure 2A.5**), however, compounds **9-12** did not show emission in solid-state.

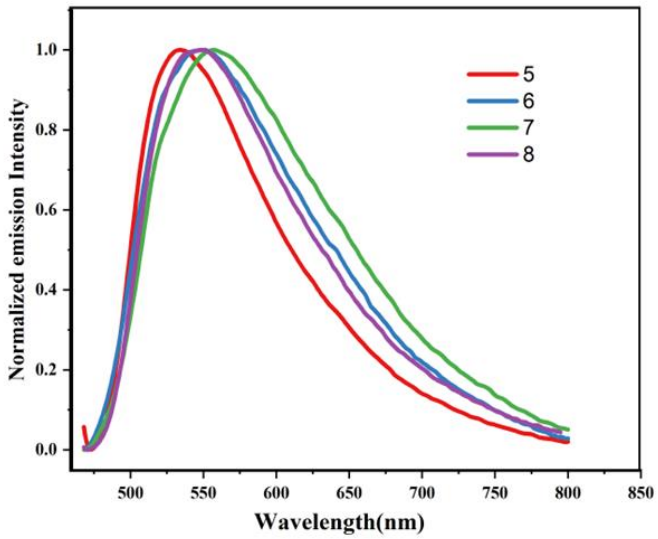

Figure 2A.4: Normalized emission spectra of boron compounds **5-12** (3.5×10^{-5} M) in dichloromethane.

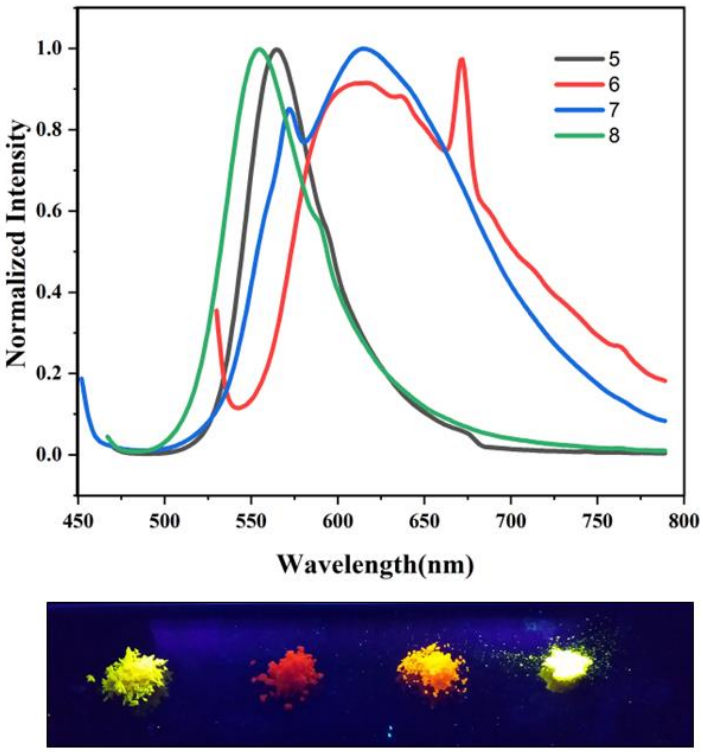

Figure 2A.5: Normalized solid-state emission spectra of boron compounds **5-8** (top), photographs of solid-state image of boron compounds **5-8** under hand held UV-light at 365 nm (bottom).

2A.2.3 Electrochemical Studies

The electrochemical properties of the compounds **5-12** were investigated using cyclic voltammetry in N_2 bubbled dichloromethane (CH_2Cl_2) at 298 K. All the boron compounds **5-12** showed one reversible peak ranging from -1.097 to -1.327 V (**Figure 2A.6**). The electrochemical potential of the boron centre is hugely affected by changing the groups on the boron centre. The bis(pentaflurophenyl) boron compounds (**5-8**) showed less negative potential over diphenylboron compounds (**9-12**). The reduction potential of compound **9** showed more negative value of -1.327 V due to the presence of an electron-donating methoxy group present in the periphery of one of the phenyl ring, whereas compound **12** showed the less negative value of -1.225 V due to more stabilized

LUMO level. A similar trend was observed for the bis(penfluorophenyl) derivatives, also ($E_{1/2}$ for **5** is -1.190 V and for **9** is -1.097 V).

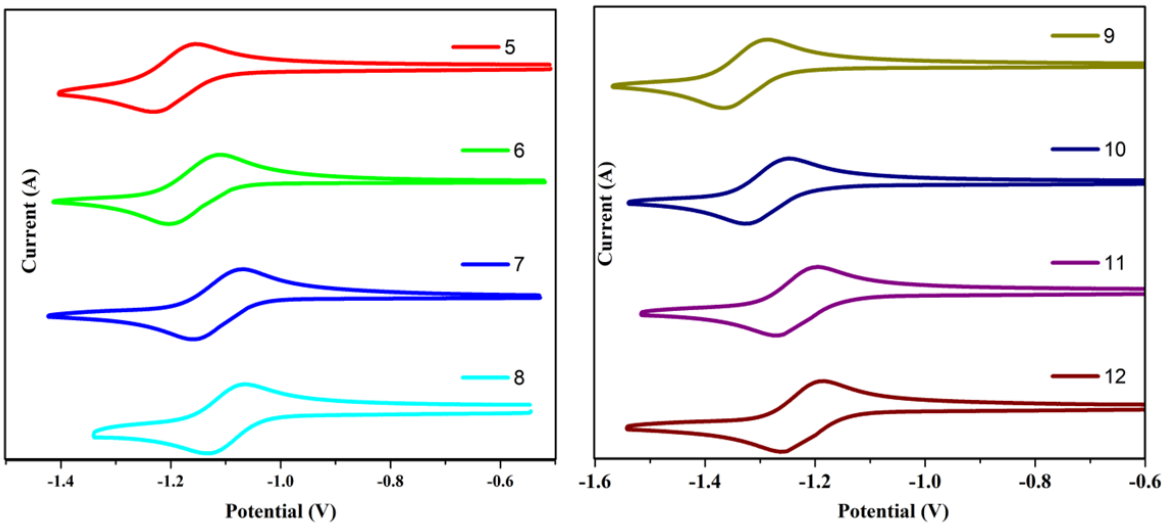

Figure 2A.6: Cyclic voltammogram (reduction potential) of compounds **5-12** (vs Ferrocene/Ferrocenium) with 0.1 M of $^{n}Bu_4N[PF_6]$ in CH_2Cl_2 as the supporting electrolyte (scan rate 50 mV/s).

Table 2A.8 HOMO and LUMO levels derived from UV-Vis onset absorption and electrochemical data.

Compounds	E_{pc}	HOMO-LUMO gap[a]	LUMO[b]	HOMO[c]	HOMO-LUMO gap[d]
5	-1.190	2.47	-3.44	-5.92	3.300
6	-1.155	2.49	-3.46	-5.95	3.444
7	-1.115	2.50	-3.51	-6.01	3.493
8	-1.097	2.43	-3.52	-5.95	3.131
9	-1.327	2.41	-3.39	-5.80	3.321
10	-1.287	2.39	-3.39	-5.79	3.410
11	-1.233	2.40	-3.38	-5.78	3.420
12	-1.225	2.34	-3.43	-5.77	3.183

[#]E_{pc} = cathodic peak potential. [a]Absorption onset of the longest wavelength of UV band. [b]Calculated from E_{pc} of the reduction wave with reference to Fc/Fc^+. [c]Calculated from HOMO-LUMO gap and LUMO. [d]Obtained from DFT calculations.

2A.2.4 DFT Studies

We used density functional theory (DFT) calculations to optimize the geometries (B3LYP/6-31-g-(d,p)) and time-dependent density functional theory (TD-DFT)

calculations to compute the excitation in order to learn more about the absorption behavior of boron compounds **5–12** and the orbitals involved in the electronic transitions. The highest and lowest occupied (HOMO & LUMO) molecular orbitals of the boron compounds **5-12** are shown in **Table 2A.9** This shows that the HOMOs are localized on the thioketonate skeleton and substituted aromatic ring especially the aryl attached to the keto moiety whereas LUMO orbitals are localized on the thioketonate central ring and both the aryl moieties. A similar energy band gap was observed for **5-12** ranging from 3.131 eV (**8**) to 3.493 eV (**7**). In general a lower energy band gap was observed for -C_6F_5 (**R**$_2$) compounds over their respective -Ph (**R**$_2$) substituted compounds. The electron withdrawing nature of -C_6F_5 on **5-8** are responsible for the observed low LUMO values. This lowest LUMO values further justifies the lower reduction potential realized in **5-8.**

Table 2A.9 Computed HOMO and LUMO molecular orbital for compounds **5-12.**

Compound	HOMO	LUMO
5	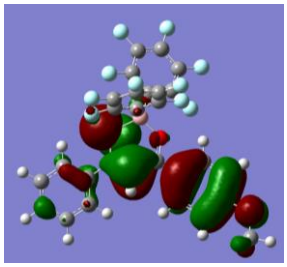 -6.212(154)	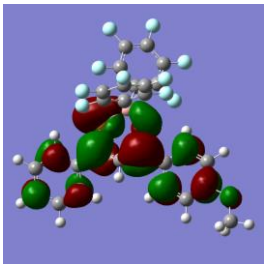 -2.910(155)
6	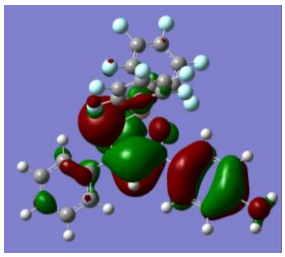 -6.442(150)	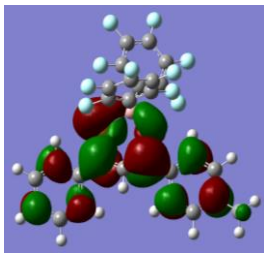 -2.998(151)

7	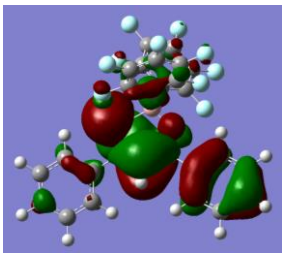 -6.539(146)	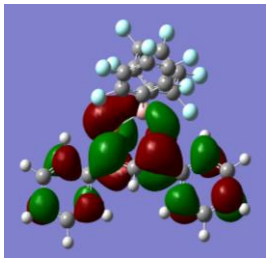 -3.046(147)
8	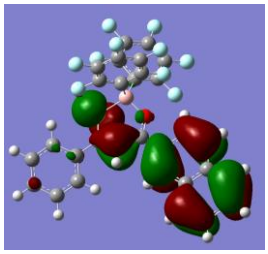 -6.187(159)	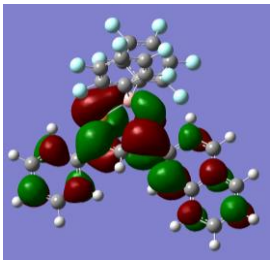 -3.056(160)
9	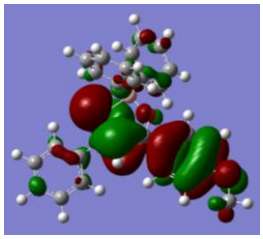 -6.132(114)	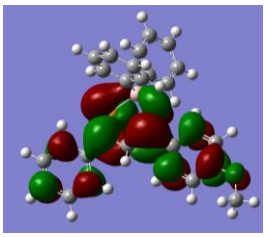 -2.811(115)
10	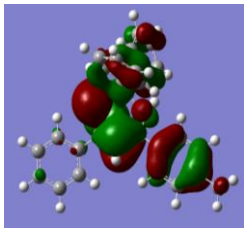 -6.302(110)	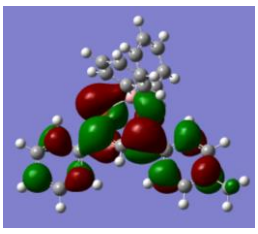 -2.892(111)

11	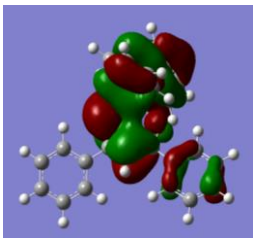 -6.361(106)	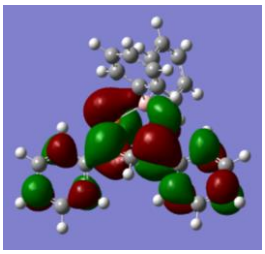 -2.941(107)
12	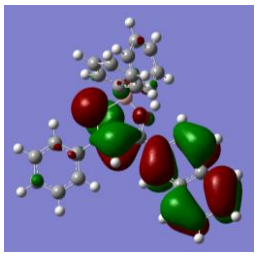 -6.130(119)	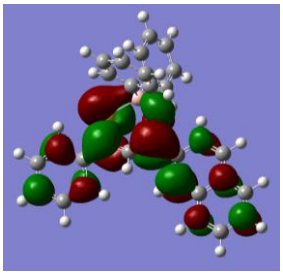 -2.947(120)

Table 2A.10 Calculated electronic transitions for compounds **5-12** from TD-DFT (B3LYP (6-31G(d,p)) calculations

Compound	Transition	MO contributions	Energy gap eV (nm)	Oscillator strength/f
5	$S_0 \rightarrow S_1$	HOMO→LUMO	2.92 (424)	0.6505
	$S_0 \rightarrow S_2$	HOMO-2→LUMO HOMO-1→LUMO	3.21 (385)	0.0010
	$S_0 \rightarrow S_3$	HOMO-3→LUMO HOMO-2→LUMO	3.29 (376)	0.0013
6	$S_0 \rightarrow S_1$	HOMO→LUMO	3.01 (411)	0.4975
	$S_0 \rightarrow S_2$	HOMO-2→LUMO HOMO-1→LUMO	3.14 (394)	0.0059

	$S_0 \rightarrow S_3$	HOMO-3→LUMO HOMO-2→LUMO HOMO-1→LUMO	3.21 (385)	0.0012
7	$S_0 \rightarrow S_1$ $S_0 \rightarrow S_2$ $S_0 \rightarrow S_3$	HOMO→LUMO HOMO-1→LUMO HOMO-2→LUMO HOMO-1→LUMO HOMO→LUMO HOMO-3→LUMO HOMO-2→LUMO HOMO-1→LUMO	3.05 (406) 3.10 (399) 3.16 (391)	0.3532 0.0414 0.0011
8	S0→S1 S0→S2 S0→S3	HOMO→LUMO HOMO-1→LUMO HOMO-3→LUMO HOMO-2→LUMO	2.70 (459) 3.06 (404) 3.10 (399)	0.3147 0.2948 0.0375
9	S0→S1 S0→S2 S0→S3	HOMO-2→LUMO HOMO-1→LUMO HOMO→LUMO HOMO-2→LUMO HOMO→LUMO HOMO-2→LUMO HOMO-1→LUMO	2.88 (430) 2.92 (424) 2.94 (420)	0.1595 0.3601 0.0188
10	S0→S1	HOMO-2→LUMO HOMO-1→LUMO	2.81 (440)	0.0129

	S0→S2	HOMO →LUMO HOMO-2→LUMO HOMO-1→LUMO HOMO→LUMO	2.88 (429)	0.0044
	S0→S3	HOMO-2→LUMO HOMO-1→LUMO HOMO→LUMO	2.95 (419)	0.3217
11	S0→S1	HOMO-2→LUMO HOMO →LUMO	2.78 (445)	0.0075
	S0→S2	HOMO-2→LUMO HOMO-1→LUMO HOMO→LUMO	2.84 (436)	0.0034
	S0→S3	HOMO-4→LUMO HOMO-2→LUMO HOMO-1→LUMO HOMO→ LUMO	2.96 (418)	0.2198
12	S0→S1	HOMO-2→LUMO HOMO→ LUMO	2.74 (452)	0.3270
	S0→S2	HOMO-2→LUMO HOMO-1→LUMO HOMO→LUMO	2.79 (443)	0.0488
	S0→S3	HOMO-2→LUMO HOMO–1→LUMO	2.84 (435)	0.0037

2A.3 Conclusion

In summary, we have synthesized bis(pentafluorophenyl) boron and diphenyl boron substituted monothio-β-diketonates with different substituents on one side of the thioketonate. X-ray analysis reveal that the B-O and B-S bond lengths of diphenyl boron compounds are significantly longer than the -$B(C_6F_5)_2$ compounds. The photophysical properties of these boron compounds were studied in four different solvents. In general the -$B(C_6F_5)_2$ compounds showed blue shifted absorption compared to diphenyl boron compounds. The bis(pentafluorophenyl) boron compounds displayed lower reduction potential values than the diphenyl boron compounds. This study reveal that the HOMO-LUMO gap was tuned by varying the substituents on the boron centre.

2A.4.1 Experimental procedure

General information:

All the reactions were carried out under N_2 atmosphere using standard glove box, Schlenk line and vacuum line techniques. Dry solvents used for the reactions were dried according to the standard procedures. All the reactions were monitored by thin-layer chromatography. Nuclear magnetic resonance spectra were recorded on a 400 MHz or 700 MHz Fourier transform NMR spectrometer (JEOL or Bruker) with $CDCl_3$ as a solvent. ^{11}B and ^{19}F NMR spectra were externally referenced to $BF_3.Et_2O$ in $CDCl_3$ (δ=0 ppm) and α,α,α-trifluoro toluene in $CDCl_3$ (δ=-63.73 ppm), respectively. Chemical shifts are reported in δ ppm (parts per million) using residual solvent protons as the internal standard (δ 7.26 for $CDCl_3$ in ^1H NMR, δ 77.16 for $CDCl_3$ in ^{13}C NMR). Coupling constants are reported as J values in hertz (Hz). Splitting patterns are designated as s(singlet), d(doublet), t(triplet), q(quartet), dd(doublet of doublet), dt(doublet of triplet), m(multiplet) and br(broad). HRMS were recorded using Waters XEVO G2-XS QTOF mass spectrometer. UV – Visible spectra were recorded on Agilent Technologies Cary 60

UV/Visible spectrometer. Fluorescence spectra were measured using Edinburgh specrofluorimeter instrument FS5. Relative luminescence quantum yields are calculated by comparing the emission intensities of the standard sample (Fluorescein dye in ethanol). A Rigaku Super Nova fine-focused dual diffractometer, fitted with a PILATUS200K, was utilised to gather single crystal X-ray diffraction data using Cu Kα radiation (λ = 1.54178 Å). The structures were solved using Olex2 and the ShelXS structure solution program using Direct Methods. The ShelXL refinement tool was then used to refine the structures using Least Squares minimization. Anisotropic displacement coefficients were utilised in the refinement of all non-hydrogen atoms. The H atoms were placed at calculated positions and were refined as riding atoms. The standard three electrode arrangement used for cyclic voltammetry included an Ag wire serving as the reference electrode, a Pt wire serving as the secondary electrode, and a glassy carbon working electrode. About 1.0 x 10^{-3} M solution in CH_2Cl_2 with $[Bu_4N][PF_6]$ (0.1 M) as a supporting electrolyte was used to record the voltammogram. The scans were referenced with a small amount of ferrocene as an internal standard. Starting materials: methyl benzodithioate was prepared according to the literature procedure.[20] Commercially available 4-methoxy acetophenone, 4-methyl acetophenone, acetophenone, 2-acetyl naphthalene, tris(pentafluorophenyl)borane, triphenylborane were purchased from Sigma-Aldrich, Spectrochem, Alfa-Aaser.

2A.4.2 General procedure for the preparation for 1,3-monothio-β-diketones:

To a stirred suspension of NaH (2.2 mmol, 50%) in DMF (10mL) under N_2 atmosphere was added dropwise a solution of aryl methyl ketone (1.0 mmol) and methyl benzodithioate (1.2 mmol) in DMF (10mL) at 0 °C. The reaction mixture was further stirred at room temperature for 5 h (monitored by TLC) and was poured into ice-cold water (40mL) and acidified with acetic acid. Precipitated red colour solid was filtered off

and the product was isolated through column chromatography using *n*-hexane/EtOAc as eluent.

Synthesis of compound 1

The quantities involved are: Methyl benzodithioate (1.80 g, 10.7 mmol), 4-methoxyacetophenone (1.3 g, 8.9 mmol), and NaH (0.47 g, 19.6 mmol). Red colour solid, yield: 1.40 g, (60.0 %). **^{1}H NMR** (400 MHz, $CDCl_3$) δ 15.42 (s, 1H), 8.01 (d, *J* = 8.0 Hz, 2H), 7.81 (d, *J* = 8.0 Hz, 2H), 7.52 – 7.39 (m, 4H), 6.99 (d, *J* = 8.8 Hz, 2H), 3.90 (s, 3H). **^{13}C NMR** (101 MHz, $CDCl_3$) δ 202.07, 179.66, 163.64, 145.84, 131.01, 129.60, 128.61, 127.97, 126.96, 114.41, 110.32, 55.70. **HRMS**(ESI) m/z calcd for $C_{16}H_{14}O_2S([M+Na]^+)$ 293.0612, found: 293.0603.

Synthesis of compound 2

The quantities involved are: Methyl benzodithioate (1.80 g, 10.7 mmol), 4-methylacetophenone (1.20 g, 8.9 mmol), and NaH (0.47 g, 19.7 mmol). Red colour solid, yield: 1.30 g, (58.0 %). ^{1}H NMR (400 MHz, $CDCl_3$) δ 15.38 (s, 1H), 7.92 (d, *J* = 8.0 Hz, 2H), 7.81 (d, *J* = 8.0 Hz, 2H), 7.53 – 7.36 (m, 4H), 7.30 (d, *J* = 8.0 Hz, 2H), 2.43 (s, 3H). **^{13}C NMR** (101 MHz, $CDCl_3$) δ 203.50, 179.94, 145.78, 143.82, 132.93, 131.14, 129.77, 128.63, 127.46, 126.96, 110.55, 21.87. **HRMS**(ESI) m/z calcd for $C_{16}H_{14}OS$ $([M+H]^+)$ 255.0838, found: 255.0819.

Synthesis of compound 3

The quantities involved are: Methyl benzodithioate (1.80 g, 10.7 mmol), acetophenone (1.10 g, 8.9 mmol), and NaH (0.57 g, 23.6 mmol). Red colour solid, yield: 1.50 g, (47.0 %). **^{1}H NMR** (400 MHz, $CDCl_3$) δ 15.24 (s, 1H), 8.02 (d, *J* = 8.0 Hz, 2H), 7.89 – 7.79 (m, 2H), 7.61 – 7.40 (m, 7H). **^{13}C NMR** (101 MHz, $CDCl_3$) δ 203.65, 179.89, 145.62,

135.81, 132.77, 131.25, 129.01, 128.66, 127.38, 126.96, 110.75. **HRMS**(ESI) m/z calcd for $C_{15}H_{12}OS$ ($[M+H]^+$) 241.0682, found: 241.0649.

Synthesis of compound 4

The quantities involved are: Methyl benzodithioate (1.80 g, 10.7 mmol), acetophenone (1.50 g, 8.8 mmol), and NaH (0.46 g, 19.4 mmol). Red colour solid, yield: 1.60 g, (62.0 %). **^{1}H NMR** (400 MHz, $CDCl_3$) δ 15.41 (s, 1H), 8.58 (s, 1H), 8.06 – 7.84 (m, 6H), 7.64 – 7.44 (m, 6H). **^{13}C NMR** (101 MHz, $CDCl_3$) δ 204.02, 179.57, 145.79, 135.49, 132.98, 132.95, 131.25, 129.56, 128.81, 128.72, 128.68, 128.53, 127.96, 127.09, 127.00, 123.25, 111.03. **HRMS**(ESI) m/z calcd for $C_{19}H_{14}OS$ ($[M+H]^+$) 291.0844, found: 291.0822.

General procedure for the preparation for boron derivatives (5-8):

An oven dried pressure tube was charged with 1,3-monothio-β-diketones (1.0 mmol) and tris(pentafluorophenyl) borane (1.2 mmol) in 10mL of toluene in N_2 glove box. Then the reaction mixture was heated to 110 °C for 24 h and transferred to round bottom flask, concentrated under vacuum. Product were purified using neutral alumina column chromatography and *n*-hexane/EtOAc.

Synthesis of compound 5

The quantities involved are: compound **1** (0.40 g, 1.5 mmol) and tris (pentafluorophenyl) borane (0.90 g, 1.7 mmol). Light orange colour solid, yield: 0.50 g, (56.0 %). **^{1}H NMR** (700 MHz, $CDCl_3$) δ 8.26 (d, *J* = 8.0 Hz, 2H), 7.89 (d, *J* = 8.0 Hz, 2H), 7.64 – 7.59 (m, 2H), 7.51 (t, *J* = 7.8 Hz, 2H), 7.08 (d, *J* = 8.0 Hz, 2H), 3.96 (s, 3H). **^{13}C NMR** (176 MHz, $CDCl_3$) δ 188.44, 181.47, 166.26, 147.88 (d, *J* = 236 Hz), 140.36 (d, J = 250 Hz), 139.70, 137.30 (d = 262 Hz) 136.56, 133.65, 132.97, 129.22, 128.54, 126.11, 115.05, 110.49, 56.02. **^{19}F NMR** (376 MHz, $CDCl_3$) δ -134.28 (d, 4F, Pf), -156.68 (t, 2F, Pf), -163.35 (t,

4F, Pf). **^{11}B NMR** (128 MHz, $CDCl_3$) δ 1.76. **HRMS**(ESI) m/z calcd for $C_{28}H_{13}BF_{10}O_2S$ ($[M]^+$) 614.0606, found: 614.0568.

Synthesis of compound 6

The quantities involved are: compound **2** (0.50 g, 1.9 mmol) and tris (pentafluorophenyl) borane (1.20 g, 2.3 mmol). Red colour crystal, yield: 0.78 g, (67.0 %). **^{1}H NMR** (700 MHz, $CDCl_3$) δ 8.18 (d, *J* = 8.0 Hz, 2H), 7.91 (d, *J* = 8.0 Hz, 2H), 7.69 (s, 1H), 7.64 (t, *J* = 8.0 Hz, 1H), 7.53 (t, *J* = 8.0 Hz, 2H), 7.41 (d, *J* = 8.1 Hz, 2H), 2.51 (s, 3H). **^{13}C NMR** (176 MHz, $CDCl_3$) δ 190.40, 182.43, 147.89 (d, J = 246 Hz), 147.72, 140.42 (d, J = 250 Hz), 139.51, 137.28 (d, J = 253 Hz), 133.95, 131.00, 130.31, 129.26, 128.59, 110.79, 22.19. **^{19}F NMR** (376 MHz, $CDCl_3$) δ -134.24 (d, 4F, Pf), -156.49 (t, 2F, Pf), -163.24 (t, 4F, Pf). **^{11}B NMR** (128 MHz, $CDCl_3$) δ 1.77. **HRMS**(ESI) m/z calcd for $C_{28}H_{13}BF_{10}OS$ ($[M-H]^+$) 597.0579, found: 597.0650.

Synthesis of compound 7

The quantities involved are: compound **3** (0.75 g, 3.1 mmol) and tris (pentafluorophenyl) borane (1.90 g, 3.7 mmol). Yellowish orange crystal, yield: 1.45 g, (79.0 %). **^{1}H NMR** (700 MHz, $CDCl_3$) δ 8.26 (d, *J* = 8.0 Hz, 2H), 7.92 (d, *J* = 8.0 Hz, 2H), 7.74 (t, *J* = 8.0 Hz, 1H), 7.69 (s, 1H), 7.66 (t, *J* = 8.0 Hz, 1H), 7.61 (t, *J* = 8.0 Hz, 2H), 7.54 (t, *J* = 8.0 Hz, 2H). **^{13}C NMR** (176 MHz, $CDCl_3$) δ 191.85, 182.47, 147.85 (J = 243 Hz), 140.47 (d, J = 252 Hz), 139.47, 137.32 (d, J = 250 Hz), 135.70, 134.18, 133.68, 130.12, 129.50, 129.35, 128.66, 110.93, 77.34, 77.16, 76.98. **^{19}F NMR** (376 MHz, $CDCl_3$) δ -134.24 (d, 4F, Pf), -156.31 (t, 2F, Pf), -163.14 (t, 4F, Pf). **^{11}B NMR** (128 MHz, $CDCl_3$) δ 1.85. **HRMS**(ESI) m/z calcd for $C_{27}H_{11}BF_{10}OS$ ($[M+H]^+$) 584.0500, found: 584.0539.

Synthesis of compound 8

The quantities involved are: compound **4** (0.50 g, 1.7 mmol) and tris (pentafluorophenyl) borane (1.10 g, 2.1 mmol). Yellow colour solid, yield: 0.75 g, (69.0 %). **^{1}H NMR** (400 MHz, $CDCl_3$) δ 8.85 (s, 1H), 8.20 (d, *J* = 8.0 Hz, 1H), 8.08 (d, *J* = 8.0 Hz, 1H), 8.04 – 7.91 (m, 4H), 7.83 (s, 1H), 7.74 – 7.60 (m, 3H), 7.56 (t, *J* = 8.0 Hz, 2H). **^{13}C NMR** (176 MHz, $CDCl_3$) δ 191.20, 182.17, 147.91 (d, J = 246 Hz), 140.49 (d, J = 260 Hz), 139.62, 137.38 (J = 271 Hz), 136.86, 134.10, 132.94, 132.79, 130.99, 130.47, 130.24, 129.39, 129.36, 128.66, 128.14, 127.62, 124.48, 111.23. **^{19}F NMR** (377 MHz, $CDCl_3$) δ -134.16 (d, 4F, Pf), -156.36 (t, 2F, Pf), -163.13 (t, 4F, Pf). **^{11}B NMR** (128 MHz, $CDCl_3$) δ 1.82. **HRMS**(ESI) m/z calcd for $C_{31}H_{13}BF_{10}OS$ ($[M-H]^+$) 633.0657, found: 633.0659.

General procedure for the preparation of boron biphenyl (BPh_2) derivatives:

An oven-dried pressure tube was charged with 1,3-monothio-β-diketones (1.0 mmol) and triphenyl borane (1.2 mmol) in 10 mL of toluene in N_2 glove box. The reaction mixture was heated to 110 °C for 24 h and transferred to a round bottom flask, concentrated under vacuum. To this 50 mL of hexane was added and sonicated until precipitate was observed. Hexane layer was decanted and the same process was repeated 3 times. The solid thus obtained was dried under vacuum.

Synthesis of compound 9

The quantities involved are: compound **1** (0.40 g, 1.5 mmol) and triphenyl borane (0.43 g, 1.7 mmol). Light orange colour solid, yield: 0.52 g, (81.0 %). **^{1}H NMR** (400 MHz, $CDCl_3$) δ 8.27 (d, *J* = 8.0 Hz, 2H), 7.89 (d, *J* = 8.0 Hz, 2H), 7.58 (d, *J* = 8.0 Hz, 5H), 7.50 – 7.43 (m, 3H), 7.30 – 7.16 (m, 6H), 7.05 (d, *J* = 8.0 Hz, 2H), 3.94 (s, 3H). **^{13}C NMR** (101 MHz, $CDCl_3$) δ 189.36, 180.78, 165.27, 140.63, 132.80, 132.23, 131.82, 128.93, 128.15, 127.25, 126.58, 114.79, 111.44, 55.91. **^{11}B NMR** (128 MHz, $CDCl_3$) δ 6.34. **HRMS**(ESI) m/z calcd for $C_{28}H_{24}BO_2S$ ($[M+H]^+$) 435.1626, found: 435.1591.

Synthesis of compound 10

The quantities involved are: compound **2** (0.50 g, 1.9 mmol) and triphenyl borane (0.57 g, 2.4 mmol). Light orange colour solid, yield: 0.54 g, (65.0 %). **^{1}H NMR** (400 MHz, $CDCl_3$) δ 8.18 (d, *J* = 8.0 Hz, 2H), 7.95 – 7.88 (m, 2H), 7.63 – 7.53 (m, 6H), 7.48 (d, *J* = 8.0 Hz, 2H), 7.37 (d, *J* = 8.0 Hz, 2H), 7.31 – 7.15 (m, 6H), 2.49 (s, 3H). **^{13}C NMR** (101 MHz, $CDCl_3$) δ 191.04, 181.46, 146.21, 140.51, 133.02, 132.24, 130.12, 129.35, 128.97, 128.19, 127.27, 126.64, 111.68 , 22.13. **^{11}B NMR** (128 MHz, $CDCl_3$) δ 6.13. **HRMS**(ESI) m/z calcd for $C_{28}H_{23}BOS$ ($[M]^+$) 418.1677, found: 418.1649.

Synthesis of compound 11

The quantities involved are: compound **3** (0.50 g, 2.0 mmol) and triphenyl borane (0.60 g, 2.5 mmol). Light orange colour solid, yield: 0.46 g, (54.0 %). **^{1}H NMR** (700 MHz, $CDCl_3$) δ 8.26 (d, *J* = 8.0 Hz, 2H), 7.91 (d, *J* = 8.0 Hz, 2H), 7.69 (d, *J* = 8.0 Hz, 1H), 7.63 – 7.53 (m, 8H), 7.48 (t, *J* = 7.8 Hz, 2H), 7.29 – 7.24 (m, 4H), 7.22 (d, *J* = 8.0 Hz, 2H). **^{13}C NMR** (176 MHz, $CDCl_3$) δ 192.29, 181.42, 140.43, 134.93, 134.60, 133.22, 132.26, 129.34, 129.17, 129.04, 128.21, 127.32, 126.71, 111.79. **^{11}B NMR** (128 MHz, $CDCl_3$) δ 5.06. **HRMS**(ESI) m/z calcd for $C_{27}H_{22}BOS$ ($[M+H]^+$) 405.1521, found: 405.1511.

Synthesis of compound 12

The quantities involved are: compound **4** (0.50 g, 1.7 mmol) and triphenyl borane (0.5 g, 2.0 mmol). Light orange colour solid, yield: 0.52 g, (67.0 %). **NMR** (400 MHz, $CDCl_3$) δ 8.90 (s, 1H), 8.27 (d, *J* = 8.0 Hz, 1H), 8.09 (d, *J* = 8.0 Hz, 1H), 8.05 – 7.95 (m, 4H), 7.75 – 7.61 (m, 8H), 7.54 (t, *J* = 7.6 Hz, 2H), 7.37 – 7.21 (m, 6H). **^{13}C NMR** (101 MHz, $CDCl_3$) δ 191.81, 181.16, 140.53, 136.35, 133.19, 132.90, 132.37, 132.15, 131.37, 130.12, 129.58, 129.18, 129.04, 128.25, 128.06, 127.46, 127.32, 126.75, 124.13, 112.15.

^{11}B NMR (128 MHz, $CDCl_3$) δ 5.23. **HRMS**(ESI) m/z calcd for $C_{31}H_{24}BOS$ ($[M+H]^+$) 455.1677, found: 455.1630.

2A.5 References

1. Rao, Y.-L.; Amarne, H.; Wang, S. *Coord. Chem. Rev.* **2012,** *256*, 759-770.

2. Li, D.; Zhang, H.; Wang, Y. *Chem. Soc. Rev.* **2013,** *42*, 8416-8433.

3. Suresh, D.; Gomes, P. T., Advances in Luminescent Tetracoordinate Organoboron Compounds. In *Advances in Organometallic Chemistry and Catalysis*, 2013; pp 485-492.

4. DeRosa, C. A.; Fraser, C. L., Tetracoordinate Boron Materials for Biological Imaging. In *Main Group Strategies towards Functional Hybrid Materials*, 2017; pp 111-140.

5. Murali, A. C.; Nayak, P.; Venkatasubbaiah, K. *Dalton Trans.* **2022,** *51*, 5751-5771.

6. Shi, J.; Ran, Z.; Peng, F. *Dyes Pigm.* **2022,** *204*, 110383.

7. Padilha, L. A.; Webster, S.; Przhonska, O. V.; Hu, H.; Peceli, D.; Ensley, T. R.; Bondar, M. V.; Gerasov, A. O.; Kovtun, Y. P.; Shandura, M. P.; Kachkovski, A. D.; Hagan, D. J.; Stryland, E. W. V. *J. Phys. Chem. A* **2010,** *114*, 6493-6501.

8. Ono, K.; Hashizume, J.; Yamaguchi, H.; Tomura, M.; Nishida, J.-i.; Yamashita, Y. *Org. Lett.* **2009,** *11*, 4326-4329.

9. Mamiya, M.; Suwa, Y.; Okamoto, H.; Yamaji, M. *Photochem. Photobiol. Sci.* **2016,** *15*, 928-936.

10. Nagai, A.; Kokado, K.; Nagata, Y.; Chujo, Y. *Macromolecules* **2008,** *41*, 8295-8298.

11. Chen, P.-Z.; Niu, L.-Y.; Chen, Y.-Z.; Yang, Q.-Z. *Coord. Chem. Rev.* **2017,** *350*, 196-216.

12. Xu, S.; Evans, R. E.; Liu, T.; Zhang, G.; Demas, J. N.; Trindle, C. O.; Fraser, C. L. *Inorg. Chem.* **2013,** *52*, 3597-3610.

13. Ono, K.; Yoshikawa, K.; Tsuji, Y.; Yamaguchi, H.; Uozumi, R.; Tomura, M.; Taga, K.; Saito, K. *Tetrahedron* **2007,** *63*, 9354-9358.

14. Gon, M.; Tanaka, K.; Chujo, Y. *Bull. Chem. Soc. Jpn.* **2018,** *92*, 7-18.

15. Tanaka, K.; Chujo, Y. *NPG Asia Mater.* **2015,** *7*, e223-e223.

16. Yoshii, R.; Hirose, A.; Tanaka, K.; Chujo, Y. *J. Am. Chem. Soc.* **2014,** *136*, 18131-18139.

17. Macedo, F. P.; Gwengo, C.; Lindeman, S. V.; Smith, M. D.; Gardinier, J. R. *Eur. J. Inorg. Chem.* **2008,** *2008*, 3200-3211.

18. Murali, A. C.; Nayak, P.; Nayak, S.; Das, S.; Senanayak, S. P.; Venkatasubbaiah, K. *Angew. Chem. Int. Ed.* **2023,** *62*, e202216871.

19. Murali, A. C.; Nayak, P.; Panda, R.; Das, R.; Venkatasubbaiah, K. *ACS Appl. Opt. Mater.* **2023,** *1*, 1033-1042.

20. Ramesha, A. B.; Sandhya, N. C.; Pavan Kumar, C. S.; Hiremath, M.; Mantelingu, K.; Rangappa, K. S. *New J. Chem.* **2016,** *40*, 7637-7642.

CHAPTER 2B

Far red/near infrared emissive boron-thioketonates: A new class of boranes as acceptors in optoelectronic devices

2B.1 Introduction

Tri- and four-coordinated boron compounds have drawn a great deal of attention owing to their properties such as light absorption, emission, electron acceptability, and high stability.[1-14] Among the several boron based dyes investigated, boron-β-diketonates are important category of compounds.[15-18] The optical properties of the boron-β-diketonates were tuned by using different methodology, such as a) by altering the R groups on the 1,3-positions of diketonates, b) by altering the substituents on the 'boron' center, and c) by substituting oxygen of the diketonates with other hetero atoms (**Figure 2B.1**). For example, Fraser and co-workers[19-23] reported various β-diketonate boranes that exhibit room temperature phosphorescence, tunable fluorescence, and mechanochromism; Yam and co-workers[24] and Adachi and co-workers[25] investigated the near-infrared emitting property of boron-β-diketonates and studied them as photochromic and light emitting materials respectively utilizing the first strategy mentioned above. Chujo and co-workers[26, 27] described the synthesis of boron-β-ketoiminates and -diiminates and their AIE properties by utilizing the third strategy. In spite of these advances, there are no reports that involve synthesis of boron compounds of β-thioketones with one oxygen in diketonate substituted by a sulfur atom. It should be mentioned that different β-thioketones were studied as ligands to make complexes employing various elements,[28-32] however, boron-β-thioketonates are not investigated yet.

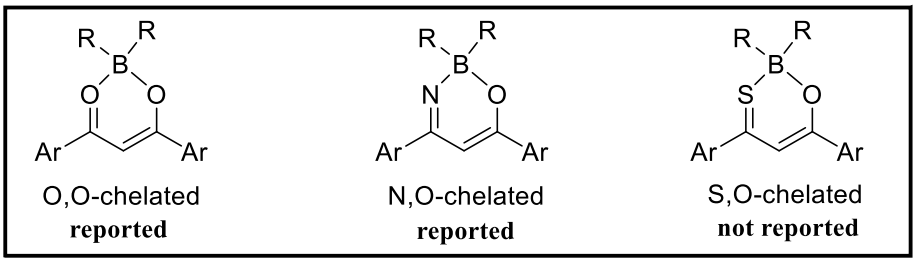

Figure 2B.1. Molecular chem-draw structures of compounds (a) boron-β-diketonate, (b) boron-β-ketoiminate and (c) boron-β-thioketonate**.**

Organic electronics such as organic field-effect transistors, organic light-emitting diodes, organic photovoltaic devices and memories is a growing interdisciplinary field of research which require both hole-conducting (p-type) and electron-conducting (n- type) semiconductors. Considerable progress has been made in developing hole-conducting organic semiconductors, however, the growth of electron-conducting materials is slow owing to the limited molecular diversity and lack of knowledge of electron transport property. Different synthetic protocols were adopted to make n-type semiconductors with high electron affinities.[33-38] For instance, fluorine and trifluromethyl substituted arenes, tetracarboxylic diimides, electron deficient heteropolycyclic compounds and quinone derivatives have been investigated as building block for electron-conducting materials. Owing to the rich photophysical properties, tetra-coordinated boron compounds gained attention in making various optoelectronic materials. For instance, Yam and co-workers[39] demonstrated the potential of boron-β-diketonates in making electronic memory storage, and organic solar cells, Ono and co-workers[40, 41] synthesized various BF_2-complexes (tetracene, perylene, octafluorotetracene, and π-extended diketones) and studied their electron-conducting behavior in organic field-effect transistors. In this chapter, we discuss the design, synthesis, and characterization of a new class of boron compounds viz. β-thioketonates of perfluorinated diphenylboranes and their photophysical, electrochemical, and electron transport properties. Further, we also studied their potential application as a photodetector and as an ON/OFF fluorescent acid sensor.

2B.2 Results and discussion

2B.2.1 Synthesis and characterization

The 1,3-monothio-β-diketones (MTDKH) (**6-9)** were readily synthesized (**Scheme 2B.1**) in good yields by the Claisen condensation of methylbenzodithioate derivatives (**1-3**) and acetophenone derivatives (**4 and 5)** in the presence of sodium hydride according to

literature methods.[42, 43] The desired boron monothioketonate compounds (MTDKB) **10-13** were prepared in good yields by the reaction of $(C_6F_5)_3B$ with MTDKH (**6-9**) in dry toluene at 110 °C. All the four MTDKH ligands (**6-9)** and MTDKB (**10-13)** compounds were completely characterized using multi-nuclear NMR spectroscopy, HRMS, and also using single crystal X-ray diffraction analysis in the case of **8** and **10-13**. Formation of compound **6** was further verified from the literature data.[43] All the four MTDKH ligands (**6-9)** have shown down fielded proton signal at 16-17 ppm which indicates the presence of enol tautomer. Furthermore, the ^{13}C NMR showed the expected C=S signal at around 200 ppm. The disappearance of the down fielded enolic peak and shift in the aliphatic, as well as aromatic peak positions in ^{1}H-NMR of all four MTDKB (**10-13)**, indicates the formation of boron compounds. Formation of the target compounds was further confirmed using $^{19}F\{^{1}H\}$ NMR and $^{11}B\{^{1}H\}$ NMR. The $^{19}F\{^{1}H\}$ NMR of all four compounds show a set of three resonances, which indicates the presence of pentafluorophenyl groups and a broad singlet at around 0 ppm was observed in the boron NMR, which is indicative of a tetra-coordinated boron centre.

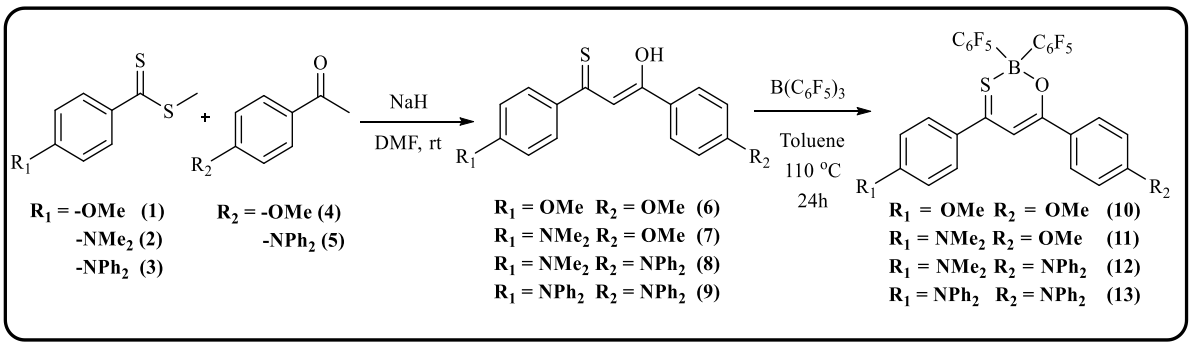

Scheme 2B.1: Synthetic route to the compounds **10-13**.

The molecular structure of compounds **10-13** (**Figure 2B.2**) were unambiguously confirmed by X-ray crystallography. Fortunately, we got crystals of the ligand **8**, which got crystallized in the monoclinic C2/c space group. Selected bond lengths and bond angles for the ligand and boron compounds are presented in **Table 2B.1.** Ligand **8** shows

a nearly planar conformation of thioketone skeleton consisting of C_3SO with intramolecular H-bonding.

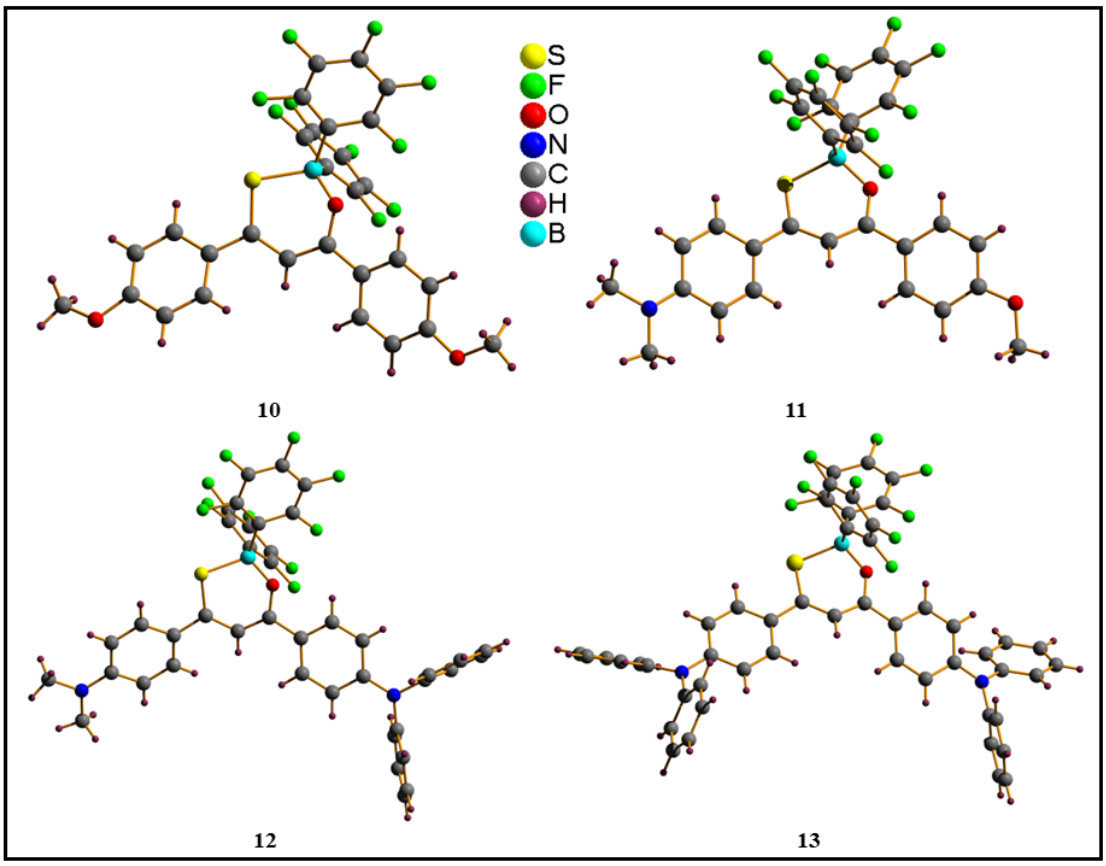

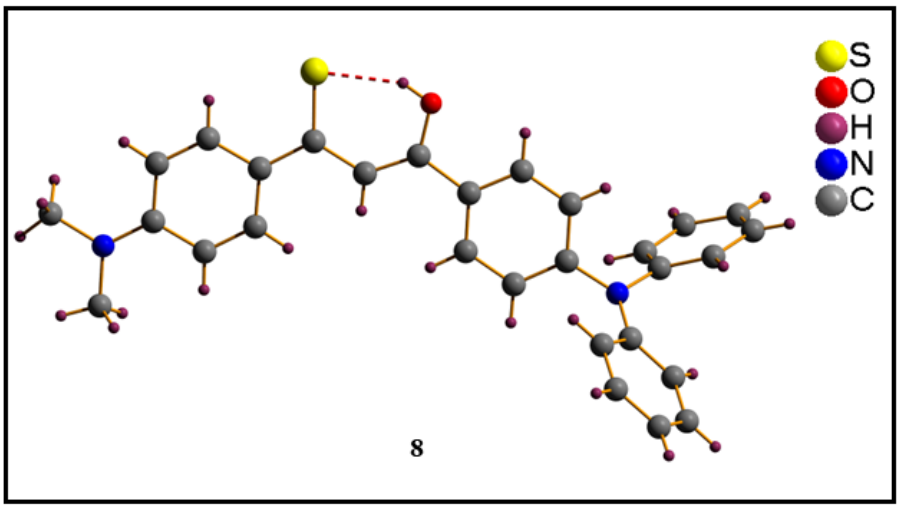

Figure 2B.2. Molecular structures of **10-13** and **8** with ball and stick model.

The C1-C2 bond length is longer than C2-C3 bond; the S-C1 and O-C3 bond lengths are 1.696 & 1.327 Å, respectively. This indicates that ligand **8** exist in the enolic form

represented in **Table 2B.1**. The C1-C2 and C2-C3 bond distances of the MTDKB (**10-13)** compounds are nearly equal and falls in between C-C and C=C bond distances. The S-C1 and O-C3 bond lengths fall in between the single and double bond distances of sulfur-carbon and oxygen-carbon, respectively. These data suggest that the electrons on the thioketonate C_3SO ring in MTDKB compounds are delocalized due to chelation. In all four MTDKB compounds, the boron atom deviates from the plane defined by the thioketones C_3SO plane by ~0.70 Å (**Table 2B.1**). The observed B-O (1.477-1.491 Å) bond lengths are comparable to the bond length reported for bis(pentafluorophenyl)boron diketonate; however the B-S (1.946-1.955 Å) bond lengths are slightly shorter than what is observed in bis(phenyl)boron quinolone-8-thiolate,[44] and also bis(phenyl)boron thioketonate which indicates that electron-withdrawing $–C_6F_5$ plays a key role for this shorter bond length.

Table 2B.1 Selected geometrical parameters for compounds **10-13** and **8**

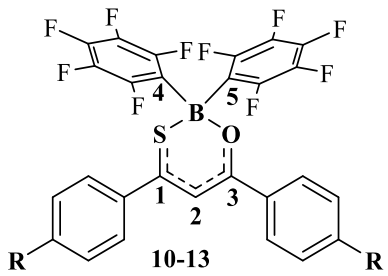

10-13

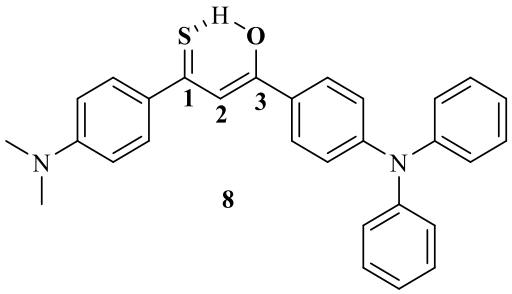

8

	10	**11**	**12**	**13**	**8**
S-C1 (Å)	1.719 (3)	1.722 (4)	1.711 (18)	1.719 (4)	1.696 (3)
O-C3 (Å)	1.308 (4)	1.315 (5)	1.309 (2)	1.302 (5)	1.327 (4)
B-S (Å)	1.950 (3)	1.955 (4)	1.946 (19)	1.955 (5)	-
B-O (Å)	1.486 (4)	1.491 (5)	1.477 (2)	1.481 (5)	-
B-C4 (Å)	1.629 (4)	1.620 (6)	1.638 (3)	1.621 (7)	-
B-C5 (Å)	1.632 (4)	1.640 (5)	1.619 (3)	1.627 (6)	-

C1-C2 (Å)	1.394 (4)	1.396 (5)	1.387 (2)	1.365 (6)	1.426 (5)
C2-C3 (Å)	1.394 (4)	1.390 (5)	1.382 (2)	1.398 (6)	1.365 (5)
S-B-O (deg)	106.99 (19)	108.4 (2)	107.38 (12)	106.7 (3)	-
S-B-C4 (deg)	113.0 (2)	114.3 (2)	107.51 (11)	108.8 (3)	-
O-B-C5 (deg)	105.2 (2)	113.2 (3)	106.19 (14)	104.8 (3)	-
C4-B-C5 (deg)	109.9 (2)	108.5 (5)	110.22 (14)	111.2 (3)	-
C1-C2-C3 (deg)	124.4 (3)	125.4 (4)	124.90 (17)	124.7 (4)	127.7 (3)
Deviation of B from C_3SO plane (Å)	0.68	0.73	0.69	0.73	-

Table 2B.2: Crystal data and structure refinement for compounds **10-13**.

	Compound **10**	Compound **11**	Compound **12**
Empirical formula	$C_{29}H_{15}BF_{10}O_3S$	$C_{30}H_{18}BF_{10}NO_2S$	$C_{41}H_{25}BF_{10}N_2OS$
Formula weight	644.28	657.32	794.50
Temperature/K	114.5(4)	172(70)	293(2)
Crystal system	orthorhombic	monoclinic	triclinic
Space group	Pbca	C2/c	P-1
a/Å	14.40588(16)	19.9074(4)	10.8195(3)
b/Å	22.6363(3)	11.9311(2)	13.9924(5)
c/Å	31.8510(3)	23.6783(8)	16.6177(6)
α/°	90	90	106.701(3)
β/°	90	101.373(3)	104.180(3)
γ/°	90	90	106.242(3)
Volume/$Å^3$	10386.5(2)	5513.5(2)	2163.87(14)
Z	16	8	2
$\rho_{calc}g/cm^3$	1.648	1.584	1.219
μ/mm^{-1}	2.083	1.956	0.149
F(000)	5184.0	2656.0	808.0
Radiation	CuKα (λ = 1.54184)	CuKα (λ = 1.54184)	MoKα (λ = 0.71073)

2Θ range for data collection/°	7.786 to 133.172	7.616 to 133.198	6.742 to 49.994
Index ranges	$-16 \le h \le 17$, $-26 \le k \le 26$, $-27 \le l \le 37$	$-23 \le h \le 23$, $-9 \le k \le 14$, $-28 \le l \le 28$	$-12 \le h \le 12$, $-16 \le k \le 16$, $-19 \le l \le 19$
Reflections collected	42967	15405	34534
Independent reflections	9166 [R_{int} = 0.0507, R_{sigma} = 0.0264]	4676 [R_{int} = 0.0490, R_{sigma} = 0.0387]	7590 [R_{int} = 0.0284, R_{sigma} = 0.0202]
Data/restraints/parameters	9166/0/797	4676/0/409	7590/0/507
Goodness-of-fit on F^2	1.047	1.137	1.029
Final R indexes [I>=2σ (I)]	R_1 = 0.0554, wR_2 = 0.1417	R_1 = 0.0682, wR_2 = 0.2084	R_1 = 0.0420, wR_2 = 0.1124
Final R indexes [all data]	R_1 = 0.0568, wR_2 = 0.1428	R_1 = 0.0832, wR_2 = 0.2657	R_1 = 0.0520, wR_2 = 0.1198
Largest diff. peak/hole / e $Å^{-3}$	1.84/-0.69	0.70/-0.88	0.23/-0.20

Table 2B.3. Crystal data and structure refinement for compound **13** and **8**.

	Compound **13**	Compound **8**
Empirical formula	$C_{51}H_{29}BF_{10}N_2OS$	$C_{29}H_{26}N_2OS$
Formula weight	918.63	450.58
Temperature/K	293(2)	100.00(10)
Crystal system	monoclinic	monoclinic
Space group	$P2_1/n$	C2/c
a/Å	10.5735(5)	27.1145(4)
b/Å	17.2153(8)	9.6525(2)
c/Å	27.7127(14)	35.9344(8)
α/°	90	90
β/°	91.842(5)	97.906(2)
γ/°	90	90
Volume/$Å^3$	5041.8(4)	9315.5(3)
Z	4	16
$\rho_{calc}g/cm^3$	1.210	1.285
μ/mm^{-1}	0.137	1.416
F(000)	1872.0	3808.0
Radiation	MoKα (λ = 0.71073)	CuKα (λ = 1.54184)
2Θ range for data collection/°	6.722 to 49.998	7.682 to 151.46
Index ranges	$-12 \le h \le 12$, $-23 \le k \le 21$, $-37 \le l \le 35$	$-32 \le h \le 33$, $-6 \le k \le 12$, $-41 \le l \le 44$
Reflections collected	51195	34859
Independent reflections	8836 [R_{int} = 0.1011, R_{sigma} = 0.0909]	9034 [R_{int} = 0.1371, R_{sigma} = 0.0936]
Data/restraints/parameters	8836/0/595	9034/0/601

Goodness-of-fit on F^2	1.053	1.026
Final R indexes [I>=2σ (I)]	R_1 = 0.0931, wR_2 = 0.2675	R_1 = 0.0986, wR_2 = 0.2467
Final R indexes [all data]	R_1 = 0.1307, wR_2 = 0.2994	R_1 = 0.1304, wR_2 = 0.2623
Largest diff. peak/hole / e $Å^{-3}$	0.77/-0.22	1.25/-0.83

2B.2.2 Optical properties

The photophysical properties of the MTDKB compounds (**10-13**) were investigated in different solvents such as toluene, tetrahydrofuran (THF), dichloromethane, acetonitrile, and dimethyl formamide (DMF) and the results are presented in **Table 2B.4** The absorption spectra of MTDKB compounds (**10-13)** in CH_2Cl_2 solution (**Figure 2B.3**) displayed strong absorption in the range of 461-562 nm that corresponds to the π-π* transition. By changing the peripheral substitution from –OMe to different amine functionality, a remarkable red shift in the absorption maxima was observed due to intramolecular charge transfer (ICT) character induced by amine functional groups and also by extended conjugation. The boron compounds (**10-13**) exhibited emission from cyan to NIR in the solution as well as in the thin film state. A comparison of MTDKB compounds (**10-13)** in CH_2Cl_2 reveals that compound **11** & **12** showed red-shifted emission over compound **10** due to electron-donating nature of -NMe_2. A further red shift was achieved by replacing -NMe_2 with –NPh_2 due to extended conjugation. The emission of **13** exhibited 178 nm red-shift compared to **10** and fell in the NIR region (λ_{em} = 708 nm in CH_2Cl_2). Emission studies in different solvents reveal that compounds **11-13** showed solvatochromism; however compound **10** did not show emission changes with an increase of solvent polarity. These results indicate that the dipole moment of compounds **11-13** increases in the excited state, probably due to ICT. A comparison of the absorption and emission maximum of compound **10** (O,S-chelation) with O,O-chelated boron compound showed a red shift of 20 nm and 89 nm

respectively.[45] This implies that replacement of the oxygen by sulfur has huge impact on the photophysical properties which will be discussed below. Moreover, the emission of compounds **10-13** in the thin film state varies from 596 nm to 710 nm and is red shifted in comparison to their solution state (CH_2Cl_2) emissions.

Table 2B.4: Photophysical data of the boron compounds **10-13**.

Compounds	Solvent	λ_{max}[a] (nm)	$\varepsilon_{max}x10^3/M^{-1}cm^{-1}$	λ_{em}[b] (nm)	Δ (cm^{-1})	ϕ_F[c] (%)	τ(ns)
10	Toluene	396,462	29.9	525	2597	<0.1	
	THF	395,463	27.9	513	2104	0.7	
	CH_2Cl_2	393, 461	35.6	530	2823	0.5	2.00
	DMF	397,467	25.4	513	1919	0.9	
	ACN	392,460	35.5	516	2359	0.2	
	Thin film	499		596		1.4	
11	Toluene	439,512	40.8	573	2078	2.4	
	THF	434,518	44.7	585	2210	2.3	
	CH_2Cl_2	434, 517	46.1	583	2189	1.6	1.99
	DMF	433,532	41.1	611	2429	0.2	
	ACN	430,522	25.8	594	2321	<0.1	
	Thin film	583		659		6.7	
12	Toluene	464,551	68.2	609	1727	5.9	
	THF	463,556	71.0	638	2311	0.4	
	CH_2Cl_2	461, 555	63.8	661	2889	10.2	1.83
	DMF	465,568	57.8	653	2671	1.7	
	ACN	460,558	29.5	706	3756	<0.1	
	Thin film	628		674		10.2	
13	Toluene	479,560	45.8	644	2329	8.8	
	THF	478,563	53.3	701	3495	3.7	
	CH_2Cl_2	473, 562	74.4	708	3668	3.6	3.58
	DMF	481,568	49.3	739	4073	1.9	
	ACN	473,558	30.7	762	4797	<0.1	
	Thin film	644		710		12.8	

[a]absorption maximum ($1.5x10^{-5}$ M). [b]excited at the higher wavelength of absorption maximum. [c]absolute fluorescence quantum yields using integrating sphere.

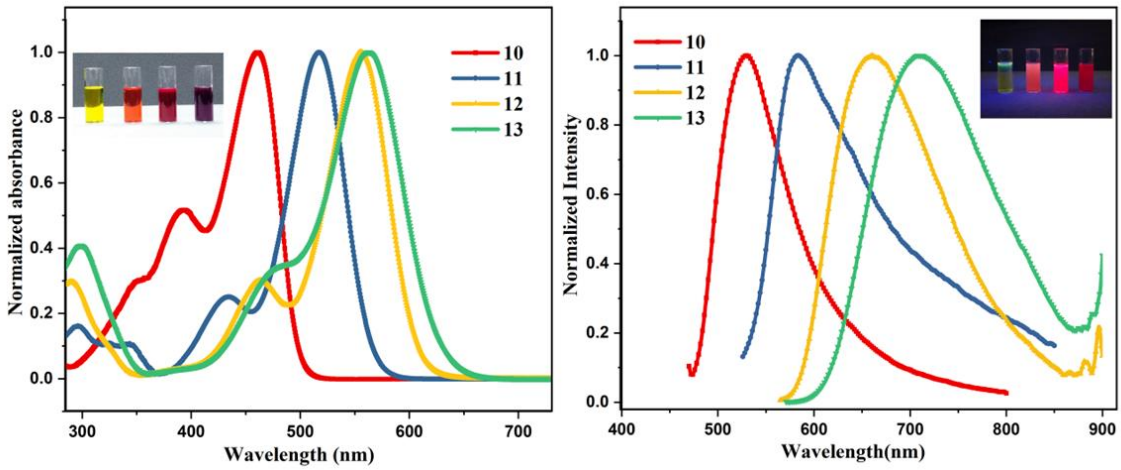

Figure 2B.3: Normalized absorption spectra (Left) and emission spectra (Right) of boron compounds **10-13** (1.5×10^{-5} M) in CH_2Cl_2, excited at higher wavelength absorption maxima. Inset (Left): photograph of compounds **10-13** in CH_2Cl_2 under day light. Inset (Right): photograph of compounds **10-13** in CH_2Cl_2 under a hand-held UV lamp at 365 nm.

2B.2.3 DFT Studies

To gain more insight into absorption behavior of MTDKB compounds and the orbitals involved in the electronic transitions, we optimized the geometries using density funtional theory (DFT) calculations (B3LYP/6-31g(d,p)) and computed the excitations using TD-DFT calculations. **Figure 2B.4**, represents the energy level of the highest occupied and the lowest unoccupied (HOMO & LUMO) molecular orbitals of MTDKB compounds, which indicates that both HOMO and LUMO orbitals are delocalized over β-thioketonate moiety and the aryl groups attached at the 1- and 3-position. Apart from that the HOMO's of compounds **10-13** also have contributions from $-NMe_2$ and $-NPh_2$. TD-DFT calculations were nicely reproduced the red shift observed for these compounds. Introduction of more electron-donating $-NMe_2$ and $-NPh_2$ increases the HOMO energy level, thereby reducing the energy gap of the MTDKB compounds. The calculations further indicate that compounds **11-13** showed bathochromic shift because of intramolecular charge transfer (ICT) from electron donating $-NMe_2$ and $-NPh_2$ to the

electron accepting β-thioketonate boron moiety. A comparison of the HOMO & LUMO energy levels of the O,O-chelated compound[45] with O,S-chelated compound (**10**) reveals that the later has lower energy band gap. A significant increase in HOMO energy level is realized over LUMO level. The cumulative effect of this helps in reducing the band gap considerably and thus leads to a bathochromic shift in the absorption of compound **10** compared to the analogues O,O-chelated compound.[45] Sulphur plays a crucial role in reducing the band gap as the primary difference between compound **10** and O,O-chelated compound reported by Chujo and co-workers is the presence of sulfur instead of oxygen.

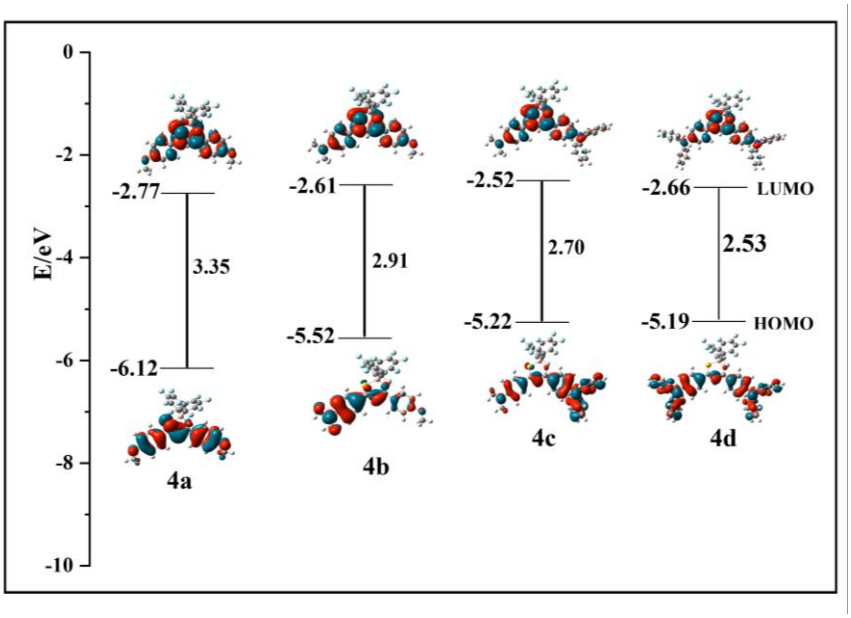

Figure 2B.4. Calculated HOMO and LUMO's of compounds **10-13** with their 3D representation.

Table 2B.5. Calculated electronic transitions for compounds **10-13** from TD-DFT (B3LYP) calculations

Compound	Transition	MO contributions	Energy gap eV (nm)	Oscillator strength/f
10	$S_0 \rightarrow S_1$	HOMO→LUMO	2.90 (426)	0.7895
	$S_0 \rightarrow S_2$	HOMO-5→LUMO	3.15 (392)	0.1945
		HOMO-4→LUMO		

		HOMO-1→LUMO		
	$S_0 \rightarrow S_3$	HOMO-4→LUMO	3.30 (375)	0.0017
		HOMO-3→LUMO		
		HOMO-2→LUMO		
	$S_0 \rightarrow S_4$	HOMO-4→LUMO	3.37 (367)	0.0350
		HOMO-3→LUMO		
		HOMO-2→LUMO		
		HOMO-1→LUMO		
	$S_0 \rightarrow S_5$	HOMO-6→LUMO	3.41 (362)	0.0396
		HOMO-4→LUMO		
		HOMO-3→LUMO		
		HOMO-1→LUMO		
	$S_0 \rightarrow S_6$	HOMO-9→LUMO	3.53 (350)	0.0384
		HOMO-6→LUMO		
		HOMO-5→LUMO		
		HOMO-1→LUMO		
11	$S_0 \rightarrow S_1$	HOMO→LUMO	2.58 (480)	0.8661
	$S_0 \rightarrow S_2$	HOMO-1→LUMO	3.06 (404)	0.2957
	$S_0 \rightarrow S_3$	HOMO-3→LUMO	3.41(363)	0.0042
		HOMO-2→LUMO		
	$S_0 \rightarrow S_4$	HOMO-6→LUMO	3.44 (360)	0.0382
		HOMO-4→LUMO		
		HOMO-3→LUMO		
		HOMO-2→LUMO		

	$S_0 \rightarrow S_5$	HOMO-4→LUMO HOMO-3→LUMO HOMO-2→LUMO	3.51 (352)	0.0022
	$S_0 \rightarrow S_6$	HOMO-6→LUMO HOMO-5→LUMO	3.62 (342)	0.0347
12	$S_0 \rightarrow S_1$	HOMO→LUMO	2.29 (539)	1.1262
	$S_0 \rightarrow S_2$	HOMO-1→LUMO	2.73 (453)	0.3159
	$S_0 \rightarrow S_3$	HOMO-2→LUMO	3.23 (383)	0.0471
	$S_0 \rightarrow S_4$	HOMO-4→LUMO HOMO-3→LUMO	3.44 (359)	0.0012
	$S_0 \rightarrow S_5$	HOMO-5→LUMO HOMO-4→LUMO HOMO-3→LUMO	3.51 (353)	0.0154
	$S_0 \rightarrow S_6$	HOMO-5→LUMO HOMO-4→LUMO HOMO-3→LUMO	3.54 (349)	0.0037
13	$S_0 \rightarrow S_1$	HOMO→LUMO	2.14 (576)	1.1830
	$S_0 \rightarrow S_2$	HOMO-1→LUMO	2.48 (498)	0.2897
	$S_0 \rightarrow S_3$	HOMO-5→LUMO HOMO-2→LUMO	3.19 (388)	0.0527
	$S_0 \rightarrow S_4$	HOMO-4→LUMO HOMO-3→LUMO	3.36 (368)	0.0021
	$S_0 \rightarrow S_5$	HOMO-5→LUMO HOMO-4→LUMO	3.42 (361)	0.0305

	$S_0 \rightarrow S_6$	HOMO-3→LUMO HOMO-5→LUMO HOMO-4→LUMO HOMO-3→LUMO	3.46 (357)	0.0071

Table 2B.6. Computed orbitals for compounds **10-13.**

Compound	**10**	**11**
LUMO+2	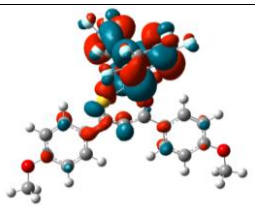 -0.6881 eV	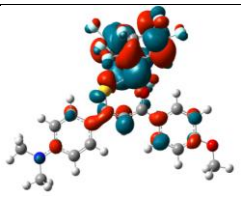 -0.6256 eV
LUMO+1	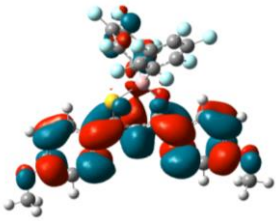 -0.8568 eV	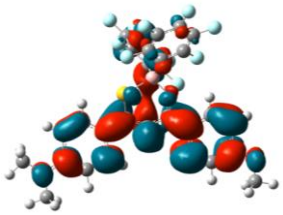 -0.7344 eV
LUMO	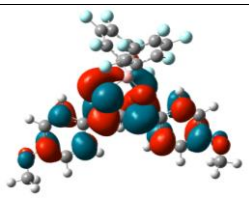 -2.7744 eV	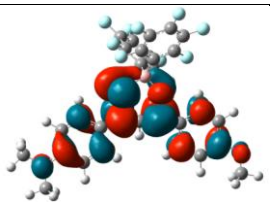 -2.6112 eV
HOMO	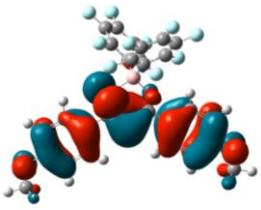 -6.12 eV	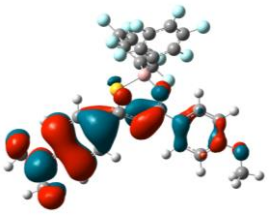 -5.5216 eV

HOMO-1	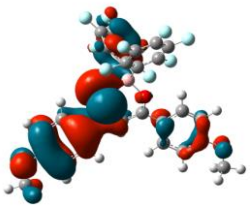 -6.392 eV	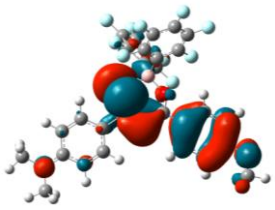 -6.1472 eV
HOMO-2	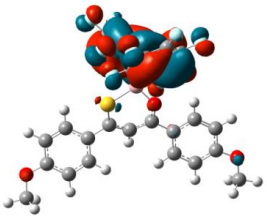 -6.6096 eV	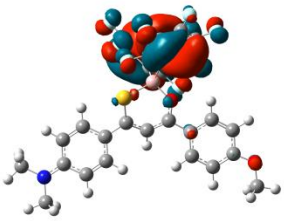 -6.5824 eV

Compound	**12**	**13**
LUMO+2	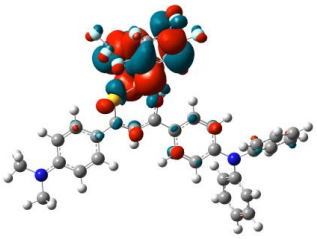 -0.5984 eV	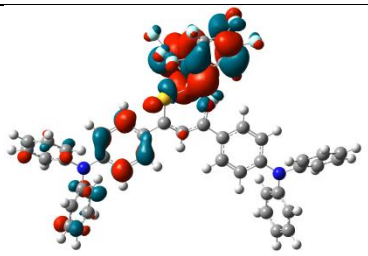 -0.6528 eV
LUMO+1	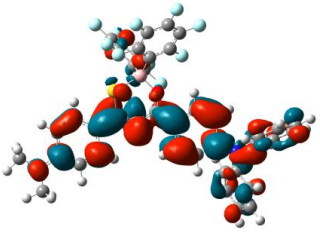 -0.816 eV	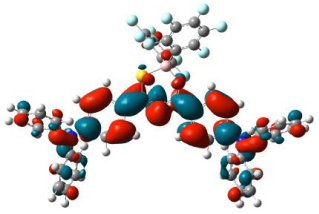 -0.9792 eV

LUMO	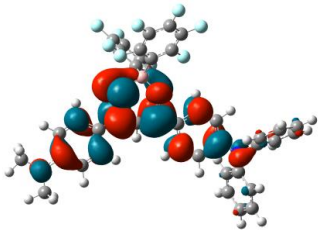 -2.5284 eV	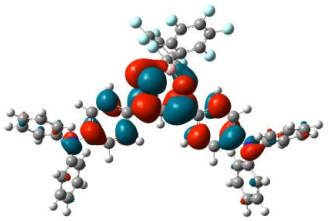 -2.6656 eV
HOMO	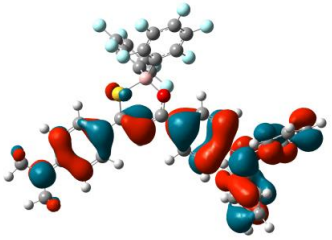 -5.2224 eV	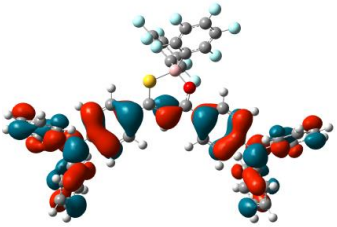 -5.1952 eV
HOMO-1	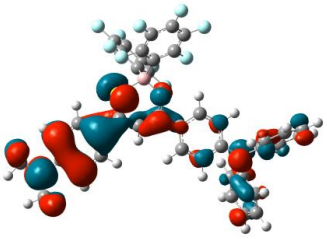 -5.576 eV	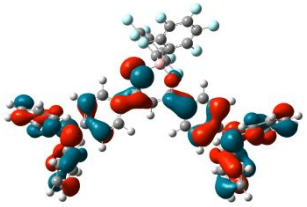 -5.4128 eV
HOMO-2	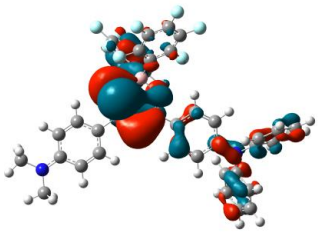 -6.3376 eV	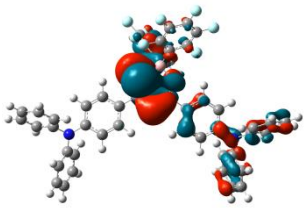 -6.3648 eV

2B.2.4 Electrochemical properties

Table 2B.7. HOMO and LUMO levels derived from UV-Vis onset absorption and electrochemical data.

Compounds	HOMO-LUMO gap[a]	LUMO[b]	HOMO[c]
10	1.952	-2.917	-4.869
11	1.685	-2.614	-4.299
12	1.505	-2.586	-4.091
13	1.406	-2.769	-4.175

[a]Absorption onset of the longest wavelength of UV band. [b]Calculated from E_{pc} of the reduction wave with reference to Fc/Fc^{+}. [c]Calculated from HOMO-LUMO gap and LUMO.

Table 2B.8. Electrochemical data for **10-13**

Compounds	E_{pc}	E_{pa} (1^{st} and 2^{nd} peak)
10	-1.185	-
11	-1.442	0.734
12	-1.483	0.614, 0.790
13	-1.343	0.680, 0.837

[#]E_{pc} = cathodic peak potential, [#]E_{pa} = anodic peak potential

Cyclic voltammetry studies of compounds **10-13** (vs Ferrocene/Ferrocenium) were performed with 0.1M of $NBu_4(PF_6)$ in CH_2Cl_2 as the supporting electrolyte (scan rate 100 mV/s).

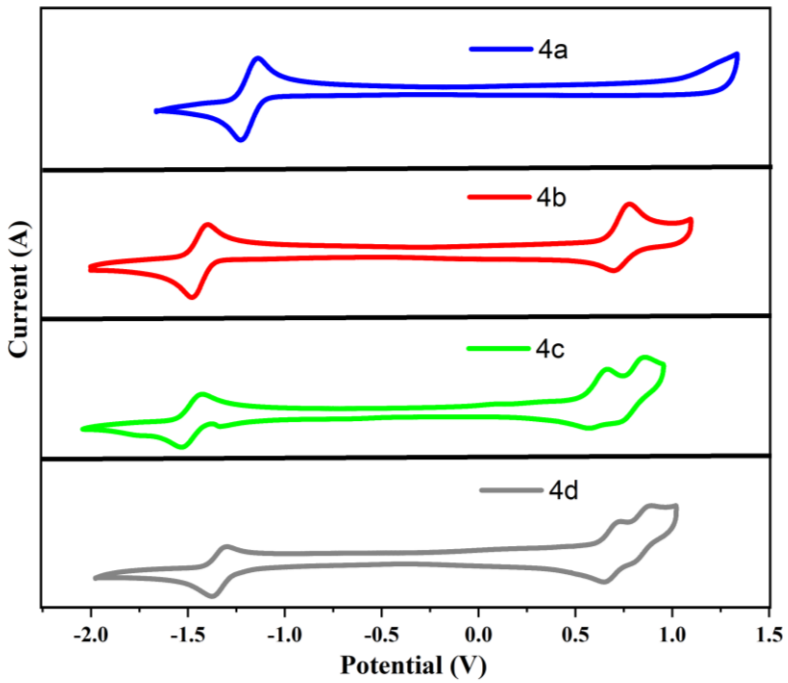

Figure 2B.5: Cyclic voltammogram of compounds **10-13** (vs Ferrocene/Ferrocenium) with 0.1M of $NBu_4(PF_6)$ in CH_2Cl_2 as the supporting electrolyte (scan rate 100 mV/s).

The electrochemical properties of MTDKB compounds were studied using cyclic voltammetry (CV) in N_2 purged dichloromethane (CH_2Cl_2) at 298K. All MTDKB compounds exhibit one reversible reduction peak ranging from -1.185 to -1.483 V (**Figure 2B.5**) and are comparable or lower the values reported for boron-diketonate compounds.[45, 46] The potentials of the reduction process centred on the boron moiety are only slightly affected by the electronic nature on the periphery of the phenyl groups. The reduction potential of **11** & **12** is slightly more negative than that of **10** owing to the presence of electron-donating -NMe_2 moieties. As expected, compound **10** did not show any oxidation peak, whereas compound **12** showed one reversible oxidation, and compound **12** & **13** showed two quasi reversible oxidation peaks centered on amine functionality. The frontier molecular orbital (FMO) energies (HOMO and LUMO) were also calculated from the onset absorption and E_{pc}. The calculated energy gap values are in good agreement with TD-DFT computation values. A comparison of the reduction potential of **10** with O,O-chelated compound[45] reveal that the former is less negative over the later which correlates with the observed low band gap using DFT calculations.

2B.2.5 Charge transport properties

To explore the potential of MTDKB as charge transport material, and understand the nature of charge carrier we fabricated both electron-only (Ag/Molecule/Ag) and hole only (ITO/PEDOT:PSS/Molecule/Au) devices from all the MTDKB molecules. To optimize the film formation, firstly the devices were prepared where the films were dried at room temperature and then annealed at 110 ºC for 10 min and another set of devices which were annealed at 110 ºC for 10 min during the drying process. We observe an enhancement of mobility by at least two orders of magnitude for the devices where films were annealed during drying process. Hence for all the semiconducting films we utilized this method of fabrication. Devices fabricated from such optimized semiconducting films

exhibit reliable trap-free space charge limited regime for voltage values within 5- 7 V indicating relatively low degree of disorder prevalent in this class of materials (Figure **2B.5a,b**).[47] The charge carrier mobility (μ) was estimated by using Mott Gurney law, given by, $J = \frac{9}{8}\epsilon_0\epsilon_r\mu\frac{V^2}{d^3}$, where J is the current density, d is the thickness of the semiconducting material, V is the applied voltage, ϵ_0 is the vacuum permittivity, and ϵ_r is the dielectric constant of the material which was estimated to be in the range 2 - 4 for all the molecules (**10-13**).[48] Maximum electron mobility of 0.003 $cm^2V^{-1}s^{-1}$ was obtained for **10** which decreases to ~ 10^{-5} $cm^2V^{-1}s^{-1}$ for molecule **12** and **13** (**Figure 2B.6**).

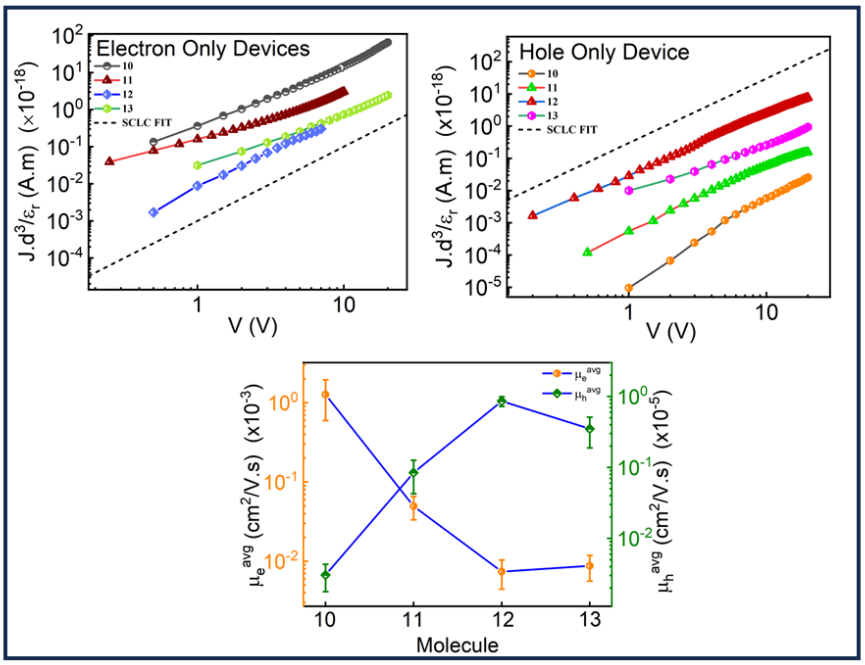

Figure 2B.6: J-V characteristics of a**)** electron only devices (Ag/Sample/Ag); b) hole only devices (Ag/PEDOT:PSS/ Sample/Au) used to estimate the SCLC mobility of the samples. Note that J is scaled with sample thickness (d) and dielectric constant (ε_r). c) The trends of μ_e and μ_h of molecules **10-13**.

Hole mobility exhibited exactly an opposite trend with the maximum bulk hole mobility of ~ 10^{-5} $cm^2V^{-1}s^{-1}$ thereby confirming that all molecules are acceptor type and hole transport is difficult irrespective of the electrodes chosen (**Figure 2B.6a and 2B.6c**). To

understand this trend in transport, we performed detailed structural characterization of the molecules. XRD patterns depict a direct correlation between the charge transport and the crystallinity. Intensity of the XRD pattern was observed to be consistent with the single crystal XRD obtained on these materials. Intense XRD peaks with a FWHM value of ~ 0.05˚ are obtained with molecule **10** indicating higher degree of order prevalent in this molecule which is consistent with the higher mobility observed. FWHM of the XRD pattern increases to a higher value of 0.11˚ for molecules **12** and **13** which exhibit the lowest electron mobility. To further probe the transport dynamics, we performed temperature dependent transport measurement on these molecules. All the devices exhibited a typical Arrhenius temperature dependence with a maximum activation energy of ~ 90 meV indicating relatively ordered landscape for charge transport attributed to the inherent crystalline structure of this material. Interestingly such a wide variation in mobility is observed irrespective of the same conjugated core which highlights the impact of the peripheral substitution on the molecular packing which ultimately decides the transport parameters.[49] At a molecular level, our measurement suggests that incorporation of phenyl substitution compared to the methyl substitution (bulkier peripheral group compared to smaller peripheral group) disrupts the inherent crystallinity of the system and decreases the charge carrier mobility. Finally, we utilized these molecules to design a single component photodetector device. These vertical devices exhibit outstanding photo response with responsivity reaching ~ 6 mA/W which is comparable to inorganic semiconductors (*a*-Si). This level of performance is possibly attributed to the combination of the high electron mobility and high dielectric constant of the molecule **10** which allows efficient dissociation of the photogenerated charge carriers.

2B.2.6 Thermal Properties

The thermal properties of boron compounds **10-13** were analysed with thermogravimetric analysis (TGA) under N_2 atmosphere at a heating rate of 20 °C/min. All the boron compounds displyed good thermal stability and decomposition of the boron compounds **10-12** begins with above 300 °C (**Figure 2B.7**).

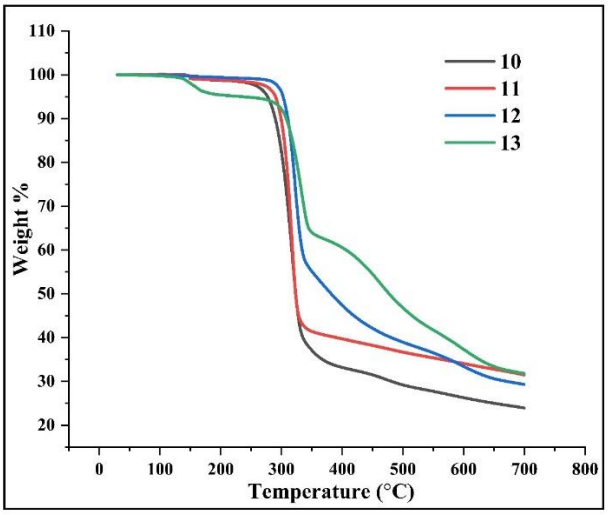

Figure 2B.7. TGA curve of **10-13** at a heating rate of 20 °C/min.

2B.2.7 Sensing Properties

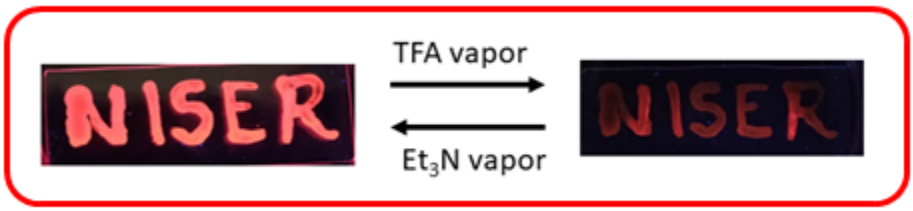

Figure 2B.8. The image of compound **11** (wt 5%) with PMMA support under UV light, exposing after TFA fume and Et_3N fume.

Finally, the electron donating capability of N,N-dimethylamino and N,N-diphenylamino groups of compounds **11-13**, have been utilized for sensing acid. The PMMA thin film (5 wt%) of compound **11** exhibits a red color under day light and emits bright red color luminescence under UV light. When the film was exposed to TFA vapor in a closed chamber, the red emission of the film got quenched in ~ 1 min. Interestingly, the NIR

luminescence of compound **11** regained by the exposure of Et_3N vapor, indicating that the optical properties can be tuned reversibly by fuming acid-base (**Figure 2B.8**).

2B.3 Conclusion

We have developed a new family of bis(pentafluorophenyl)boron monothio-β-diketonates (MTDKB). The emission of these O,S-chelated boranes could be tuned from far red to near-IR. These molecules showed outstanding electron transport with mobility reaching values of upto 0.003 cm^2/Vs. To understand the relevance of our chemical design for dissociation of photogenerated carrier with these we employed these molecules in a single component photodetector which exhibited reasonable responsivity of upto 6 mA/W. These results indicate the efficacy of our chemical design in tuning the optoelectronic properties of these semiconductors and opens up the strategy for designing photoactive acceptor molecules as an alternative to fullerene. Moreover, the amine functionality allowed us to use these molecules as reversible ON/OFF fluorescence sensor. Furthermore, this methodology will help to develop other, O,S-chelated organoboron compounds that will find applications in chemosensors, organic light emitting diodes, etc.

2B.4 Experimental section

2B.4.1 General information

All the reactions were carried out under N_2 atmosphere using standard glove box, Schlenk line and vacuum line techniques. Dry solvents used for the reactions were dried according to the standard procedures. All the reactions were monitored by thin layer chromatography. Nuclear magnetic resonance spectra were recorded on a 400 MHz or 700MHz Fourier transform NMR spectrometer (JEOL or Bruker) with $CDCl_3$ as a solvent. ^{11}B and ^{19}F NMR spectra were externally referenced to $BF_3.Et_2O$ in $CDCl_3$ (δ=0

ppm) and α,α,α-trifluoro toluene in $CDCl_3$ (δ=-63.73 ppm), respectively. Chemical shifts are reported in δ ppm (parts per million) using residual solvent protons as the internal standard (δ 7.26 for $CDCl_3$ in ^1H NMR, δ 77.16 for $CDCl_3$ in ^{13}C NMR). Coupling constants are reported as J values in hertz (Hz). Splitting patterns are designated as s(singlet), d(doublet), t(triplet), q(quartet), dd(doublet of doublet), dt(doublet of triplet), m(multiplet) and br(broad). HRMS were recorded using Waters XEVO G2-XS QTOF mass spectrometer. Elemental analyses were performed in a Euro Vector EA 3000 CHNS analyzer. UV – Visible spectra were recorded on Agilent Technologies Cary 60 UV/Visible spectrometer. Fluorescence spectra and quantum yield were measured using Edinburgh specrofluorimeter instrument FS5. For the measurement of absolute quantum yield, the concentration of the boron compounds was such as to give an absorbance of around 0.1 at excitation wavelength. Absolute total quantum yields were measured using an integrating sphere (Edinburgh instrument FS5) mounted in SC-30 compartment of the spectrofluorimeter, with data processing by software supplied by Edinburgh instrument FS5. The time-resolved fluorescence studies, a time-correlated single-photon counting (TCSPC) spectrometer (Edinburgh, OB920) has been used with a laser of 405 nm as a source of excitation and an MCP photomultiplier (Hamamatsu R3809U-50) is used as a detector. In order to check the laser profile, a water:ludox (4:1) solution has been used. Using water:ludox (4:1) solution, the instrument response function (IRF) has been obtained. The experimentally obtained fluorescence decay traces, I(t), has been evaluated as the sum of triexponential function (eq 1) and have been analysed using the nonlinear least-squares iterative convolution method based on the Levenberg-Marquardt algorithm.[50]

$$I(t) = \alpha_1 e^{-t/\tau_1} + \alpha_2 e^{-t/\tau_2} + \alpha_3 e^{-t/\tau_3} \qquad 1$$

Where α_1, α_2, and α_3 are the pre-exponential factors of the components having lifetimes τ_1,τ_2, and τ_3, respectively. The data has been analyzed using F900 software, the goodness of the fit has been observed through chi square ($\chi 2$) values and relative amplitude can be obtained. These three lifetime components have been averaged to obtain an average lifetime using eq 2

$$<\tau> = \sum \alpha_i \tau_i \qquad 2$$

Single-crystal X-ray diffraction data for compound **10-13** & **8** were collected on a Rigaku Super Nova fine-focused dual diffractometer, fitted with a PILATUS200K, was utilised to using Cu Kα radiation (λ = 1.54178 Å). The structures were solved using Olex2 and the ShelXS structure solution program using Direct Methods. The ShelXL refinement tool was then used to refine the structures using Least Squares minimization. Anisotropic displacement coefficients were utilised in the refinement of all non-hydrogen atoms. The H atoms were placed at calculated positions and were refined as riding atoms. The standard three electrode arrangement used for cyclic voltammetry included an Ag wire serving as the reference electrode, a Pt wire serving as the secondary electrode, and a glassy carbon working electrode. About 1.0 x 10^{-3} M solution in CH_2Cl_2 with $[Bu_4N][PF_6]$ (0.1 M) as a supporting electrolyte was used to record the voltammogram. The scans were referenced with a small amount of ferrocene as an internal standard. The scans were referenced with small amount of ferrocene as an internal standard. DFT computations were carried out using the Gaussian 16 software.[51] Using 6-31G(d,p) (B3LYP) as the basis set, the structures were optimized. Frequency calculations confirmed the optimized structures to be local minimum structures. Excitation data were determined using TD-DFT (B3LYP/631g(d,p))–PCM solvation (THF))) calculations. The films were prepared by mixing of polymethylmethacrylate (PMMA) (95 mg) and

compound **MTDKB** (5 mg) in distilled CH_2Cl_2, stirred (1h) and coated in a glass plate, then dried at open air for 24h.

Starting materials: Commercially available 4-methoxyacetophenoene (**4**), 4-aminoacetophenone, 4-bromo-N,N-dimethylaniline, triphenylamine, tris(pentafluorophenyl)borane, were purchased from Sigma-Aldrich, Spectrochem and Alfa-Aaser and used without further purification. 1-(4-(Diphenylamino)phenyl)ethenone (**5**), methyl-4-methoxybenzodithioate (**1**), 4-bromo-N,N-diphenylaniline, methyl 4-(dimethylamino)benzodithioate (**2**), and methyl 4-(diphenylamino)benzodithioate (**3**) are synthesized by following the literature reported procedures.[52-55]

2B.4.2 Synthetic procedure and spectral characterization

General procedure for the preparation for 1,3-monothio-β-diketones (MTDKH):

To a stirred suspension of NaH (2.2 mmol, 50%) in DMF(10mL) under N_2 atmosphere was added dropwise to a solution of aryl methyl ketone (1.0 mmol) and derivatives of methylbenzodithioate (1.2 mmol) in DMF (10mL) at 0 °C. The reaction mixture was further stirred at room temperature for 5-8h (monitored by TLC) and was poured into ice-cold water (40mL) then acidified with acetic acid. The precipitated red coloured solid was filtered and was purified by 100-200 silica gel chromatography using *n*-hexane/EtOAc as the eluent.

Synthesis of compound 6:[43] The quantities involved are as follows; 4-methoxyacetophenone (1.13g, 7.53 mmol), methyl 4-methoxybenzodithioate (1.80 g, 9.04 mmol) and NaH (50%, 0.40g, 16.66 mmol). Light red solid, Yield: 0.80 g (53%). **^{1}H NMR:** (400 MHz, $CDCl_3$) δ = 16.12 (s, 1H), 7.99 (d, *J*=8.7 Hz, 2H), 7.89 (d, *J*=8.7 Hz, 2H), 7.41 (s, 1H), 6.99 (d, *J*=8.0 Hz, 2H), 6.93 (d, *J*=8.0 Hz, 2H), 3.89 (s, 3H), 3.87 (s, 3H).**^{13}C NMR:** (101 MHz, $CDCl_3$) δ = 204.6, 178.1, 163.4, 162.5, 138.6, 129.3, 128.9,

127.8, 114.4, 113.8, 108.4, 55.7, 55.6. **HRMS** (ESI) m/z calcd for $C_{17}H_{16}O_3S$ ($[M+Na]^+$): 323.0724, found: 323.0712.

Synthesis of compound 7: The quantities involved are as follows; 4-methoxyacetophenone (0.25 g, 1.66 mmol), methyl 4-(dimethylamino)benzodithioate (0.42g, 2.0 mmol) and NaH (50%, 0.088g, 3.66 mmol). Dark red solid, Yield: 0.30 g (58%). **^{1}H NMR:** (400 MHz, $CDCl_3$) δ = 16.55 (s, 1H), 7.97 (dd, *J*=9.0 Hz, 3.3, 4H), 7.40 (s, 1H), 6.98 (d, *J*=8.9 Hz, 2H), 6.69 (d, *J*=8.5 Hz, 2H), 3.88 (s, 3H), 3.07 (s, 6H). **^{13}C NMR:** (101 MHz, $CDCl_3$) δ = 206.1, 175.8, 162.9, 152.9, 129.3, 128.9, 128.1, 114.3, 111.3, 111.2, 106.2, 55.6, 40.4. **HRMS** (ESI) m/z calcd for $C_{18}H_{19}NO_2S$ ($[M+H]^+$): 314.1207, found: 314.1209.

Synthesis of compound 8: The quantities involved are as follows; 1-(4-(methyl(phenyl)amino)phenyl)ethan-1-one (1.00 g, 3.48 mmol), methyl 4-(dimethylamino)benzodithioate (0.88g, 4.18 mmol)and NaH (50%, 0.18 g, 7.62 mmol). Reddish green solid, Yield: 0.70 g (45%).**^{1}H NMR:** (400 MHz, $CDCl_3$) δ = 16.61 (s, 1H), 7.96 (d, *J*=9.1 Hz, 2H), 7.84 (d, *J*=8.9 Hz, 2H), 7.39(s, 1H), 7.35 – 7.30 (m, 4H), 7.19 – 7.12 (m, 6H), 7.04 (d, *J*=8.9 Hz, 2H), 6.73 (d, *J*=8.8 Hz, 2H), 3.07 (s, 6H).**^{13}C NMR:** (101 MHz, $CDCl_3$) δ = 205.6, 175.5, 152.8, 151.6, 146.6, 134.0, 129.7, 129.3, 128.4, 127.6, 125.9, 124.7, 120.5, 111.2, 106.2, 40.4. **HRMS** (ESI) m/z calcd for $C_{29}H_{26}N_2OS$ ($[M+H]^+$): 451.1845, found: 451.1839.

Synthesis of compound 9: The quantities involved are as follows; 1-(4-(methyl(phenyl)amino)phenyl)ethan-1-one (0.62 g, 2.16 mmol), methyl 4-(diphenylamino)benzodithioate (0.86 g, 2.38 mmol) and NaH (50%, 0.11 g, 4.75 mmol). Dark reddish green solid, Yield: 0.60 g (48%). **^{1}H NMR:** (400 MHz, $CDCl_3$) δ = 16.46 (s, 1H), 7.84 (d, *J*=8.7 Hz, 2H), 7.79 (d, *J*=8.5 Hz, 2H), 7.38 (s, 1H), 7.35 – 7.29 (m, 8H),

7.18 – 7.11 (m, 12H), 7.01 (t, *J*=9.3 Hz, 4H). **^{13}C NMR:** (176 MHz, $CDCl_3$) δ = 204.9, 176.9, 151.9, 151.1, 146.8, 146.5, 138.8, 129.7, 129.6, 128.6, 128.5, 126.9, 126.1, 125.7, 124.9, 124.4, 120.5, 120.2, 107.8. **HRMS** (ESI) m/z calcd for $C_{39}H_{30}N_2OS$ ($[M+H]^+$) :575.2196, found: 575.2152.

General procedure for the preparation for pentafluoro biphenyl borane derivatives (MTDKB):

An oven dried pressure tube was charged with 1,3-monothio-β-diketone (MTDKH) (1.00 mmol) and tris(pentafluorophenyl)borane (1.2 mmol) in 10mL of toluene under N_2 atmosphere. The reaction mixture was continuously stirred at 110 °C for 24 h. The crude mixture was transferred to a round bottom flask and concentrated using rotary evaporator. The crude product was purified using neutral alumina using *n*-hexane/EtOAc as the eluent.

Synthesis of compound 10: The quantities involved are as follows; compound **6** (0.25 g, 0.83 mmol) and tris(pentafluorophenyl)borane (0.50 g, 0.99 mmol). Red compound, Yield: 0.35 g (65%). **^{1}H NMR:** (400 MHz, $CDCl_3$) δ = 8.23 (d, *J*=9.0, 2H), 7.94 (d, *J*=8.9, 2H), 7.56 (s, 1H), 7.07 (d, *J*=9.0, 2H), 7.00 (d, *J*=8.8, 2H), 3.95 (s, 3H), 3.91 (s, 3H).**^{13}C NMR:** (101 MHz, $CDCl_3$) δ = 186.9, 180.7, 165.8, 164.8, 147.9 (d, *J*=246 Hz), 140.3 (d, *J*=246 Hz), 137.3 (d, *J*=255 Hz), 132.6, 132.0, 130.8, 126.4, 114.9, 114.6, 108.6, 55.9, 55.8. **^{11}B NMR:** (128 MHz, $CDCl_3$) δ = 0.50 (s). **^{19}F NMR:** (376 MHz, $CDCl_3$) δ = -134.0 – -134.2 (m, 4F, Pf), -156.9 (t, *J*=19.2 Hz, 2F, Pf), -163.4 (t, *J* = 21.8 Hz, 4F, Pf). **HRMS** ($ASAP^+$) m/z calcd for $C_{29}H_{15}BF_{10}O_3S$ ($[M+H]^+$): 645.0712, found: 645.0768. Anal. Calcd for $C_{29}H_{15}BF_{10}O_3S$: C, 54.06; H, 2.35; S, 4.98. Found: C, 53.84; H, 2.03; N, 5.49.

Synthesis of compound 11: The quantities involved are as follows; compound **7** (0.25 g, 0.798 mmol) and tris(pentafluorophenyl)borane (0.49 g, 0.96 mmol). Greenish red crystal, Yield: 0.40 g (77%). **^{1}H NMR:** (400 MHz, $CDCl_3$) δ = 8.19 (d, *J*=8.9, 2H), 7.98 (d, *J*=9.1, 2H), 7.50 (s, 1H), 7.05 (d, *J*=9.0, 2H), 6.85 (br, 2H), 3.93 (s, 3H), 3.15 (s, 6H). **^{13}C NMR:** (176 MHz, $CDCl_3$) δ = 185.1, 178.2, 164.8, 154.9, 147.9 (d, *J*=238 Hz), 140.1 (d, *J*=253 Hz), 137.2 (d, *J*=243 Hz), 131.8, 131.2, 127.3, 126.4, 114.6, 111.6, 105.7, 55.8, 40.3. **^{11}B NMR:** (128 MHz, $CDCl_3$) δ = -0.01 (s). **^{19}F NMR:** (377 MHz, $CDCl_3$) δ = -134.2 (dd, *J*=23.8, 8.4, 4F, Pf), -157.6 (t, *J*=20.4, 2F, Pf), -163.7– -164.0 (m, 4F, 2f). **HRMS** (ASAP$^+$) m/z calcd for $C_{30}H_{19}BF_{10}NO_2S$ ($[M+H]^+$): 658.1106, found: 658.1052. Anal. Calcd for $C_{30}H_{18}BF_{10}NO_2S.CH_2Cl_2$: C, 50.16; H, 2.72; N, 1.89; S, 4.32. Found: C, 50.87; H, 2.38; N, 1.75; S, 5.03.

Synthesis of compound 12: The quantities involved are as follows; compound **8** (0.35 g, 0.77 mmol) and tris(pentafluorophenyl)borane (0.48 g, 0.93 mmol). Greenish red crystal, Yield: 0.46 g (75%). **^{1}H NMR:** (400 MHz, $CDCl_3$) δ = 8.03 (d, *J*=9.1, 2H), 7.94 (d, *J*=9.1, 2H), 7.46 (s, 1H), 7.39– 7.23 (m, 4H), 7.25 – 7.19 (m, 6H), 7.02 (d, *J*=9.1, 2H), 6.75 (d, *J*=9.2, 2H), 3.12 (s, 6H).**^{13}C NMR:** (101 MHz, $CDCl_3$) δ = 182.8, 177.7, 154.2, 153.7, 147.9 (d, *J*=256Hz), 147.1, 142.5 (d, *J*=254 Hz), 137.1 (d, *J*=254 Hz), 132.9, 131.5, 130.9, 129.9, 127.2, 126.9, 126.7, 125.8, 125.9, 118.9, 111.9, 106.1, 40.5. **^{11}B NMR:** (128 MHz, $CDCl_3$) δ = -0.02 (s). **^{19}F NMR:** (377 MHz, $CDCl_3$) δ = -134.2 (dd, *J*=22.7, 7.2, 4F, Pf), -157.8 (t, *J*=20.4, 2F, Pf), -163.9 (td, *J*=24.8, 9.1, 4F, Pf). **HRMS** (ASAP$^+$) m/z calcd for $C_{41}H_{26}BF_{10}N_2OS$ ($[M+H]^+$): 795.1735, found: 795.1664. Anal. Calcd for $C_{41}H_{25}BF_{10}N_2OS$: C, 61.98; H, 3.17; N, 3.53; S, 4.04. Found: C, 62.74; H, 2.72; N, 3.26; S, 4.61.

Synthesis of compound 13: The quantities involved are as follows; compound **9** (0.23 g, 0.40 mmol) and tris(pentafluorophenyl)borane (0.25 g, 0.48 mmol). Light greenish red

crystal, Yield: 0.12 g (34%). **^{1}H NMR:** (400 MHz, $CDCl_3$) δ = 8.04 (d, *J*=8.9, 2H), 7.81 (d, *J*=8.9, 2H), 7.47 (s, 1H), 7.47 – 7.33 (m, 8H), 7.24 – 7.17 (m, 12H), 7.01 – 6.99 (m, 4H). **^{13}C NMR:** (101 MHz, $CDCl_3$) δ = 182.8, 178.7, 154.1, 153.2, 147.9 (d, *J*=246 Hz), 145.9, 140.1 (d, *J*=253 Hz), 137.1 (d, *J*=239 Hz),131.8, 131.2, 130.1, 130.0, 129.9, 126.8, 126.4, 126.0, 125.5, 125.2, 119.7, 118.7, 107.7, 100.0. **^{11}B NMR:** (128 MHz, $CDCl_3$) δ = 0.27 (s). **^{19}F NMR:** (377 MHz, $CDCl_3$) δ = -134.0 (d, *J*=24.2, 4F, Pf), -157.1 (t, *J*=19.7, 2F, Pf), -163.7 (t, *J*=21.4, 4F, Pf). **HRMS** ($ASAP^+$) m/z calcd for $C_{51}H_{29}BF_{10}N_2OS$ ($[M+H]^+$): 919.1970, found: 919.2010. Anal. Calcd for $C_{51}H_{29}BF_{10}N_2OS$: C, 66.68; H, 3.18; N, 3.05; S, 3.49. Found: C, 67.39; H, 2.79; N, 2.69; S, 4.00.

2B.5 References

1. Entwistle, C. D.; Marder, T. B. *Chem. Mater.* **2004,** *16*, 4574-4585.
2. Jia, W.-L.; Bai, D.-R.; McCormick, T.; Liu, Q.-D.; Motala, M.; Wang, R.-Y.; Seward, C.; Tao, Y.; Wang, S. *Chem. Eur. J.* **2004,** *10*, 994-1006.
3. Fukazawa, A.; Yamaguchi, S. *Chem. Asian J.* **2009,** *4*, 1386-1400.
4. Jäkle, F. *Chem. Rev.* **2010,** *110*, 3985-4022.
5. Araneda, J. F.; Piers, W. E.; Sgro, M. J.; Parvez, M. *Chem. Sci.* **2014,** *5*, 3189-3196.
6. Neena, K. K.; Sudhakar, P.; Dipak, K.; Thilagar, P. *Chem. Commun.* **2017,** *53*, 3641-3644.
7. Kaese, T.; Trageser, T.; Budy, H.; Bolte, M.; Lerner, H.-W.; Wagner, M. *Chem. Sci.* **2018,** *9*, 3881-3891.
8. Hirai, M.; Tanaka, N.; Sakai, M.; Yamaguchi, S. *Chem. Rev.* **2019,** *119*, 8291-8331.
9. Liu, K.; Lalancette, R. A.; Jäkle, F. *J. Am. Chem. Soc.* **2019,** *141*, 7453-7462.

10. Mukundam, V.; Sa, S.; Kumari, A.; Das, R.; Venkatasubbaiah, K. *J. Mater. Chem. C* **2019,** *7*, 12725-12737.

11. Taylor, J. W.; Harman, W. H. *Chem. Commun.* **2020,** *56*, 4480-4483.

12. Berger, S. M.; Ferger, M.; Marder, T. B. *Chem. Eur. J.* **2021,** *27*, 7043-7058.

13. Sa, S.; Murali, A. C.; Nayak, P.; Venkatasubbaiah, K. *Chem. Commun.* **2021,** *57*, 10170-10173.

14. Su, X.; Bartholome, T. A.; Tidwell, J. R.; Pujol, A.; Yruegas, S.; Martinez, J. J.; Martin, C. D. *Chem. Rev.* **2021,** *121*, 4147-4192.

15. Chen, P.-Z.; Niu, L.-Y.; Chen, Y.-Z.; Yang, Q.-Z. *Coord. Chem. Rev.* **2017,** *350*, 196-216.

16. Bellinger, S.; Hatamimoslehabadi, M.; Bag, S.; Mithila, F.; La, J.; Frenette, M.; Laoui, S.; Szalda, D. J.; Yelleswarapu, C.; Rochford, J. *Chem. Eur. J.* **2018,** *24*, 906-917.

17. Bellinger, S.; Hatamimoslehabadi, M.; Borg, R. E.; La, J.; Catsoulis, P.; Mithila, F.; Yelleswarapu, C.; Rochford, J. *Chem. Commun.* **2018,** *54*, 6352-6355.

18. Murali, A. C.; Nayak, P.; Venkatasubbaiah, K. *Dalton Trans.* **2022,** *51*, 5751-5771.

19. Morris, W. A.; Kolpaczynska, M.; Fraser, C. L. *J. Phys. Chem. C* **2016,** *120*, 22539-22548.

20. Morris, W. A.; Butler, T.; Kolpaczynska, M.; Fraser, C. L. *Mater. Chem. Front.* **2017,** *1*, 158-166.

21. Butler, T.; Zhuang, M.; Fraser, C. L. *J. Phys. Chem. C* **2018,** *122*, 19090-19099.

22. Wang, F.; Song, D.; Dickie, D. A.; Fraser, C. L. *Chem. Asian J.* **2019,** *14*, 1849-1859.

23. Wang, F.; Song, D.; Dickie, D. A.; Fraser, C. L. *J. Fluoresc.* **2021,** *31*, 39-49.

24. Poon, C.-T.; Lam, W. H.; Wong, H.-L.; Yam, V. W.-W. *J. Am. Chem. Soc.* **2010,** *132*, 13992-13993.

25. Kim, D.-H.; D'Aléo, A.; Chen, X.-K.; Sandanayaka, A. D. S.; Yao, D.; Zhao, L.; Komino, T.; Zaborova, E.; Canard, G.; Tsuchiya, Y.; Choi, E.; Wu, J. W.; Fages, F.; Brédas, J.-L.; Ribierre, J.-C.; Adachi, C. *Nat. Photon.* **2018,** *12*, 98-104.

26. Yoshii, R.; Hirose, A.; Tanaka, K.; Chujo, Y. *J. Am. Chem. Soc.* **2014,** *136*, 18131-18139.

27. Ito, S.; Yaegashi, M.; Tanaka, K.; Chujo, Y. *Chem. Eur. J.* **2021,** *27*, 9194-9194.

28. Uhlemann, E.; Thomas, P. *J. Prakt. Chem.* **1966,** *34*, 180-189.

29. Siiman, O.; Titus, D. D.; Cowman, C. D.; Fresco, J.; Gray, H. B. *J. Am. Chem. Soc.* **1974,** *96*, 2353-2359.

30. Hoskins, B. F.; Pannan, C. D. *J. inorg. nucl. chem.* **1975,** *11*, 409-413.

31. Das, M.; Haworth, D. T. *Transit. Met. Chem.* **1996,** *21*, 442-446.

32. Andrews, P. C.; Blair, V. L.; Ferrero, R. L.; Junk, P. C.; Kedzierski, L.; Peiris, R. M. *Dalton Trans.* **2014,** *43*, 1279-1291.

33. Katz, H. E.; Lovinger, A. J.; Johnson, J.; Kloc, C.; Siegrist, T.; Li, W.; Lin, Y. Y.; Dodabalapur, A. *Nature* **2000,** *404*, 478-481.

34. Sakamoto, Y.; Suzuki, T.; Kobayashi, M.; Gao, Y.; Fukai, Y.; Inoue, Y.; Sato, F.; Tokito, S. *J. Am. Chem. Soc.* **2004,** *126*, 8138-8140.

35. Naraso; Nishida, J.-i.; Kumaki, D.; Tokito, S.; Yamashita, Y. *J. Am. Chem. Soc.* **2006,** *128*, 9598-9599.

36. Jones, B. A.; Facchetti, A.; Wasielewski, M. R.; Marks, T. J. *J. Am. Chem. Soc.* **2007,** *129*, 15259-15278.

37. Wang, Z.; Kim, C.; Facchetti, A.; Marks, T. J. *J. Am. Chem. Soc.* **2007,** *129*, 13362-13363.

38. Mamada, M.; Nishida, J.-i.; Tokito, S.; Yamashita, Y. *Chem. Commun.* **2009**, 2177-2179.

39. Li, P.; Liang, Q.; Hong, E. Y.-H.; Chan, C.-Y.; Cheng, Y.-H.; Leung, M.-Y.; Chan, M.-Y.; Low, K.-H.; Wu, H.; Yam, V. W.-W. *Chem. Sci.* **2020,** *11*, 11601-11612.

40. Ono, K.; Yamaguchi, H.; Taga, K.; Saito, K.; Nishida, J.-i.; Yamashita, Y. *Org. Lett.* **2009,** *11*, 149-152.

41. Kojima, Y.; Sugiura, S.; Suzuki, K.; Yisilamu, Y.; Ono, K. *Chem. Asian J.* **2022,** *17*, e202101262.

42. Kumar, S. V.; Yadav, S. K.; Raghava, B.; Saraiah, B.; Ila, H.; Rangappa, K. S.; Hazra, A. *J. Org. Chem.* **2013,** *78*, 4960-4973.

43. Yugandar, S.; Konda, S.; Ila, H. *Organic Letters* **2017,** *19*, 1512-1515.

44. Tokoro, Y.; Nagai, A.; Kokado, K.; Chujo, Y. *Macromolecules* **2009,** *42*, 2988-2993.

45. Nagai, A.; Kokado, K.; Nagata, Y.; Arita, M.; Chujo, Y. *J. Org. Chem.* **2008,** *73*, 8605-8607.

46. Wang, L.; Zhang, Z.; Cheng, X.; Ye, K.; Li, F.; Wang, Y.; Zhang, H. *J. Mater. Chem. C* **2015,** *3*, 499-505.

47. Senanayak, S. P.; Ashar, A. Z.; Kanimozhi, C.; Patil, S.; Narayan, K. S. *Phys. Rev. B.* **2015,** *91*, 115302.

48. Abdi-Jalebi, M.; Dar, M. I.; Sadhanala, A.; Senanayak, S. P.; Giordano, F.; Zakeeruddin, S. M.; Grätzel, M.; Friend, R. H. *J. Phys. Chem. Lett.* **2016,** *7*, 3264-3269.

49. Vasimalla, S.; Senanayak, S. P.; Sharma, M.; Narayan, K. S.; Iyer, P. K. *Chem. Mater.* **2014,** *26*, 4030-4037.

50. Lakowicz, J. R., *Principles of fluorescence spectroscopy*. Springer: 2006.

51. Frisch, M.; Trucks, G.; Schlegel, H.; Scuseria, G.; Robb, M.; Cheeseman, J.; Scalmani, G.; Barone, V.; Petersson, G.; Nakatsuji, H. *Wallingford CT* **2016,** *421*.

52. Usha Gangan, T. V.; Reddy, M. L. P. *Dalton Trans.* **2015,** *44*, 15924-15937.

53. Ramesha, A. B.; Sandhya, N. C.; Pavan Kumar, C. S.; Hiremath, M.; Mantelingu, K.; Rangappa, K. S. *New J. Chem.* **2016,** *40*, 7637-7642.

54. Raikwar, M. M.; Avhad, K. C.; Varghese, M.; Mathew, E.; Joe, I. H.; Sekar, N. *Opt. Mater.* **2019,** *92*, 100-110.

55. Wei, J.; Ma, Y.; Liu, C.; Li, J.; Shen, J.; Zhang, K. Y.; Liu, S.; Zhao, Q. *J. Mater. Chem. C* **2021,** *9*, 5945-5951.

CHAPTER 2C

Tetraphenylethylene-based Boron Thioketonates: Effect of Substitution, Cyanide ion Sensing and Study of Non-linear Optical Properties

2C.1 Introduction

Boron containing luminescent materials especially tetra-coordinated boron containing luminescent materials have attracted considerable interest in various fields such as photovoltaics, organic field-effect transistors, light-emitting devices, and sensors owing to their tuneable and strong absorption, emission and stability over three-coordinated boron compounds.[1-7] Among the different tetra-coordinated boron containing luminescent materials boron-β-diketonates have been studied to a greater extent due to their large molar extinction coefficients and high fluorescence quantum yields. Much effort has been paid to tune the photophysical properties of boron-β-diketonates by chemically modifying the π-conjugation *via* the substituents.[8-10] For example, Fraser and co-workers explored the substituent effect of boron-β-diketonates and studied them as stimuli responsive materials,[11, 12] Chujo and co-workers described the effect of B-F vs B-aryl.[13, 14] More recently, Adachi and co-workers demonstrated the use of boron-β-diketonates as NIR emissive materials.[15] Furthermore, efforts also been made to tune the photophysical properties by replacing one or two of the oxygen's present on the diketone moiety. For instance, Gardinier and Chujo groups reported the synthesis of boron-β-ketoiminate and boron-β-diiminate compounds and their rich photophysical properties.[16-18] We recently reported the first synthesis of monothio-β-diketonate boron compounds and studied their applications in making organic electronics.[19]

Tetraphenylethylene (TPE) is one of the attractive building block widely studied for its inherent aggregation-induced emission (AIE) phenomenon.[20, 21] The AIE realized in TPE molecule is an important class of anti-aggregation caused quenching effect that showed strong emission in the solid state.[22] Apart from that the ease of synthesis made this moiety as an attractive synthon to convert aggregation caused quenching (ACQ) molecules into AIE molecules.[23, 24] Taking advantage of the TPE unit, we designed and synthesized TPE

and N,N-dimethyl aniline (DMA) substituted O,S-chelated organoboron material and studied their structural-property relationship. The synthesized boron compounds **1-4** have shown red emission in the solution as well as in the solid state. The substitution effect, aggregation-induced emission properties, cyanide ion sensing, and their impact on the nonlinear optical (NLO) properties are presented.

2C.2 Results and discussion

2C.2.1 Synthesis and characterization

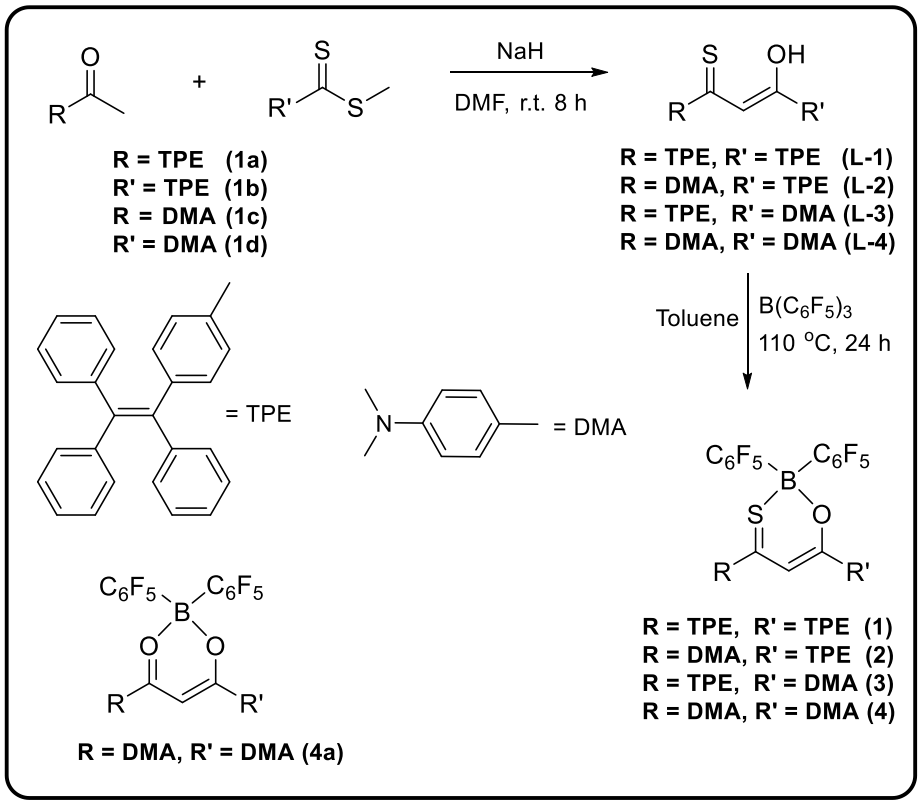

Scheme 2C.1: Synthetic route to the ligands **L1-L4** and boron compounds **1-4**.

The boron monothio-β-diketonate compounds **1-4** were synthesized by refluxing $B(C_6F_5)_3$ and tetraphenylethylene (TPE) and N,N-dimethylaniline (DMA) derivatives of 1,3-monothio-β-diketones (**L1-L4)** in dry toluene at 110 °C as shown in Scheme **2C.1.** The ligands **L1-L4** were synthesized by adopting a similar protocol as reported in the literature.[19, 25, 26] Formation of the ligands **(L1-L4)** and the boron compounds **(1-4)** characterized using multi-nuclear NMR spectroscopy, HRMS, and single crystal X-ray

diffraction in case of **2-4**. The ^{1}H NMR of all four ligands **1-4** shows the hydrogen bonded enolic proton resonating between 15-17 ppm. The disappearance of this signal in the boron compounds **1-4**, indicates the formation of the desired boron compounds. All the boron compounds showed a $^{11}B\{^{1}H\}$ NMR resonating at ~0 ppm which confirms the tetra-coordinated nature of the boron. The presence of boron-centred bis(pentafluorophenyl) rings was confirmed with $^{19}F\{^{1}H\}$ NMR. All the boron compounds **1-4** showed three sets of peaks resonating at the range of ~ -133.0 to -164.0 ppm.

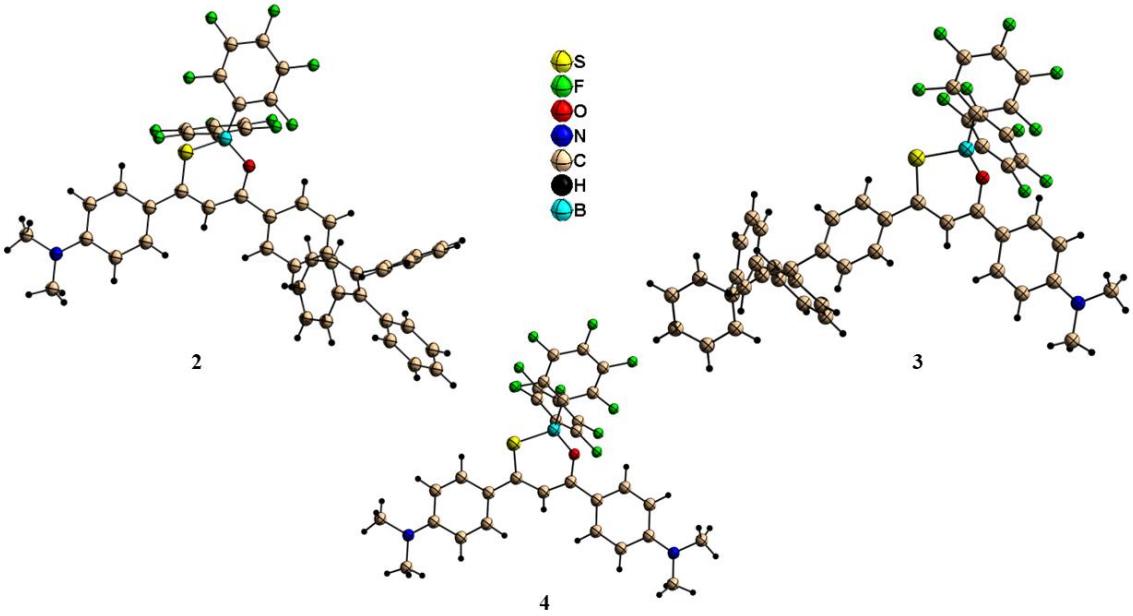

Figure 2C.1. Molecular structure of **2-4** with ball and stick model.

Single crystals of boron compounds **2-4** suitable for X-ray diffraction were grown by slow evaporation of the respective compounds from a mixture of solvents (**2** and **3** from $CHCl_3$/*n*-hexane mixture; **4** from CH_2Cl_2/diethylether mixture). All the boron compounds (**Figure 2C.1**) crystallized in the triclinic P-1 space group; selected bond lengths and bond angles are presented in **Table 2C.1.** The observed B-S bond lengths (1.936(3) for **2**; 1.952(4) for **3** and 1.957(3) for **4**) are significantly longer than typical B-S single (1.89 Å) and B-S double bond (1.69).[27, 28] The C-S bond distances (1.718(3) for **2**; 1.726(4) for **3**

and 1.738(3) for **4**) are longer than that observed in $Ph_2C=S$ (1.636(9) Å).[29] The B-O bond distances and S-B-O bond angles are comparable to other monothio-β-diketonate boron compounds reported in the literature.[14, 19] In all three compounds, the six-membered cyclic ring formed by the boron coordination takes a twisted conformation and the deviation of the boron atom from plane C is 0.66 Å, 0.52 Å, and 0.56 Å for compounds **2-4** respectively. The angle between plane A and plane C varies from 15.4 to 35.3°, and that of plane B and plane C vary from 11.5 to 15.0° (**Table 2C.1**).

Table 2C.1 Selected geometrical parameters for compounds **1-4** in tetrahydrofuran.

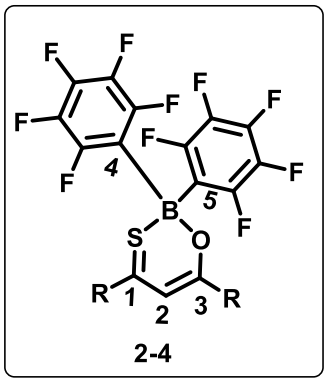

2-4

	2	**3**	**4**
S-C1 (Å)	1.718 (3)	1.726 (4)	1.738 (3)
O-C3 (Å)	1.318 (3)	1.313 (5)	1.313 (4)
B-S (Å)	1.936 (3)	1.952 (4)	1.957 (3)
B-O (Å)	1.484 (3)	1.491 (5)	1.484 (4)
B-C4 (Å)	1.651 (4)	1.635 (6)	1.627 (5)
B-C5 (Å)	1.622 (4)	1.628 (6)	1.641 (5)
C1-C2 (Å)	1.409 (4)	1.376 (6)	1.387 (4)
C2-C3 (Å)	1.388 (3)	1.418 (5)	1.406 (4)
S-B-O (deg)	105.9 (2)	107.8 (3)	106.3 (2)
S-B-C4 (deg)	113.3 (2)	108.7 (3)	112.3 (2)
O-B-C5 (deg)	105.2 (2)	106.2 (3)	113.2 (2)
C4-B-C5 (deg)	111.4 (2)	108.2 (3)	108.3 (2)
C1-C2-C3 (deg)	124.7 (2)	124.2 (4)	125.3 (3)

Plane A/C	15.8 (5)	35.3 (7)	15.4 (6)
Plane B/C	13.1 (5)	11.5 (7)	15.0 (7)
Deviation of B from C_3SOB plane (Å)	0.66	0.52	0.56

Table 2C.2: Crystal data and structure refinement for compounds **2-4**.

Compound	**2**	**3**	**4**
Empirical formula	$C_{49}H_{30}BF_{10}NOS$	$C_{50}H_{31}BCl_3F_{10}NOS$	$C_{31}H_{21}BF_{10}N_2OS$
Formula weight	881.61	1000.98	670.37
Temperature/K	100.00(10)	100.00(10)	293(2)
Crystal system	triclinic	triclinic	triclinic
Space group	P-1	P-1	P-1
a/Å	10.0495(3)	9.18485(14)	8.9816(2)
b/Å	15.1708(5)	15.4471(2)	13.0571(3)
c/Å	15.2134(6)	17.3977(3)	13.7444(3)
α/°	68.639(4)	94.6902(13)	65.886(2)
β/°	75.402(3)	104.3423(13)	89.929(2)
γ/°	72.901(3)	90.2448(12)	77.543(2)
Volume/$Å^3$	2037.05(14)	2382.67(6)	1429.72(6)
Z	2	2	2
$\rho_{calc}g/cm^3$	1.437	1.395	1.557
μ/mm^{-1}	1.462	2.829	1.880
F(000)	900.0	1016.0	680.0
Crystal size/mm^3	0.2 × 0.2 × 0.2	0.12 × 0.12 × 0.12	0.18 × 0.15 × 0.13
Radiation	CuKα (λ = 1.54184)	CuKα (λ = 1.54184)	CuKα (λ = 1.54184)
2Θ range for data collection/°	7.466 to 150.272	7.452 to 150.62	7.08 to 151.352
Index ranges	$-9 \le h \le 12$, $-18 \le k \le 18$, $-15 \le l \le 19$	$-11 \le h \le 11$, $-19 \le k \le 18$, $-19 \le l \le 21$	$-8 \le h \le 11$, $-16 \le k \le 16$, $-17 \le l \le 17$
Reflections collected	28967	34036	20644
Independent reflections	8148 [R_{int} = 0.0384, R_{sigma} = 0.0298]	9601 [R_{int} = 0.0541, R_{sigma} = 0.0320]	5803 [R_{int} = 0.0701, R_{sigma} = 0.0483]
Data/restraints/ parameters	8148/0/570	9601/0/607	5803/0/419

Goodness-of-fit on F^2	1.055	1.032	1.157
Final R indexes [I>=2σ (I)]	R_1 = 0.0513, wR_2 = 0.1254	R_1 = 0.0635, wR_2 = 0.1727	R_1 = 0.0738, wR_2 = 0.2299
Final R indexes [all data]	R_1 = 0.0674, wR_2 = 0.1364	R_1 = 0.0647, wR_2 = 0.1737	R_1 = 0.0810, wR_2 = 0.2357
Largest diff. peak/hole / e $Å^{-3}$	0.49/-0.28	0.65/-0.78	1.50/-0.78

2C.2.2 Photophysical properties

The absorption and emission of boron compounds **1-4** were measured in different solvents and the results are presented in **Table 2C.3, Figure 2C.2.** For comparative study we also synthesized compound **4a**, (**Scheme 2C.1**) a diketonate boron compound and studied its photophysical properties. The UV-Vis spectra of **1-4** in tetrahydrofuran (THF) solvent showed a strong absorption band ranging from 494 to 547 nm. A remarkable red shift in absorption was observed for compounds **2-4** relative to **1**, may be ascribed to strong electron donating nature of $–NMe_2$ groups. The λ_{max} of compound **4** showed a red shift of 46 nm compared to compound **4a** due to the exchange of oxygen atom with sulphur atom. On excitation at their absorption maxima, the emission of these compounds tuned from 597 nm to 688 nm in THF solvent. With increase in solvent polarity the emission maxima of all the compounds got red shifted; in some instance the emission reached to NIR region (761 nm for compound **1** in CH_3CN, **Table 2C.3**). The observed emission and Stokes shift (7478 cm^{-1} in CH_3CN) for compound **1** are quite high among all boron compounds reported here (**Table 2C.3**). Compound **4** exhibit a low Stokes shift (1531 cm^{-1}) and narrow band width which is due to the presence of $–NMe_2$ on both sides of the phenyl ring makes the molecule more symmetrical and planar. The emission maximum of compound **4** showed a pronounced red shift of 62 nm compared to compound **4a**, due to the sulphur effect. The fluorescence quantum yields of compounds **1-4** in different solvents was determined using integrating sphere method. Compared with

4a, compounds **1-4** exhibits a low quantum yield due to the presence of heavier sulphur atom, which enhances the intersystem crossing rate.[30] Among the monothio-β-diketonate boron compounds studied, **1** showed a high fluorescence quantum yield of 16% in THF. Symmetrically substituted compounds **1** and **4** showed better quantum yields over unsymmetrically substituted compounds **2** and **3**. The fluorescence lifetime of **1-4** in THF are in the range of 1.27 to 7.45 ns.

Table 2C.3: Photophysical data of the boron compounds **1-4**.

Compounds	**Solvent**	**λ_{abs}[a] /nm (ε x 10^4/M^{-1} cm^{-1})**	**λ_{em}[b] (nm)**	**Stokes Shift (cm^{-1})**	**ϕ_F[c] (%)**	**τ (ns)**
1	Toluene	304 (3.8), 498 (4.3)	623	4029	9.9	
	THF	312 (2.1), 494 (2.5)	688	5708	15.9	7.45
	CH_2Cl_2	303 (2.2), 491 (2.6)	700	6081	14.2	
	CH_3CN	283 (3.5), 485 (3.9)	761	7478	7.5	
	Thin film	580[d]	660		14.1	
2	Toluene	460 (2.3), 531 (7.0)	593	1969	0.1	
	THF	455 (1.3), 536 (4.3)	620	2527	1.5	1.28
	CH_2Cl_2	456 (1.4), 534 (4.4)	616	2493	2.1	
	CH_3CN	450 (1.3), 539 (4.3)	632	2730	1.4	
	Thin film	608[d]	675		1.0	
3	Toluene	423 (1.3), 526 (6.4)	601	2373	10.5	
	THF	409 (0.8), 530 (4.0)	628	2944	0.6	1.27
	CH_2Cl_2	411 (0.8), 528 (4.2)	623	2888	4.5	
	CH_3CN	397 (0.79), 530 (4.2)	641	2952	2.0	
	Thin film	597[d]	670		5.8	
4	Toluene	447 (1.8), 539 (6.7)	581	1341	9.2	
	THF	447 (1.7), 547 (6.4)	597	1531	3.8	2.04
	CH_2Cl_2	446 (2.1), 545 (7.5)	601	1710	12.2	

	CH_3CN	447 (1.54), 551 (5.3)	623	1888	1.6	
	Thin film	607[d]	670		7.2	
4a	THF	387 (1.0), 501 (6.0)	535	1269	88.8	

[a]absorption maximum ($1.5x10^{-5}$ M). [b]excited at the higher wavelength of absorption maximum. [c]absolute fluorescence quantum yields using integrating sphere.

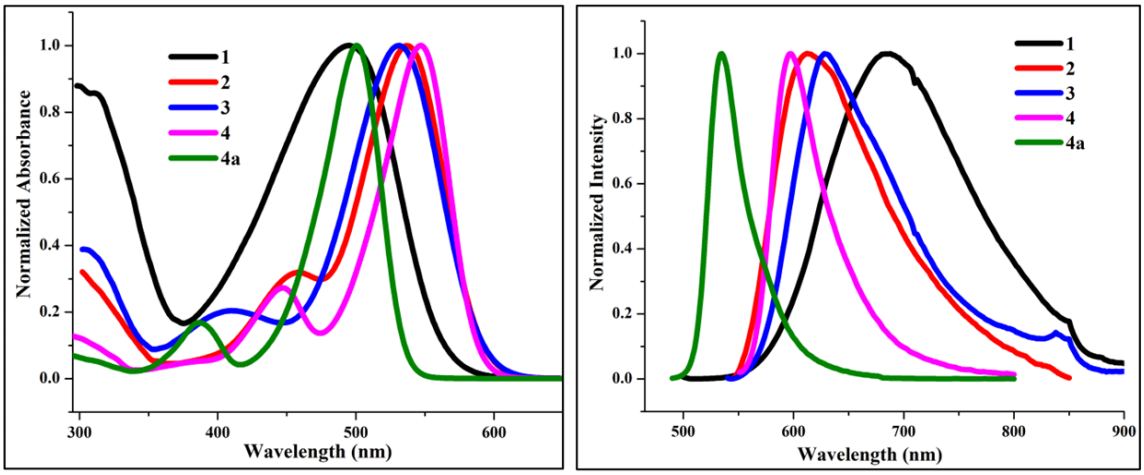

Figure 2C.2: Normalized absorption spectra (Left) and emission spectra (Right) of boron compounds **1-4** and **4a** (1.5×10^{-5} M) in THF, excited at higher wavelength absorption maxima.

2C.2.3 AIE studies

Tetraphenylethylene unit is a well-known structural motif which leads to aggregation induced enhancement emission (AIEE). To investigate the AIEE properties of the boron compounds, the photoluminescence of **1-4** in dilute THF and H_2O/THF mixtures were studied. Compounds **1**, **2**, and **3** showed AIEE phenomenon; however, **4** showed aggregation caused quenching (**Figure 2C.6**). As shown in **Figure 2C.4 and 2C.5**, the emission intensity of **6** and **7** was increased upon adding H_2O to THF solution while keeping the concentration of the solution same. At 60 % water fraction (H_2O/THF; 60/40) the emission intensity reached higher. On further increasing the water fraction resulted in a decrease in emission intensity. However, **1** showed a decrease in emission intensity upto 50% water fraction (**Figure 2C.3**). The PL intensity showed enhancement after 50% water fraction, which may be due to the formation of different molecular aggregates with

the change of water fraction. A similar trend was realized from the plot of quantum yield vs water fraction of compounds **1-3** (**Figure 2C.7**). Absorption spectra of **2** and **3** (**Figure 2C.7**) showed (~10 nm) marginal red shift at 60% water in THF. A decrease in absorption intensity with marginal blue shift (~10 nm) and level-off tails at higher water fraction was realized. However, **5** showed a decrease in absorption intensity, and level-off tails with increase in water fraction was observed.

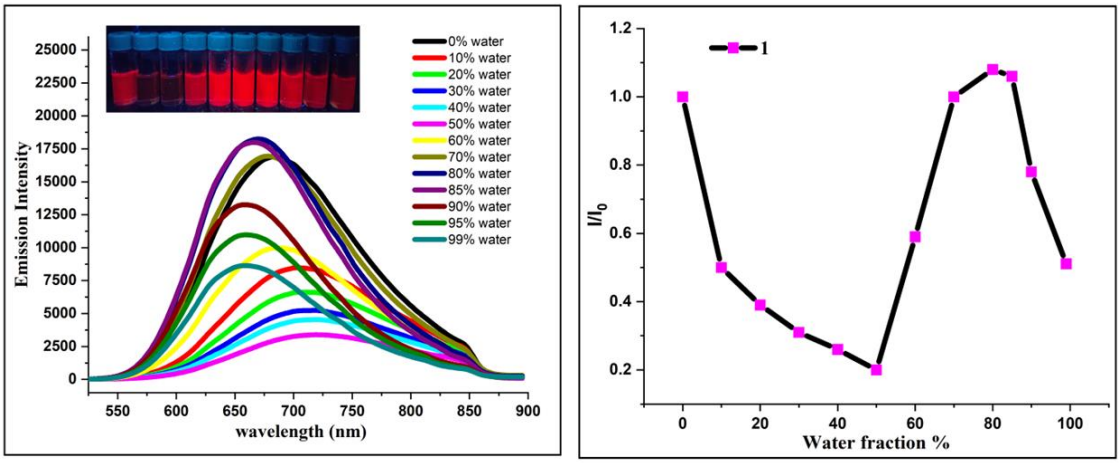

Figure 2C.3. Fluorescence spectra of compound **1** (1.5×10^{-5} M) in a THF/H_2O mixture with different waterfraction (f_w) (left). I/I_0 Vs water fraction (%) plot of **1** with the addition of water (vol%) (right). Inset (left): Photograph of compound **1** with increasing water fraction (0–99%) under handheld UV lamp excited at 365 nm.

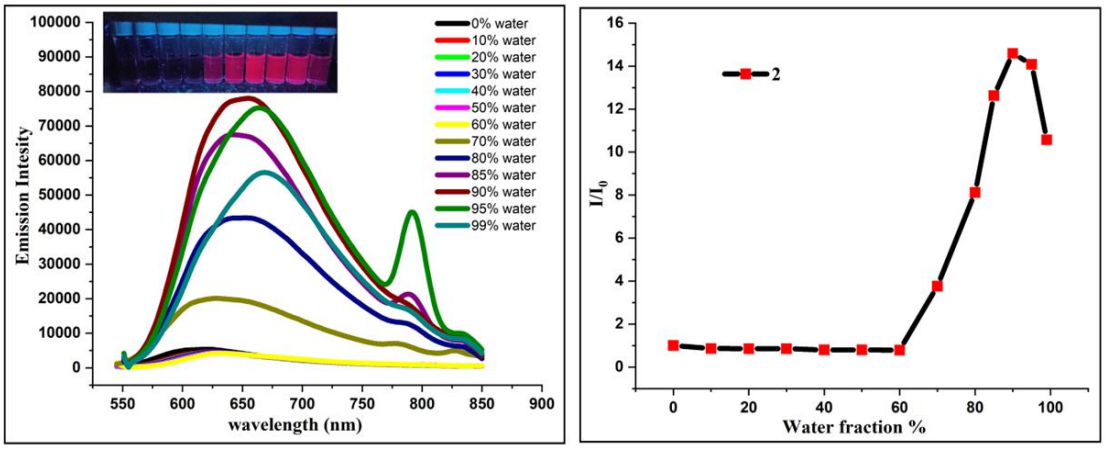

Figure 2C.4. Fluorescence spectra of compound **2** (1.5×10^{-5} M) in a THF/H_2O mixture with different waterfraction (f_w) (left). I/I_0 Vs water fraction (%) plot of **2** with the addition of water (vol%) (right). Inset (left): Photograph of compound **2** with increasing water fraction (0–99%) under handheld UV lamp excited at 365 nm.

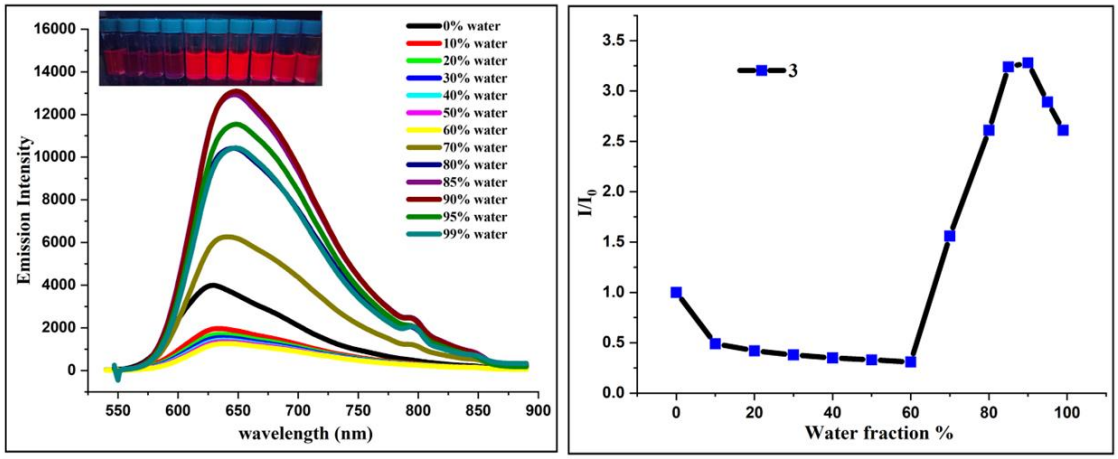

Figure 2C.5. Fluorescence spectra of compound **3** (1.5 x 10^{-5} M) in a THF/H_2O mixture with different waterfraction (f_w) (left). I/I_0 Vs water fraction (%) plot of **3** with the addition of water (vol%) (right). Inset (left): Photograph of compound **3** with increasing water fraction (0–99%) under handheld UV lamp excited at 365 nm.

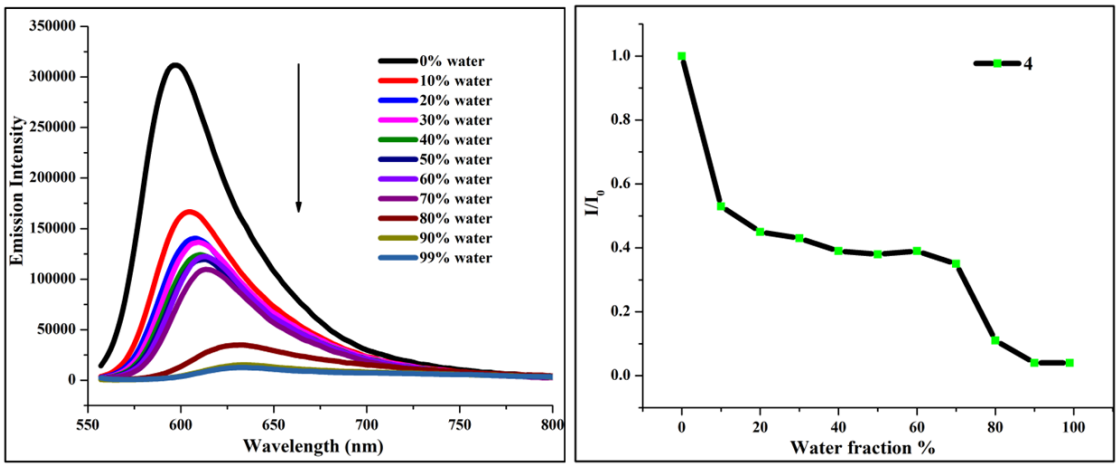

Figure 2C.6. Fluorescence spectra of compound **4** (1.5 x 10^{-5} M) in a THF/H_2O mixture with different waterfraction (f_w) (left). I/I_0 Vs water fraction (%) plot of **4** with the addition of water (vol%) (right). Inset (left): Photograph of compound **4** with increasing water fraction (0–99%) under handheld UV lamp excited at 365 nm.

Table 2C.4. Relative quantum yield (%) of the aggregates of complexes **1-3** in THF/H_2O.

THF: H_2O (%)	**1**	**2**	**3**
100:0	4.3	0.12	0.76
80:20	1.7	0.08	0.36
60:40	1.0	0.08	0.26
40:60	4.4	0.11	0.26
20:80	5.0	0.76	3.0
10:90	2.3	1.2	3.8

[#]Fluorescein dye in ethanol used as a reference standard for measuring relative fluorescence quantum yield (%).

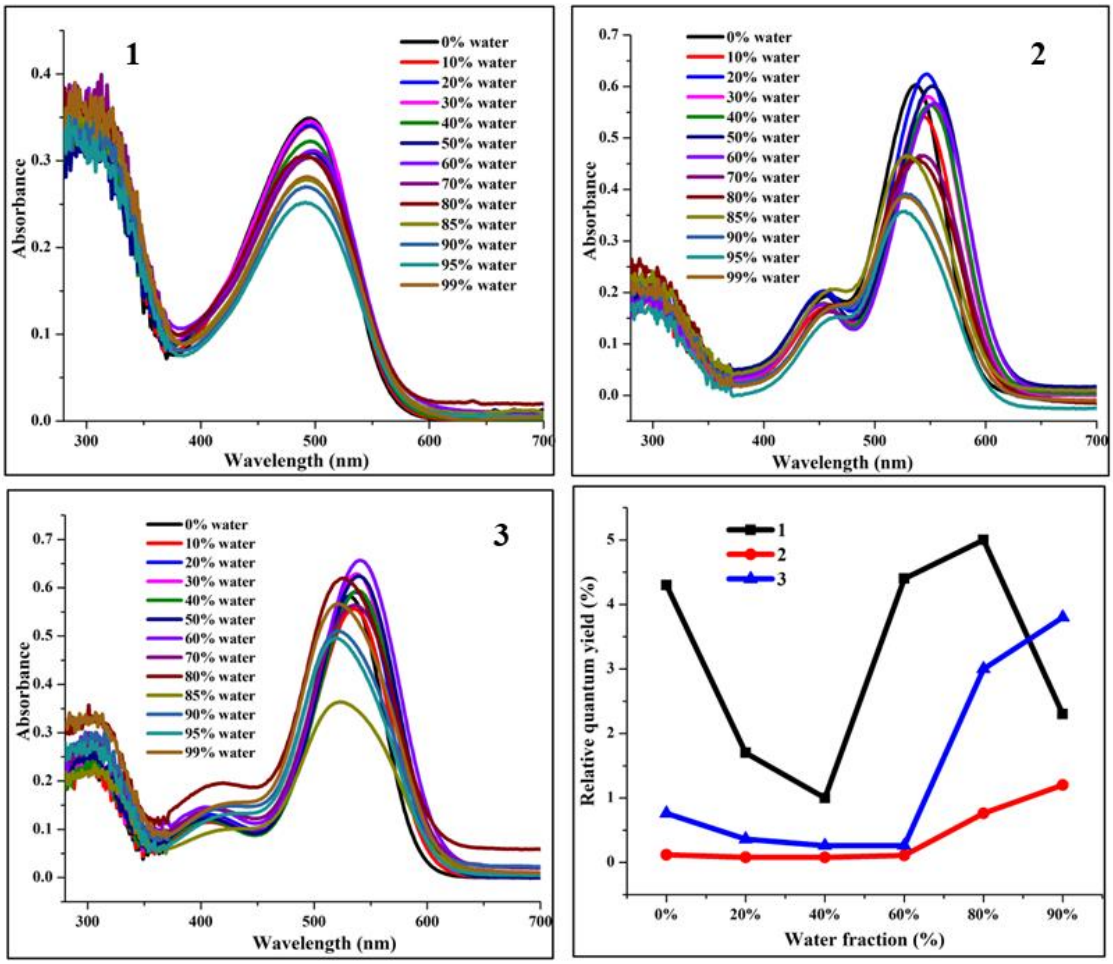

Figure 2C.7. UV-Vis spectra of compounds **1-3** (1.5 x 10^{-5} M) in a THF/H_2O mixture with different waterfraction (f_w). Relative quantum yield (%) plot of **1-3** with different percentage of water (bottom right).

2C.2.4 Electrochemical studies

The electrochemical properties of compounds **1-4** were studied by cyclic voltammetry (CV) in N_2 purged dichloromethane at 298 K using $^nBu_4N[PF_6]$ as a supporting electrolyte. All the boron compounds **1-4** exhibit one boron-centred reversible reduction ranging from -1.16 to -1.49 V (**Figure 2C.8 and Table 2C.6**). Compounds **2** and **3** showed reduction potential similar to each other (-1.31 V) indicating that TPE and DMA interchange does not affect the electronic nature on the boron. Compound **4**, showed the reversible reduction (-1.49 V) at more negative due to the presence of electron-donating -NMe_2 groups. Apart from that, all four compounds showed quasi-reversible oxidations

ranging from 0.66 V to 1.28 V (**Figure 2C.8 and Table 2C.6**). Compounds **2** and **3** showed similar oxidation potentials (first oxidation potential is located at 0.83 V for **2** and 0.88 V for **3**; the second oxidation potential is located at 1.13 V for **2** and 1.18 V for **3**) whereas, compound **4** showed less positive value (first oxidation potential is located at 0.66 V; the second oxidation potential is located at 0.88 V). The first oxidation wave is related to $–NMe_2$ groups (in case of **2-4**) and the second oxidation wave is corresponding to the oxidation of the TPE unit in case of **1-3** and NMe_2 in case of **4**. For comparison, we also performed CV of compound **4a** in dichloromethane, which showed the reversible reduction at -1.78 V. This observed value is more negative than the O,S-chelated boron compounds (**1-4**), and also showed quasi-reversible oxidations at 0.66 V and 1.04 V (Table 3). The first oxidation potential of **4a** and **4** are similar (0.66 V), and the second oxidation potential of **4a** showed a higher value (1.04 V) compared to compound **4** (0.88 V). The obtained notable change in the oxidation potential may be due to the presence of sulphur atom in the case of **4.**

The HOMOs and LUMOs of compounds **1-4** are estimated using UV-Vis absorption and cyclic voltammetry data (**Table 2C.5**). The HOMO levels fall in the range of -5.23 to -5.63 eV whereas the LUMOs fall in the range of -3.12 to -3.44 eV. Electron-donating $-NMe_2$ group destabilize the HOMOs and LUMOs of compounds **2-4** in comparison with **1**. A comparison of compound **4** (O,S-chelated) vs compound **4a** (O,O-chelated) reveal that the HOMO-LUMO gap significantly reduced upon replacement of ‘O’ atom with ‘S’ atom, which is responsible for the red shift realized in the absorption and emission in **4** as well as the less negative potential realized in CV (**4**).

Table 2C.5. HOMO and LUMO levels derived from UV-Vis onset absorption and electrochemical data.

Compounds	HOMO-LUMO gap[a]	LUMO[b]	HOMO[c]
1	2.19	-3.44	-5.63
2	2.09	-3.28	-5.37

3	2.08	-3.33	-5.41
4	2.11	-3.12	-5.23
4a	2.33	-2.84	-5.17

[a]Absorption onset of the longest wavelength of UV band. [b]Calculated from E_{pc} of the reduction wave with reference to Fc/Fc^{+}. [c]Calculated from HOMO-LUMO gap and LUMO.

Table 2C.6. Electrochemical data for **1-4** and **4a**

Compounds	E_{pc}	E_{pa} (1and 2nd peak)
1	-1.16	1.15, 1.28
2	-1.31	0.83, 1.13
3	-1.31	0.88, 1.18
4	-1.49	0.66, 0.88
4a	-1.78	0.66, 1.04

[#]E_{pc} = cathodic peak potential, [#]E_{pa} = anodic peak potential

Cyclic voltammetry studies of compounds **1-4** and **4a** (vs Ferrocene/Ferrocenium) were performed with 0.1M of $NBu_4(PF_6)$ in CH_2Cl_2 as the supporting electrolyte (scan rate 100 mV/s).

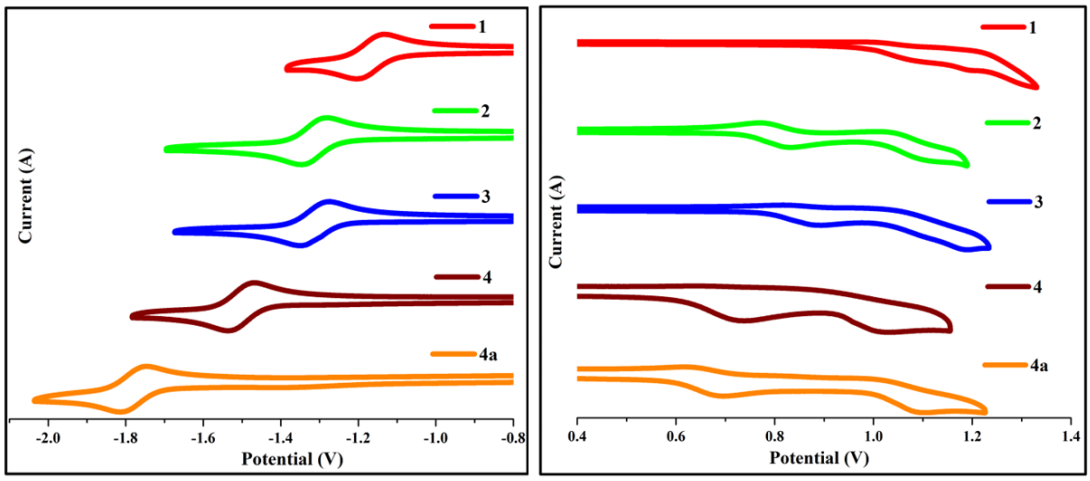

Figure 2C.8: Cyclic voltammogram of compounds **1-4** and **4a** (vs Ferrocene/Ferrocenium) with 0.1M of $NBu_4(PF_6)$ in CH_2Cl_2 as the supporting electrolyte (scan rate 100 mV/s). [reduction potential (left) and oxidation potential (right)].

2C.2.5 Cyanide ion sensing

Cyanide ion is one of the chemical widely used in chemical and industrial process.[31] Moreover, cyanide ion is also know for its extreme toxicity to human health.[32] Hence, detection of cyanide ion is important and has attracted attention of different groups. Different strategies for detecting cyanide ion have been developed.[33] Among the various methods, boron based cyanide detecting methods attracted to a greater attention. The

reversible binding of cyanide and fluorides to tri-coordinated boranes were exploited by different groups.[34] However, the use of tetra-coordinated boranes as probes for cyanide detection is scarcely reported.[35] Inspired by theses studies we explored the utility of our red emissive O,S-chelated boron compounds for detecting cyanide ion. To determine the sensing property of the compounds **1-4**; different equivalents of cyanide ion was added and the absoption and emission of the compounds were monitored (**Figure 2C.9 – 2C.12)**. As shown in **Figure 2C.9**, the absoprtion band at 486 nm and the emission band at 761 nm of compound **1** gradually decreased upon sequential addition of cyanide ion. When 3 equivalents of cyanide ion was added to the solution of compound **1**, the absorption band at 441 nm and the emission band at 684 nm disappeared and can be noticed by naked eye.

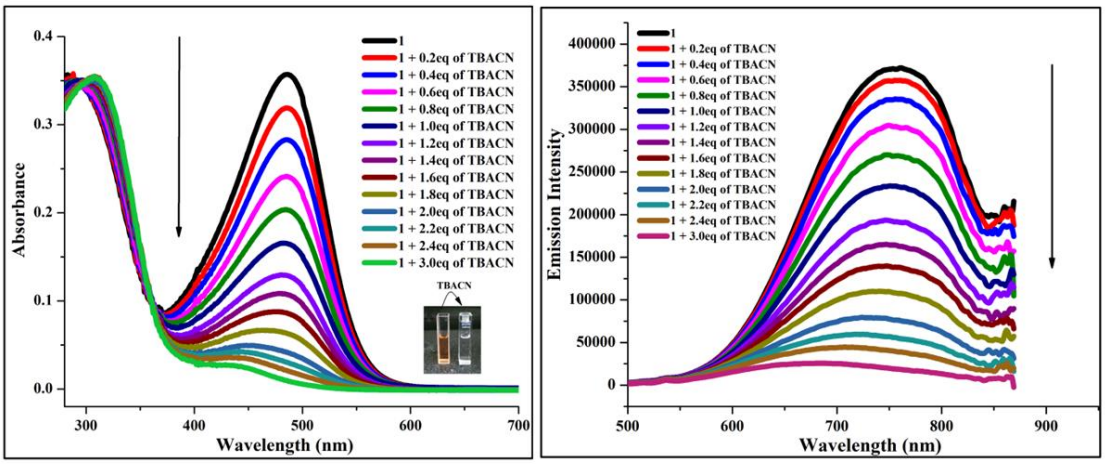

Figure 2C.9. Absorption spectra (Left) and emission spectra (Right) of boron compound **1** (1.0×10^{-5} M) with the addition of TBACN in acetonitrile

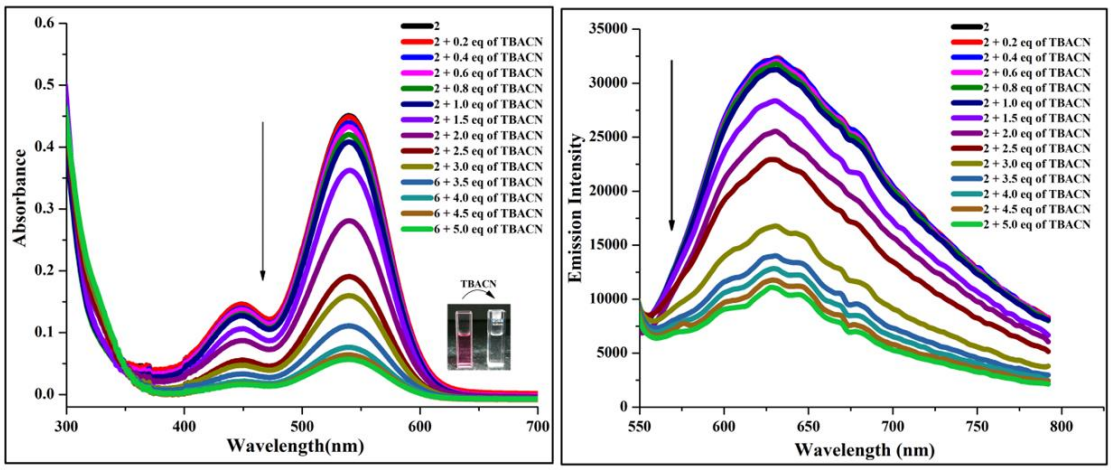

Figure 2C.10. Absorption spectra (Left) and emission spectra (Right) of boron compound **2** (1.0 x 10^{-5} M) with the addition of TBACN in acetonitrile

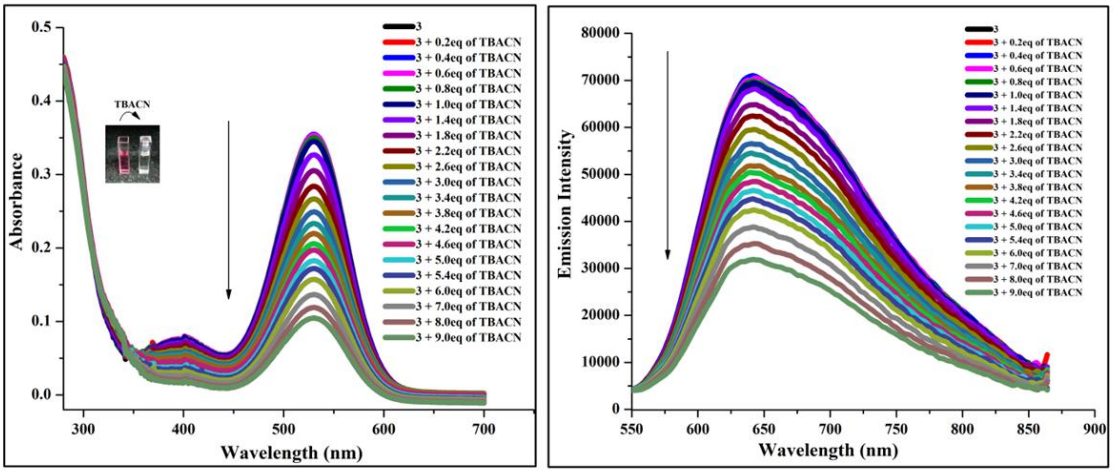

Figure 2C.11. Absorption spectra (Left) and emission spectra (Right) of boron compound **3** (1.0 x 10^{-5} M) with the addition of TBACN in acetonitrile

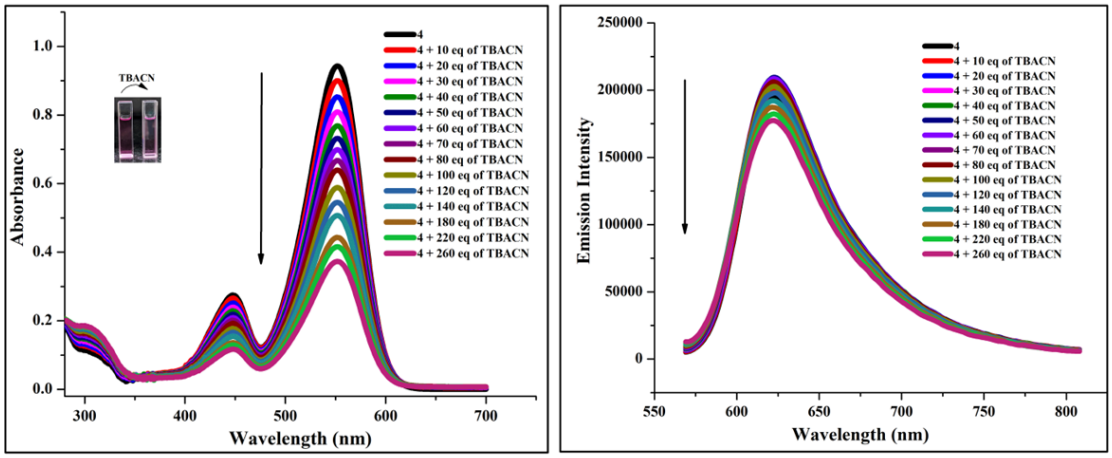

Figure 2C.12. Absorption spectra (Left) and emission spectra (Right) of boron compound **4** (1.0 x 10^{-5} M) with the addition of TBACN in acetonitrile

As selectivity is an important criteria for the success of a probe, we measured the fluorescence spectra of compound **1** with various other anions such as F^-, Br^-, Cl^-, I^-, HSO_4^-, NO_3^-, AcO^-, PF_6^-. As shown in **Figure 2C.13**, non of these anions showed any significant change upon addition of these anions to a solution of compound **1**. This result suggest that compound **1** act as a selective probe for detecting cyanide ion. Although compounds **2** and **3** showed a similar quenching behaviour (**Figure 2C.14 and Figure 2C.15**), they required 5 and 9 equivalents of cyanide ion respectively inorder to notice the quenching with nacked eye. On the other hand, compound **4** did not show appreciable quenching even after adding 240 equivalents of cyanide ion (**Figure 2C.16**).

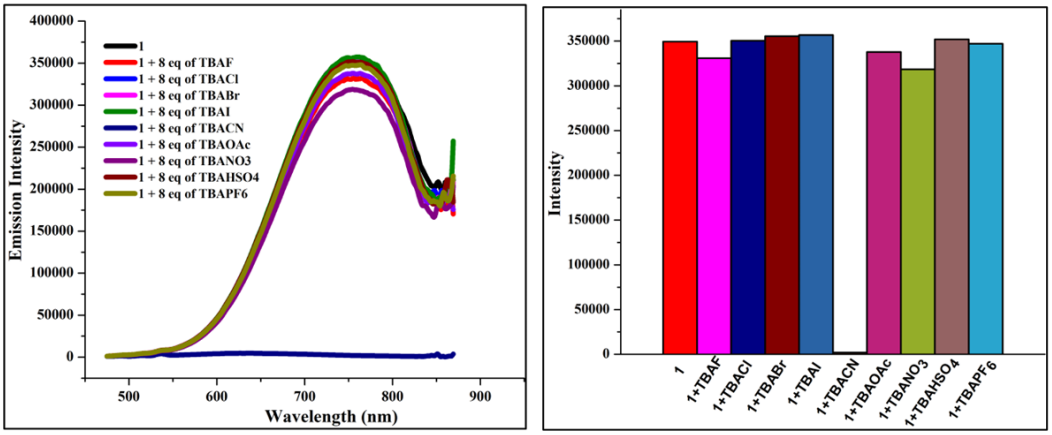

Figure 2C.13. Emission spectra (Left) of compound **1** (1 x 10^{-5} M) with various anions (8.0 equiv) in acetonitrile and selectivity bar diagram (Right) of compound **1** in presence of various anions (F^-, Cl^-, Br^-, I^-, CN^-, OAc^-, NO_3^-, HSO_4^-, PF_6^-) (8.0 equiv) in acetonitrile.

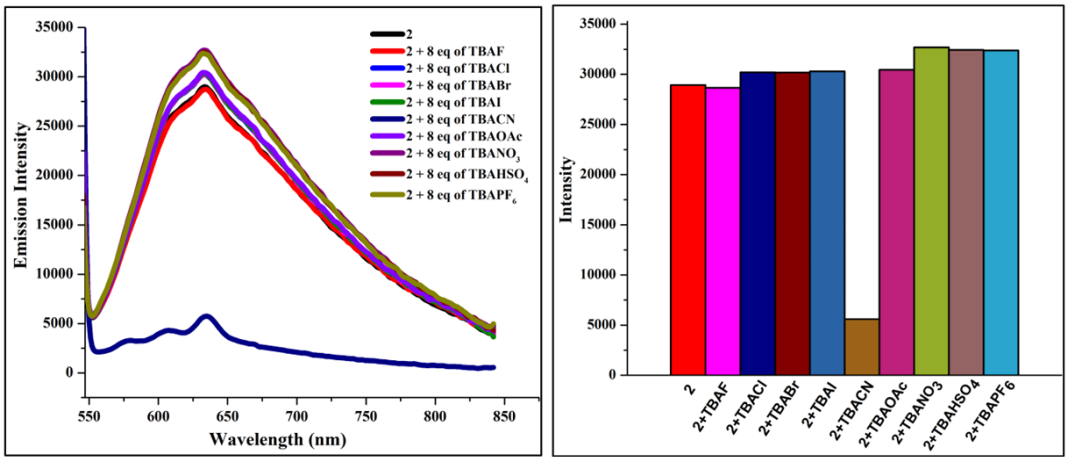

Figure 2C.14. Emission spectra (Left) of compound **2** (1 x 10^{-5} M) with various anions (8.0 equiv) in acetonitrile and selectivity bar diagram (Right) of compound **2** in presence of various anions (F^-, Cl^-, Br^-, I^-, CN^-, OAc^-, NO_3^-, HSO_4^-, PF_6^-) (8.0 equiv) in acetonitrile.

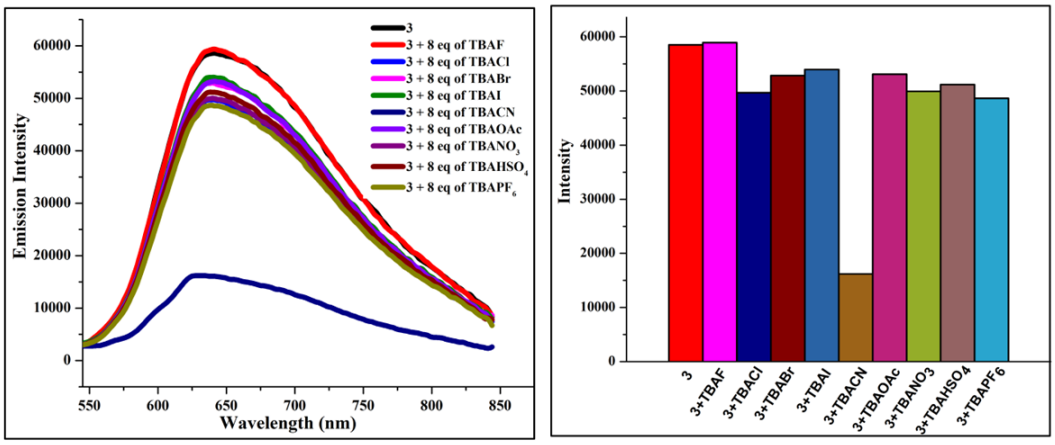

Figure 2C.15. Emission spectra (Left) of compound **3** (1 x 10^{-5} M) with various anions (8.0 equiv) in acetonitrile and selectivity bar diagram (Right) of compound **3** in presence of various anions (F^-, Cl^-, Br^-, I^-, CN^-, OAc^-, NO_3^-, HSO_4^-, PF_6^-) (8.0 equiv) in acetonitrile.

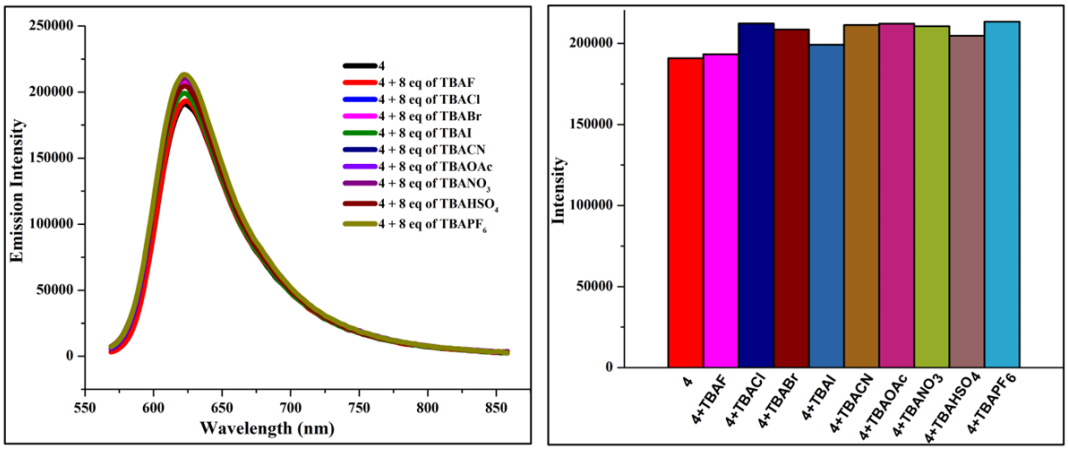

Figure 2C.16. Emission spectra (Left) of compound **4** (1 x 10^{-5} M) with various anions (8.0 equiv) in acetonitrile and selectivity bar diagram (Right) of compound **4** in presence of various anions (F^-, Cl^-, Br^-, I^-, CN^-, OAc^-, NO_3^-, HSO_4^-, PF_6^-) (8.0 equiv) in acetonitrile.

To realize the detection mechanism, we carried out NMR experiments. In the ^1H NMR of compound **2** the olefenic proton (H_e) appeared at 7.64 ppm. Upon sequential addition of cyanide ion, the proton H_e got upfield shifted to 5.96 ppm. The ^{11}B NMR of compound **2** is reminescent after the addition of cyanide ion which indicates that the coordination around boron center has not changed (**Figure 2C.19**). The ^{19}F {^1H} NMR of compound **2**

showed three sets of peaks, however, upon addition of cyanide ion six sets of peaks were observed which indicates that both $–C_6F_5$ experienced different enviornment **Figure 2C.18**.

(a)

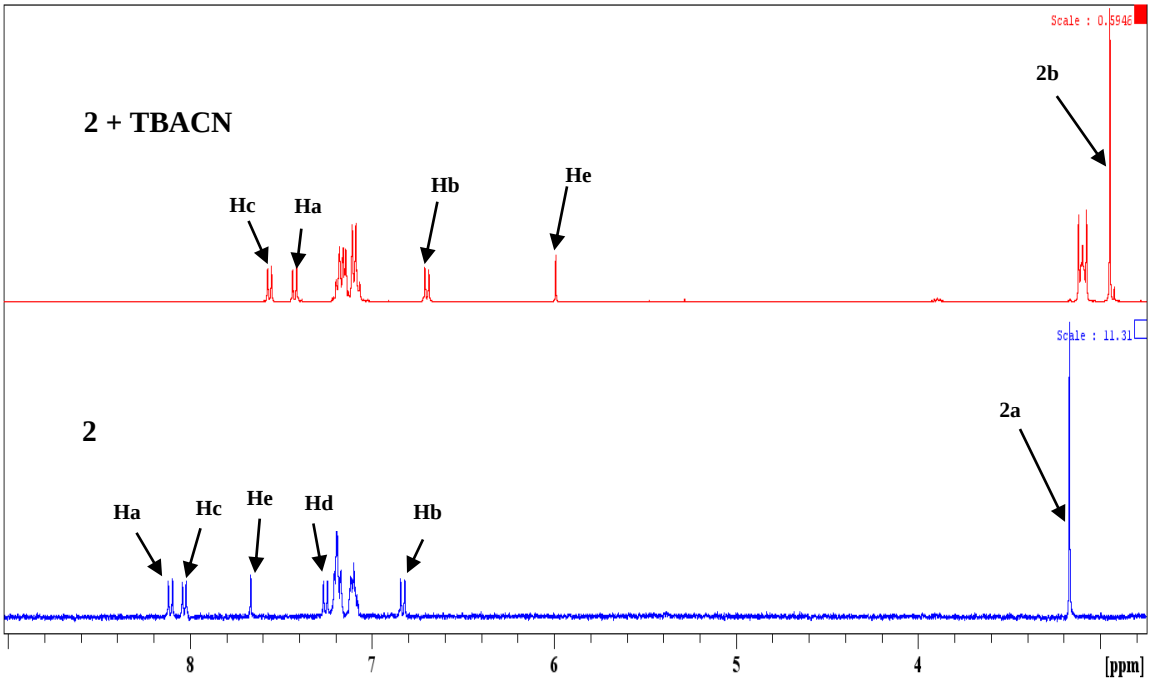

(b)

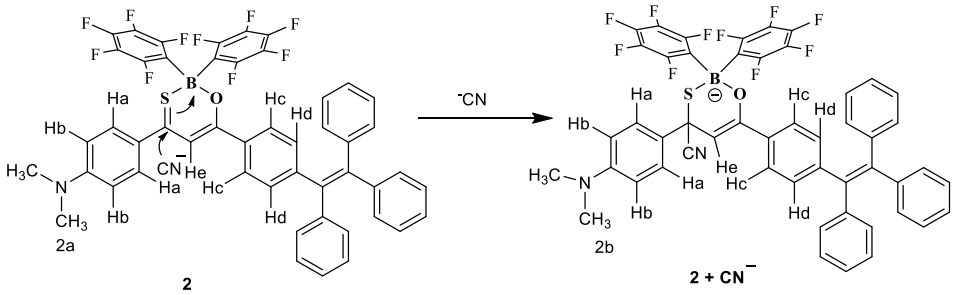

(c)

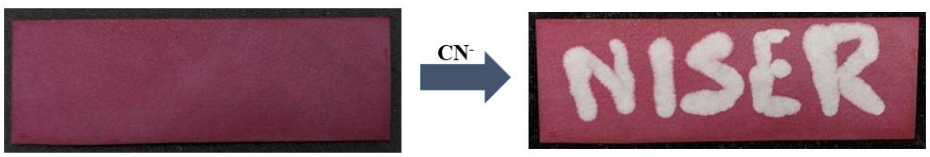

Figure 2C.17. (a) ^{1}H-NMR spectrum of **2** and **2** + TBACN (2.0 equvi) (CD_3CN) 400MHz. (b) Plausible sensing mechanism. (c) Test strip detection using compound **2**.

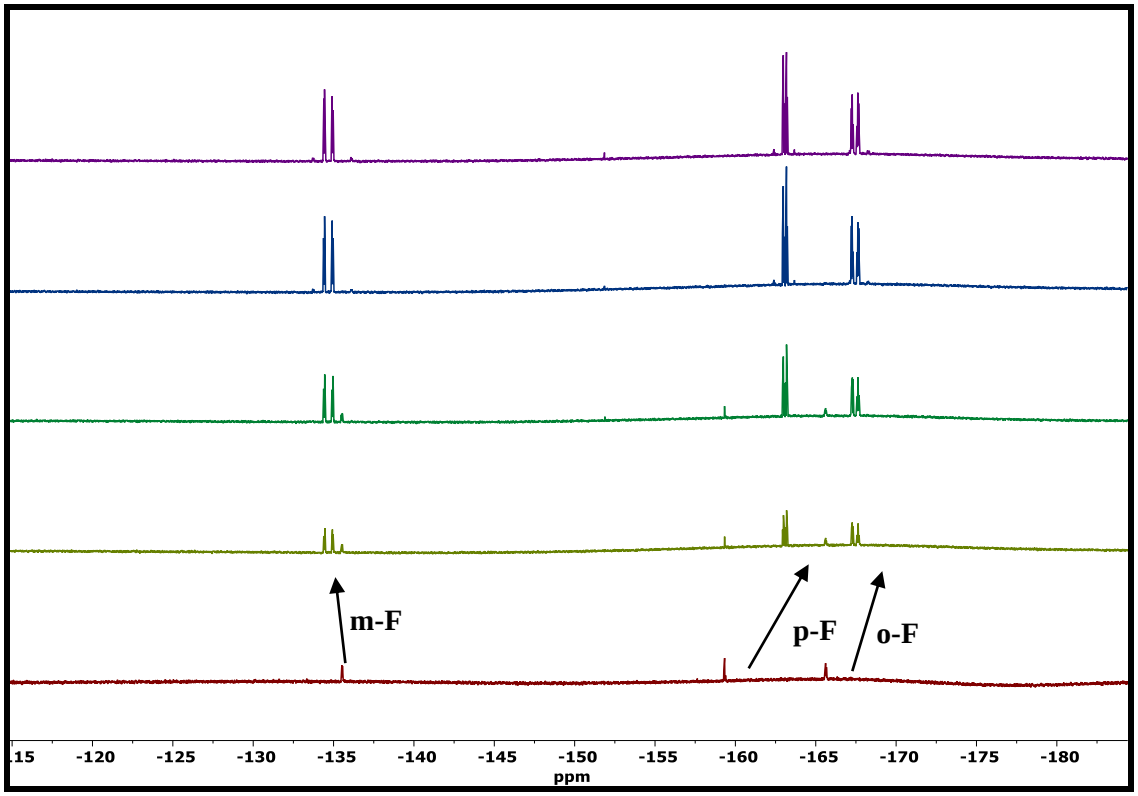

Figure 2C.18. ^{19}F-NMR spectrum of **2** with sequential addition of 0.4eq of TBACN (CD_3CN) in 400 MHz

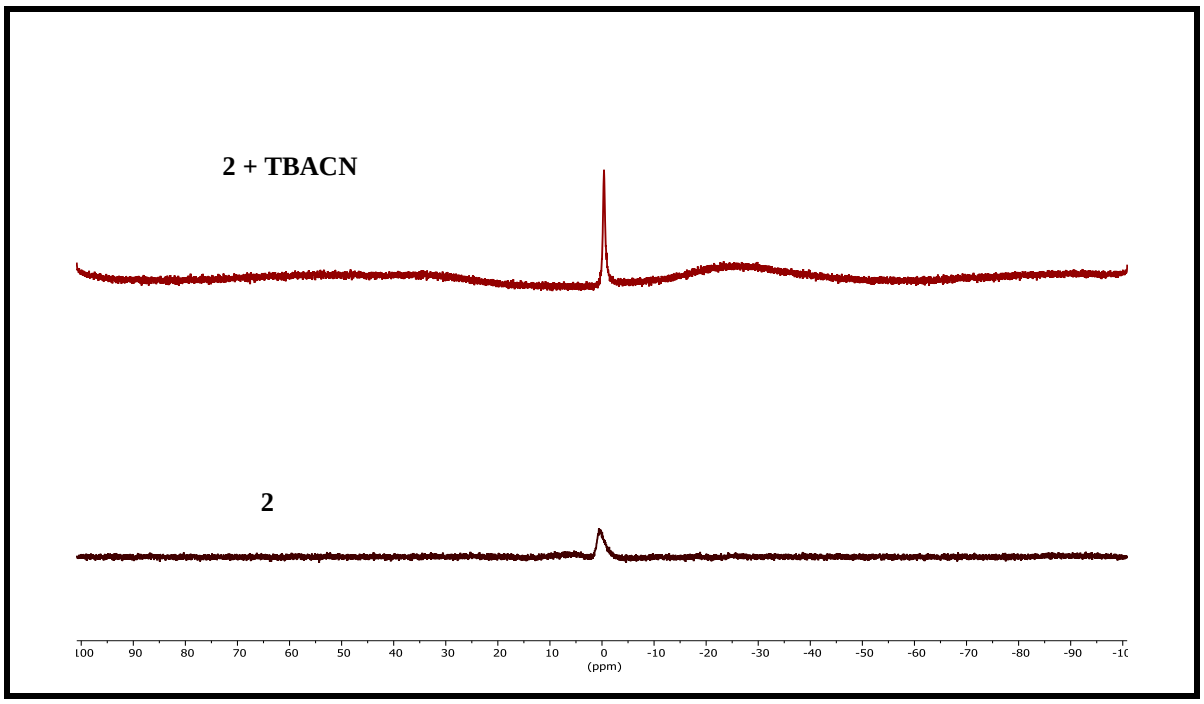

Figure 2C.19. Stacked ^{11}B-NMR spectrum of **2** and **2+TBACN** (2.0 equvi) (CD_3COCD_3) in 400 MHz

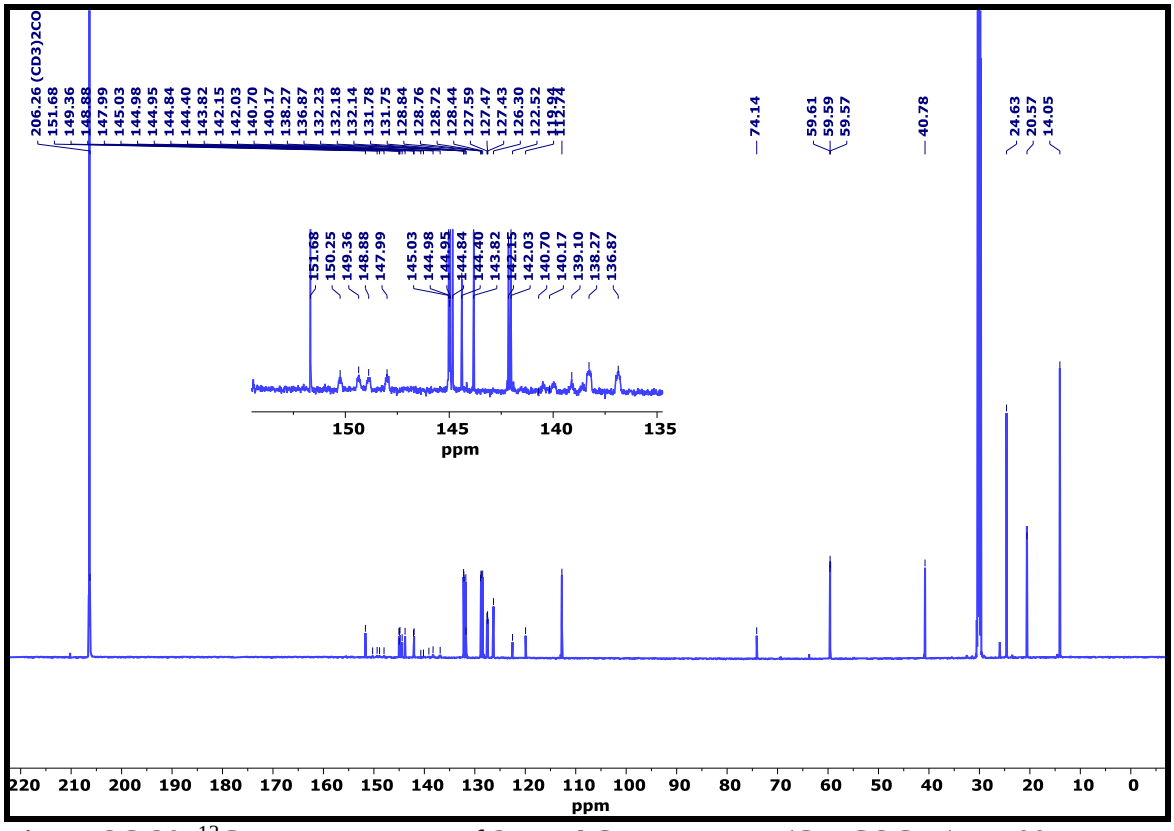

Figure 2C.20. ^{13}C-NMR spectrum of **2+TBACN** (2.0 equvi) (CD_3COCD_3) in 700 MHz

Furthermore, compound **2** showed peaks at 185 and 177 ppm in the ^{13}C NMR which corresponds to C=S and C=O groups respectively (**Figure 2C.20**). Upon addition of cyanide ion they disappeared and got upfield shifted. Based on these studies, we propose a plausible attacking site of the molecule and the detection mechanism involved in this system as shown in **Figure 2C.17 (b).**

2C.2.6 Non-linear optical properties

In order to explore the $\chi^{(3)}$ induced NLO response of the compounds **1-4** and **4a**, we carried out single-beam Z-scan transmission measurements using an ultrashort pulse fiber laser emitting ≈ 400 fs pulses centred at 1030 nm wavelength. The details of the experimental configuration are provided in the **2C.4.2** Z-scan experiment. The measured open-aperture (OA) normalized transmittance for compounds **1-4** and **4a** is presented in **Figure 2C.21**, (black dots), which exhibits a characteristic TPA signature. It is apparent

that the transmission minima at the focus for **1** and **2** is relatively higher as compared to the transmission minima for **3**, **4**, and **4a**. It is worthwhile to note that all the measurements were carried out at on-axis peak intensity (at focal point) of $I_0 = 1.3 \times 10^{12} W/cm^2$. In order to quantitatively estimate the TPA coefficient (β), the experimental measurements were fitted using the relation as given below.[36, 37]

$$T(x) = 1 - \frac{\beta I_0 L_{eff}}{2^{3/2}(1+x^2)} \quad \ldots\ldots\ldots\ldots\ldots\ldots\ldots\ldots (1)$$

The estimated values of β for all the compounds are tabulated in **Table 2C.5**. The β for compound **1** is the least whereas compounds **4** and **4a** exhibit the largest values of β. In general, the first-order hyperpolarizability (responsible for NLO response) bears an inverse variation with the HOMO-LUMO gap owing to the ease of electron delocalization upon optical excitation.[38, 39] This provides an acceptable basis for a small value of β for **1** and a greater value of β for **3**. A significant jump in the value of β could be observed in the case of compound **2** with respect to that of **1**. This is essentially a consequence of introducing the group 'NMe_2' which exhibits a strong tendency of donating electron for attaining thermodynamic equilibrium. Consequently, this results in an overall increase in conjugation length that manifests through a significant enhancement in β. It is interesting to note that compound **4** exhibits the largest value of β despite a higher HOMO-LUMO gap. This is essentially a consequence of introducing two 'NMe_2' groups that brings down the dihedral angle (see **Table 2C.1**). In fact, compounds **4** and **4a** could be assumed to be planar. A smaller dihedral angle provides a low resistive charge-transfer path, thereby increasing the possibility of high first-order hyperpolarizability.[40] With respect to the compound **4**, the compound **4a** has a smaller β owing to the absence of sulphur; in general stronger change in dipole moment (of the molecule) upon excitation through π-delocalization is responsible for high β, which is facilitated by the presence of Sulphur.

Table 2C.7: Nonlinear optical coefficients of the compounds **1-4** and **4a** at the fixed excitation wavelength of 1030 nm.

Sample	***β (cm/W)***	***n_2 (cm^2/W)***
Compound **1**	1.604×10^{-12}	1.040×10^{-16}
Compound **2**	4.121×10^{-12}	1.246×10^{-16}
Compound **3**	5.442×10^{-12}	8.226×10^{-17}
Compound **4**	6.236×10^{-12}	1.400×10^{-16}
Compound **4a**	5.542×10^{-12}	1.237×10^{-16}

Further, we have carried out closed-aperture (CA) Z-scan experiment to ascertain the applicability of the compounds for optical switching applications. It is worth mentioning that the depth and speed of optical switching is determined by the underlying mechanism driving the third-order optical nonlinearity. Usually, the thermal nonlinearities are slow, but they result in a large nonlinear refractive index (n_2). The optical nonlinearity arising due to electron transport are, in general, very fast (a few tens of femtosecond time-scale). In order to measure n_2 having a predominant electronic origin, we carry out the Z-scan transmittance measurements using ultrashort pulses (< 400 fs) and a low repetition rate laser. The measured normalized transmittance in CA Z-scan for compound **1** is presented in **Figure 2C.22** (black dots). A valley-to-peak variation is exhibited by all the compounds which is a signature of positive value of nonlinear refractive index (n_2). In other words, all the compounds exhibit self-focusing characteristics. In order to quantitatively estimate n_2, we use the following expression to carry out a theoretical fitting to the experimental measurements.[41]

$$T(x) = 1 - \frac{4\Delta\phi_0 x}{(x^2+9)(x^2+1)} - \frac{2(x^2+3)\Delta\Psi_0}{(x^2+9)(x^2+1)} \quad \ldots\ldots\ldots\ldots\ldots(2)$$

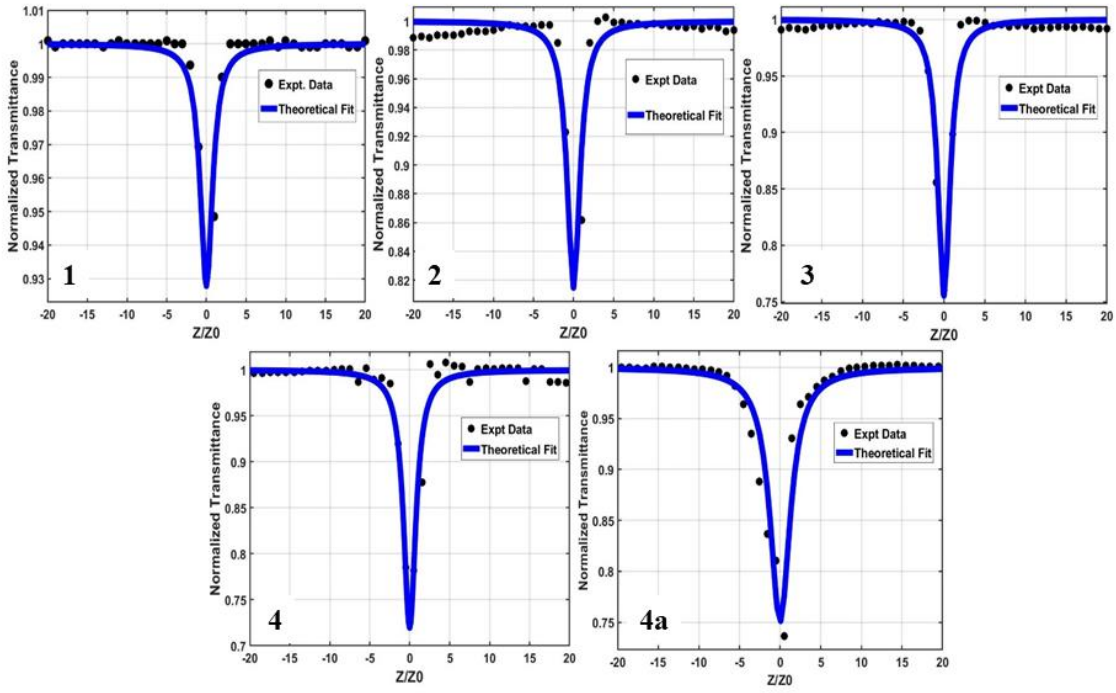

Figure 2C.21. The plot of normalized transmittance as a function of sample position for open-aperture Z-scan of compounds **1-4** and **4a** in THF (10^{-5} M) respectively.

The n_2 values are estimated to be 1.040×10^{-16}, 1.246×10^{-16}, 8.226×10^{-17}, 1.400×10^{-16} and 1.237×10^{-16} cm^2/W for compounds **1-4** and **4a** respectively. The non-linear refractive indices (n_2) for all the compounds remain almost in the similar range with n_2 for compound **3** being marginally smaller than the rest. In CA Z-scan measurements, it is apparent that the coplanarity in the molecular structure plays a discernible role. For example, the difference between the angular orientation of planes A and C is maximum for compound **3** resulting in a higher dihedral angle. This manifests through a smaller value of n_2. On the other hand, the dihedral angle is very small in case of compound **4**, which results in the highest value for n_2. It could also be observed that the impact of NMe_2 on n_2 is weak implying that the role of conjugation length on n_2 is relatively weaker in this case.

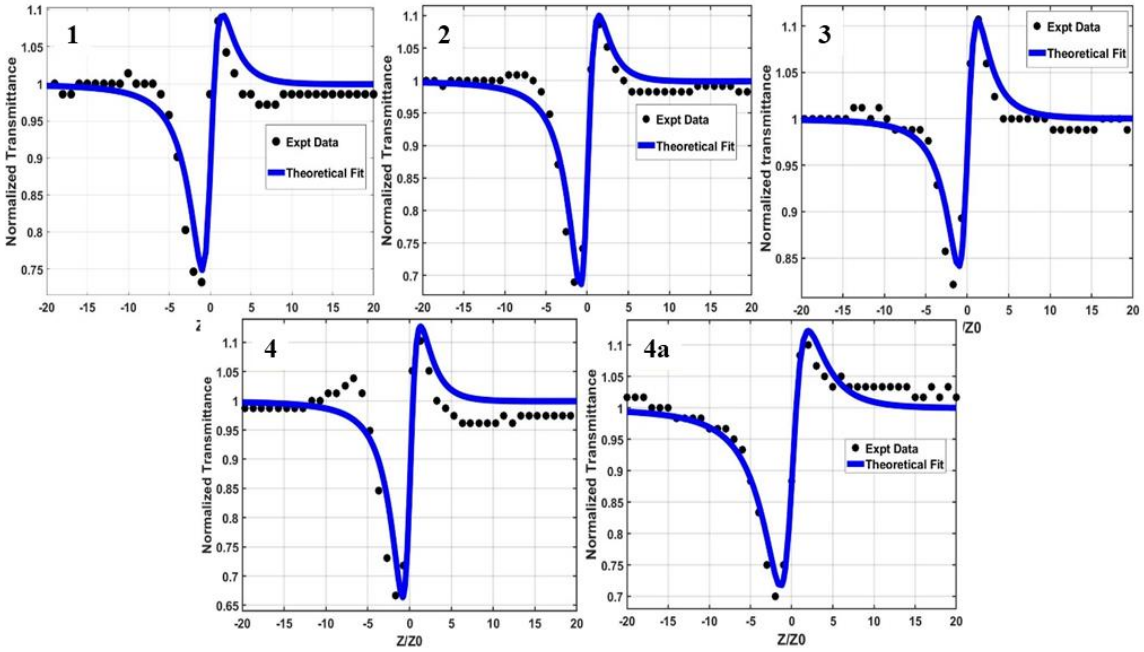

Figure 2C.22. The plot of normalized transmittance as a function of sample position for closed-aperture Z-scan of compounds **1-4** and **4a** in THF (10^{-5} M) respectively.

2C.3 Conclusion

In summary, we have designed and successfully synthesized a series of TPE and DMA decorated monothio-β-diketonate boron compounds. All these compounds exhibit red emission both in solution and in the solid state. TPE motif substituted molecules **1-3** showed AIEE phenomenon, whereas the DMA substituted on both sides exhibited aggregation caused quenching. The electrochemical studies reveal that these molecules showed one electron reversible reduction and two separate irreversible one-electron oxidation events. The OA and CA Z-scan measurements reveal that all the compounds exhibit a TPA behaviour at infrared excitation wavelength and self-focusing effect. The impact of π-electron delocalization and the dihedral angle on the NLO response is analyzed for all the compounds. The strong TPA signature indicates the possibility of potential deployment in optoelectronics-based information transport and in optical limiting architectures. Furthermore, monothio-β-diketonate boron compounds (**1-3**) offer

selective detection of cyanide ion both colorimetrically and fluorimetrically. These results indicate that O,S-chelation is a promising strategy to make red emissive materials. This strategy is expected to further tune the optical properties to make red or near-IR emissive O,S-chelated dyes for OLED and biomedical applications.

2C.4 Experimental section

2C.4.1 General information

All the reactions were carried out under N_2 atmosphere using standard glove box, Schlenk line and vacuum line techniques. Dry solvents used for the reactions were dried according to the standard procedures. All the reactions were monitored by thin layer chromatography. Nuclear magnetic resonance spectra were recorded on a 400 MHz or 700 MHz Fourier transform NMR spectrometer (JEOL or Bruker) with $CDCl_3$ as a solvent. ^{11}B and ^{19}F NMR spectra were externally referenced to $BF_3.Et_2O$ in $CDCl_3$ (δ=0 ppm) and α,α,α-trifluoro toluene in $CDCl_3$ (δ=-63.73 ppm), respectively. Chemical shifts are reported in δ ppm (parts per million) using residual solvent protons as the internal standard (δ 7.26 for $CDCl_3$ in ^1H NMR, δ 77.16 for $CDCl_3$ in ^{13}C NMR). Coupling constants are reported as J values in hertz (Hz). Splitting patterns are designated as s(singlet), d(doublet), t(triplet), q(quartet), dd(doublet of doublet), dt(doublet of triplet), m(multiplet) and br(broad). HRMS were recorded using Waters XEVO G2-XS QTOF mass spectrometer. Elemental analyses were performed in a Euro Vector EA 3000 CHNS analyzer. UV – Visible spectra were recorded on Agilent Technologies Cary 60 UV/Visible spectrometer. Fluorescence spectra and quantum yield were measured using Edinburgh specrofluorimeter instrument FS5. For the measurement of absolute quantum yield, the concentration of the boron compounds was such as to give an absorbance of around 0.1 at excitation wavelength. Absolute total quantum yields were measured using an integrating sphere (Edinburgh instrument FS5) mounted in SC-30 compartment of the

spectrofluorimeter, Single crystal X-ray diffraction data were collected on a Bruker APEX-II CCD diffractometer using CuKα (λ = 1.54184) radiation. The structure were solved by direct methods using SHELXT program and refined with least squares minimization with SHELXL using Olex2. The standard three electrode arrangement used for cyclic voltammetry included an Ag wire serving as the reference electrode, a Pt wire serving as the secondary electrode, and a glassy carbon working electrode. About 1.0 x 10^{-3} M solution in CH_2Cl_2 with $[Bu_4N][PF_6]$ (0.1 M) as a supporting electrolyte was used to record the voltammogram. The scans were referenced with a small amount of ferrocene as an internal standard.

In view of the strong emission characteristics of AIE of the complex **1-3**, relative luminescence quantum yields are calculated by comparing the emission intensities of the standard sample (Fluorescein dye in ethanol) and the unknown sample using the following equation:

$$\Phi_{unk} = \Phi_{std}(I_{unk}/I_{std})(A_{std}/A_{unk})(\eta_{unk}/\eta_{std})^2$$

where Φ_{unk} and Φ_{std} are the luminescence quantum yields of the unknown sample and standard sample, respectively, and I_{unk} and I_{std} are the integrated emission intensities of the unknown sample and standard sample solution, respectively. A_{unk} and A_{std} are the absorbances of the unknown sample and standard sample solution at their excitation wavelengths, respectively.

The η_{unk} and η_{std} (ethanol) terms represent the refractive indices of the corresponding solvents

$$\eta_{unk} = \chi_{THF}\,\eta_{THF} + \chi_{water}\,\eta_{water}$$

χ = mole fraction

2B.4.2 Z-scan experiment

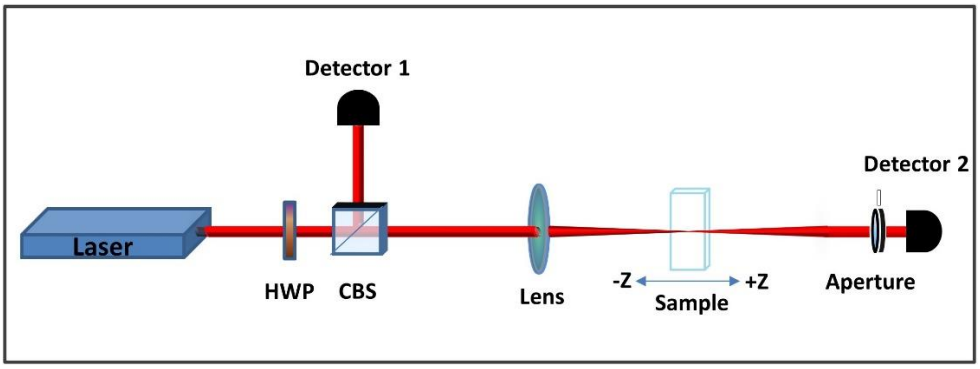

Figure 2C.23. Schematic diagram of the Z-scan experimental setup. (HWP: half-wave plate; CBS: cube-beam splitter)

The schematics of the Z-scan experimental set-up used for the NLO coefficient measurement is shown in **Figure 2C.23**. An Yb-doped fiber laser (Cazadero,M/S Calmar Inc., USA) emitting pulses of pulse duration 400 fs at 1 kHz repetition rate is used for the experiment. The fundamental laser beam at excitation wavelength 1030 nm is used to measure the nonlinear optical (NLO) coefficients such as nonlinear refractive index coefficient (n_2) and absorption coefficient (β). Spatially, the laser beam is 5 mm wide (diameter) with a near Gaussian spatial profile ($M^2 < 1.05$) and it is polarized in the plane of the optical table (horizontal polarization). A combination of half wave plate and a cube-beam splitter is to variably attenuate the beam and control the fluence on the sample. The beam is focused to a spot-size of ≈ 52 μm using a plano-convex lens of 100 mm focal length. The samples are translated by ≈ 10 cm about the focal point. The transmitted optical power is measured using a photodetector with an aperture of suitable diameter (for closed-aperture). It is worth noting that the reported compounds exhibit linear absorption bands in the visible spectral band of the electromagnetic-spectrum (see **Figure 2C.2**). Consequently, the nonlinear absorption measurements are carried out at near-infrared *i.e.* at 1030 nm excitation wavelength. All the calculations of NLO

coefficients for the complexes were carried out with respect to the standard CS_2 solvent under identical experimental conditions.

Starting materials: 1-Bromo-4-(1,2,2-triphenylethynyl)-benzene, 1-(4-(1,2,2-triphenylvinyl)phenyl)ethan-1-one (**1a)**, 1-(4-(dimethylamino)phenyl)ethan-1-one (**1c**), were prepared according to the reported literature procedure.[42-44] Compound **1a** can also prepared by Friedel Craft acylation reaction. 1,1,2,2-Tetraphenylethylene, 4-bromo-N,N-dimethylaniline, 4-bromoaniline, Methyl iodide, Carbon disulphide, Potassium carbonate, Acetyl chloride, Anhydrous Aluminium trichloride, Magnesium flakes, Anhydrous Zinc chloride, Titanium tetrachloride, Sodium hydride, Tris(pentafluorophenyl)borane were purchased from Sigma-Aldrich, Spectrochem, Alfa-Aesar.

2C.4.3 Synthetic procedure and spectral characterization

General procedure for the synthesis of 1,3-monothio-β-diketones (L1-L4):

A two neck RB was charged with acetophenone derivative (1.0 mmol) and DMF (10 mL) then NaH (2.2 mmol, 50%) was added under nitrogen atmosphere and stirred for 5 min. Then methyl benzodithioate derivative (1.2 mmol) in DMF (10 mL) was added dropwise at 0 °C. The reaction mixture was continuously stirred at room temperature for 5-8 h. After the completion of the reaction, (starting material consumption was monitored by TLC) it was poured into ice-cold water (40 mL), acidified with glacial acetic acid. The resultant orange coloured solid was filtered and purified using column chromatography (eluent: *n*-hexane/CH_2Cl_2). For compound **L1**, after the acidification, solid formation was not detected hence, the crude mixture was extracted with ethyl acetate (3 x 30 mL). The combined organic layers were washed with ice water, dried over Na_2SO_4 and concentrated under vacuum. The obtained viscous liquid was purified by silica gel column chromatography using *n*-hexane/ CH_2Cl_2 as eluent.

Synthesis of L1: The quantities involved are: 1-(4-(1,2,2-Triphenylvinyl)phenyl)ethan-1-one (0.50 g, 1.3 mmol), methyl 4-(1,2,2-triphenylvinyl)benzodithioate (0.62 g, 1.5 mmol) and NaH (50%, 0.07g, 2.9 mmol). Red solid, yield: 0.60 g (60%). **^{1}H NMR:** (400 MHz, $CDCl_3$) δ 15.86 (s, 1H), 7.73 (d, *J* = 8.4 Hz, 2H), 7.59 (d, *J* = 8.3 Hz, 2H), 7.36 (s, 1H), 7.16-7.08 (m, 22H), 7.06-6.99 (m, 13H). **^{13}C NMR:** (101 MHz, $CDCl_3$) δ 205.6, 178.1, 148.8, 147.4, 143.5, 143.4, 143.3, 143.3, 143.1, 142.8, 142.3, 140.0, 140.0, 133.1, 131.9, 131.6, 131.5, 131.5, 131.4, 131.4, 131.4, 128.0, 128.0, 127.9, 127.8, 127.8, 127.1, 127.0, 126.9, 126.8, 126.7, 126.4, 109.7. **HRMS** (ESI) m/z calcd for $C_{55}H_{39}OS$ ($[M-H]^+$): 747.2722, found: 747.2801.

Synthesis of L2: The quantities involved are: 1-(4-(1,2,2-Triphenylvinyl)phenyl)ethan-1-one (1.0 g, 2.7 mmol) , methyl 4-(dimethylamino)benzodithioate (0.62 g, 2.9 mmol) and NaH (50%, 0.14 g, 5.9 mmol). Red solid, yield: 1.15 g (80%). **^{1}H NMR:** (400 MHz, $CDCl_3$) δ 16.57 (s, 1H), 7.98 (d, *J* = 8.5 Hz, 2H), 7.74 (d, *J* = 8.1 Hz, 2H), 7.38 (s, 1H), 7.19-7.10 (m, 11H), 7.09-7.01 (m, 6H), 6.65 (d, *J* = 8.6 Hz, 2H), 3.07 (s, 6H). **^{13}C NMR:** (101 MHz, $CDCl_3$) δ 207.7, 174.7, 153.1, 147.9, 143.4, 143.3, 143.2, 142.4, 140.1, 133.6, 133.5, 131.8, 131.4, 131.4, 131.3, 129.4, 128.0, 127.9, 127.8, 127.0, 126.8, 126.2, 110.9, 106.3, 40.2. **HRMS** (ESI) m/z calcd for $C_{37}H_{30}NOS$ ($[M-H]^+$): 536.2060, found: 536.2043.

Synthesis of L3: The quantities involved are: 1-(4-(Dimethylamino)phenyl)ethan-1-one (0.60 g, 3.7 mmol), methyl 4-(1,2,2-triphenylvinyl)benzodithioate (1.7 g, 4.4 mmol) and NaH (50%, 0.19 g, 8.1 mmol). Dark red solid, yield: 0.70 g (36%). **^{1}H NMR:** (400 MHz, $CDCl_3$) δ 16.47 (s, 1H), 7.93 (d, *J* = 9.1 Hz, 2H), 7.63 (d, *J* = 8.4 Hz, 2H), 7.41 (s, 1H), 7.15-7.09 (m, 9H), 7.08-7.07 (m, 2H), 7.06 – 7.02 (m, 6H), 6.70 (d, *J* = 9.1 Hz, 2H), 3.09 (s, 6H). **^{13}C NMR:** (101 MHz, $CDCl_3$) δ 202.0, 179.0, 153.7, 146.6, 143.9, 143.7, 143.5, 142.1, 140.3, 131.5, 131.4, 131.4, 129.6, 128.0, 127.9, 127.8, 126.9, 126.7, 126.4, 121.4,

111.4, 109.0, 40.2. **HRMS** (ESI) m/z calcd for $C_{37}H_{30}NOS$ ($[M-H]^+$): 536.2048, found: 536.2043.

Synthesis of L4: The quantities involved are: 1-(4-(Dimethylamino)phenyl)ethan-1-one (1.0 g, 6.1 mmol), methyl 4-(dimethylamino)benzodithioate (1.6 g, 7.4 mmol) and NaH (50%, 0.32 g, 14.0 mmol). Dark red solid, yield: 0.72 g (36%). **^{1}H NMR:** (400 MHz, $CDCl_3$) δ = 16.78 (s, 1H), 7.96 (d, *J* = 8.0 Hz, 2H), 7.93 (d, *J* = 8.0 Hz, 2H), 7.43 (s, 1H), 6.71 (d, *J* = 8.0 Hz, 2H), 6.68 (d, *J* = 8.0 Hz, 2H), 3.08 (s, 6H), 3.06 (s, 6H). **^{13}C NMR:** (101 MHz, $CDCl_3$) δ = 203.7, 176.8, 153.2, 152.7, 130.5, 129.1, 129.0, 122.0, 111.4, 111.0, 105.9, 40.3, 40.2. **HRMS** (ESI) m/z calcd for $C_{19}H_{21}N_2OS$ ($[M-H]^+$): 325.1361, found: 325.1369.

General procedure for the synthesis of boron compounds (1-4):

1,3-Monothio β-diketone (1.0 mmol) and tris(pentafluorophenyl)borane (1.2 mmol) were taken in a nitrogen flushed pressure tube. Dry toluene (10 mL) was transferred to the tube and the reaction mixture was continuously stirred at 110 °C for 24 h. The crude mixture was transferred to 100 mL RB flask; the solvent was removed using rota-evaporator; the obtained crude product was subjected to column chromatography on neutral alumina using *n*-hexane/EtOAc mixtures to yield the desired boron compounds.

Synthesis of boron compound 1: The quantities involved are: Compound **L1** (0.35 g, 0.46 mmol) and tris(pentafluorophenyl)borane (0.26 g, 0.51 mmol). Red powder, yield: 0.30 g (60%). **^{1}H NMR:** (400 MHz, $CDCl_3$) δ 7.93 (d, *J* = 8.4 Hz, 2H), 7.64 (d, *J* = 8.3 Hz, 2H), 7.51 (s, 1H), 7.21 (d, *J* = 8.3 Hz, 2H), 7.17 – 7.15 (m, 8H), 7.14 – 7.09 (m, 9H), 7.07-6.97 (m, 14H). **^{13}C NMR:** (101 MHz, $CDCl_3$) δ 189.0, 181.1, 152.0, 150.6, 147.7 (d, *J* = 241 Hz), 144.1, 143.6, 143.1, 143.1, 143.0, 142.8, 140.4 (d, *J* = 257 Hz), 139.7, 139.5, 137.2 (d, *J* = 251 Hz), 137.0, 132.3, 132.2, 131.5, 131.4, 131.4, 129.4, 128.2, 128.1, 128.0, 127.8, 127.4, 127.3, 127.1, 127.1, 110.2. **^{11}B NMR:** (128 MHz, $CDCl_3$) δ =

0.77 (s). **^{19}F NMR:** (376 MHz, $CDCl_3$) δ -134.03 (d, 4F, Pf), -156.51 (t, 2F, Pf), -163.22 (t, 4F, Pf). **HRMS** (TOF MS ASAP+) m/z calcd for $C_{67}H_{40}BF_{10}OS$ ($[M+H]^+$): 1093.2770, found: 1093.2993. Anal. Calcd for $C_{67}H_{40}BF_{10}OS.CH_2Cl_2$: C, 69.34; H, 3.51; S, 2.72. Found: C, 69.64; H, 3.85; S, 3.28.

Synthesis of boron compound 2: The quantities involved are: Compound **L2** (0.40 g, 0.74 mmol) and tris(pentafluorophenyl)borane (0.45 g, 0.89 mmol). Greenish red solid, yield: 0.35 g (54%). Single crystals of **2** were obtained from a mixture of chloroform/hexane. **^{1}H NMR:** (400 MHz, $CDCl_3$) δ 7.97 (d, *J* = 9.2 Hz, 1H), 7.91 (d, *J* = 8.6 Hz, 1H), 7.48 (s, 1H), 7.20 (d, *J* = 8.5 Hz, 1H), 7.16-7.10 (m, 9H), 7.08-7.01 (m, 6H), 6.69 (d, *J* = 9.2 Hz, 1H), 3.14 (s, 6H). **^{13}C NMR:** (101 MHz, $CDCl_3$) δ 186.0, 177.8, 155.1, 150.3, 147.8 (d, *J* = 242 Hz), 143.4, 143.3, 143.2, 143.1, 140.0, 140.1 (d, *J* = 257 Hz), 137.1 (d, *J* = 256 Hz), 132.6, 132.0, 131.5, 131.5, 131.4, 131.3, 128.7, 128.1, 128.1, 127.8, 127.2, 127.0, 126.3, 111.6, 106.1, 40.3. **^{11}B NMR:** (128 MHz, $CDCl_3$) δ = 0.12 (s). **^{19}F NMR:** (376 MHz, $CDCl_3$) δ -133.87 – -134.03 (d, 4F, Pf), -157.43 (t, 2F, Pf), -163.60 – -163.80 (t, 4F, Pf). **HRMS** (TOF MS ASAP$^+$) m/z calcd for $C_{49}H_{30}BF_{10}NOS$ ($[M]^+$): 881.2018, found: 881.2053. Anal. Calcd for $C_{49}H_{30}BF_{10}NOS$: C, 66.76; H, 3.43; N, 1.59; S, 3.64. Found: C, 66.76; H, 3.44; N, 0.86; S, 4.25.

Synthesis of boron compound 3: The quantities involved are: Compound **L3** (0.50 g, 0.93 mmol) and tris(pentafluorophenyl)borane (0.57 g, 1.1 mmol). Red powder, yield: 0.44 g (53%). Single crystals of **3** were obtained from a mixture of chloroform/hexane. **^{1}H NMR:** (400 MHz, $CDCl_3$) δ 8.13 (d, *J* = 8.8 Hz, 2H), 7.63 (d, *J* = 8.4 Hz, 1H) 7.46 (s, 1H), 7.16 – 7.09 (m, 11H), 7.07-6.98 (m, 6H), 6.74 (d, *J* = 8.9 Hz, 2H), 3.18 (s, 6H). **^{13}C NMR** (176 MHz, $CDCl_3$) δ 180.6, 179.6, 155.4, 149.0, 147.8 (d, *J* = 242 Hz), 143.3, 143.2, 143.2, 142.9, 140.1 (d, *J* = 248 Hz), 139.8, 137.1 (d, *J* = 252 Hz), 137.7, 133.1, 131.9, 131.5, 131.4, 131.4, 128.1, 128.0, 127.8, 127.7, 127.1, 126.9, 111.9, 109.6, 40.4.

^{11}B NMR: (128 MHz, $CDCl_3$) δ = 0.28 (s). **^{19}F NMR:** (376 MHz, $CDCl_3$) δ -133.96 – -134.14 (d, 4F, Pf), -157.49 (t, 2F, Pf), -163.61 – -163.81 (t, 4F, Pf). **HRMS** (TOF MS ASAP$^+$) m/z calcd for $C_{49}H_{30}BF_{10}NOS$ ($[M]^+$): 881.2018, found: 881.1992. Anal. Calcd for $C_{49}H_{30}BF_{10}NOS.0.2CHCl_3$: C, 65.26; H, 3.36; N, 1.55; S, 3.54. Found: C, 64.78; H, 3.59; N, 0.86; S, 4.04.

Synthesis of boron compound 4: The quantities involved are: Compound **L4** (0.35 g, 1.1 mmol) and tris(pentafluorophenyl)borane (0.66 g, 1.3 mmol). Greenish red solid, yield: 0.38 g (53%). Single crystals of **4** were obtained from a mixture of CH_2Cl_2/diethyl ether. **^{1}H NMR:** (400 MHz, $CDCl_3$ δ 8.12 (d, *J* = 9.2 Hz, 1H), 7.93 (d, *J* = 9.2 Hz, 1H), 7.46 (s, 1H), 6.75 (d, *J* = 9.2 Hz, 1H), 6.70 (d, *J* = 9.1 Hz, 1H), 3.15 (s, 4H), 3.10 (s, 4H). **^{13}C NMR:** (176 MHz, $CDCl_3$) δ = 180.4, 178.2, 154.7, 153.9, 147.9 (d, *J* = 238 Hz), 139.9 (d, *J* = 252 Hz), 137.1 (d, *J* = 257 Hz), 132.3, 130.5, 127.1, 121.4, 111.6, 107.9, 105.9, 40.3, 40.3. **^{11}B NMR:** (128 MHz, $CDCl_3$) δ = 0.17 (s). **^{19}F NMR:** (377 MHz, $CDCl_3$) δ = -134.00 – -134.21 (d, 4F, Pf), -158.21 (t, 2F, Pf), -164.02 – -164.29 (t, 4F, Pf). **HRMS** (TOF MS ASAP$^+$) m/z calcd for $C_{31}H_{21}BF_{10}N_2OS$ ($[M]^+$): 670.1344, found: 670.1382. Anal. Calcd for $C_{31}H_{21}BF_{10}N_2OS$: C, 55.54; H, 3.16; N, 4.18; S, 4.78. Found: C, 54.99; H, 3.16; N, 3.28; S, 4.95.

2C.5 References

1. Entwistle, C. D.; Marder, T. B. *Chem. Mater.* **2004,** *16*, 4574-4585.
2. Hu, K.; Zhang, Z.; Burke, J.; Qin, Y. *J. Am. Chem. Soc.* **2017,** *139*, 11004-11007.
3. Ji, L.; Griesbeck, S.; Marder, T. B. *Chem. Sci.* **2017,** *8*, 846-863.
4. Jia, W.-L.; Bai, D.-R.; McCormick, T.; Liu, Q.-D.; Motala, M.; Wang, R.-Y.; Seward, C.; Tao, Y.; Wang, S. *Chem. Eur. J.* **2004,** *10*, 994-1006.
5. Mukherjee, S.; Thilagar, P. *J. Mater. Chem. C* **2016,** *4*, 2647-2662.

6. Murali, A. C.; Nayak, P.; Venkatasubbaiah, K. *Dalton Trans.* **2022,** *51*, 5751-5771.

7. Yuan, Z.; Entwistle, C. D.; Collings, J. C.; Albesa-Jové, D.; Batsanov, A. S.; Howard, J. A. K.; Taylor, N. J.; Kaiser, H. M.; Kaufmann, D. E.; Poon, S.-Y.; Wong, W.-Y.; Jardin, C.; Fathallah, S.; Boucekkine, A.; Halet, J.-F.; Marder, T. B. *Chem. Eur. J.* **2006,** *12*, 2758-2771.

8. Chen, P.-Z.; Niu, L.-Y.; Chen, Y.-Z.; Yang, Q.-Z. *Coord. Chem. Rev.* **2017,** *350*, 196-216.

9. Bellinger, S.; Hatamimoslehabadi, M.; Bag, S.; Mithila, F.; La, J.; Frenette, M.; Laoui, S.; Szalda, D. J.; Yelleswarapu, C.; Rochford, J. *Chem. Eur. J.* **2018,** *24*, 906-917.

10. Bellinger, S.; Hatamimoslehabadi, M.; Borg, R. E.; La, J.; Catsoulis, P.; Mithila, F.; Yelleswarapu, C.; Rochford, J. *Chem. Commun.* **2018,** *54*, 6352-6355.

11. Morris, W. A.; Butler, T.; Kolpaczynska, M.; Fraser, C. L. *Mater. Chem. Front.* **2017,** *1*, 158-166.

12. Wang, F.; Song, D.; Dickie, D. A.; Fraser, C. L. *Chem. Asian J.* **2019,** *14*, 1849-1859.

13. Nagai, A.; Kokado, K.; Nagata, Y.; Chujo, Y. *Macromolecules* **2008,** *41*, 8295-8298.

14. Nagai, A.; Kokado, K.; Nagata, Y.; Arita, M.; Chujo, Y. *J. Org. Chem.* **2008,** *73*, 8605-8607.

15. Aoki, R.; Komatsu, R.; Goushi, K.; Mamada, M.; Ko, S. Y.; Wu, J. W.; Placide, V.; D'Aléo, A.; Adachi, C. *Adv. Opt. Mater.* **2021,** *9*, 2001947.

16. Macedo, F. P.; Gwengo, C.; Lindeman, S. V.; Smith, M. D.; Gardinier, J. R. *Eur. J. Inorg. Chem.* **2008,** *2008*, 3200-3211.

17. Tanaka, K.; Yanagida, T.; Hirose, A.; Yamane, H.; Yoshii, R.; Chujo, Y. *RSC Adv.* **2015,** *5*, 96653-96659.

18. Yoshii, R.; Hirose, A.; Tanaka, K.; Chujo, Y. *J. Am. Chem. Soc.* **2014,** *136*, 18131-18139.

19. Murali, A. C.; Nayak, P.; Nayak, S.; Das, S.; Senanayak, S. P.; Venkatasubbaiah, K. *Angew. Chem.* **2023,** *135*, e202216871.

20. Chen, Z.; Deng, D.-d.; Pu, S. *Tetrahedron Lett.* **2022,** *107*, 154096.

21. Liu, X.; Zhu, C.; Tang, B. Z. *Acc. Chem. Res* **2022,** *55*, 197-208.

22. Bi, X.; Hao, W.; Liu, H.; Chen, X.; Xie, M.; Wang, Y.; Zhao, Y. *Dyes Pigm.* **2021,** *189*, 109267.

23. Liu, W.; Wang, Y.; Ge, G.; Ma, L.; Ren, L.; Zhang, Y. *Dyes Pigm.* **2019,** *171*, 107704.

24. Yang, H.; Zhang, W.; Lu, X.; Liu, W.; Wang, Y.; Li, H.; Yang, Y. *Dyes Pigm.* **2021,** *192*, 109396.

25. Kumar, S. V.; Yadav, S. K.; Raghava, B.; Saraiah, B.; Ila, H.; Rangappa, K. S.; Hazra, A. *J. Org. Chem.* **2013,** *78*, 4960-4973.

26. Nagaraju, C.; Ashok, S. H.; Shamanth, S.; Nagarakere, S. C.; Sunilkumar, M. P.; Subbegowda, R. K.; Mantelingu, K. *Synth. Commun.* **2020,** *50*, 2647-2654.

27. Hommer, H.; Nöth, H.; Knizek, J.; Ponikwar, W.; Schwenk-Kircher, H. *Eur. J. Inorg. Chem.* **1998,** *1998*, 1519-1527.

28. Wang, H.; Zhang, J.; Hu, H.; Cui, C. *J. Am. Chem. Soc.* **2010,** *132*, 10998-10999.

29. Rindorf, G.; Carlsen, L. *Acta. Crystallogr. B.* **1979,** *35*, 1179-1182.

30. Jędrzejewska, B.; Zakrzewska, A.; Mlostoń, G.; Budzák, Š.; Mroczyńska, K.; Grabarz, A. M.; Kaczorowska, M. A.; Jacquemin, D.; Ośmiałowski, B. *J. Phys. Chem. A* **2016,** *120*, 4116-4123.

31. Chaaban, M. A. *J. Mater. Process. Technol.* **2001,** *119*, 336-343.

32. Xu, Z.; Chen, X.; Kim, H. N.; Yoon, J. *Chem. Soc. Rev.* **2010,** *39*, 127-137.

33. Jackson, R.; Logue, B. A. *Anal. Chim. Acta* **2017,** *960*, 18-39.

34. Perumal, S.; Karuppannan, S.; Gandhi, S.; Subramanian, S.; Govindasamy, A.; Gopal, S. K. *Appl. Organomet. Chem.* **2020,** *34*, e5257.

35. Li, S.; Huo, F.; Ma, K.; Zhang, Y.; Yin, C. *New J. Chem.* **2021,** *45*, 1216-1220.

36. Sheik-Bahae, M.; Said, A. A.; Wei, T. H.; Hagan, D. J.; Stryland, E. W. V. *IEEE J. Quantum Electron.* **1990,** *26*, 760-769.

37. Singh, A.; Dey, P.; Kumari, A.; Sikdar, M. K.; Sahoo, P. K.; Das, R.; Maiti, T. *Phys. Chem. Chem. Phys.* **2022,** *24*, 4065-4076.

38. Rodríguez, M.; Castro-Beltrán, R.; Ramos-Ortiz, G.; Maldonado, J. L.; Farfán, N.; Domínguez, O.; Rodríguez, J.; Santillan, R.; Meneses-Nava, M. A.; Barbosa-García, O.; Peon, J. *Synth. Met.* **2009,** *159*, 1281-1287.

39. Yuan, Z.; Taylor, N. J.; Ramachandran, R.; Marder, T. B. *Appl. Organomet. Chem.* **1996,** *10*, 305-316.

40. Mukundam, V.; Sa, S.; Kumari, A.; Das, R.; Venkatasubbaiah, K. *J. Mater. Chem. C* **2019,** *7*, 12725-12737.

41. Yin, M.; Li, H. P.; Tang, S. H.; Ji, W. *Appl. Phys. B* **2000,** *70*, 587-591.

42. Usha Gangan, T. V.; Reddy, M. L. P. *Dalton Trans.* **2015,** *44*, 15924-15937.

43. Liu, W.; Wang, Y.; Yang, J.; Li, X.; Wang, X.; Ma, L. *Dyes Pigm.* **2020,** *175*, 108149.

44. Yang, F.; Zhang, J.; Zang, Q.; Shen, T.; Ni, J.; Zhang, H.; Sun, J. Z.; Tang, B. Z. *Mater. Chem. Front.* **2022,** *6*, 368-378.

CHAPTER 2D

Carbazole-based Boron-thioketonates: Synthesis, Optical, Electrochemical, and TADF Properties

2D.1 Introduction

Thermally activated delayed fluorescence (TADF) materials have gained popularity in recent years due to their application in organic light-emitting diodes (OLEDs), where they can replace phosphorescent emitters made of metal-based organic compounds.[1] Theoretical perspective of the TADF-based materials can show an internal quantum efficiency of 100% with the utilization of triplet excitons through the reverse intersystem crossing (RISC) mechanism.[2] Emitters with a small energy gap between the singlet and triplet excited states (ΔE_{ST}) are essential requirements to achieve a quick RISC process.[3] Hence, the combination of electron-donor and electron-withdrawing acceptor units play a crucial role in frontier molecular orbital (FMO) distribution to achieve a very less energy gap between singlet and triplet states.[3, 4] Recent reports indicate that successful blue and green TADF emitters with high colour purity are being developed.[5] However, the inherent non-radiative process from the lower laying singlet excited energy levels makes it difficult to produce effective orange-red TADF materials. There are different approaches for achieving orange-red TADF emitters, for example, acceptor with cyano substitution, incorporation of rigid donor and acceptor, and incorporation of boron atom in the TADF core.[6] Taking advantage of boron's empty p-orbital, the boron incorporated tri- and tetra-coordinated boron compounds play a crucial role in OLED devices.[7] Among them, tetra-coordinated boron-β-diketonates were studied by various research groups,[8] and we explored the replacement of one oxygen of the diketones with a sulphur atom as a strategy to obtain molecule that can be emissive in the red-region of the spectral band.[9, 10] Carbazole is one of the rigid donor units widely used in TADF materials due to its tuneable nature of energy gap (ΔE_{ST}) and τ of TADF materials.[11] Taking advantage of the carbazole, we designed and synthesized carbazole substituted boron-β-thioketonate and and studied their optical, electrochemical and TADF properties.

2D.2 Result and Discussion

2D.2.1 Synthesis and characterization

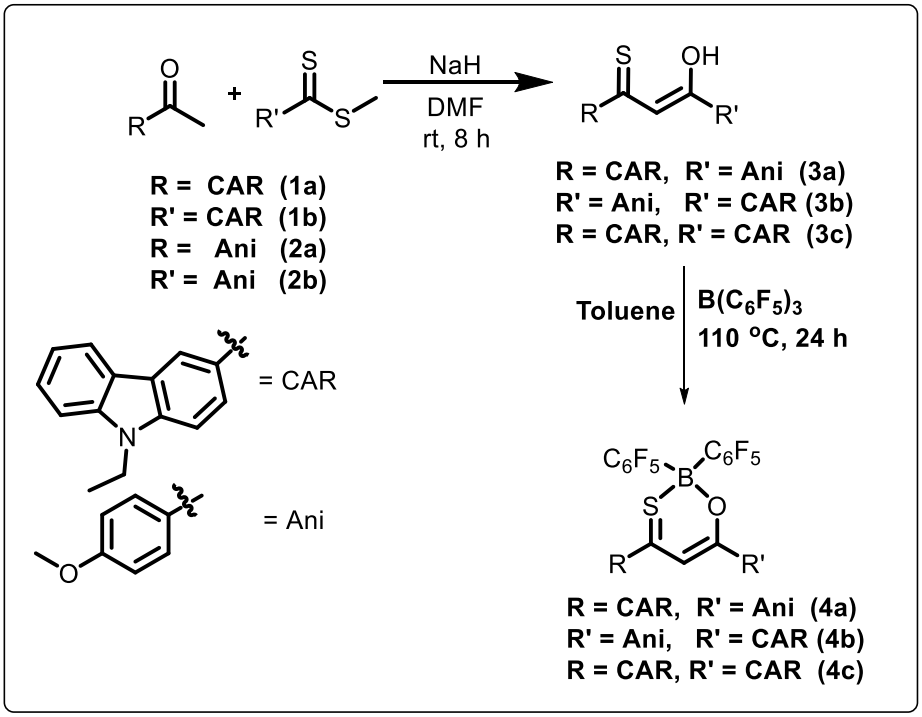

Scheme 2D.1: Synthetic routes for the ligands (**3a-3c**) and boron compounds (**4a-4c**).

The required boron monothio-β-diketonate compounds **4a-4c** were prepared by refluxing $B(C_6F_5)_3$ with respective N-ethyl carbazole (CAR) and p-anizole (Ani) derivatives of 1,3-monothio-β-diketones (**3a-3c**) ligands in dry toluene at 110 °C (**Scheme 2D.1**). The required ligands were prepared by adopting the reported procedure.[10] All the synthesized ligands (**3a-3c**) and boron complexes **(4a-4c)** were confirmed using ^{1}H, ^{13}C, ^{11}B (in case of **4a-4c**), ^{19}F NMR (in case of **4a-4c**) spectroscopy, HRMS, and single crystal X-ray diffraction (in case of **4a** and **4b**). ^{1}H-NMR spectrum of all three ligands **(3a-3c)** shows a broad singlet of intramolecular hydrogen bonded enolic proton resonating at ~16-17 ppm. The $^{11}B\{^{1}H\}$ NMR of all three boron complexes **(4a-4c)** showed a peak at ~0-1 ppm, which represents the formation of four coordinated boron complex, and $^{19}F\{^{1}H\}$ NMR spectra gives three different sets of peaks (ortho, meta, para) resonating peaks between ~ -130.0 to -170.0 ppm.

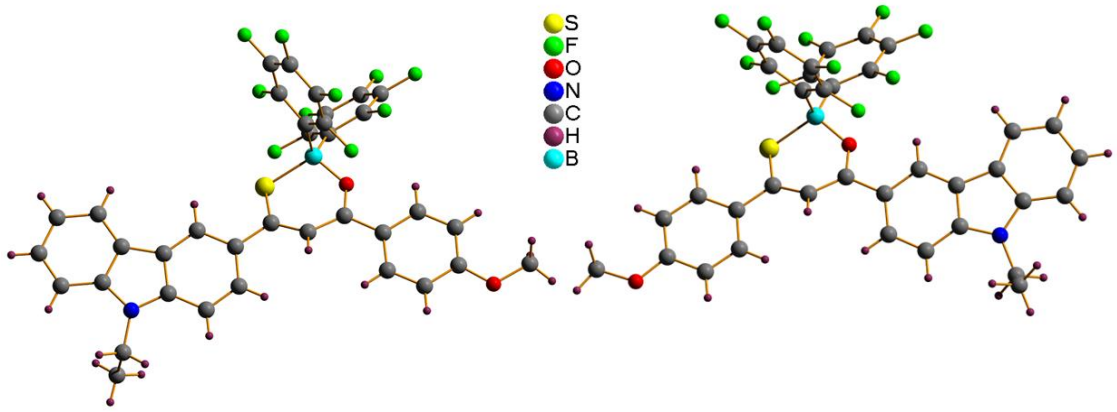

Figure 2D.1: Molecular structure of compounds **4a** and **4b** (from left to right) with ball and stick model.

The molecular structure of the boron compounds **4a** and **4b** were confirmed by X-ray crystallography. Single crystals of boron compounds **4a** and **4b** were grown by slow evaporation of CH_2Cl_2/*n*-hexane solvent mixture. Both compounds (**Figure 2D.1**) were crystallized in the triclinic P-1 space group. The selected bond angles and bond lengths are shown in **Table 2D.1** The observed B-S and B-O bond lengths are (1.947 (2), 1.481 (2) for **4a** and 1.944 (2), 1.485 (3) for **4b**) are comparable with our previously reported monothio-β-diketonate boron compounds.[9, 10] The deviation of the boron atom from C3SOB plane of compound **4a** (0.292 Å) is significantly lower than the value observed for compound **4b** (0.362 Å).

Table 2D.1 Comparison of bond lengths, bond angles, and other structural data for compounds **4a** and **4b.**

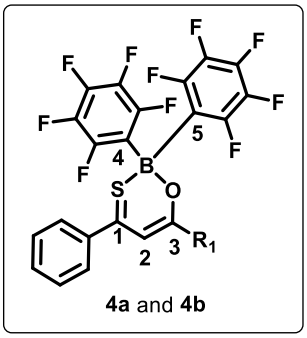

4a and **4b**

	4a	**4b**

S-C1 (Å)	1.715 (2)	1.729 (2)
O-C3 (Å)	1.304 (2)	1.313 (2)
B-S (Å)	1.947 (2)	1.944 (2)
B-O (Å)	1.481 (2)	1.485 (3)
B-C4 (Å)	1.630 (3)	1.644 (3)
B-C5 (Å)	1.633 (3)	1.626 (3)
C1-C2 (Å)	1.385 (3)	1.383 (3)
C2-C3 (Å)	1.401 (3)	1.395 (3)
S-B-O (deg)	108.2 (1)	106.4 (1)
S-B-C4 (deg)	108.5 (1)	108.6 (1)
O-B-C5 (deg)	104.2 (1)	105.0 (2)
C4-B-C5 (deg)	110.1 (1)	110.7 (2)
C1-C2-C3 (deg)	124.7 (1)	124.3 (2)
Deviation of B from C3SOB plane (Å)	0.292	0.362

Table 2D.2 Crystal data and structure refinement for compound **4a** and **4b.**

	4a	**4b**
Empirical formula	$C_{36}H_{20}BF_{10}NO_2S$	$C_{36}H_{20}BF_{10}NO_2S$
Formula weight	731.40	731.40
Temperature/K	296(2)	100.01(10)
Crystal system	triclinic	triclinic
Space group	P-1	P-1
a/Å	9.6329(3)	10.8140(4)
b/Å	13.5959(6)	12.6316(5)
c/Å	13.7543(3)	13.5128(6)
α/°	100.343(2)	113.316(4)
β/°	110.433(2)	107.654(4)
γ/°	104.952(4)	99.543(3)
Volume/Å^3	1556.88(10)	1526.67(12)
Z	2	2
ρ_{calc}g/cm^3	1.560	1.591
μ/mm^{-1}	1.801	0.205
F(000)	740.0	740.0
Crystal size/mm^3	0.15 × 0.14 × 0.12	0.15 × 0.12 × 0.11
Radiation	CuKα (λ = 1.54184)	MoKα (λ = 0.71073)

2Θ range for data collection/°	7.05 to 156.672	6.532 to 60.696
Index ranges	$-12 \le h \le 12$, $-16 \le k \le 17$, $-17 \le l \le 12$	$-13 \le h \le 14$, $-15 \le k \le 16$, $-15 \le l \le 17$
Reflections collected	27477	27850
Independent reflections	6423 [R_{int} = 0.0481, R_{sigma} = 0.0280]	7338 [R_{int} = 0.0685, R_{sigma} = 0.0585]
Data/restraints/parameters	6423/0/463	7338/0/462
Goodness-of-fit on F^2	1.065	1.033
Final R indexes [I>=2σ (I)]	R_1 = 0.0450, wR_2 = 0.1261	R_1 = 0.0598, wR_2 = 0.1523
Final R indexes [all data]	R_1 = 0.0518, wR_2 = 0.1354	R_1 = 0.0838, wR_2 = 0.1667
Largest diff. peak/hole / e $Å^{-3}$	0.47/-0.33	1.03/-0.46

2D.2.2 Optical properties

Table 2D.3 Photophysical data of compounds **4a-4c** at 298K

Compounds	**Solvent**	**λ_{abs}[a] /nm**	**λ_{ems}[b] /nm**	**Stokes shift (cm^{-1})**	**ϕ_F[c] (%)**	**τ_{PF} (ns)[d]**
4a	Toluene	490	533	1647	0.14	
	THF	491	580	3125	0.91	0.16
	DCM	488	582	3309	0.12	
	DMF	499	630	4167	0.22	
	ACN	489	632	4627	0.14	
4b	Toluene	501	549	1746	2.72	
	THF	501	574	2539	12.02	0.40
	DCM	498	574	2659	11.46	
	DMF	506	624	3737	1.41	
	ACN	498	623	4029	0.71	
4c	Toluene	514	554	1405	3.12	
	THF	518	568	1700	3.62	0.25
	DCM	514	573	2003	4.49	
	DMF	527	596	2197	7.80	

	ACN	516	593	2516	7.33	

[a]Absorption maximum ($1.5*10^{-5}$ M). [b]Excited at the absorption maximum. [c]Absolute fluorescence quantum yields (%), [d]Prompt fluorescence life-time.

Table 2D.4 Photophysical data of compounds **4a-4c** at 298K

Compounds	**Solvent**	$\lambda_{abs}{}^{a}$ **/nm**	$\lambda_{ems}{}^{b}$ **/nm**	$\lambda_{DF}{}^{c}$ **/nm**	τ_{DF} **(µs)**[d]
4a	THF	491	568	580	2.7
	Thin film	-	595	592	87.5, 189.0[e]
4b	THF	501	574	574	5.4
	Thin film	-	582	583	6.3, 285.0[e]
4c	THF	518	568	570	3.5
	Thin film	-	603	602	27.0, 55.0[e]

[a]Absorption maximum. [b]PL spectra at room temperature using xenon arc lamp. [c]Delayed PL spectra at room temperature using xenon flash lamp. [d]Delayed fluorescence life time. [e]Delayed fluorescence life-time under vacuum.

The UV-Vis absorption and emission of boron compounds **(4a-4c)** were investigated in various solvents such as toluene, tetrahydrofuran (THF), dichloromethane (DCM), dimethylformamide (DMF), and acetonitrile (ACN) and the data is presented in **Table 2D.3, 2D.4,** and **Figure 2D.2.** The UV-Vis spectra of **4a-4c** show intense absorption lower energy band in tetrahydrofuran (THF) from 471-527nm which arises from the typical π-π* transition (**Figure 2D.2**). Compound **4c** displayed a remarkable bathochromic shift of absorption maxima over **4a** and **4b** due to the stronger intramolecular charge transfer (ICT) character shown by two carbazole functional groups. THF solution of the synthesized boron compounds (**4a-4c**) displayed λ_{max} emission from 533 nm to 632 nm (**Table 2D.3**). Introduction of the carbazole unit observed a remarkable blue shift in the emission spectrum compared to the reported boron thioketone based molecules.[9, 10] Compound **4c** displayed narrow bandwidth in comparison with other compounds (59 nm). The PL quantum yield (ϕ_F) of compounds **4a-4c** were measured, as shown in **Table 2D.3** compound **4c** showed a significantly larger quantum yield in polar solvent. Time-resolved fluorescence of compounds **4a-4c** showed bi- or tri-exponential decay profile (τ_{PF}**)** in the nanosecond time domain (0.16 – 0.40 ns). To get further insight

into the excited state behavior of compounds **4a-4c** in solution and film-state (1 wt%), we studied using xenon flash lamp. At ambient conditions, THF solution of compounds **4a-4c** showed delayed fluorescence peak maxima ranging of 570 nm – 580 nm (**Table 2D.3**). Among them, compounds **4b** and **4c** are smoothly overlap with prompt emission spectra whereas compound **4a** showed 12 nm red shift with prompt emission spectra. Moreover, compounds **4a-4c** showed tri-exponential decay with lifetimes in the microsecond range of 2.7 μs – 5.4 μs in THF which maybe corresponds to T_n to S_0 through S_1 transition. The thin-film of delayed PL spectra of compounds **4a-4c** showed significantly high intense peaks at ambient conditions than the peaks observed at 90 K which is strongly suggest that compounds **4a-4c** showed TADF property (**Figure 2D.3d, 2D.4d, 2D.5d**). Thin film of compound **4a** showed delayed emission band at 592 nm, compound **4b** at 583 nm, and compound **4c** at 602 nm which overlap with prompt emission spectra of these boron compounds (see **Table 2D.4**). Moreover, delayed emission spectra of compounds **4a-4c** were also recorded under vacuum, as expected, they showed stronger luminescence behaviour which indicates that triplet state is involved in the luminescence processes of these compounds. The PL decay (**τ_{DF}**) of thin film of the compounds **4a-4c** showed 87.5 μs, 6.3 μs, 27.0 μs respectively whereas PL decay got increased to 189.0, 285.0, 55.0 μs under vacuum (**Figure 2D.3 - Figure 2D.5**). In general, long lived decay time scale can be assigned as phosphorescence, however, the observed energy emission maxima from both xenon arc and flash lamp, hence, obtained longer decay (**τ_{DF}**) time can be ascribed to delayed fluorescence. Due to the complete overlapping of both prompt and delayed emission spectra (ambient and 90 K conditions), the splitting energy (ΔE_{ST}) of singlet (S_1) and triplet (T_1) could not able to calculate experimentally. To get further insight into the delayed luminescence characteristics of compounds **4a-4c,** $S_0 \rightarrow S_1$, $S_1 \rightarrow S_0$ and $T_n \rightarrow S_0$ transition were calculated theoretically which will be discussed below (see **DFT section**).

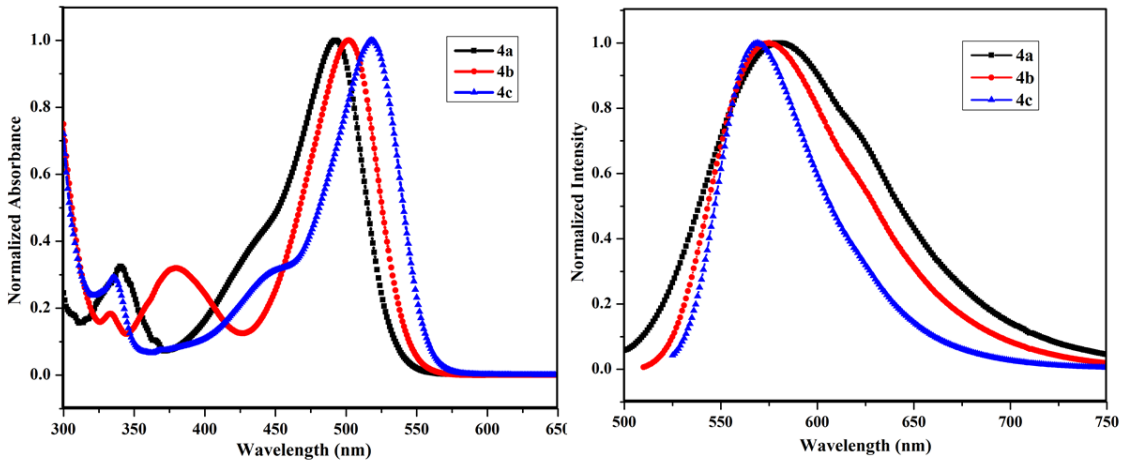

Figure 2D.2: Normalized absorption spectra (Left) and emission spectra of boron compounds **4a-4c** (1.5 x 10^{-5} M) in tetrahydrofuran, excited at a higher wavelength of absorption maxima (Right).

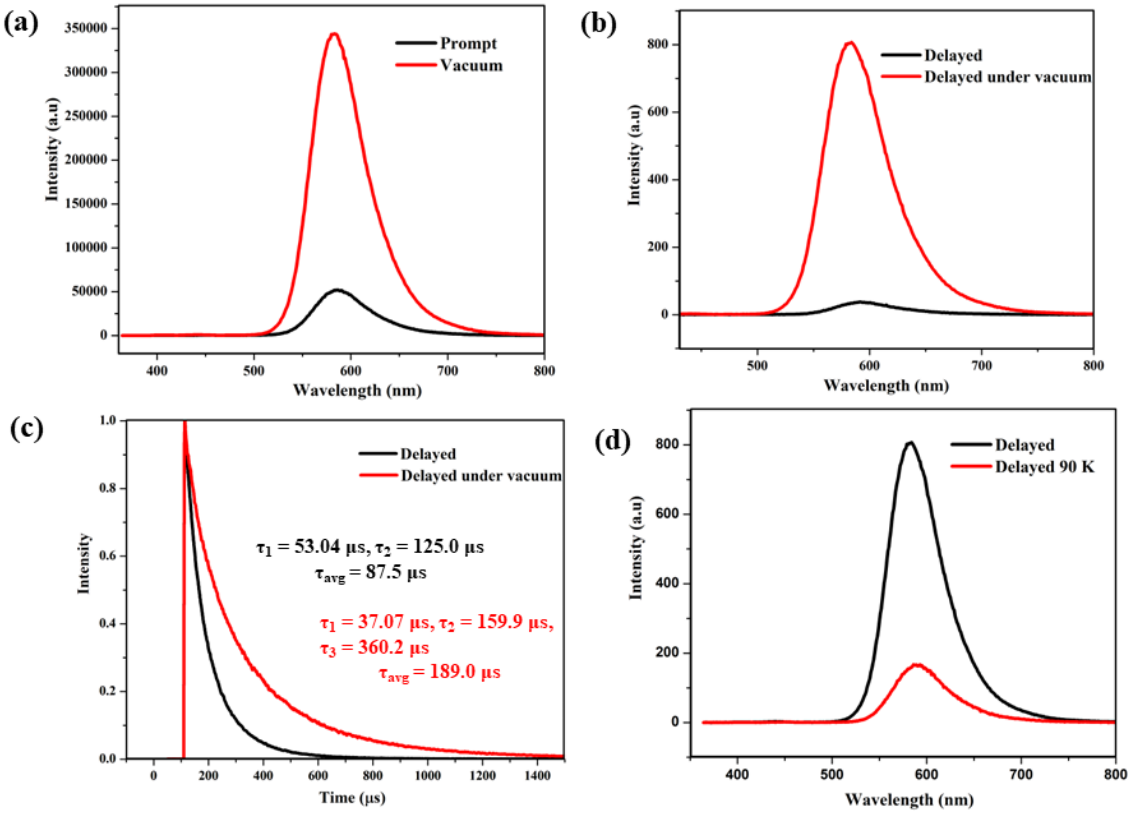

Figure 2D.3: (a) Thin film emission spectra of boron compound **4a.** (b) Thin film delayed luminescence spectra of boron compound **4a.** (c) Thin film delayed luminescence life-time of boron compound **4a.** (d) Temperature dependent thin film delayed luminescence spectra of boron compound **4a.**

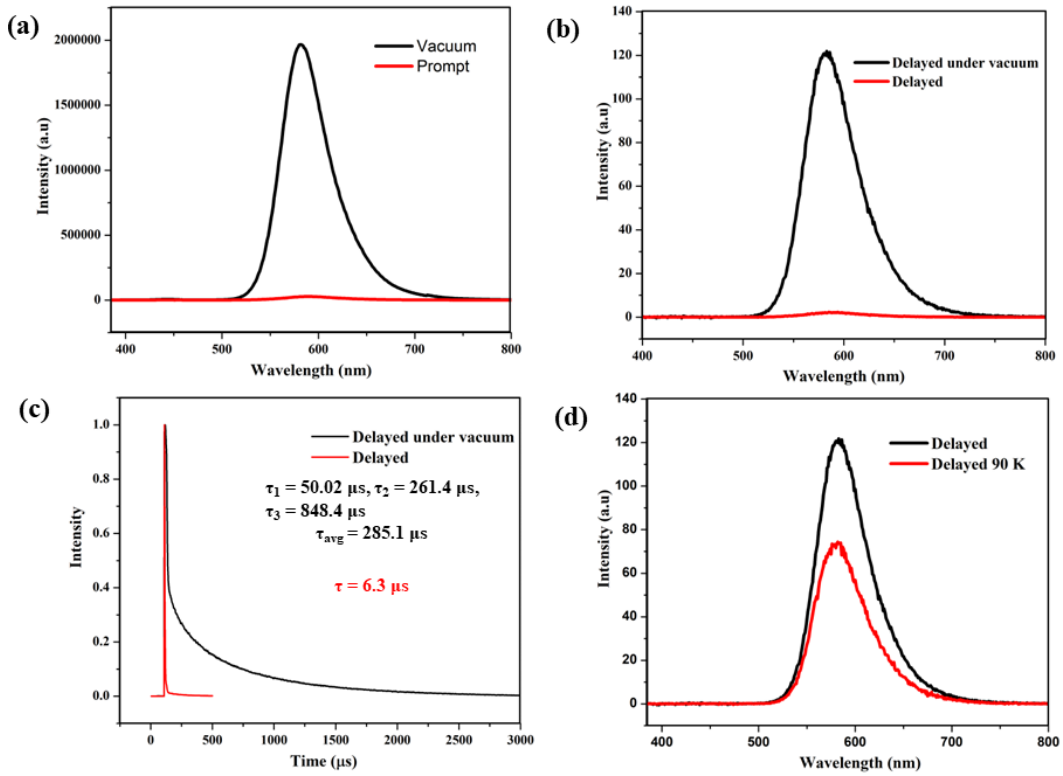

Figure 2D.4: (a) Thin film emission spectra of boron compound **4b.** (b) Thin film delayed luminescence spectra of boron compound **4b.** (c) Thin film delayed luminescence life-time of boron compound **4b.** (d) Temperature dependent thin film delayed luminescence spectra of boron compound **4b.**

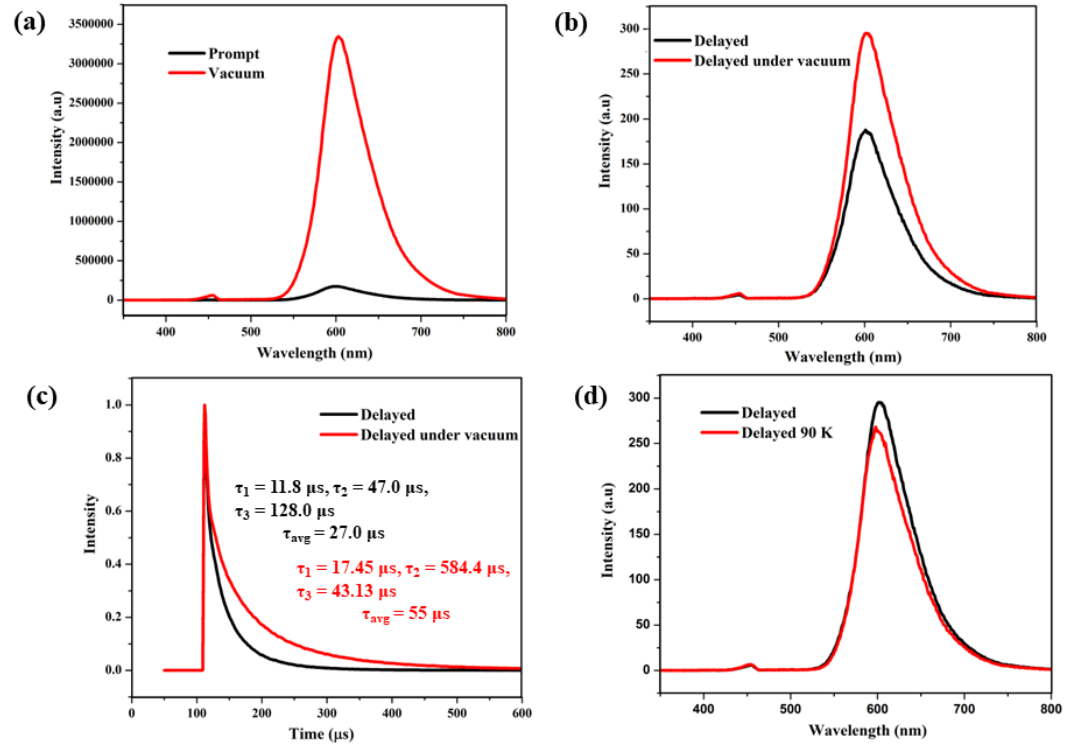

Figure 2D.5: (a) Thin film emission spectra of boron compound **4c.** (b) Thin film delayed luminescence spectra of boron compound **4c.** (c) Thin film delayed luminescence life-

time of boron compound **4c.** (d) Temperature dependent thin film delayed luminescence spectra of boron compound **4c.**

2D.2.3 Electrochemical properties

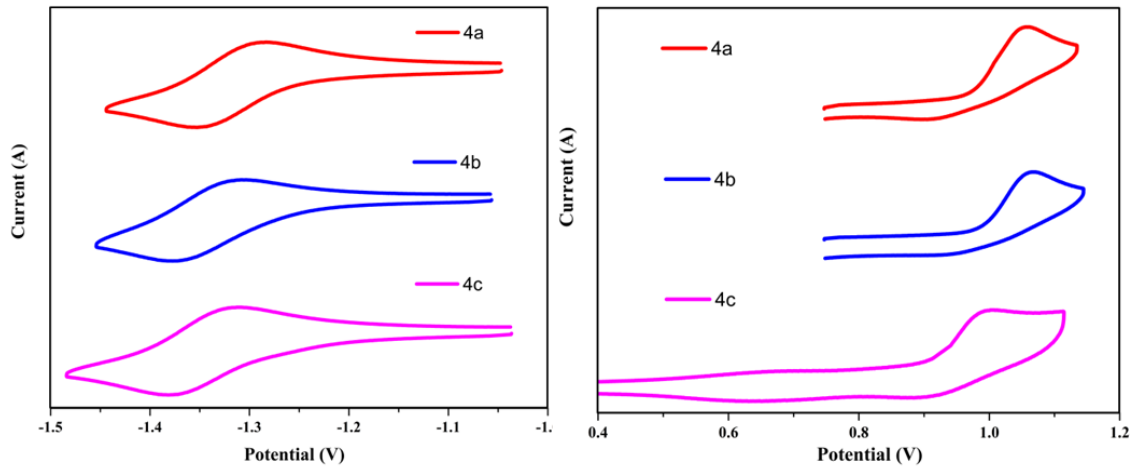

Figure 2D.6: Cyclic voltammogram of reduction potential (left) and oxidation potential (right) of compounds **4a-4c** (vs Ferrocene/Ferrocenium) with 0.1 M of $^{n}Bu_4N[PF_6]$ in CH_2Cl_2 as the supporting electrolyte (scan rate 50 mV/s).

The electrochemical behaviour of the boron compounds **4a-4c** were investigated by cyclic voltammetry in degassed dichloromethane at 298 K using $^{n}Bu_4[PF_6]$ as a supporting electrolyte. All three boron compounds **4a-4c** displayed one reversible reduction cycle ranging from -1.31 to -1.38 V (**Figure 2D.6** and **Table 2D.5**). Similar to our previous report,[10] compounds **4a** and **4b** displayed almost the same reduction potential value while interchanging the carbazole and anisole substituent. Compound **4c** showed reduction potential at a more negative due to the presence of two carbazole (CAR) groups. Moreover, the introduction of two anisole (Ani) groups showed less negative reduction potential at -1.18 V.[9] Apart from that all three boron compounds showed a quasi-reversible oxidation cycle ranging from 0.64 to 0.99 V (**Table 2D.5**). Similar to the reduction profile, the oxidation peaks of the boron compounds also showed almost similar potential (for **4a** and **4b** 0.98 V, 0.99 V). Moreover, compound **4c** showed two quasi-oxidation potentials, one peak (0.94 V) with a similar potential region of compound **4a**

and **4b** and another peak (0.64 V) at a less positive region. The HOMO-LUMO gap of compounds **4a-4c** are calculated using electrochemical data (**Table 2D.5**).

Table 2D.5 Electrochemical data of complexes **4a-4c.**

Complexes	E_{pc}	E_{pa} (1and 2nd peak)	HOMO-LUMO gap[a]
4a	-1.31	0.98	2.29
4b	-1.33	0.99	2.32
4c	-1.38	0.64, 0.94	2.02

[#]E_{pc} = cathodic peak potential, [#]E_{pa} = anodic peak potential. [a]Electrochemical band gap (difference between oxidation wave and reduction waves).

2D.2.4 DFT Studies

We used density functional theory (DFT) calculations to optimize the geometries (B3LYP/6-31-g-(d,p)) and time-dependent density functional theory (TD-DFT) in order to learn more about the singlet ground state (S_0), singlet (S_1) and triplet (T_1) excited states of boron compounds **4a-4c.** Ground states of computed wavelength values are nicely reproduces the trend observed by experiments. TD-DFT calculations reveal that the observed energy difference between the S_1 and T_1 states is high, however, T_9, T_{10}, T_{12} triplet states of compounds **4a-4c** are very close to S_1 state. These are the possible triplet states responsible for delayed fluorescence *via* reversible inter system crossing ($T_n \rightarrow S_1$) observed in these boron compounds **4a-4c.**

Table 2D.6. Calculated electronic transitions for compound **4a-4c** from TD-DFT (B3LYP) calculations

Compounds	Transition	Wavelength	Energy	Oscillator strength
4a	$S_0 \rightarrow S_1$	450	2.97	0.4997
	$S_1 \rightarrow S_0$	677	1.83	0.0008
	$T_9 \rightarrow S_0$	691	1.79	0.0018

	$T_1 \rightarrow S_0$	2444	0.50	0.0366
4b	$S_0 \rightarrow S_1$	413	2.99	0.6022
	$S_1 \rightarrow S_0$	601	2.06	0.1120
	$T_{10} \rightarrow S_0$	648	1.91	0.0207
	$T_1 \rightarrow S_0$	1721	0.72	0.0203
4c	$S_0 \rightarrow S_1$	457	2.71	0.9320
	$S_1 \rightarrow S_0$	571	2.17	0.1785
	$T_{12} \rightarrow S_0$	594	2.08	0.0547
	$T_1 \rightarrow S_0$	2399	0.51	0.0368

2D.3 Conclusion

In summary, we successfully synthesized carbazole substituted monothio-β-diketonate tetra-coordinated bis(pentaflurophenyl)boron compounds. Detailed characterization, optical, and electrochemical properties were presented. All these O,S-chelated carbazole based boron compounds showed orange to red emission in the liquid state and solid state. Further, the TADF of these materials were studied in solution as well as in the film state.

2D.4.1 Experimental procedure

General information: All the reactions were carried out under N_2 atmosphere using standard glove box, Schlenk line and vacuum line techniques. Dry solvents used for the reactions were dried according to standard procedures. All the reactions were monitored by thin-layer chromatography. Nuclear magnetic resonance spectra were recorded on a 400 MHz or 700MHz Fourier transform NMR spectrometer (JEOL or Bruker) with $CDCl_3$ as a solvent. ^{11}B and ^{19}F NMR spectra were externally referenced to $BF_3.Et_2O$ in $CDCl_3$ (δ=0 ppm) and α,α,α-trifluoro toluene in $CDCl_3$ (δ=-63.73 ppm), respectively. Chemical shifts are reported in δ ppm (parts per million) using residual solvent protons as the internal standard (δ 7.26 for $CDCl_3$ in ^1H NMR, δ 77.16 for $CDCl_3$ in ^{13}C NMR).

Coupling constants are reported as J values in hertz (Hz). Splitting patterns are designated as s(singlet), d(doublet), t(triplet), q(quartet), dd(doublet of doublet), dt(doublet of triplet), m(multiplet) and br(broad). HRMS were recorded using Waters XEVO G2-XS QTOF mass spectrometer. Elemental analyses were performed in a Euro Vector EA 3000 CHNS analyzer. UV – Visible spectra were recorded on Agilent Technologies Cary 60 UV/Visible spectrometer. Fluorescence spectra and quantum yields were measured using Edinburgh spectrofluorimeter instrument FS5. For the measurement of absolute quantum yield, the concentration of the boron compounds were such as to give an absorbance of around 0.1 at the excitation wavelength. Absolute total quantum yields were measured using an integrating sphere (Edinburgh instrument FS5) mounted in the SC-30 compartment of the spectrofluorimeter. A Rigaku Super Nova fine-focused dual diffractometer, fitted with a PILATUS200K, was utilised to gather single crystal X-ray diffraction data using Cu Kα radiation (λ = 1.54178 Å) or MoKα radiation (λ = 0.71073). The structures were solved using Olex2 and the ShelXS structure solution program using Direct Methods. The ShelXL refinement tool was then used to refine the structures using Least Squares minimization. Anisotropic displacement coefficients were utilised in the refinement of all non-hydrogen atoms. The H atoms were placed at calculated positions and were refined as riding atoms. The standard three electrode arrangement used for cyclic voltammetry included an Ag wire serving as the reference electrode, a Pt wire serving as the secondary electrode, and a glassy carbon working electrode. About 1.0 x 10^{-3} M solution in CH_2Cl_2 with $[Bu_4N][PF_6]$ (0.1 M) as a supporting electrolyte was used to record the voltammogram. The scans were referenced with a small amount of ferrocene as an internal standard.Starting materials: Carbazole, ethyl iodide, acetyl chloride, N-bromosuccinimide, carbon disulphide, methyl iodide, sodium hydride, 4-methoxy acetophenone, Tris(pentafluorophenyl)borane, were purchased from Sigma-Aldrich,

Spectrochem and Alfa-Aaser. 9-ethyl-9H-carbazole, 3-bromo-9-ethyl-9H-carbazole, 1-(9-ethyl-9H-carbazol-3-yl)ethan-1-one, methyl 4-methoxybenzodithioate were prepared according to the reported literature procedure.[12-14]

Synthetic routes of methyl 9-ethyl-9H-carbazole-3-carbodithioate and 1-(9-ethyl-9H-carbazol-3-yl)ethan-1-one:

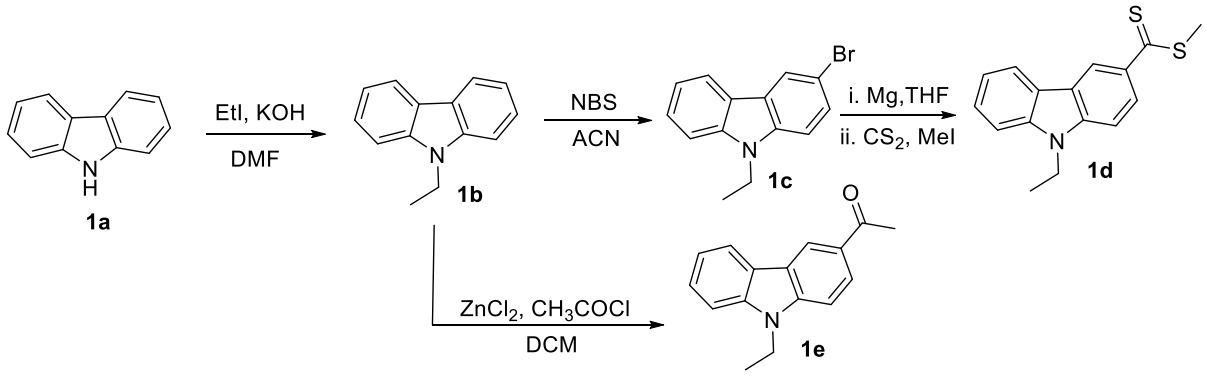

Synthesis of methyl 4-methoxybenzodithioate:[9]

Magnesium (0.52g, 21.39 mmol) and a catalytic amount of iodine was taken in a two-necked round bottom flask. THF was added under a nitrogen atmosphere and warmed the solution till the brisk effervescence is observed. Add a solution of 1-bromo-4-methoxybenzene (2.00g, 10.69 mmol) dropwise to the mixture at 0 °C and stirred for 2 h at 65 °C. The Grignard solution was transferred into another round bottom flask and cooled to 0 °C, CS_2 (0.97g, 1.27 mmol) was added dropwise to the solution and it becomes orange colour. The reaction mixture was stirred further 2 h at room temperature. Then methyl iodide (1.98g, 12.83 mmol) was added to the mixture dropwise at 0 °C. Then the reaction mixture was stirred for 3-5 h. The completion of the reaction was monitored by TLC. After completion of reaction, THF was concentrated under vacuum, extracted with ethyl acetate (50mL x 3). The separated ethyl acetate layer dried over anhydrous Na_2SO_4, and removed the solvent under reduced pressure. The product was isolated through column chromatography using *n*-hexane. Yield: 2.06g (98.0%). **^{1}H NMR** (400

MHz, $CDCl_3$) δ = 8.10 (d, *J* = 8.0, 2H), 6.88 (d, *J* = 8.0, 2H), 3.86 (s, 3H), 2.77 (s, 3H). **^{13}C NMR** (101 MHz, $CDCl_3$) δ = 226.98, 163.64, 138.22, 128.98, 113.56, 55.64, 20.47.

Synthesis of methyl 9-ethyl-9H-carbazole-3-carbodithioate (1d):

Magnesium (0.56g, 23.44 mmol) and a catalytic amount of iodine were taken in a two-necked round bottom flask. THF was added under a nitrogen atmosphere and warmed the solution till the brisk effervescence is observed. Add a solution of 3-bromo-9-ethyl-9H-carbazole (3.20g, 11.72 mmol) dropwise to the mixture at 0 °C and stirred for 2 h at 65 °C. Obtained Grignard solution was transferred into another round bottom flask and cooled to 0 °C, CS_2 (1.33g, 17.50 mmol) was added dropwise to the solution and it becomes orange colour. The reaction mixture was stirred further 2 h at room temperature. Then methyl iodide (2.48g, 17.58 mmol) was added to the mixture dropwise at 0 °C. Then the reaction mixture was stirred for 3-5 h. The completion of the reaction was monitored by TLC. After completion of reaction, THF was concentrated under vacuum, extracted with ethyl acetate (50mL x 3). The separated ethyl acetate layer dried over anhydrous Na_2SO_4, and removed the solvent under reduced pressure. The product was isolated through column chromatography using of *n*-hexane as a solvent. Red colour liquid, Yield: 2.50g (76%). **^{1}H NMR** (400 MHz, $CDCl_3$) δ 8.84 (s, 1H), 8.24 (d, *J* = 8.0 Hz, 1H), 8.08 (d, *J* = 8.0 Hz, 1H), 7.46 – 7.38 (m, 1H), 7.34 (d, *J* = 8.0 Hz, 1H), 7.28 – 7.17 (m, 2H), 4.28 (q, *J* = 7.3 Hz, 2H), 2.76 (s, 3H), 1.36 (t, *J* = 7.2 Hz, 3H). **^{13}C NMR** (101 MHz, $CDCl_3$) δ = 227.95, 143.00, 140.85, 137.03, 126.61, 125.83, 123.61, 122.75, 121.02, 120.15, 120.11, 109.15, 107.92, 38.01, 20.69, 13.96. **HRMS** (ESI) m/z calcd for $C_{16}H_{15}NS_2$ ($[M+H]^+$): 286.0724, found: 286.0710.

2D.4.2 General procedure for the synthesis of 1,3-monothio-β-diketones:

Two neck RB was charged with NaH (2.2 mmol, 50%) and acetophenone derivatives, then DMF (10 mL) was added under nitrogen atmosphere, and stirred for 5min. Derivatives of methyl benzodithioate (1.2 mmol) in DMF (10 mL) was added dropwise at 0 °C. Then the reaction mixture was stirred at room temperature for 5-8 h. The progress of the reaction was monitored by TLC. After the completion of the reaction, the mixture was poured into ice-cold water (40 mL) and acidified with glacial acetic acid and observed orange coloured solid was filtered and the product was isolated through column chromatography using *n*-hexane/CH_2Cl_2 as eluent (or) crude mixture was extracted with ethyl acetate (3 x 30 mL) and combined ethyl acetate layers were washed with ice water, dried over Na_2SO_4 and concentrated under vacuum. The viscous liquid was purified by silica gel column chromatography using *n*-hexane/CH_2Cl_2 as eluent.

Synthesis of ligand (3a):

The quantities are involved are as follows: 4-Methoxyacetophenone (0.38g, 2.55 mmol), methyl 9-ethyl-9H-carbazole-3-carbodithioate (0.80g, 2.80 mmol) and sodium hydride (50%, 0.14g, 5.61 mmol). Orange solid, Yield: 0.45g (46%). **^{1}H NMR** (400 MHz, $CDCl_3$) δ = 16.38 (s, 1H), 8.70 (s, 1H), 8.19 (d, *J* = 8.0, 1H), 8.11 (d, *J* = 8.0, 1H), 8.04 (d, *J* = 8.0, 2H), 7.60 (s, 1H), 7.51 (t, *J* = 8.0, 1H), 7.45 – 7.36 (m, 2H), 7.30 (t, *J* = 8.0, 1H), 7.01 (d, *J* = 8.0, 2H), 4.39 (q, *J* = 7.3, 2H), 3.90 (s, 3H), 1.46 (t, *J* = 7.1 Hz, 3H). **^{13}C NMR** (101 MHz, $CDCl_3$) δ = 206.8, 177.3, 163.3, 142.2, 140.8, 137.4, 129.3, 128.0, 126.4, 125.7, 123.5, 123.0, 120.9, 120.0, 119.9, 114.3, 109.1, 108.5, 108.2, 55.6, 38.0, 13.9. **HRMS** (ESI) m/z calcd for $C_{24}H_{22}NO_2S$ ($[M+H]^+$): 388.1371, found: 388.1360.

Synthesis of ligand (3b):

The quantities involved are as follows: 1-(9-ethyl-9H-carbazol-3-yl)ethan-1-one (1.08g, 4.59 mmol), methyl 4-methoxybenzodithioate (1.0g, 5.05 mmol) and sodium hydride

(50%, 0.24g, 10.0 mmol). orange solid, Yield: 0.63g (36%). **^{1}H NMR** (400 MHz, $CDCl_3$) δ 16.49 (s, 1H), 8.79 (s, 1H), 8.20 – 8.10 (m, 2H), 7.95 (d, *J* = 8.0 Hz, 2H), 7.63 (s, 1H), 7.53 (ddd, *J* = 8.2, 7.0, 1.2 Hz, 1H), 7.50 – 7.38 (m, 2H), 7.37 – 7.27 (m, 1H), 6.99 – 6.93 (m, 2H), 4.44 – 4.36 (m, 2H), 3.89 (s, 3H), 1.47 (t, *J* = 7.2 Hz, 3H). **^{13}C NMR** (101 MHz, $CDCl_3$) δ = 204.1, 179.3, 162.4, 142.8, 140.7, 138.9, 129.0, 126.7, 125.7, 125.2, 123.4, 123.1, 120.9, 120.6, 120.2, 113.7, 109.2, 108.8, 108.7, 55.6, 38.0, 14.0. **HRMS** (ESI) m/z calcd for $C_{24}H_{22}NO_2S$ ($[M+H]^+$): 388.1371, found: 388.1360.

Synthesis of ligand (3c):

The quantities involved are as follows: 1-(9-ethyl-9H-carbazol-3-yl)ethan-1-one (0.65g, 2.77 mmol), methyl 9-ethyl-9H-carbazole-3-carbodithioate (0.87g, 3.05 mmol) and sodium hydrate (50%, 0.15g, 6.03 mmol). Orange solid, Yield: 0.79g (60%). **^{1}H NMR** (400 MHz, $CDCl_3$) δ 16.73 (s, 2H), 8.85 (s, 1H), 8.75 (s, 1H), 8.24 – 8.12 (m, 3H), 7.81 (s, 1H), 7.59 – 7.39 (m, 6H), 7.36 – 7.28 (m, 2H), 4.45 – 4.35 (m, 4H), 1.54 – 1.38 (m, 6H). **^{13}C NMR** (101 MHz, $CDCl_3$) δ = 206.2, 178.7, 142.7, 142.1, 140.8, 140.7, 137.7, 126.7, 126.4, 125.9, 125.7, 125.2, 123.5, 123.4, 123.2, 123.0, 120.9, 120.6, 120.2, 120.1, 119.8, 109.1, 109.0, 108.7, 108.1, 38.0, 37.9, 14.0. **HRMS** (ESI) m/z calcd for $C_{31}H_{25}N_2OS$ ($[M-H]^+$): 473.1688, found: 473.1686.

General procedure for the synthesis of bis(pentafluoro)phenyl boron compounds:

In a degassed nitrogen purged pressure tube 1,3-monothio-β-diketone (**3a – 3c**) derivatives (1.0 mmol), tris(pentafluorophenyl)borane (1.2 mmol) and dry. toluene (10 mL) were added and the reaction mixture was stirred at 110 °C for 24 h. Then the solvent was removed by rota evaporator, crude product was purified using neutral alumina column chromatography.

Synthesis of compound 4a:

The quantities involved are: Compound **3a** (0.35g, 0.90 mmol) and tris(pentafluorophenyl)borane.(0.55g, 1.08 mmol). Dark orange powder, Yield: 0.41g (62%). **^{1}H NMR** (700 MHz, $CDCl_3$) δ 8.74 (s, 1H), 8.30 – 8.23 (m, 3H), 8.11 (d, *J* = 8.0, 1H), 7.73 (s, 1H), 7.56 (t, *J* = 8.0 Hz, 1H), 7.49 – 7.43 (m, 2H), 7.36 (t, *J* = 8.0 Hz, 1H), 7.11 – 7.07 (m, 2H), 4.42 (q, *J* = 7.1 Hz, 1H), 3.96 (s, 3H), 1.48 (t, *J* = 7.3 Hz, 3H). **^{13}C NMR** (176 MHz, $CDCl_3$) δ 188.1, 179.8, 165.5, 147.9 (d, *J* = 241 Hz), 143.8, 140.9, 139.6 (d, *J* = 260 Hz), 137.2 (d, *J* = 248 Hz), 132.4, 130.5, 127.2, 126.8, 123.8, 123.1, 122.1, 121.2, 120.7, 114.8, 109.4, 108.9, 108.4, 55.9, 38.2, 13.9. **^{19}F NMR** (376 MHz, $CDCl_3$) δ = -134.08 (d, 4f, Pf), -156.99 (t, 2f, Pf), -163.40 (d, 4f, Pf). **^{11}B NMR** (128 MHz, $CDCl_3$) δ 0.53. **HRMS** (ESI) m/z calcd for $C_{36}H_{21}BF_{10}NO_2S$ ($[M+H]^+$): 732.1263, found: 732.1210.

Synthesis of compound 4b:

The quantities involved are: Compound **3b** (0.40g, 1.03 mmol) and tris(pentafluorophenyl)borane.(0.63g, 1.24 mmol). Orange powder, Yield: 0.57g (76%). **^{1}H NMR** (700 MHz, $CDCl_3$) δ 8.99 (s, 1H), 8.40 – 8.37 (m, 1H), 8.23 (d, *J* = 8.0 Hz, 1H), 8.01 - 7.97 (m, 2H), 7.76 (s, 1H), 7.57 (t, *J* = 8.0 Hz, 1H), 7.53 – 7.47 (m, 2H), 7.03 (d, *J* = 8.0 Hz, 2H), 4.43 (q, *J* = 7.0 Hz, 2H), 3.92 (s, 3H), 1.51 (t, *J* = 7.3 Hz, 3H). **^{13}C NMR** (176 MHz, $CDCl_3$) δ 184.6, 181.4, 164.3, 147.8 (d, *J* = 243 Hz),, 144.3, 140.8, 140.1 (d, *J* = 250 Hz), 137.1 (d, *J* = 246 Hz), 132.2, 130.5, 128.2, 127.2, 124.4, 123.8, 123.7, 123.0, 121.0, 120.9, 114.4, 109.4, 109.1, 109.0, 55.7, 38.1, 13.8. **^{19}F NMR** (376 MHz, $CDCl_3$) δ -134.03 (d, 4f, Pf), -157.03 (t, 2f, Pf), -163.42 (d, 4f, Pf). **^{11}B NMR** (128 MHz, $CDCl_3$) δ 0.37. **HRMS** (ESI) m/z calcd for $C_{36}H_{21}BF_{10}NO_2S$ ($[M+H]^+$): 732.1263, found: 732.1277.

Synthesis of compound 4c:

The quantities involved are: Compound **3c** (0.40g, 0.84 mmol) and tris(pentafluorophenyl)borane. (0.51g, 1.01 mmol). Dark Red powder, Yield: 0.41g (60%). ^{1}H NMR (400 MHz, $CDCl_3$) δ 8.99 (s, 1H), 8.75 (s, 1H), 8.41 – 8.35 (m, 1H), 8.27 – 8.18 (m, 2H), 8.12 (dd, *J* = 8.0, 1.9 Hz, 1H), 7.89 (s, 1H), 7.62 – 7.30 (m, 9H), 4.50 - 4.28 (m, 4H), 1.54 – 1.42 (m, 6H). **^{19}F NMR** (376 MHz, $CDCl_3$) δ -133.93 (d, 4f, Pf), -157.22 (t, 2f, Pf), -163.51 (d, 4f, Pf). **^{11}B NMR** (128 MHz, Acetone-D_6) δ 0.52. **HRMS** (ESI) m/z calcd for $C_{43}H_{26}BF_{10}N_2OS$ ($[M+H]^+$): 819.1735, found: 819.1761.

2D.5 References

1. Liang, X.; Tu, Z.-L.; Zheng, Y.-X. *Chem. Eur. J.* **2019,** *25*, 5623-5642.

2. Goushi, K.; Yoshida, K.; Sato, K.; Adachi, C. *Nat. Photonics* **2012,** *6*, 253-258.

3. Endo, A.; Sato, K.; Yoshimura, K.; Kai, T.; Kawada, A.; Miyazaki, H.; Adachi, C. *Appl. Phys. Lett.* **2011,** *98*, 083302.

4. Braveenth, R.; Lee, H.; Park, J. D.; Yang, K. J.; Hwang, S. J.; Naveen, K. R.; Lampande, R.; Kwon, J. H. *Adv. Funct. Mater.* **2021,** *31*, 2105805.

5. Chen, Y.; Zhang, D.; Zhang, Y.; Zeng, X.; Huang, T.; Liu, Z.; Li, G.; Duan, L. *Adv. Mater.* **2021,** *33*, 2103293.

6. Rayappa Naveen, K.; Prabhu Cp, K.; Braveenth, R.; Hyuk Kwon, J. *Chem. Eur. J.* **2022,** *28*, e202103532.

7. Huang, Z.; Wang, S.; Dewhurst, R. D.; Ignat'ev, N. V.; Finze, M.; Braunschweig, H. *Angew. Chem. Int. Ed.* **2020,** *59*, 8800-8816.

8. Murali, A. C.; Nayak, P.; Venkatasubbaiah, K. *Dalton Trans.* **2022,** *51*, 5751-5771.

9. Murali, A. C.; Nayak, P.; Nayak, S.; Das, S.; Senanayak, S. P.; Venkatasubbaiah, K. *Angew. Chem. Int. Ed.* **2023,** *62*, e202216871.

10. Murali, A. C.; Nayak, P.; Panda, R.; Das, R.; Venkatasubbaiah, K. *ACS Appl. Opt. Mater* **2023,** *1*, 1033-1042.

11. Im, Y.; Kim, M.; Cho, Y. J.; Seo, J.-A.; Yook, K. S.; Lee, J. Y. *Chem. Mater.* **2017,** *29*, 1946-1963.

12. Rowland, C. A.; Lorzing, G. R.; Bhattacharjee, R.; Caratzoulas, S.; Yap, G. P. A.; Bloch, E. D. *Chem. Commun.* **2020,** *56*, 9352-9355.

13. Przypis, L.; Walczak, K. Z. *J. Org. Chem.* **2019,** *84*, 2287-2296.

14. Raikwar, M. M.; Mohbiya, D. R.; Sekar, N. *ChemistrySelect* **2019,** *4*, 11966-11978.

CHAPTER 3

Synthesis, Structural, and Optical Properties of Pyrazolyl Anchored Bis(pentafluorophenyl)boron Complexes

3.1 Introduction

The study of organic luminescent materials has evolved into an important topic owing to their potential applications in organic lasers, photoswitches and organic electronics.[1-3] Different strategies have been employed to tune the electronic and, photophysical properties, stability, and durability of such materials.[4-7] Attractive photophysical properties were achieved by incorporating main-group elements in the framework of organic molecules.[8-10] Among the different main-group incorporated organic fluorophores, boron-embedded fluorophores[11-13] have gained attention due to their stability, electron acceptability and tuneable luminescence.[14-17] In particular, tetra-coordinated N,O-chelated boron compounds have emerged as promising candidates due to their interesting photophysical properties such as solvatochromism, aggregation induced enhanced emission (AIEE), and mechanochromism, as well as their exhibited potential applications in electroluminescent and bio-imaging materials.[17-21]

Pyrazoles are heterocyclic compounds that have attracted interest owing to their use in pharmaceutical industry.[22-25] In addition, substituted pyrazoles are also used as herbicides, pesticides, supramolecular entity units, UV stabilizer, ligands in coordination chemistry and catalysis, and also in photoinduced electron transfer systems.[26-37] However, their applications as fluorescent materials are not well studied. Hence, there is a growing interest in the preparation of structurally diverse pyrazoles and investigation of their fluorescent behaviour. We have recently shown that tetra-aryl pyrazoles with their unique propeller arrangement exhibited aggregation induced emission.[38] Furthermore, we also showed that one can tune the optical properties of tri-aryl pyrazoles by utilizing B-N coordination and subsequently investigated the interesting non-linear optical behavior and electroluminescent properties of these materials.[39-41]

It is well known that multiple factors such as electronic structure, molecular geometry, crystal packing, position of coordination/chelation, etc., play a vital role in determining the photophysical properties of such materials. There remains a huge scope to synthesize structurally diverse organoboron complexes and explore their properties. Here, we report the synthesis, structure, and photophysical properties of two different types of tetra-aryl pyrazole anchored N,O-chelated boron compounds. We subsequently investigate the AIEE properties of these compounds. We also perform density functional theory (DFT) calculations to obtain insights into the electronic structure of the compounds. Finally, we demonstrate the application of our synthesized compounds for picric acid sensing.

3.2 Results and discussion

3.2.1 Synthesis and characterization

The starting materials **1b**-**3b** were synthesized by using appropriate reagents and following the methodology reported by us previously,[38, 39] whereas the starting materials **4b**-**6b** were synthesized by following the method reported by Vijay Kumar *et al.*[42] The ligands **1a**-**6a** were synthesized by demethylation of **1b**-**6b** using BBr_3. The desired boron compounds **1-6** were synthesized in good yields by the reaction of $(C_6F_5)_3B$ with ligands **1a-6a** in dry toluene at 110 °C (**Scheme 3.1**). The ligands **1a-6a** and the boron compounds **1-6** were characterized using ^{1}H and ^{13}C NMR spectroscopy (^{11}B and ^{19}F NMR in case of **1**-**6**), HRMS/elemental analysis, and X-ray diffraction analysis in case of **1, 4,** and **5**. The ^{1}H NMR of ligands **1a-6a** showed a singlet between 9-11 ppm which corresponds to the phenolic -OH. It should be noted that ligands **1a-3a** have shown phenolic -OH signal at ~9.6 ppm, however, the phenolic -OH signal appeared at ~11.0 ppm for ligands **4a-6a**. This noticeable shift in the chemical shift of the -OH proton can be attributed to effective intramolecular hydrogen bonding prevailing in compounds **4a-6a** over **1a-3a.** Representative ^{1}H NMR spectra of ligands **1a**, **4a** and compound **1** are

presented in **Figure 3.1**. The disappearance of the downfield phenolic -OH peak and the shifts in the aliphatic and aromatic peak positions in the ^{1}H-NMR spectra of all six compounds (**1-6**) hints towards the formation of the boron compounds. The ^{19}F{^{1}H} NMR spectra of all compounds **1-6**, showed three set of resonances, which indicates the presence of pyrazole coordinated pentafluorophenyl groups. The ^{11}B{^{1}H} NMR spectra recorded for compounds **1-6** showed a broad singlet at ~ 0 ppm, which confirms the tetra-coordinated nature of the desired organoboron compounds.

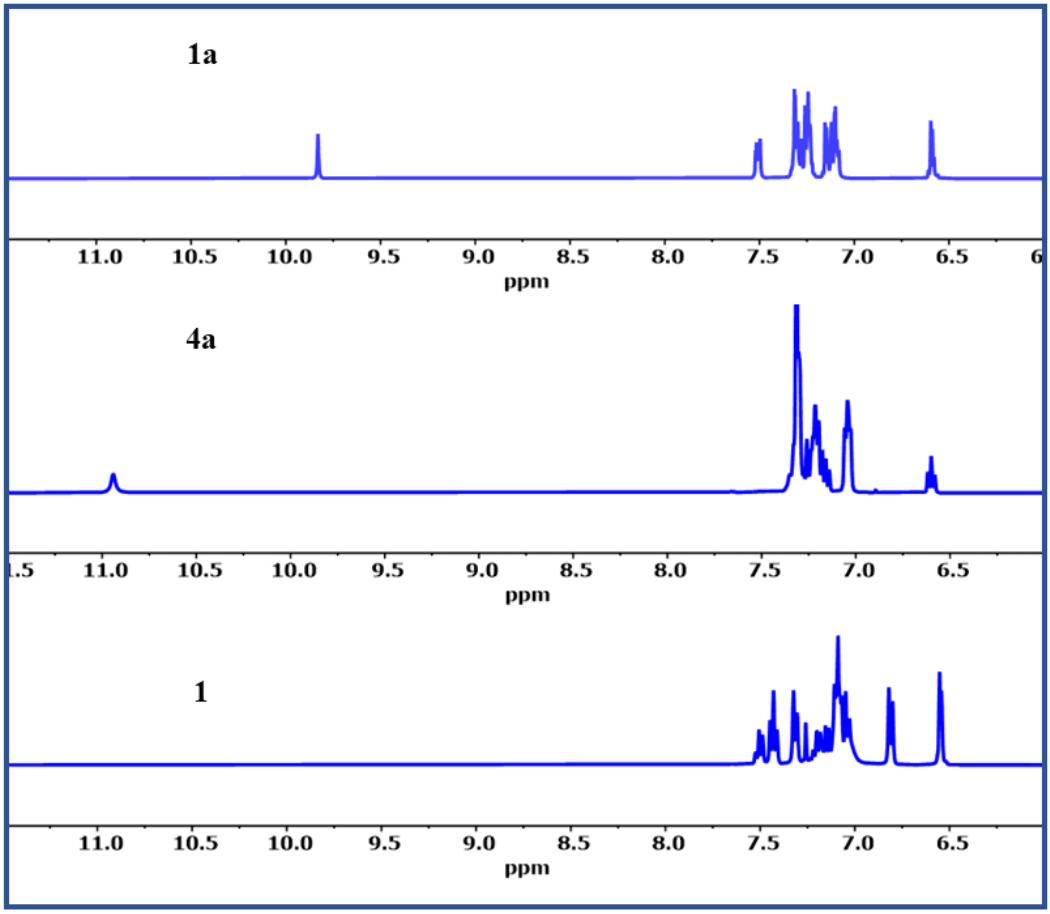

Figure 3.1: ^{1}H-NMR spectra of ligands **1a, 4a** and compound **1** in $CDCl_3$

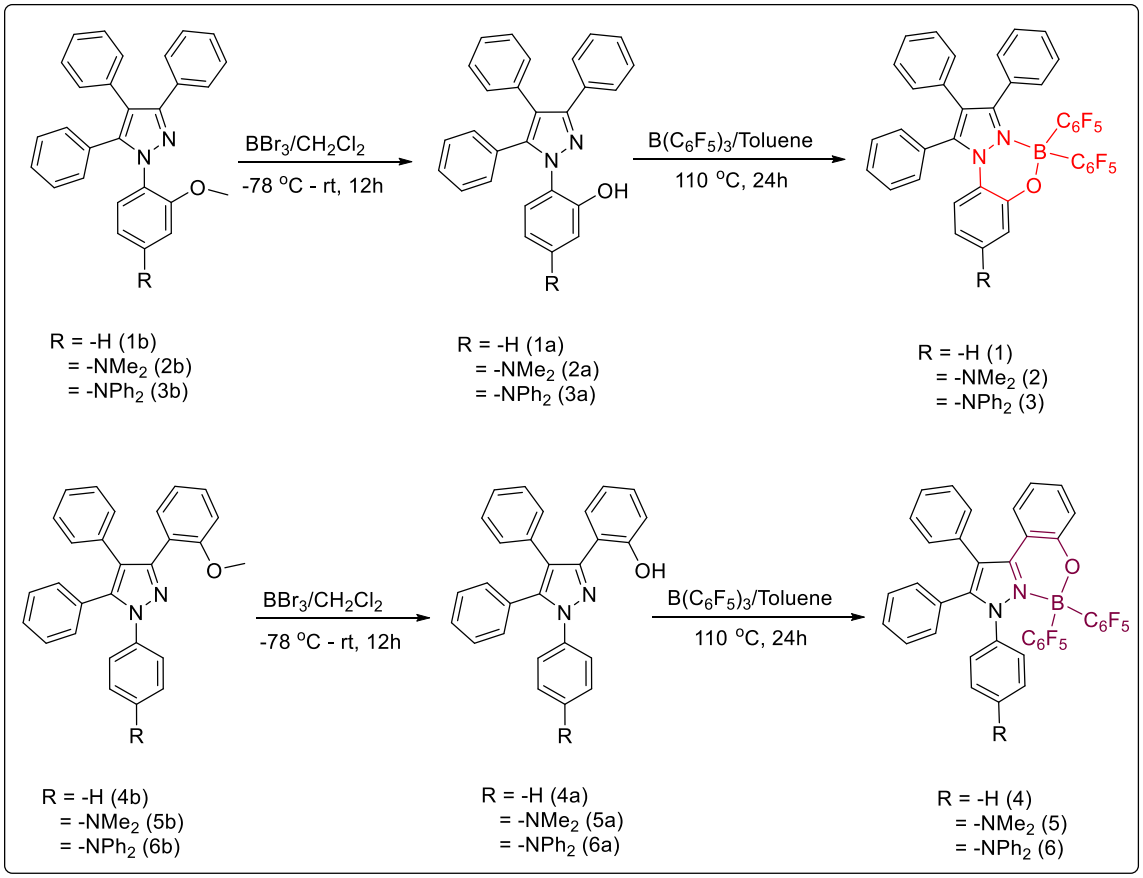

Scheme 3.1: Synthetic route for pyrazole-anchored N,O-chelated bis(pentafluorophenyl) boron compounds **1-3** (top) and **4-6** (bottom)

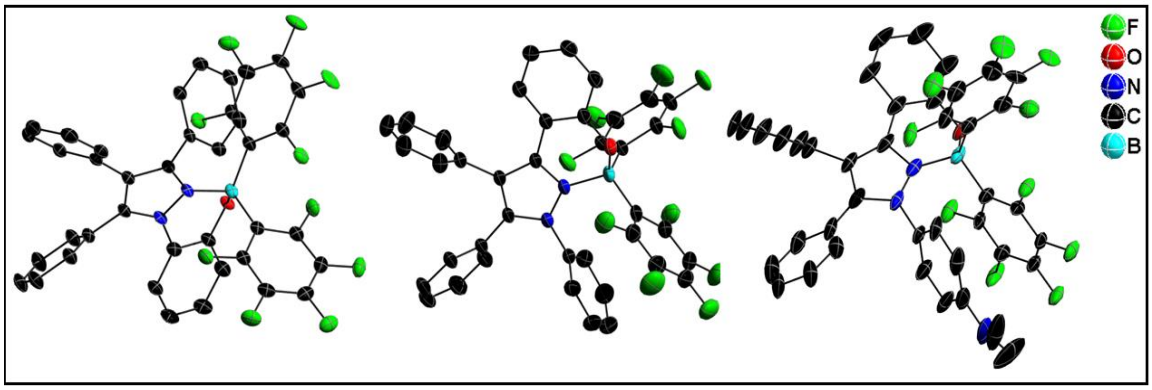

Figure 3.2: Molecular structure of compounds **1, 4,** and **5** (from left to right) with 50%, 20%, 30% probability level of thermal ellipsoids (hydrogen atoms are omitted for clarity).

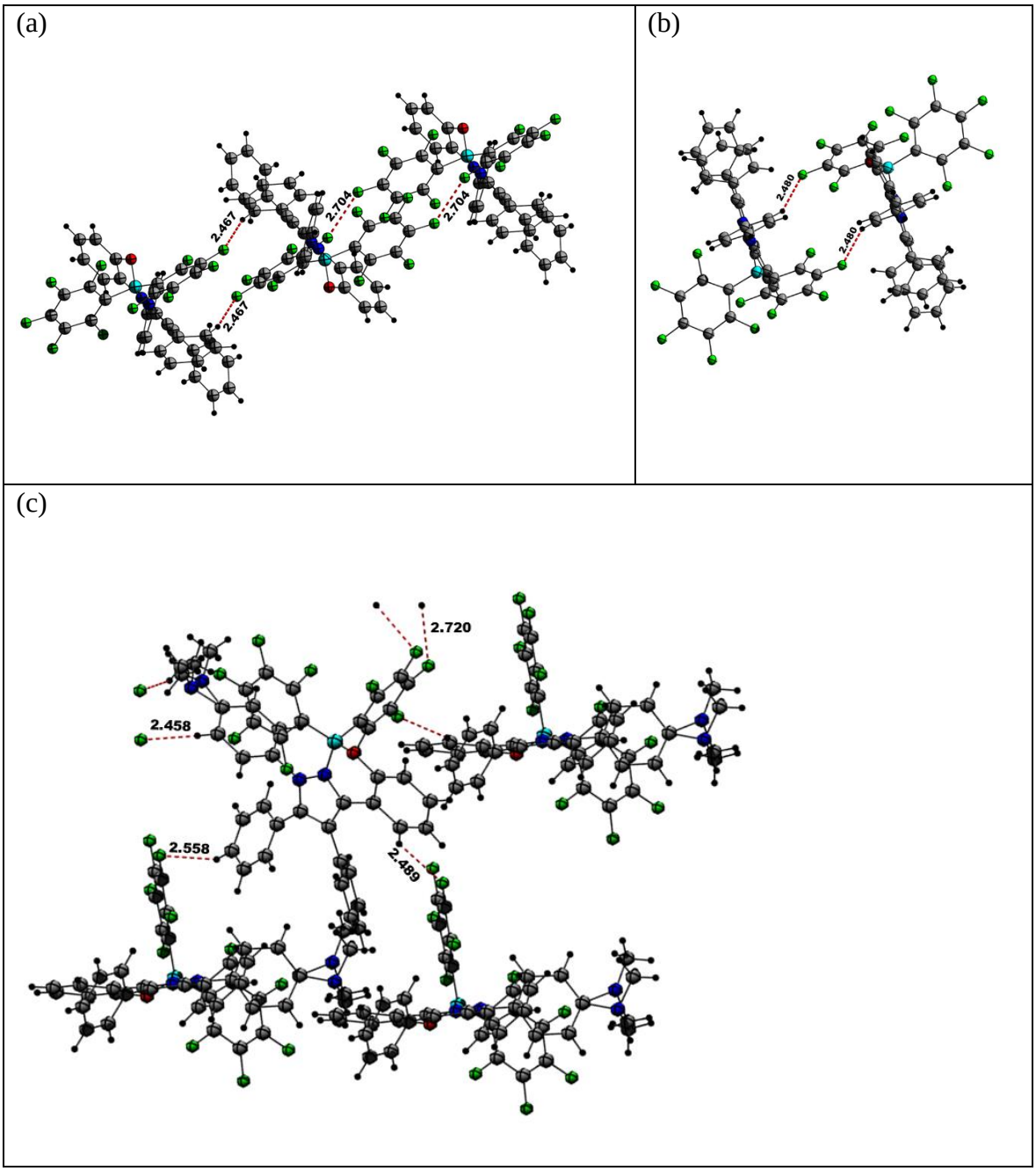

Figure 3.3: (a) Intermolecular interactions (C-H…F and F…F) in compound **1**; (b) Intermolecular interactions (C-H…F) in compound **4**; (c) Intermolecular interactions (C-H…F) in compound **5**.

The molecular structure of compounds **1, 4,** and **5** were confirmed with X-ray crystallography analysis. Single crystals of the compounds **1, 4,** and **5** were obtained by slow evaporation of a chloroform and hexane mixture. The X-ray structures showed that compounds **1** and **5** crystallized in triclinic crystal system with P1 space group whereas

compound **4** crystallized in a monoclinic crystal system with $P2_1$ space group. The molecular structures of **1**, **4**, and **5** are presented in **Figure 3.2**, and the selected bond lengths and bond angles are provided in **Table 3.1.** The B-N bond distances (1.596 (2) Å for **1**; 1.602 (2) Å for **4**; 1.577 (10) Å for **5**) and the B-O bond distances (1.474 (2) Å for **1**; 1.462 (2) Å for **4**; 1.468 (12) Å for **5**) are comparable to the literature reported values.[43-46] The boron atom deviates (0.40 Å for **1**; 0.36 Å for **4**; 0.34 Å for **5**) from the six-membered ring defined by N_2C_2OB in case of **1** and NC_3OB in case of **4** and **5**. There is a drastic difference between the interplanar angle between the pyrazole and the N-phenyl (Plane A) of compound **1** (62.67 Å) and compounds **4** and **5** (11.1 Å for **4**; 14.2 Å for **5**). A reverse trend was observed for the interplanar angle between the pyrazole ring and the plane D (**Table 3.1**). The interplanar angle between the pyrazole and the plane B or C varies from 41.5 ° to 82.2 °. Compounds **1**, **4**, and **5** showed weak intermolecular interactions like C–H···F hydrogen bonds (**Figure 3.3**). These interactions help in restricting the intramolecular rotation which leads to enhanced quantum yields in the aggregated state (see photophysical section).

Table 3.1. Bond length, bond angle and plane deviation measurement data for compounds **1**, **4**, and **5**.

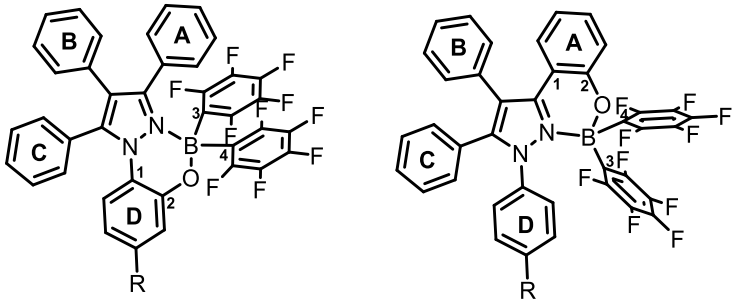

Compound	**1**	**4**	**5**
B-N (Å)	1.596 (2)	1.602 (2)	1.577 (10)
B-O (Å)	1.474 (2)	1.462 (2)	1.468 (12)
B-C3 (Å)	1.644 (2)	1.626 (3)	1.646 (10)

B-C4 (Å)	1.627 (2)	1.650 (3)	1.659 (10)
N-B-O (deg)	105.1 (1)	104.2 (1)	104.4 (6)
N-B-C3 (deg)	109.7 (1)	111.8 (1)	110.7 (6)
O-B-C4 (deg)	107.1 (1)	108.8 (1)	105.1 (6)
C3-B-C4 (deg)	117.3 (1)	114.8 (1)	116.4 (5)
Deviation of B from N_2C_2OB plane (Å)	0.405 (1)	-	-
Deviation of B from NC_3OB plane (Å)	-	0.361 (1)	0.343 (1)
Angle between pyrazole ring and plane A (Å)	62.7 (5)	11.1 (6)	14.2 (2)
Angle between pyrazole ring and plane B (Å)	45.2 (5)	82.2 (7)	60.9 (3)
Angle between pyrazole ring and plane C (Å)	58.6 (4)	54.7 (7)	41.5 (3)
Angle between pyrazole ring and plane D (Å)	26.5 (5)	85.8 (8)	78.5 (3)

Table 3.2. Crystal data and structure refinement for compounds 1, 4 and **5.**

	Compound 1	**Compound 4**	**Compound 5**
Empirical formula	$C_{39}H_{19}BF_{10}N_2O$	$C_{39}H_{19}BF_{10}N_2O$	$C_{41}H_{24}BF_{10}N_3O$
Formula weight	732.37	732.37	775.44
Temperature/K	100.00(10)	299.6(9)	113(18)
Crystal system	triclinic	triclinic	monoclinic
Space group	P-1	P-1	$P2_1$
a/Å	7.88670(10)	8.8799(2)	12.4589(13)
b/Å	13.1605(3)	14.0601(3)	12.9868(9)
c/Å	17.5175(4)	16.9083(3)	12.6311(11)
α/°	109.877(2)	75.691(2)	90
β/°	90.082(2)	81.675(2)	107.763(10)
γ/°	107.239(2)	78.457(2)	90
Volume/$Å^3$	1622.45(6)	1994.05(8)	1946.3(3)
Z	2	2	2
$\rho_{calc}g/cm^3$	1.499	1.220	1.323
μ/mm^{-1}	0.130	0.922	0.113
F(000)	740.0	740.0	788.0

Crystal size/mm^3	0.15 × 0.12 × 0.11	0.14 × 0.13 × 0.11	0.14 × 0.12 × 0.11
Radiation	MoKα (λ = 0.71073)	CuKα (λ = 1.54184)	MoKα (λ = 0.71073)
2Θ range for data collection/°	6.94 to 49.998	7.53 to 156.84	6.668 to 52.732
Index ranges	-9 ≤ h ≤ 9, -15 ≤ k ≤ 15, -20 ≤ l ≤ 20	-11 ≤ h ≤ 11, -17 ≤ k ≤ 17, -20 ≤ l ≤ 20	-15 ≤ h ≤ 14, -15 ≤ k ≤ 16, -15 ≤ l ≤ 15
Reflections collected	22626	37407	32402
Independent reflections	5704 [R_{int} = 0.0314, R_{sigma} = 0.0223]	8039 [R_{int} = 0.0632, R_{sigma} = 0.0320]	7671 [R_{int} = 0.1186, R_{sigma} = 0.0627]
Data/restraints/parameters	5704/0/478	8039/0/478	7671/1107/516
Goodness-of-fit on F^2	1.035	1.081	1.066
Final R indexes [I>=2σ(I)]	R_1 = 0.0332, wR_2 = 0.0871	R_1 = 0.0589, wR_2 = 0.1737	R_1 = 0.0859, wR_2 = 0.1948
Final R indexes [all data]	R_1 = 0.0361, wR_2 = 0.0892	R_1 = 0.0679, wR_2 = 0.1837	R_1 = 0.0927, wR_2 = 0.2002
Largest diff. peak/hole / e Å^{-3}	0.30/-0.23	0.20/-0.32	0.49/-0.38
Flack parameter	-	-	-1.3(5)

3.2.2 Photophysical properties

The optical properties of compounds **1-6** were investigated in different solvents such as toluene, tetrahydrofuran (THF), and acetonitrile (CH_3CN) and the results are presented in **Table 3.3**, and **Figures 3.4 – 3.8**.

Table 3.3. Photophysical data of compounds **1-6** in different solvents

Compound	**Solvent**	**λ_{abs}[a] /nm (ε x 10^4/M^{-1} cm^{-1})**	**λ_{ems}[b] (nm)**	**Stokes Shift (cm^{-1})**	**ϕ_F[d] (%)**	**τ_{av} (ns)**
1	Toluene	312 (1.28)	506	12289	4.6,	
	THF	307 (1.18)	515	13156	1.4(5.6)[f]	1.3 (0.7)[g]
	ACN	307 (1.17)	517	13231	0.5	
			380[c]		3.7[e]	
2	Toluene	356 (1.42)	500	8089	1.7,	
	THF	352 (1.85)	533	9648	0.5(41.6)[f]	0.2 (6.2)[g]
	ACN	348 (1.71)	555	10717	0.7	
			485[c]		30.8[e]	

3	Toluene	367 (1.86)	477	6283	16.4,	
	THF	365 (1.56)	508	7712	14.0(32.1) [f]	1.6 (3.2)[g]
	ACN	360 (1.73)	541	9293	12.0	
			(452, 549)[c]		11.8 [e]	
4	Toluene	323 (0.74)	434	7918	20.4,	
	THF	319 (1.00)	440	8620	18.9(19.6) [f]	3.8 (2.6)[g]
	ACN	318 (1.04)	446	9025	14.5	
			380 [c]		5.4 [e]	
5	Toluene	318 (1.81)	438	8615	<0.1	
	THF	318 (1.27)	475	10394	<0.1(15.5) [f]	2.2 (3.6)[g]
	ACN	316 (1.44)	500	11645	0.2	
			408 [c]		28.2 [e]	
6	Toluene	328 (1.99)	432	7339	4.0,	
	THF	324 (1.65)	446	8443	1.6(29.6) [f]	2.9 (3.3)[g]
	ACN	320 (1.99)	468	9883	5.3	
			438 [c]		23.2 [e]	

[a]Absorption maximum (concentration = 5.0 x 10^{-5} M), [b]Excited at λ_{max}, [c]Solid state emission maxima, [d]Absolute quantum yield using integrating sphere module, [e]Solid state quantum yield using integrating sphere module, [f]Absolute fluorescence quantum yield of the aggregates (f_w=99%) using integrating sphere. [g]Fluorescence lifetime of aggregates in H_2O/THF (f_w=99%).

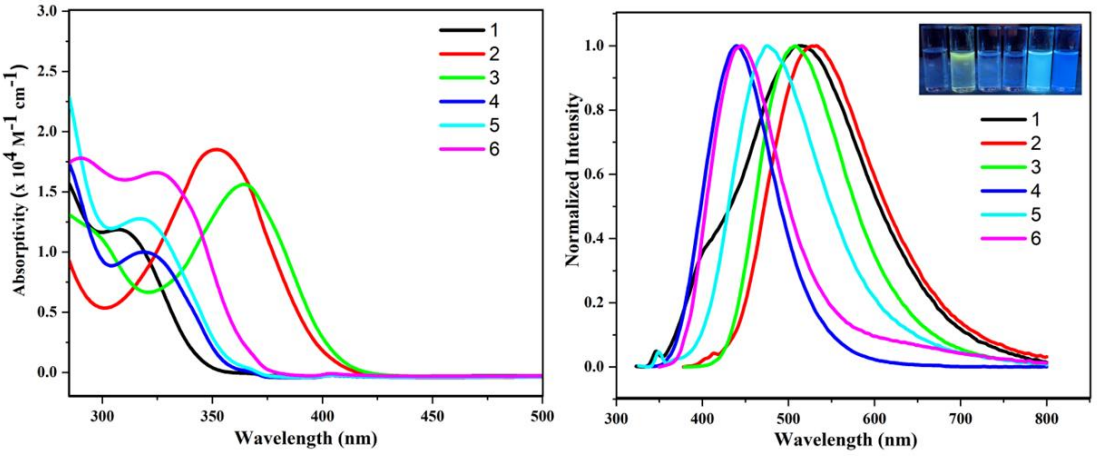

Figure 3.4: Absorption spectra of compounds **1-6** (left) and normalized emission spectra of compounds **1-6** (right) in tetrahydrofuran (5.0 x 10^{-5} M concentration). Inset (Right): photograph of compounds **1-6** in tetrahydrofuran under a hand-held UV light at 365 nm.

The absorption spectra of compounds **1-6** in THF (**Figure 3.4**) showed maxima ranging from 307-365 nm that corresponds to π-π* transition. All the six derivatives have shown similar fine structure in absorption and emission spectra. By changing the position of the boron binding site from N-phenyl to 3-phenyl, a remarkable shift in the absorption and emission maxima was observed. The absorption of compound **4** exhibited red shift over its respective isomeric compound **1**. A comparison of the absorption of **2-3** with **5-6** owing to the presence of electron donating -NMe_2/-NPh_2 along with electron accepting boron on the same phenyl group in the former, which helps in reducing the HOMO-LUMO gap. The emission of compound **1** exhibited a 75 nm red shift compared to its respective isomeric compound **4**. Similarly, compounds **2** and **3** showed 58 nm and 62 nm red shift compared to compounds **5** and **6** respectively. Owing to the reverse trend observed for compound **1**, it displayed a large Stokes shift of 13156 cm^{-1}. These observation indicates the importance of boron chelation on the N-phenyl ring *vs.* 3-phenyl and also electron donating nature of -NMe_2 and -NPh_2 groups. Detailed photophysical data for compounds **1-6** in all solvents is presented in **Table 3.3.** A positive solvatochromic emission with solvent polarity (toluene, THF, and CH_3CN) was observed for all compounds which indicates that stabilization of the excited states with solvent is significant. A drastic increase in quantum yields in the aggregated state was observed for most of the boron compounds which signifies that AIEE phenomenon prevails in these molecules which will be discussed *vide infra* (**Table 3.3**). Further, a noticeable change is the quantum yield observed for compounds **1** and **4** (**Table 3.3**, Φ_F in THF = 1.4 for **1** and 18.9 for **4**) which highlights the effect of regio-isomerism. The photoluminescence (PL) decay of **1-6** were studied by a time resolved technique.

The PL decay of **1-6** showed, no appreciable change in the average lifetime (ranging from 1.3 to 3.8 ns), in pure THF solution and in THF-water mixture (ranging from 0.2 to 6.2 ns), however, a marginal increase in average life time was observed for **2-6** over **1** and **4** in the aggregated state probably due to different types and size of aggregates prevails in **2-6.** Compounds **1-6** displayed a single exponential life-time decay in pure THF solution, and two or three exponential life-time decays, in the aggregated state suggesting that the molecules in THF-water mixture may exist in more than one environment. Additionally, we measured the lifetime decay of compound **2** in the thin film state (poly(methyl methacrylate) PMMA:**2** in 95:5 weight %) which reveal that the life time of **2** in both thin film and THF-water mixture have nearly identical values.

3.2.3 AIE properties

We have recently reported that the propeller type arrangement of phenyl around the pyrazole unit helps to induce AIEE phenomenon.[38]

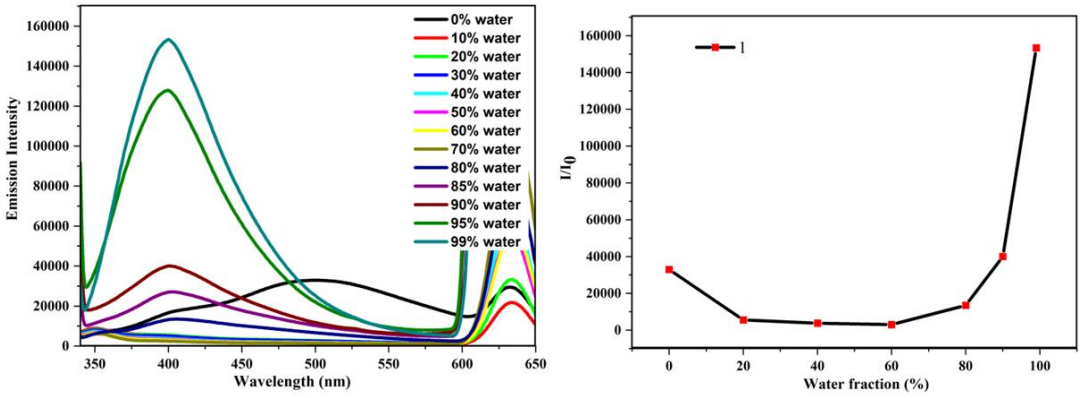

Figure 3.5: Fluorescence spectra of compound **1** (5.0 x 10^{-5} M) in a THF/H_2O mixture with different water fraction (f_w) (left). I/I_o *vs* water fraction plot for compound **1** (vol%) (right). Inset (Right): photograph of compound **1** in different THF/H_2O mixture under a hand-held UV light at 365 nm.

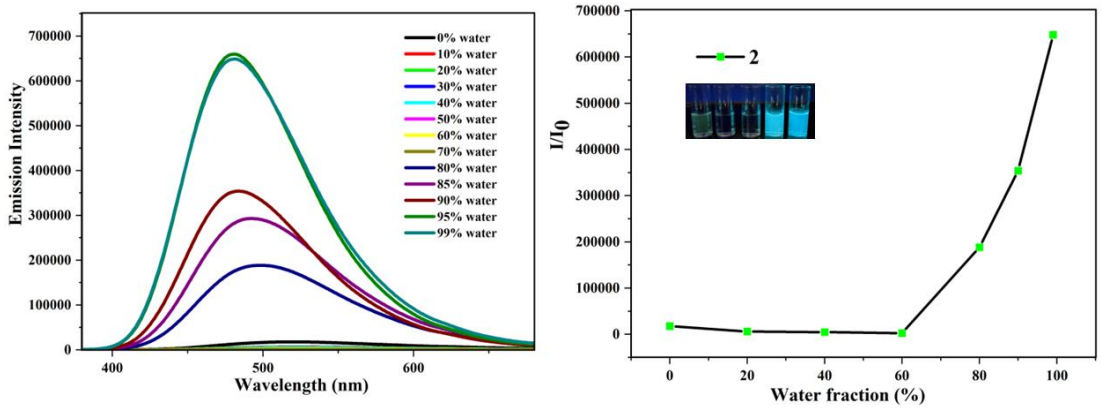

Figure 3.6: Fluorescence spectra of compound **2** (5.0 x 10^{-5} M) in a THF/H_2O mixture with different water fraction (f_w) (left). I/I_o *vs* water fraction plot for compound **2** (vol%) (right). Inset (Right): photograph of compound **2** in different THF/H_2O mixture under a hand-held UV light at 365 nm.

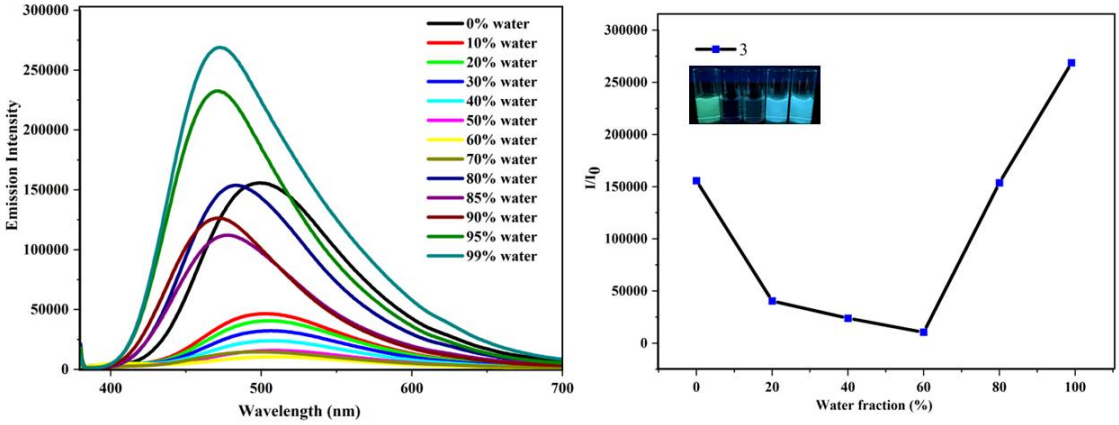

Figure 3.7: Fluorescence spectra of compound **3** (5.0 x 10^{-5} M) in a THF/H_2O mixture with different water fraction (f_w) (left). I/I_o *vs* water fraction plot for compound **3** (vol%) (right). Inset (Right): photograph of compound **3** in different THF/H_2O mixture under a hand-held UV light at 365 nm.

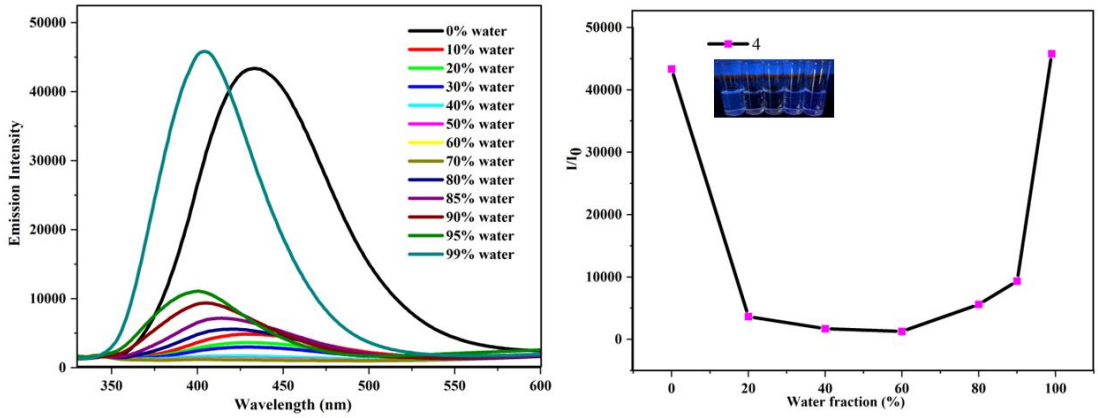

Figure 3.8: Fluorescence spectra of compound **4** (5.0 x 10^{-5} M) in a THF/H_2O mixture with different water fraction (f_w) (left). I/I_o *vs* water fraction plot for compound **4** (vol%) (right). Inset (Right): photograph of compound **4** in different THF/H_2O mixture under a hand-held UV light at 365 nm.

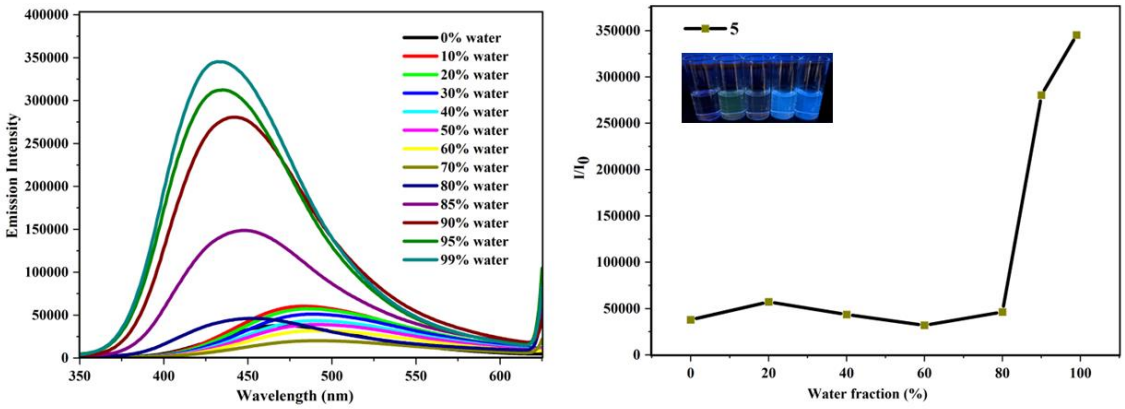

Figure 3.9: Fluorescence spectra of compound **5** (5.0 x 10^{-5} M) in a THF/H_2O mixture with different water fraction (f_w) (left). I/I_o *vs* water fraction plot for compound **5** (vol%) (right). Inset (Right): photograph of compound **5** in different THF/H_2O mixture under a hand-held UV light at 365 nm.

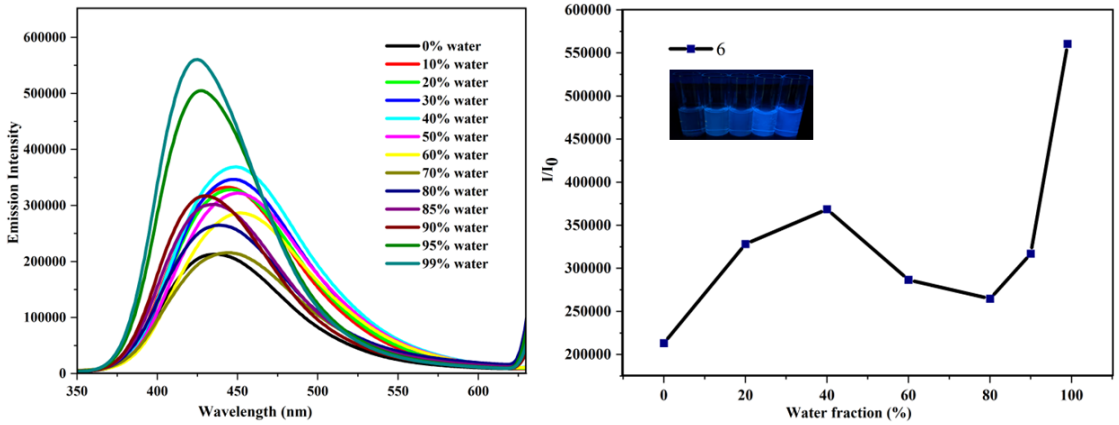

Figure 3.10: Fluorescence spectra of compound **6** (5.0 x 10^{-5} M) in a THF/H_2O mixture with different water fraction (f_w) (left). I/I_o *vs* water fraction plot for compound **6** (vol%) (right). Inset (Right): photograph of compound **6** in different THF/H_2O mixture under a hand-held UV light at 365 nm.

To examine the AIEE properties, we recorded fluorescence spectra of all pyrazole-boron compounds **1-6** in pure THF and THF/H_2O mixture with different water fractions (f_w). **Figures 3.5-3.10** show the emission spectra of compounds **1-6** in THF/H_2O mixture with different water fractions. The emission intensity I/I_0 was found to be almost identical up to ~ 70% water in THF for compounds **1, 2, 5,** and **6,** whereas **3** and **4** have shown a decrease in emission intensity with increase of water fraction from 0 % to 10 % along with slight red shift. The decrease in the emission intensity and red shift of the emission wavelength of **3** and **4** may be ascribed due to twisted intramolecular charge transfer

(TICT) as observed in other cases.[13] At high water content (f_w > 70%) the emission intensity increased drastically and reaches a maximum around 80-99% (f_w). This drastic enhancement is due to the presence of multiple phenyl rings and the non-planarity of the molecule. As discussed *vide supra* the phenyl rings around the pyrazole are arranged in a non-planar propeller shape. The molecular packing of these compounds reveals several C-H..F interactions which helps these molecules to gain better rigidity, i.e., the free rotation of the molecules is restricted which limits the conformational freedom of the molecules, thus leading to stronger emission in the aggregated state.

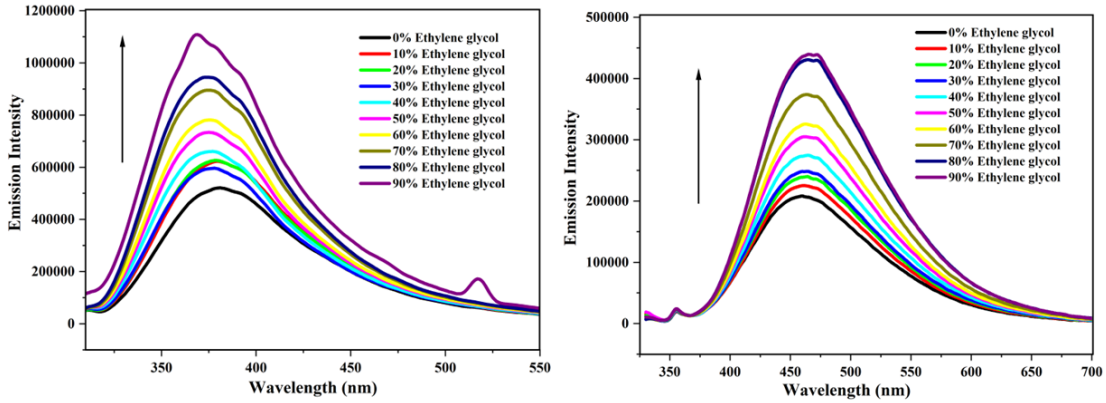

Figure 3.11: Emission spectra of compound **1** with different percentage of MeOH/ethylene glycol mixture (10^{-5} M concentration) (left). Emission spectra of compound **2** with different percentage of MeOH/ethylene glycol mixture (10^{-5} M concentration) (right).

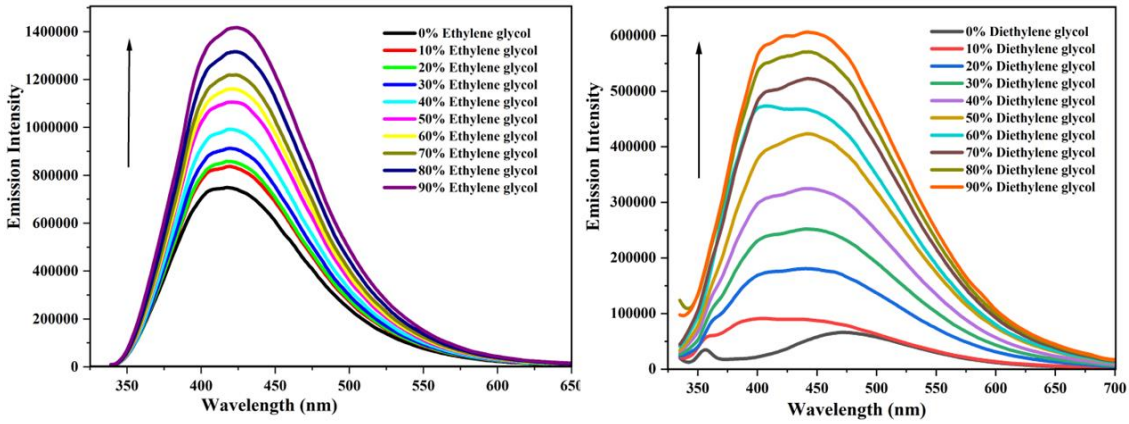

Figure 3.12: Emission spectra of compound **3** with different percentage of MeOH/ethylene glycol mixture (10^{-5} M concentration) (left). Emission spectra of compound **4** with different percentage of MeOH/diethylene glycol mixture (10^{-5} M concentration) (right).

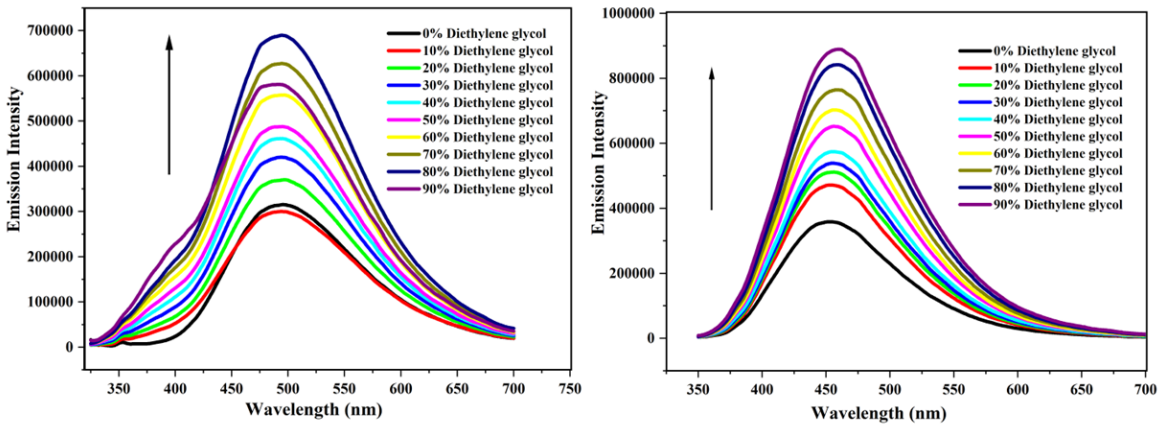

Figure 3.13: Emission spectra of compound **5** with different percentage of MeOH/diethylene glycol mixture (10^{-5} M concentration) (left). Emission spectra of compound **6** with different percentage of MeOH/diethylene glycol mixture (10^{-5} M concentration) (right).

To further understand the AIEE behaviour exhibited by compounds **1-6**, their photoluminescence was recorded at a specific concentration while varying the viscosity of the medium. With increase in viscosity the molecular rotations will decrease which will help to gain enhanced emission. As seen in **Figures 3.11-3.13**, the emission intensity of these compounds increased continuously with an increase in viscosity, which further supports the notion that restricted intramolecular rotation plays an important part in the enhanced emission observed in the aggregate state.

3.2.4 Picric acid sensing studies

Detection of picric acid is important due to its harmful effects to human health and its potential risk to act as a warfare explosive.[18] As such, we tested our compounds **1-6** for sensing picric acid to demonstrate their potential applications. Upon step-by-step addition of picric acid solution to compounds **1-6** in dichloromethane, the emission intensity of the compounds gradually decreased (**Figures 3.14-3.16**).

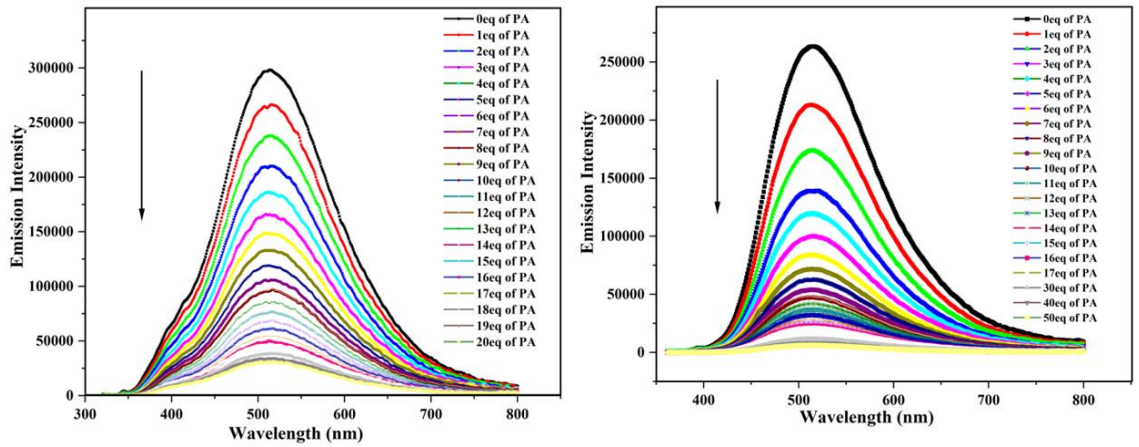

Figure 3.14: Emission spectra of compound **1** (Left) and compound **2** (Right) with the addition of different equivalents of picric acid in dichloromethane (10^{-5} M concentration).

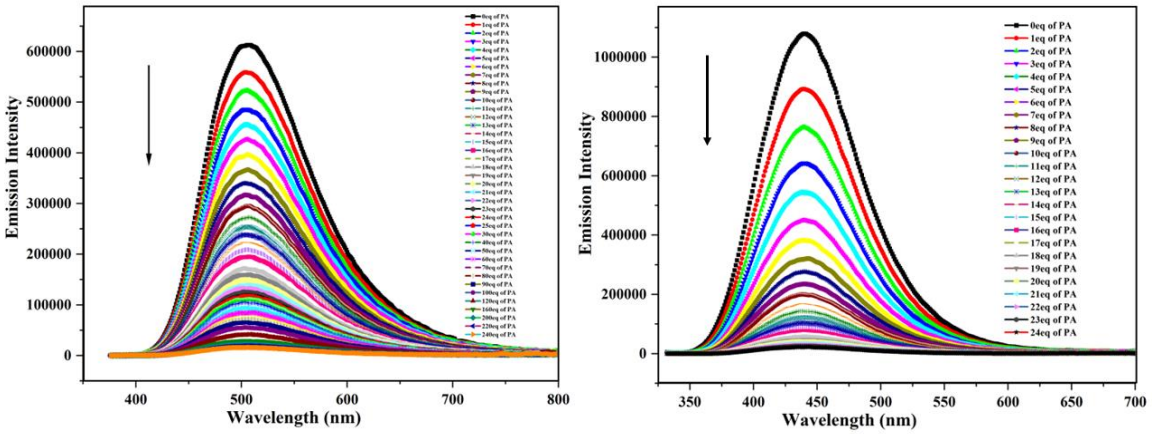

Figure 3.15: Emission spectra of compound **3** (Left) and compound **4** (Right) with the addition of different equivalents of picric acid in dichloromethane (10^{-5} M concentration).

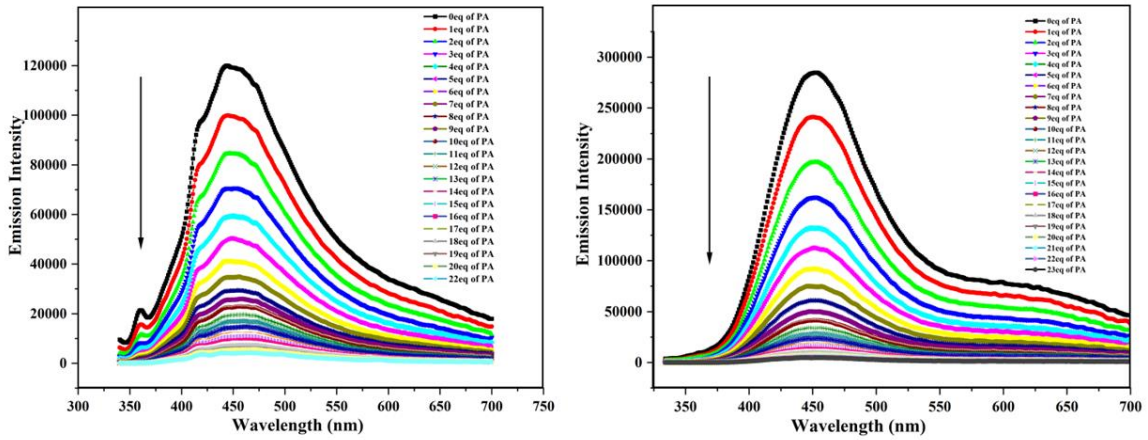

Figure 3.16: Emission spectra of compound **5** (Left) and compound **6** (Right) with the addition of different equivalents of picric acid in dichloromethane (10^{-5} M concentration).

The data were analysed at low concentration of picric acid, the Stern-Volmer plot for all compounds is linear and gave a quenching constant (K_{sv}) of 3.979 x 10^3 M^{-1}, 6.543 x 10^3 M^{-1}, 2.064 x 10^3 M^{-1}, 5.952 x 10^3 M^{-1}, 5.631 x 10^3 M^{-1}, 6.185 x 10^3 M^{-1} for compounds **1-6** respectively. The emission intensity of compounds **4-6** as a probe were quenched with 24, 22, and 23 equivalents of picric acid respectively, whereas the fluorescence intensity of compounds **1-3** were quenched with 20, 50, and 240 equivalents of picric acid respectively. This result suggests that compounds **4-6** are more effective towards sensing of picric acid over compounds **1-3**. Based on the literature precedent from our group, we propose that weak interaction between picric acid and compounds **1-6**, play an important role in the emission quenching.[47] As selectivity is an important criteria for the success of a probe, we measured the emission response of **2** with various nitro analytes (20.0 eq) such as picric acid, 2,4-dinitobenzene (2,4-DNB), 2,4-dinitrophenol (2,4-DNP), 2,4-dinitrotoluene (2,4-DNT), 4-nitrophenol, 4-nitrotoluene, nitrobenzene, nitromethane, and nitrophenol. As shown in **Figure 3.17**, picric acid showed significant fluorescence quenching than other nitro analytes tested.

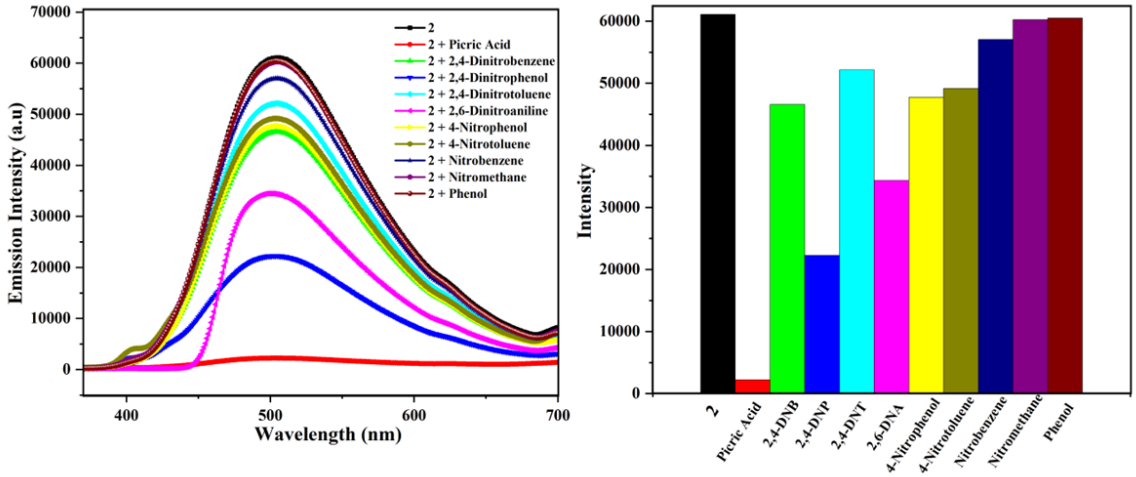

Figure 3.17: Emission spectra of compound **2** with the addition of different nitro analytes (20.0 eq) in dichloromethane at 10^{-5} M concentration (Left). Selectivity bar diagram of compound **2** in the presence of various nitro analytes (picric acid, 2,4-DNB, 2,4-DNP, 2,4-DNT, 4-nitrophenol, 4-nitrotoluene, nitrobenzene, nitromethane, nitrophenol) (Right).

3.2.5 DFT studies

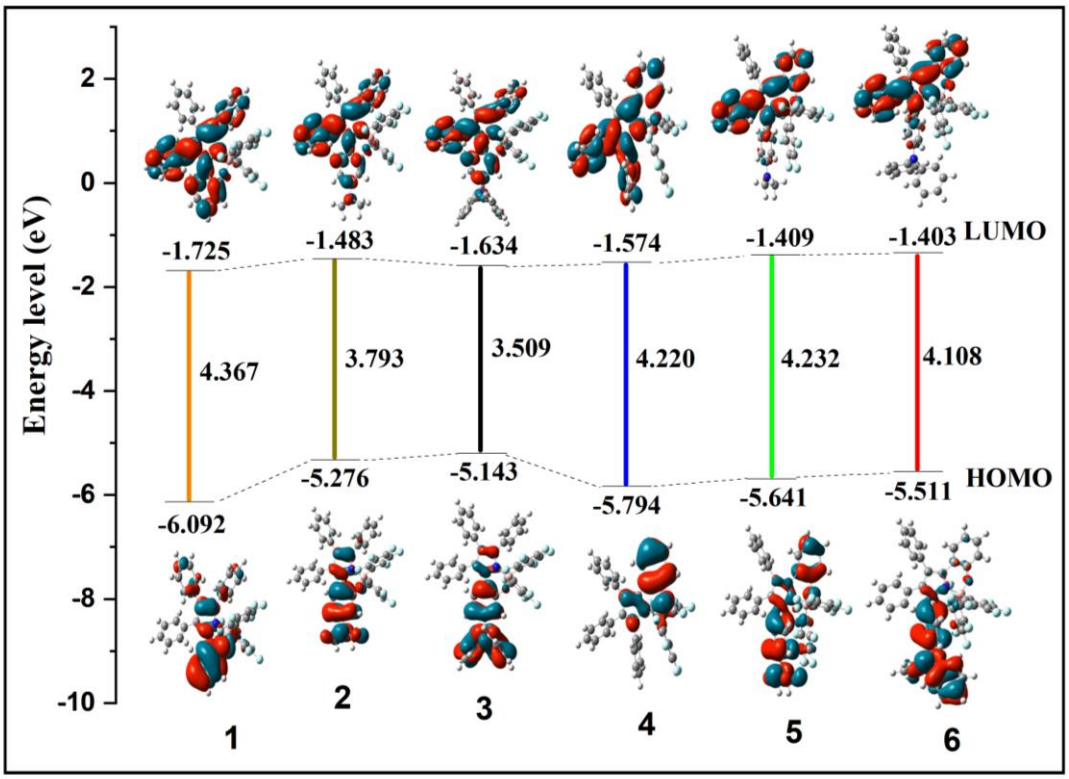

Figure 3.18: HOMO and LUMO energy level diagram of compounds **1-6.**

Density functional theory (DFT) calculations were performed on molecules **1-6** using the B3LYP functional and the 6-31G(d) basis set. As presented in **Figure 3.18**, the highest occupied molecular orbitals (HOMOs) for compounds **1-3** are mainly localized on the pyrazole and N-phenyl ring. The HOMO in compound **4** is distributed over the pyrazole and 3-phenyl ring, whereas, in compound **5**, the HOMO is localized on the pyrazole, N-phenyl, 3-phenyl and $–NMe_2$ moiety. The HOMO of compound **6** is mainly distributed over the N-phenyl and $–NPh_2$ moiety. The lowest unoccupied molecular orbitals (LUMOs) of compounds **1-4** are distributed on the N-phenyl, pyrazole, 3-phenyl and 5-phenyl moieties, however, in case of **5** and **6**, they are localized on the 3-phenyl, pyrazole and 5-phenyl moieties. Time-dependent density functional theory (TD-DFT) calculations reveal that the $S_1 \leftarrow S_0$ excitation is strongly influenced by the position of the chelation

site. In compounds **1-3** the $S_1 \leftarrow S_0$ excitation has a strong contribution while the $S_2 \leftarrow S_0$ excitation has a weak contribution in the observed optical behaviour. On the contrary, in compounds **4-6**, the $S_1 \leftarrow S_0$, $S_2 \leftarrow S_0$, and $S_3 \leftarrow S_0$ excitations contribute primarily to the observed absorption phenomenon. The computational studies nicely reproduced the trend observed experimentally.

3.3 CONCLUSION

In summary, we designed and synthesised two different types of tetra-phenyl pyrazole anchored N,O-chelated bis(pentafluorophenyl) boron compounds (**1-6**). The impact of position of boron chelation was studied using UV-Vis absorption spectroscopy, fluorescence spectroscopy, and DFT analysis. The absorption and fluorescence of compound **4** got red shifted by 11 nm and 71 nm respectively compared to its regio-isomeric compound **1** in THF solvent by simply changing the position of chelation. Similarly, the emission of compounds **2** and **5** showed a red shift in comparison to their respective compounds **3** and **6**. Moreover compounds **1-6** showed AIEE phenomenon owing to the propeller nature of the phenyl rings around the pyrazole moiety. We also exploited them as chemosensors for the detection of picric acid and found that compounds **4-6** are more effective compared to **1-3**. Overall, this study suggests that the position of boron chelation plays an important role in tuning the optical properties and sensing applications of organoboron compounds.

3.4 Experimental section

3.4.1 General information

All the reactions were carried out under N_2 atmosphere using standard glove box, Schlenk line and vacuum line techniques. Solvents and other general reagents were purified according to standard procedures. All the reactions were monitored by thin layer chromatography. Nuclear magnetic resonance spectra were recorded on a 400 MHz or 700MHz Fourier transform NMR spectrometer (JEOL or Bruker) with $CDCl_3$ as a solvent. ^{11}B and ^{19}F NMR spectra were externally referenced to $BF_3.Et_2O$ in $CDCl_3$ (δ=0 ppm) and α,α,α-trifluoro toluene in $CDCl_3$ (δ=-63.73 ppm), respectively. Chemical shifts are reported in δ ppm (parts per million) using residual solvent protons as the internal standard (δ 7.26 for $CDCl_3$ in ^1H NMR, δ 77.16 for $CDCl_3$ in ^{13}C NMR). Coupling constants are reported as J values in hertz (Hz). Splitting patterns are designated as s(singlet), d(doublet), t(triplet), q(quartet), dd(doublet of doublet), dt(doublet of triplet), m(multiplet) and br(broad). HRMS were recorded using Waters XEVO G2-XS QTOF mass spectrometer. Elemental analyses were performed in a Euro Vector EA 3000 CHNS analyzer. UV – Visible spectra were recorded on Agilent Technologies Cary 60 UV/Visible spectrometer. Fluorescence spectra and quantum yield were measured using Edinburgh spectrofluorimeter instrument FS5. For the measurement of absolute quantum yield, the concentration of the boron compounds was such as to give an absorbance of around 0.1 at excitation wavelength. Absolute total quantum yields were measured using an integrating sphere (Edinburgh instrument FS5) mounted in SC-30 compartment of the spectrofluorimeter, The time-resolved fluorescence studies, a time-correlated single-photon counting (TCSPC) spectrometer (Edinburgh, OB920) has been used with a laser of 330 nm as a source of excitation and an MCP photomultiplier (Hamamatsu R3809U-50) is used as a detector. In order to check the laser profile, a water:ludox (4:1) solution has been used. Using water:ludox (4:1) solution, the instrument response function (IRF) has been obtained. A Rigaku Super Nova fine-focused dual diffractometer, fitted with a

PILATUS200K, was utilised to gather single crystal X-ray diffraction data using Cu Kα radiation (λ = 1.54178 Å) or MoKα radiation (λ = 0.71073). The structures were solved using Olex2 and the ShelXS structure solution program using Direct Methods. The ShelXL refinement tool was then used to refine the structures using Least Squares minimization. Anisotropic displacement coefficients were utilised in the refinement of all non-hydrogen atoms. The H atoms were placed at calculated positions and were refined as riding atoms. Boron compounds **1-6** are not stable in the acidic medium. Hence, we avoided column chromatography for purification. Photo stability of compound **1** and **4** are investigated with continuous illumination of 365 nm UV light for 30 min. The ^{1}H-NMR result that both the boron compounds are stable under UV light conditions. The films were prepared by mixing of polymethylmethacrylate (PMMA) (95 mg) and compound **2** (5 mg) in distilled THF, stirred (1h) and coated in a glass plate, then dried at open air for 24h.

3.4.2 Synthetic procedure and spectral characterization

Starting materials: Commercially available 1,3-diphenylpropanedione, acetophenone, *o*-anisidine, 4-nitro-2-methoxyaniline, phenylboronic acid, stannous chloride, sodium nitrite, hydrazine monohydrate, Pd/C, 4-nitrophenylhydrazine, N-bromosuccinimide, copper(I) iodide, 1,10-phenanthroline, sodium carbonate, phenylboronic acid, iodobenzene, sodium cyanoborohydride, boron tribromide, potassium *tert*-butoxide, formaldehyde (37%) solution, magnesium flakes, carbon disulphide, methyl iodide, Palladium tetrakis(triphenylphosphine), sodium hydride, tris(pentafluorophenyl)borane were purchased from Alfa aesar and Sigma Aldrich. Glacial acetic acid, HCl, H_2SO_4 was obtained from Spectrochem.

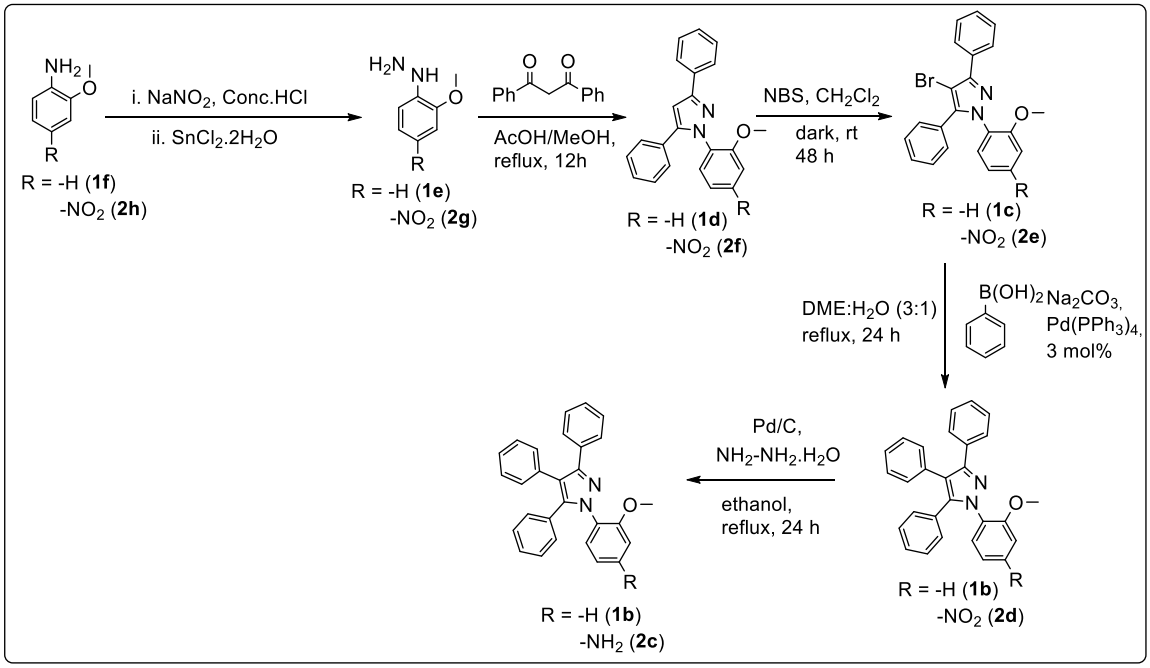

Scheme 3.2: Synthetic route for pyrazole compounds **1b** and **2c.**

Synthesis of (2-methoxyphenyl)hydrazine hydrochloride (1e) *o*-Anisidine (3.9 mL, 34.35 mmol, 1.0 eq) was added slowly to conc. HCl (50 mL) at 0 ^{o}C to form a suspension. A solution of sodium nitrite (2.40 g, 34.69 mmol, 1.1 eq) in distilled water was added dropwise to the suspension at -30 ^{o}C. The temperature was slowly allowed to reach 0 ^{o}C over a period of 2h. The reaction mixture was then added slowly to a suspension of stannous chloride (13.20 g, 69.39 mmol, 2.0 eq) in conc. HCl (25 mL) at -30 ^{o}C. The temperature was slowly allowed to reach room temperature while continuing stirring over a period of 3-4h. The reaction mixture was filtered and the precipitate was washed with cold conc. HCl and then vacuum dried. Without further purification the compound was used for the next reaction.

Synthesis of 1-(2-methoxyphenyl)-3,5-diphenyl-1*H*-pyrazole (1d) A mixture of 1,3-diphenylpropanedione (4.70 g, 20.90 mmol, 1.0 eq), (2-methoxyphenyl)hydrazine hydrochloride (**1e**) (4.80 g, 27.24 mmol, 1.3 eq), glacial acetic acid (45 mL) and methanol

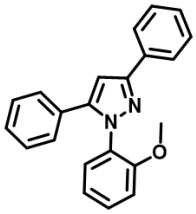

(45 mL) was refluxed for 12h. To the reaction mixture water was added (100 mL), the reaction mixture was extracted using dichloromethane (3 x 150 mL). The extracted organic phase was washed with brine and dried over anhydrous sodium sulphate. The solvent was concentrated and the product (**1d**) was purified using silica gel column chromatography (*n*-hexane/EtOAc (98:2)). Yield: 4.33 g (63.0%). **^{1}H NMR** (400 MHz, $CDCl_3$) δ 7.93 (d, *J* = 8.0 Hz, 2H), 7.54 (d, *J* = 8.0 Hz, 1H), 7.48 – 7.29 (m, 4H), 7.26 (s, 5H), 7.11 – 7.02 (m, 1H), 6.90 – 6.82 (m, 2H), 3.44 (s, 3H). **^{13}C NMR** (101 MHz, $CDCl_3$) δ 154.2, 152.0, 146.3, 133.3, 131.2, 130.1, 129.5, 129.0, 128.6, 128.3, 128.0, 127.9, 127.6, 126.0, 121.1, 112.4, 103.4, 55.5. **HR-MS** (ESI): calculated for $C_{22}H_{19}N_2O$ ($[M + H]^+$): 327.1492, observed : 327.1441.

Synthesis of 4-bromo-1-(2-methoxyphenyl)-3,5-diphenyl-1*H*-pyrazole (1c) A mixture

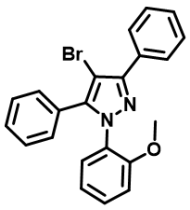

of 1-(2-methoxyphenyl)-3,5-diphenyl-1*H*-pyrazole (**1d**) (3.30 g, 10.20 mmol, 1.0 eq) and N-bromosuccinimide (2.20 g, 12.20 mmol, 1.2 eq) was taken in dichloromethane (60 mL). The reaction mixture was stirred at room temperature for 24h. After completion of the reaction, the product was extracted using water and dichloromethane (3 x 60 mL). The organic phase was collected and dried over anhydrous sodium sulphate. The solvent was concentrated and the product (**1c**) was purified using silica gel column chromatography (*n*-hexane/EtOAc (98:2)). Yield: 4.00 g (96.0%). **^{1}H NMR** (400 MHz, $CDCl_3$) δ 8.04 (d, *J* = 8.0 Hz, 2H), 7.52 – 7.45 (m, 3H), 7.43 – 7.38 (m, 1H), 7.35-7.30 (m, 6H), 7.02 (t, *J* = 7.6 Hz, 1H), 6.81 (d, *J* = 8.0 Hz, 1H), 3.44 (s, 3H). **^{13}C NMR** (101 MHz, $CDCl_3$) δ 153.8, 149.7, 143.8, 132.2, 130.3, 129.4, 129.3, 129.0, 128.8, 128.6, 128.3, 128.2, 128.0, 120.9, 112.1, 96.2, 93.1, 55.3. **HR-MS**

(ESI): calculated for $C_{22}H_{18}BrN_2O$ ($[M+H]^+$): 405.0597, 407.0578 observed : 405.0619, 407.0601.

Synthesis of 1-(2-methoxyphenyl)-3,4,5-triphenyl-1*H*-pyrazole (1b): A mixture

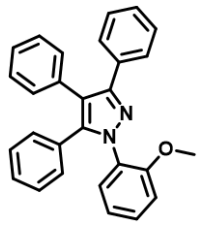

of dimethoxyethane (DME) (70 mL) and water (23 mL) was degassed for 30 minutes and added to a mixture of 4-bromo-1-(2-methoxyphenyl)-3,5-diphenyl-1*H*-pyrazole **(1c)** (3.50 g, 8.61 mmol, 1.0 eq), tetrakis(triphenylphosphine)palladium (0.40 g, 0.35 mmol, 0.04 eq), phenylboronic acid (1.40 g, 11.4 mmol, 1.2 eq) and sodium carbonate (2.70 g, 27.55 mmol, 3.0 eq) under nitrogen atmosphere. The reaction mixture was refluxed for 24h. After completion of the reaction (monitored via TLC), the reaction mixture was passed through a column of celite. The resultant mixture was extracted using water (100 mL) and dichloromethane (3 x 150 mL). The extracted organic phase was washed with brine and dried over anhydrous sodium sulphate. The solvent was concentrated and the product (**1b**) was purified using silica gel column chromatography (*n*-hexane/EtOAc (98:2)). Yield: 1.65 g (48 %). **^{1}H NMR** (400 MHz, $CDCl_3$): δ = 7.55 – 7.49 (m, 3H), 7.34 – 7.28 (m, 1H), 7.27 – 7.23 (m, 3H), 7.22 – 7.18 (m, 3H), 7.16 – 7.07 (m, 5H), 7.04 – 6.98 (m, 3H), 6.80 (d, *J* = 8.0 Hz, 1H), 3.40 (s, 3H). **^{13}C NMR** (101 MHz, $CDCl_3$): δ = 154.1, 150.2, 143.2, 133.5, 133.5, 130.9, 130.6, 130.0, 129.6, 129.3, 129.2, 128.6, 128.2, 128.2, 127.8, 127.8, 127.5, 126.6, 120.9, 119.1, 112.1, 55.3. **HR-MS** (ESI): calculated for $C_{28}H_{23}N_2O$ ($[M+H]^+$): 403.1805, observed : 403.1823.

Synthesis of 2-(3,4,5-triphenyl-1H-pyrazol-1-yl)phenol (1a): 1-(2-Methoxyphenyl)-3,4,5-triphenyl-1*H*-pyrazole (**1b**) (2.00 g, 4.95 mmol, 1.0 eq) was

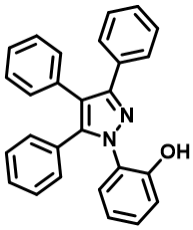

taken in dry CH_2Cl_2 (25 mL). BBr_3 (2.36 mL, 24.85mmol, 5.0 eq) in dry CH_2Cl_2 (30 mL) was added dropwise to the reaction mixture under nitrogen atmosphere at -78 ^oC. The temperature was slowly allowed to reach to room temperature while stirring for 12h. The reaction mixture was then added to ice-cold water and filtered. The filtrate was collected and extracted using water and dichloromethane (3 x 100 mL). The extracted organic phase was washed with brine and dried over anhydrous sodium sulphate. The solvent was concentrated and the product (**1a**) was purified using silica gel column chromatography (*n*-hexane/EtOAc/ CH_2Cl_2 (80:10:10)). Crystallisation was done using CH_2Cl_2/EtOH. Yield: 1.5 g (78 %). **^{1}H NMR** (400 MHz, $CDCl_3$) δ = 9.83 (s, 1H), 7.54 – 7.48 (m, 2H), 7.34 – 7.22 (m, 9H), 7.18 – 7.13 (m, 2H), 7.13 – 7.07 (m, 4H) 6.63 – 6.56 (m, 2H). **^{13}C NMR** (101 MHz, $CDCl_3$) δ = 150.8, 149.9, 142.2, 133.6, 132.4, 132.2, 130.8, 130.4, 129.6, 128.8, 128.6, 128.4, 128.4, 128.4, 128.3, 128.3, 127.1, 125.4, 120.8, 119.1, 118.6. **HR-MS** (ESI): calculated for $C_{27}H_{21}N_2O$ ($[M+H]^+$): 389.1648, observed : 389.1676.

Synthesis of complex 1: 2-(3,4,5-Triphenyl-1H-pyrazol-1-yl)phenol (**1a**) (0.30 g, 0.77 mmol, 1.0 eq) was taken in a sealed tube and tris(pentafluorophenyl)borane (0.43 g, 0.85 mmol, 1.1 eq) was added to it under nitrogen atmosphere followed by dry toluene (10 mL) and refluxed for 24h. The reaction mixture was cooled transferred to a round bottom flask and the solvent was evaporated by vacuum distillation leaving behind a glassy residue. Dry hexane (25 mL) was added to the round bottom flask and sonicated for 5 min. The white precipitate formed was collected by filtration and dried under vacuum. Crystallisation was

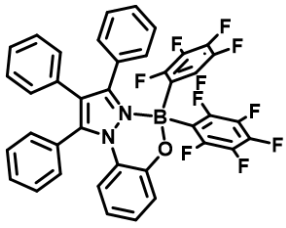

done using CH_2Cl_2/*n*-hexane. Yield: 0.30 g (54 %). **^{1}H NMR** (400 MHz, $CDCl_3$) δ = 7.51 (t, *J*=8.0, 1H), 7.43 (t, *J*=8.0, 2H), 7.35 – 7.28 (m, 2H), 7.22 – 7.12 (m, 2H), 7.11 – 6.98 (m, 8H), 6.81 (d, *J*=8.0, 2H), 6.55 (d, *J*=4.0, 2H). **^{13}C NMR** (101 MHz, $CDCl_3$) δ = 150.4, 148.1 (d, *J* = 243.41 Hz), 147.9, 140.3 (d, *J* = 260.58 Hz) 136.9 (d, *J* = 248.92 Hz) 130.6, 130.5, 130.3, 129.8, 129.6, 129.5, 128.7, 128.4, 128.2, 127.9, 127.5, 124.7, 123.8, 120.9, 120.8, 120.0. **^{19}F NMR** (376 MHz, $CDCl_3$) δ = -132.98 (bs, 4F, Pf), -156.33 (t, 2F, Pf), -164.12 (bs, 4F, Pf). **^{11}B NMR** (128 MHz, $CDCl_3$) δ -0.72. **HR-MS** (ESI): calculated for $C_{39}H_{20}BF_{10}N_2O$ ($[M+H]^+$): 733.1545, observed : 733.1591. Anal. Calcd for $C_{39}H_{19}BF_{10}N_2O$: C, 63.96; H, 2.62, N, 3.83. Found: C, 64.35; H, 1.99, N, 4.19.

Synthesis of (2-methoxy-4-nitrophenyl)hydrazine hydrochloride (2g)

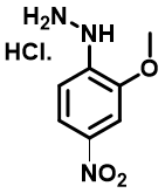

2-Methoxy-4-nitroaniline (15.10 g, 90.00 mmol, 1.0 eq) was added slowly to conc. HCl (100 mL) at 0 ^{o}C to form a suspension. A solution of sodium nitrite (9.3 g, 135.00 mmol, 1.5 eq) in distilled water was added dropwise to the suspension at -30 ^{o}C. The temperature was then slowly allowed to reach 0 ^{o}C over a period of 2h. The reaction mixture was then added slowly to a suspension of stannous chloride (40.6 g, 180.00 mmol, 2.0 eq) in conc. HCl (50 mL) at -30 ^{o}C. The temperature was slowly allowed to reach room temperature while continuing stirring over a period of 3-4h. The reaction mixture was filtered and the precipitate was washed with cold conc. HCl and then vacuum dried. Without further purification the compound was used for the next reaction.

Synthesis of 1-(2-methoxy-4-nitrophenyl)-3,5-diphenyl-1*H*-pyrazole (2f)

Compound **2f** was prepared following a procedure similar to that used for **1d**. The

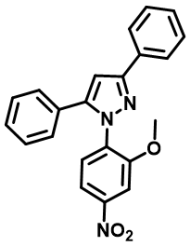

quantities involved are as follows: 1,3-Diphenylpropanedione (10.10 g, 45.09 mmol, 1.0 eq), (2-methoxy-4-nitrophenyl) hydrazine hydrochloride (**2g**) (19.00 g, 90.18 mmol, 2.0 eq), glacial acetic acid (90 mL) and methanol (90 mL). The product (**2f**) was purified using silica gel column chromatography (*n*-hexane/EtOAc (98:2)). Crystallisation was done using CH_2Cl_2/*n*-hexane. Yield: 10.2 g (60.0%). **^{1}H NMR** (400 MHz, $CDCl_3$) δ 7.99 (d, *J* = 8.0 Hz, 1H), 7.94 – 7.86 (m, 2H), 7.80 (d, *J* = 8.0 Hz, 1H), 7.70 (d, *J* = 4.0 Hz, 1H), 7.47 – 7.41 (m, 2H), 7.37 (d, *J* = 7.4 Hz, 1H), 7.32 – 7.28 (m, 3H) 7.28 – 7.18 (m, 2H), 6.87 (s, 1H), 3.45 (s, 3H). **^{13}C NMR** (101 MHz, $CDCl_3$) δ 153.9, 153.3, 148.3, 146.7, 135.1, 132.8, 130.9, 129.2, 128.8, 128.6 (2C), 128.4, 127.3, 126.0, 116.5, 107.6, 104.5, 55.9. **HR-MS** (ESI): calculated for $C_{22}H_{17}N_3O_3Na$ ($[M+Na]^+$): 394.1162, observed : 394.1185.

Synthesis of 4-bromo-1-(2-methoxy-4-nitrophenyl)-3,5-diphenyl-1*H*-pyrazole (2e)

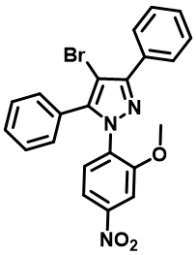

Compound **2e** was prepared following a procedure similar to that used for **1c**. The quantities involved are as follows: 1-(2-Methoxy-4-nitrophenyl)-3,5-diphenyl-1*H*-pyrazole (**2f**) (8.10 g, 21.81 mmol, 1.0 eq) and N-bromosuccinimide (4.60 g, 26.17 mmol, 1.2 eq). Yield: 9.56 g (97.0%). **^{1}H NMR** (400 MHz, $CDCl_3$) δ 8.00 (d, *J* = 8.0 Hz, 2H), 7.95 (d, *J* = 8.0 Hz, 1H), 7.73 (d, *J* = 8.0 Hz, 1H), 7.66 (s, 1H), 7.53 – 7.39 (m, 4H), 7.39 – 7.31 (m, 2H), 7.31 (d, *J* = 5.6 Hz, 2H), 3.46 (s, 3H). **^{13}C NMR** (101 MHz, $CDCl_3$) δ 153.6, 150.9, 148.4, 144.0, 134.3, 131.6, 129.1, 129.0, 129.0, 128.7, 128.4, 128.4, 128.3, 128.1, 116.2, 107.4, 94.3, 55.8. **HR-MS** (ESI): calculated for $C_{22}H_{16}BrN_3O_3Na$ ($[M+Na]^+$: 472.0267, 474.0248 observed : 472.0281, 474.0263.

Synthesis of 1-(2-methoxy-4-nitrophenyl)-3,4,5-triphenyl-1*H*-pyrazole (2d)

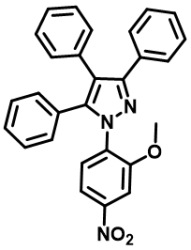

Compound **2d** was prepared following a procedure similar to that used for **1b**. The quantities involved are as follows: 4-Bromo-1-(2-methoxy-4-nitrophenyl)-3,5-diphenyl-1*H*-pyrazole (**2e**) (9.30 g, 20.52 mmol, 1.0 eq), palladium tetrakistriphenylphosphine (0.60 g, 0.51 mmol, 0.025 eq), phenylboronic acid (3.30 g, 26.67 mmol) and sodium carbonate (6.50 g, 61.54 mmol, 3.0 eq). The product (**2d**) was purified using silica gel column chromatography (*n*-hexane/EtOAc/CH_2Cl_2 (80:10:10)). Yield: 7.00 g (76.0%). **^{1}H NMR** (400 MHz, $CDCl_3$) δ 7.96 (d, *J* = 8.0 Hz, 1H), 7.78 (d, *J* = 8.0 Hz, 1H), 7.68 (s, 1H), 7.55 – 7.46 (m, 2H), 7.33 – 7.27 (m, 3H), 7.27 – 7.08 (m, 8H), 7.04 – 6.96 (m, 2H), 3.46 (s, 3H). **^{13}C NMR** (101 MHz, $CDCl_3$) δ 154.0, 151.0, 148.4, 143.5, 136.3, 134.4, 132.6, 132.5, 130.8, 130.0, 129.6, 129.2, 128.6, 128.4, 128.4, 128.2, 127.0, 120.1, 119.0, 116.3, 107.4, 55.9. **HR-MS** (ESI): calculated for $C_{28}H_{22}N_3O_3$ ($[M+H]^+$): 448.1661, observed : 448.1631.

Synthesis of 4-(3,4,5-triphenyl-1*H*-pyrazol-1-yl)-3-methoxyaniline (2c) A mixture of

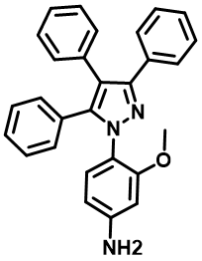

1-(2-methoxy-4-nitrophenyl)-3,4,5-triphenyl-1*H*-pyrazole (**2d**) (5.60 g, 12.6 mmol, 1.0 eq), hydrazine hydrate (6.2 mL, 126.00 mmol, 10.0 eq), Pd/C (0.13 g, 1.26 mmol, 0.1 eq) and ethanol (120 mL) was refluxed for 12h. After completion of the reaction, the reaction mixture was passed through a column of celite and was extracted using water and ethyl acetate (3 x 150 mL). The extracted organic phase was washed with brine and then dried over anhydrous sodium sulphate. The solvent was concentrated and the product (**2c**) was purified using silica gel column chromatography (*n*-hexane/EtOAc (70:30)). Crystallisation was done using CH_2Cl_2/*n*-hexane. Yield: 5.30 g (98.0%). **^{1}H NMR** (400 MHz, $CDCl_3$) δ 7.52 –

7.44 (m, 2H), 7.30 – 7.17 (m, 7H), 7.16 – 7.07 (m, 5H), 7.07 – 6.99 (m, 2H), 6.46 (d, *J* = 8.0 Hz, 1H), 6.32 (s, 1H), 4.37 (s, 2H), 3.37 (s, 3H). **^{13}C NMR** (101 MHz, $CDCl_3$) δ 155.2, 149.6, 148.1, 143.3, 133.7, 133.6, 130.8, 130.7, 130.0, 129.7, 128.6, 128.2, 128.1, 127.8, 127.6, 127.4, 126.4, 120.5, 118.8, 107.1, 99.0, 55.2. **HR-MS** (ESI): calculated for $C_{28}H_{24}N_3O$ ($[M+H]^+$): 418.1914, observed : 418.1931.

Synthesis of 3-methoxy-*N*,*N*-dimethyl-4-(3,4,5-triphenyl-1*H*-pyrazol-1-yl)aniline (2b): A mixture of 3-methoxy-4-(3,4,5-triphenyl-1*H*-pyrazol-1-yl)aniline (**2c**) (1.90 g, 4.56 mmol, 1.0 eq), sodium cyanoborohydride (1.40 g, 21.96 mmol, 5.0 eq), 37% formaldehyde solution (5.6 mL, 68.43 mmol, 15.0 eq) and acetic acid (0.52 mL, 9.12 mmol, 2.0 eq) was taken in acetonitrile (60 mL). The reaction mixture was stirred at room temperature for 6h. The reaction mixture was extracted using water and dichloromethane (3 x 100 mL). The extracted organic phase was washed with brine and then dried over anhydrous sodium sulphate. The solvent was concentrated and the product (**2b**) was purified using silica gel column chromatography (*n*-hexane/EtOAc/CH_2Cl_2 (80:10:10)). Crystallisation was done using CH_2Cl_2/Ethanol. Yield: 1.96 g (97 %). **^{1}H NMR** (400 MHz, $CDCl_3$) δ = 7.56 – 7.49 (m, 2H), 7.31 (d, *J* = 8.7 Hz, 1H), 7.28 – 7.18 (m, 6H), 7.17 – 7.10 (m, 5H), 7.08 – 7.02 (m, 2H), 6.31 (d, *J* = 8.0 Hz, 1H), 6.07 (d, *J* = 2.6 Hz, 1H), 3.43 (s, 3H), 2.96 (s, 6H). **^{13}C NMR** (101 MHz, $CDCl_3$) δ = 154.9, 152.0, 149.5, 143.2, 133.8, 133.7, 130.9, 129.7, 129.5, 128.6, 128.2, 128.1, 127.7, 127.5, 127.3, 126.4, 118.7, 118.7, 104.5, 96.1, 55.2, 40.7. **HR-MS** (ESI): calculated for $C_{30}H_{28}N_3O$ ($[M+H]^+$): 446.2227, observed : 446.2252.

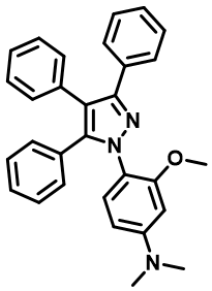

Synthesis of 5-(dimethylamino)-2-(3,4,5-triphenyl-1H-pyrazol-1-yl)phenol (2a): 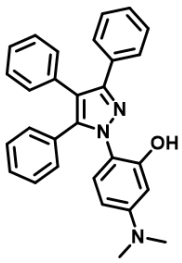 Compound **2a** was prepared following a procedure similar to that used for **1a**. The quantities involved are as follows: 3-Methoxy-*N*,*N*-dimethyl-4-(3,4,5-triphenyl-1*H*-pyrazol-1-yl)aniline (**2b**) (1.60 g, 3.59 mmol, 1.0 eq) and BBr_3 (1.7 mL, 17.91 mmol, 5.0 eq) The product (**2a**) was purified using silica gel column chromatography (*n*-hexane/EtOAc/CH_2Cl_2 (80:10:10)). Crystallisation was done using CH_2Cl_2/EtOH. Yield: 0.80 g (52 %), **^{1}H NMR** (400 MHz, $CDCl_3$) δ = 9.56 (s, 1H), 7.53 – 7.47 (m, 2H), 7.34 – 7.18 (m, 9H), 7.16 – 7.04 (m, 4H), 6.50 – 6.39 (m, 2H), 5.97 – 5.91 (m, 1H), 2.92 (s, 6H). **^{13}C NMR** (101 MHz, $CDCl_3$) δ = 151.6, 150.6, 149.2, 141.5, 132.8, 132.6, 130.8, 130.5, 129.9, 128.5(2C), 128.4, 128.3 (2C), 128.0, 126.9, 125.0, 120.1, 115.7, 103.5, 101.2, 40.4. **HR-MS** (ESI): calculated for $C_{29}H_{26}N_3O$ ($[M+H]^+$): 432.2070, observed : 432.2076.

Synthesis of complex 2: 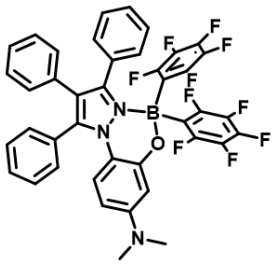 Compound **2** was prepared following a procedure similar to that used for **1**. The quantities involved are as follows: 5-(Dimethylamino)-2-(3,4,5-triphenyl-1H-pyrazol-1-yl)phenol (**2a**) (0.25 g, 0.58 mmol, 1.0 eq) and tris(pentafluorophenyl)borane (0.32 g, 0.62 mmol, 1.2 eq). Crystallisation was done using CH_2Cl_2/*n*-hexane. Yield: 0.29 g (64 %). **^{1}H NMR** (400 MHz, $CDCl_3$) δ 7.52 – 7.39 (m, 3H), 7.31 (d, *J* = 6.9 Hz, 2H), 7.22 – 6.98 (m, 8H), 6.83 – 6.75 (m, 2H), 6.38 – 6.32 (m, 1H), 6.29 (d, *J* = 4.0 Hz, 1H), 5.85 (dd, *J* = 8.0, 4.0 Hz, 1H), 2.87 (s, 6H). **^{13}C NMR** (176 MHz, $CDCl_3$) δ 151.1, 148.1 (d, *J* = 241.12 Hz) 146.4, 140.1 (d, *J* = 251.68 Hz), 139.8, 138.0, 136.8 (d, *J* = 248.16 Hz), 130.5, 130.4, 130.2, 129.6, 129.4, 129.1, 128.6, 128.3, 128.2, 128.0, 127.9,

127.6, 125.4, 122.9, 121.3, 114.6, 103.8, 102.4, 96.2, 40.2. ^{19}F NMR (376 MHz, $CDCl_3$) δ -132.82 (bs, 4F, Pf), -156.74 (t, 2F, Pf), -164.30 (s, 4F, Pf). ^{11}B NMR (128 MHz, $CDCl_3$) δ -0.85. **HR-MS** (ESI): calculated for $C_{41}H_{25}BF_{10}N_3O$ ($[M+H]^+$): 776.1967, observed : 776.2048. Anal. Calcd for $C_{41}H_{24}BF_{10}N_3O.0.2(C_6H_{14})$: C, 63.94; H, 3.41, N, 5.30. Found: C, 64.50; H, 3.15, N, 5.76.

Synthesis of 3-methoxy-*N*,*N*-diphenyl-4-(3,4,5-triphenyl-1*H*-pyrazol-1-yl)aniline (3b): A mixture of 4-(3,4,5-triphenyl-1*H*-pyrazol-1-yl)-3-methoxyaniline (**2c**) (5.20 g, 12.47 mmol, 1.0 eq), iodobenzene (4.2 mL, 37.27 mmol, 3.0 eq), copper iodide (0.14 g, 0.74 mmol, 0.06 eq), 1,10-phenanthroline (0.15 g, 0.84 mmol, 0.07 eq), potassium *tert*-butoxide (4.20 g, 37.27 mmol, 3.0 eq) was taken in a round bottom flask with degassed dry toluene (100 mL). The reaction mixture was refluxed for 36 h. After completion of the reaction, the reaction mixture was passed through a column of celite, the resultant solution was extracted using water and dichloromethane (3 x 100 mL). The extracted organic phase was washed with brine and dried over anhydrous sodium sulphate. The solvent was concentrated and the product **(3b)** was purified using silica gel column chromatography (*n*-hexane/EtOAc/CH_2Cl_2 (80:10:10)). Crystallisation was done using CH_2Cl_2/Ethanol. Yield: 5.60 g, (79 %). **^{1}H NMR** (400 MHz, $CDCl_3$) δ = 7.58 – 7.50 (m, 2H), 7.37 – 7.32 (m, 1H), 7.30 – 7.11 (m, 15H), 7.12 – 6.99 (m, 8H), 6.69 – 6.62 (m, 1H), 6.54 – 6.50 (m, 1H), 3.24 (s, 3H). **^{13}C NMR** (101 MHz, $CDCl_3$): δ = 154.8, 149.9, 149.5, 147.4, 143.2, 133.5, 133.5, 130.8, 130.7, 129.7, 129.7, 129.4, 128.6, 128.2, 128.1, 127.8, 127.7, 127.4, 126.5, 124.8, 123.5, 123.4,

118.9, 115.5, 107.0, 55.3. **HR-MS** (ESI): calculated for $C_{40}H_{32}N_3O$ ($[M+H]^+$): 570.2540, observed : 570.2564.

Synthesis of 5-(diphenylamino)-2-(3,4,5-triphenyl-1H-pyrazol-1-yl)phenol (3a): 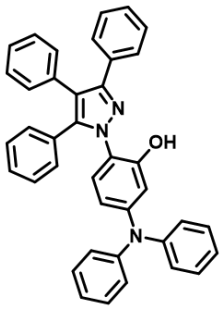 Compound **3a** was prepared following a procedure similar to that used for **1a**. The quantities involved are as follows: 3-Methoxy-*N*,*N*-diphenyl-4-(3,4,5-triphenyl-1*H*-pyrazol-1-yl)aniline (**3b**) (3.50 g, 6.13 mmol, 1.0 eq) and BBr_3 (2.9 mL, 30.67 mmol, 5.0 eq) The product **(3a)** was purified using silica gel column chromatography (*n*-hexane/EtOAc/CH_2Cl_2 (80:10:10)). Crystallisation was done using CH_2Cl_2/EtOH. Yield: 2.60 g, (76.5 %). **^{1}H NMR** (400 MHz, $CDCl_3$): δ = 9.72 (s, 1H), 7.57 – 7.46 (m, 2H), 7.35 – 7.25 (m, 13H), 7.21 – 7.02 (m, 10H), 6.83 (d, *J* = 4.0 Hz, 1H), 6.46 – 6.40 (m, 1H), 6.29 (dd, *J* = 8.0, 4.0 Hz, 1H). **^{13}C NMR** (101 MHz, $CDCl_3$): δ = 151.4, 149.5, 147.8, 147.3, 141.8, 132.5, 132.3, 130.8, 130.4, 129.7, 129.4, 128.7, 128.6, 128.44 (2C), 128.41, 128.2, 127.0, 125.1, 124.7, 123.5, 120.5, 119.8, 113.4, 111.8. **HR-MS** (ESI): calculated for $C_{39}H_{30}N_3O$ ($[M+H]^+$): 556.2389, observed : 556.2344.

Synthesis of complex 3: 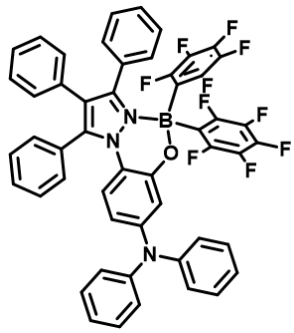 Compound **3** was prepared following a procedure similar to that used for **1**. The quantities involved are as follows: 5-(Diphenylamino)-2-(3,4,5-triphenyl-1H-pyrazol-1-yl)phenol (**3a**) (0.25 g, 0.45 mmol, 1.0eq) and tri(pentafluorophenyl)borane (0.23 g, 0.54 mmol, 1.2 eq). Crystallisation was done using CH_2Cl_2/*n*-hexane. Yield: 0.32 g (80 %). **^{1}H NMR** (400 MHz, $CDCl_3$) δ = 7.49 – 7.39 (m, 3H), 7.38 – 7.32

(m, 2H), 7.28 – 7.21 (m, 5H), 7.08 - 7.03 (m, 9H), 6.98 (d, *J* = 8.0 Hz, 4H), 6.81 (d, *J* = 8.0 Hz, 2H), 6.65 (d, *J* = 4.0 Hz, 1H), 6.34 – 6.29 (m, 1H), 6.17 (dd, *J* = 8.0, 4.0 Hz, 1H). **^{13}C NMR** (176 MHz, $CDCl_3$) δ = 151.0, 148.8, 148.2 (d, *J* = 281.6 Hz) 147.0, 146.6, 140.6, 140.1 (d, *J* = 248.16 Hz) 136.8 (d, *J* = 248.16 Hz) 130.5, 130.5, 130.3, 129.5, 129.5, 129.5, 128.8, 128.3, 128.1, 127.7, 127.6, 125.5, 124.1, 123.3, 121.0, 118.6, 112.8, 112.4. **^{19}F NMR** (376 MHz, $CDCl_3$) δ = -132.94 (bs, 4F, Pf), -156.55 (t, 2F, Pf), -164.14 (bs, 4F, Pf). **^{11}B NMR** (128 MHz, $CDCl_3$) δ = -1.02. **HR-MS** (ESI): calculated for $C_{51}H_{29}BF_{10}N_3O$ ($[M+H]^+$): 900.2280, observed : 900.2245. Anal. Calcd for $C_{51}H_{28}BF_{10}N_3O$: C, 68.09; H, 3.14, N, 4.67. Found: C, 67.89; H, 3.74, N, 4.62.

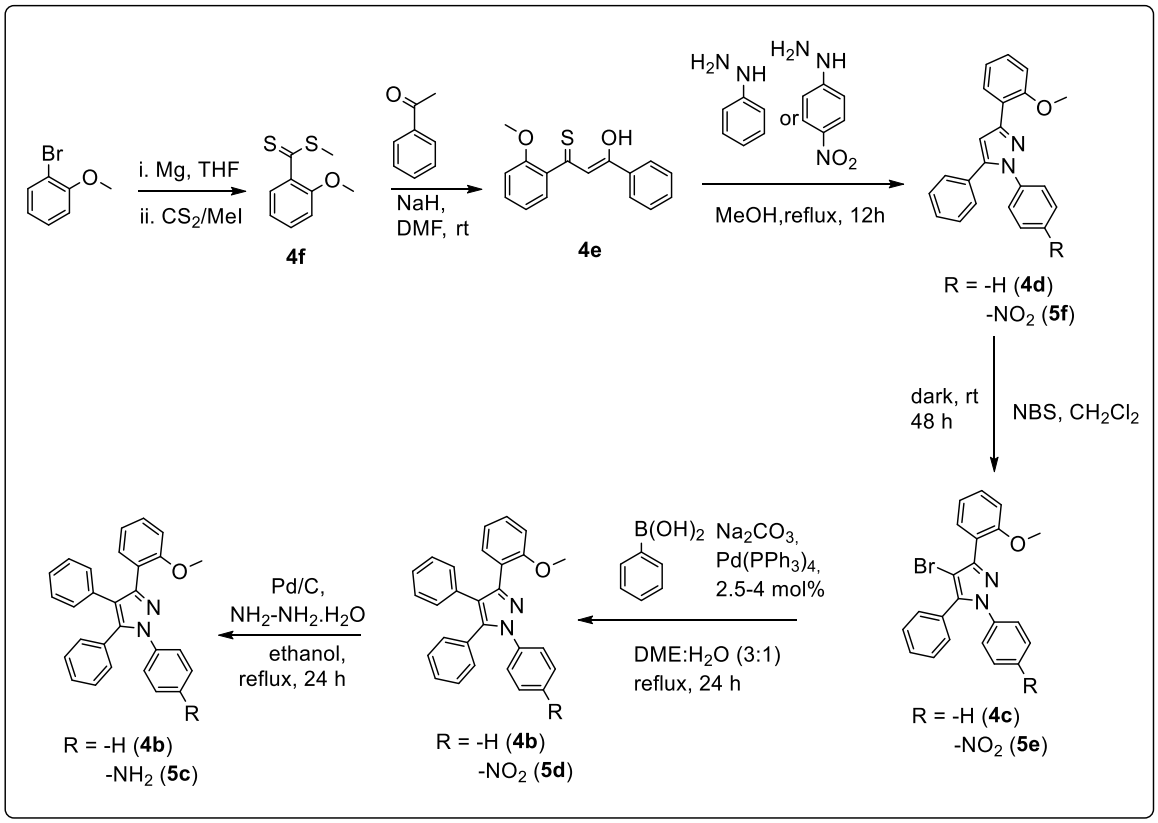

Scheme 3.3: Synthetic route for pyrazole compounds **4b** and **5c.**

Synthesis of methyl 2-methoxybenzodithiolate (4f): Activated magnesium turnings (0.84 g, 34.70 mmol, 1.3 eq) were added to 60 mL of dry THF under N_2 atmosphere to a

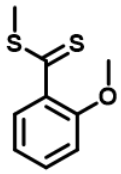

two neck RB and the solution was warmed till brisk effervescence was observed. After activation of Mg, the solution was immersed in an ice-cooled water bath and 2-bromoanisole (5.00 g, 3.33 mL, 26.69 mmol, 1.0 eq) was added dropwise. The solution was stirred for about 2h at room temperature; CS_2 (2.23 g, 1.77mL, 29.36 mmol, 1.1 eq) was added dropwise to the reaction mixture at 0 °C. Then the reaction mixture was stirred at room temperature for another 2h after which methyl iodide (4.16 g, 1.83 mL, 29.36 mmol, 1.1 eq) was added dropwise to it at 0 °C. The reaction mixture was allowed to stir at rt, overnight. After completion of the reaction, it was quenched with ice-cold water. The reaction mixture was extracted using water and ethyl acetate (3 x 100 mL). The extracted organic phase was washed with brine and dried over anhydrous sodium sulphate. The solvent was concentrated under reduced pressure and the product was purified using silica gel column chromatography (*n*-hexane/EtOAc (99.5:0.5)). Yield: 4.79 g (90.0%). **^{1}H NMR** (400 MHz,) δ 7.40 (dd, *J* = 8.0 Hz, 2.0 Hz 1H), 7.36 (dd, *J* = 8.0 Hz, 2.0 Hz, 1H), 7.00 – 6.92 (m, 2H), 3.85 (s, 3H), 2.76 (s, 3H). **^{13}C NMR** (101 MHz, $CDCl_3$) δ 229.7, 154.8, 136.6, 131.3, 129.0, 120.5, 111.9, 56.1, 21.1. HR-MS (ESI): calculated for $C_9H_{10}OS_2K$ ($[M + K]^+$): 236.9810, observed : 237.0095.

Synthesis of 3-(2-methoxyphenyl)-1-phenyl-3-thioxopropan-1-one (4e) The compound

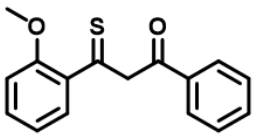

(4e) has been synthesized following a procedure reported in literature.[42, 48] To a stirred suspension of NaH (1.28 g, 26.8 mmol, 1.2 eq) in DMF (50 mL) under N_2 atmosphere was added a solution of acetophenone (2.68 g, 2.61 mL, 22.33 mmol, 1.0 eq) and methyl 2-methoxybenzodithioate **(4f)** (5.00 g, 26.8 mmol, 1.2 eq) in DMF (30 mL) at 0 ^{o}C, dropwise. The reaction mixture was further stirred at room temperature for about 5 h (monitored by TLC) and was poured into ice-cold water (100 mL) and acidified with acetic acid. The product **(4e)** was extracted using

water and EtOAc (3 x 150 mL). The extracted organic phase was washed with brine and dried over anhydrous sodium sulphate. The solvent was concentrated under reduced pressure to give crude product 3-(2-methoxyphenyl)-1-phenyl-3-thioxopropan-1-one, **(4e)** which was used for the next reaction without purification.

Synthesis of 3-(2-methoxyphenyl)-1,5-diphenyl-1*H*-pyrazole (4d) A mixture of 3-(2-

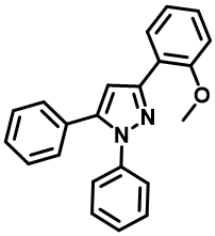

methoxyphenyl)-1-phenyl-3-thioxopropan-1-one, **(4e)** (5.00 g 18.45 mmol, 1.0 eq), phenylhydrazine (2.20 g, 20.34 mmol, 1.1 eq) in ethanol (45 mL) was refluxed for 12h. The reaction mixture was extracted using water and dichloromethane (3 x 150 mL). The extracted organic phase was washed with brine and dried over anhydrous sodium sulphate. The solvent was concentrated under reduced pressure and the product **(4d)** was purified using silica gel column chromatography (*n*-hexane/EtOAc (96:4)). Yield: 3.32 g (40%). **^{1}H NMR** (400 MHz, $CDCl_3$) δ 8.11 (dd, *J* = 7.7, 1.7 Hz, 1H), 7.41 – 7.28 (m, 11H), 7.09 (s, 1H), 7.07 – 7.00 (m, 2H), 3.95 (s, 3H). **^{13}C NMR** (101 MHz, $CDCl_3$) δ 157.0, 149.0, 143.4, 140.4, 131.0, 129.2, 129.0, 128.9 (2C), 128.5, 128.1, 127.3, 125.4, 122.1, 121.0, 111.3, 109.4, 55.6. **HR-MS** (ESI): calculated for $C_{22}H_{19}N_2O$ ($[M + H]^+$): 327.1492, observed : 327.1494.

Synthesis of 4-Bromo-3-(2-methoxyphenyl)-1,5-diphenyl-1*H*-pyrazole (4c)

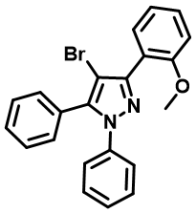

Compound **4c** was prepared following a procedure similar to that used for **1c**. The quantities involved are as follows: 3-(2-Methoxyphenyl)-1,5-diphenyl-1*H*-pyrazole **(4d)** (2.00 g, 6.12 mmol, 1.0 eq) and N-bromosuccinimide (1.31 g, 7.35 mmol, 1.2 eq). The product was purified using silica gel column chromatography (*n*-hexane/EtOAc (94:6)). Yield: 1.31 g (53.0%). **^{1}H NMR** (400 MHz, $CDCl_3$) δ 7.54 (d, *J* = 8.0 Hz, 1H), 7.45 – 7.23 (m, 11H),

7.12 – 7.00 (m, 2H), 3.90 (s, 3H). **^{13}C NMR** (101 MHz, $CDCl_3$) δ 157.7, 149.5, 141.0, 140.0, 131.9, 130.4, 130.3, 129.3, 128.9, 128.8, 128.5, 127.4, 124.9, 121.1, 120.6, 111.3, 97.8, 55.7. **HR-MS** (ESI): calculated for $C_{22}H_{18}BrN_2O$ ($[M+H]^+$): 405.0597, 407.0578 observed : 405.0574, 407.0558.

Synthesis of 3-(2-methoxyphenyl)-1,4,5-triphenyl-1*H*-pyrazole (4b): Compound **4b**

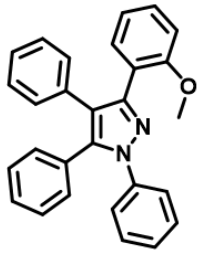

was prepared following a procedure similar to that used for **1b**. The quantities involved are as follows: 4-Bromo-3-(2-methoxyphenyl)-1,5-diphenyl-1*H*-pyrazole **(4c)** (1.67 g, 4.12 mmol, 1.0 eq), $Pd(PPh_3)_4$ (0.14 g, 0.12 mmol, 0.03 eq), phenylboronic acid (0.586 g, 4.81 mmol. 1.2 eq), and sodium carbonate (1.31 g, 12.40 mmol, 3.0 eq).. The product **(4b)** was purified using silica gel column chromatography (*n*-hexane/EtOAc (96:4)). Yield: 1.34 g (90 %). **^{1}H NMR** (400 MHz, $CDCl_3$) δ 7.53 (d, *J* = 8.0 Hz, 1H), 7.33 – 7.11 (m, 9H), 7.11 – 6.99 (m, 5H), 6.95 (t, *J* = 8.0 Hz, 1H), 6.89 – 6.84 (m, 2H), 6.72 (d, *J* = 8.0 Hz, 1H), 3.16 (s, 3H). **^{13}C NMR** (101 MHz, $CDCl_3$) δ 157.0, 148.9, 140.1, 134.3, 131.8, 130.7, 130.4, 129.7, 129.2, 129.1, 128.7, 128.4, 128.2, 127.8, 127.1, 125.9, 125.5, 122.8, 122.0, 120.8, 111.2, 54.8. **HR-MS** (ESI): calculated for $C_{28}H_{22}N_2ONa$ ($[M + Na]^+$): 425.1630, observed : 425.1639.

Synthesis of 2-(1,4,5-triphenyl-1H-pyrazol-3-yl)phenol (4a): Compound **4a** was

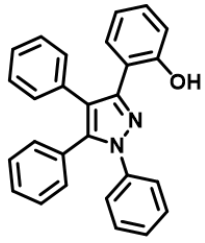

prepared following a procedure similar to that used for **1a**. The quantities involved are as follows: 3-(2-Methoxyphenyl)-1,4,5-triphenyl-1H-pyrazole **(4b)** (1.50 g, 3.73 mmol, 1.0 eq) and BBr_3 (1.41 mL, 14.92 mmol, 4.0 eq). The product **(4a)** was purified using silica gel column chromatography (*n*-hexane/EtOAc (94:06). Yield: 1.00 g

(69 %). **^{1}H NMR** (400 MHz, $CDCl_3$) δ = 10.87 (s, 1H), 7.30 – 7.20 (m, 8H), 7.10 – 7.06 (m, 6H), 7.00 – 6.93 (m, 4H), 6.53 (t, *J* = 7.6 Hz, 1H). **^{13}C NMR** (101 MHz, $CDCl_3$) δ = 156.5, 148.3, 141.8, 139.3, 133.1, 131.1, 130.4, 129.3, 129.3, 129.0, 128.6, 128.6, 128.4, 128.3, 127.6, 127.4, 124.9, 121.1, 118.8, 117.2, 116.6. **HR-MS** (ESI): calculated for $C_{27}H_{21}N_2O$ ($[M+H]^+$): 389.1648, observed : 389.1641

Synthesis of complex 4: Compound **4** was prepared following a procedure similar

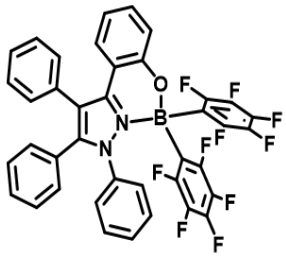

to that used for **1**. The quantities involved are as follows: 2-(1,4,5-Triphenyl-1H-pyrazol-3-yl)phenol (**4a**) (0.25 g, 0.64 mmol, 1.0 eq) and tri(pentafluorophenyl)borane (0.40 g, 0.77 mmol, 1.2 eq). Crystallisation was done using CH_2Cl_2/*n*-hexane. Yield: 0.25 g (54 %). **^{1}H NMR** (400 MHz, $CDCl_3$) δ = 7.39 (m, 3H), 7.36 – 7.29 (m, 2H), 7.24 – 7.15 (m, 3H), 7.11 (m, 6H), 6.99 (m, 4H), 6.62 (t, *J* = 8.3, 1H). **^{13}C NMR** (101 MHz, $CDCl_3$) δ = 155.5, 148.1 (d, *J* = 243.41 Hz) 147.2, 142.8, 140.1 (d, *J* = 252.5 Hz) 136.9 (d, *J* = 247.45 Hz) 134.8, 132.5, 130.9, 130.7, 130.4, 130.2, 129.8, 129.2, 129.0, 128.7, 128.5, 126.7, 126.2, 119.0, 115.1. **^{19}F NMR** (376 MHz, $CDCl_3$) δ = -134.34 (bs, 4F, Pf), -156.65 (t, 2F, Pf), -163.94 (bs, 4F, Pf). **^{11}B NMR** (128 MHz, $CDCl_3$) δ = -0.60. **HR-MS** (ESI): calculated for $C_{39}H_{20}BF_{10}N_2O$ ($[M+H]^+$): 733.1545, observed : 733.1526. Anal. Calcd for $C_{39}H_{19}BF_{10}N_2O.0.2(C_6H_{14})$: C, 64.41; H, 2.93, N, 3.74. Found: C, 64.79; H, 2.51, N, 4.20.

Synthesis of 3-(2-methoxyphenyl)-1-(4-nitrophenyl)-5-phenyl-1H-pyrazole (5f)

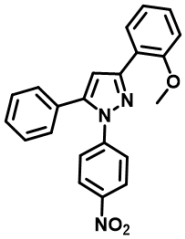

Compound **5f** was prepared following a procedure similar to that used for **4d**. The quantities involved are as follows: 3-(2-methoxyphenyl)-1-phenyl-3-thioxopropan-1-one, **(4e)** (5.00 g, 14.37 mmol, 1.0 eq), and 4-

nitrophenylhydrazine (2.20 g, 18.51 mmol, 1.3 eq). The product (**5f)** was purified using silica gel column chromatography (*n*-hexane/EtOAc (96:4)). Yield: 3.32 g (62%). **^{1}H NMR** (400 MHz, $CDCl_3$) δ 8.18 (d, *J* = 8.0 Hz, 2H), 8.09 (d, *J* = 8.0 Hz, 1H), 7.55 (d, *J* = 8.0 Hz, 2H), 7.43 – 7.36 (m, 4H), 7.34 - 7.30 (m, 2H), 7.12 – 7.00 (m, 3H), 3.95 (s, 3H). **^{13}C NMR** (101 MHz, $CDCl_3$) δ 157.2, 150.6, 145.8, 145.0, 144.0, 130.4, 129.9, 129.07 (2C), 129.01 (2C), 124.6, 124.5, 121.1, 121.1, 111.4, 111.4, 55.6. **HR-MS** (ESI): calculated for $C_{27}H_{17}N_3O_3Na$ ($[M+Na]^+$): 394.1168, observed : 394.1163.

Synthesis of 4-bromo-3-(2-methoxyphenyl)-1-(4-nitrophenyl)-5-phenyl-1H-pyrazole

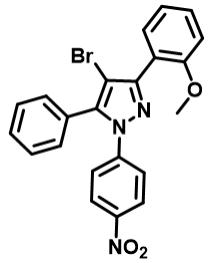

(5e) Compound **5e** was prepared following a procedure similar to that used for **1c**. The quantities involved are as follows: 3-(2-Methoxyphenyl)-1-(4-nitrophenyl)-5-phenyl-1*H*-pyrazole **(5f)** (2.30 g, 6.12 mmol, 1.0 eq) and N-bromosuccinimide (1.31 g, 7.35 mmol, 1.2 eq). The product **(5e)** was purified using silica gel column chromatography (*n*-hexane/EtOAc (94:6)). Yield: 2.28 g (83%). **^{1}H NMR** (400 MHz, $CDCl_3$) δ 8.17 – 8.11 (m, 2H), 7.51 (dd, 8.0 Hz, 2.0 Hz 1H), 7.49 – 7.44 (m, 6H), 7.41 – 7.37 (m, 2H), 7.12 – 7.01 (m, 2H), 3.91 (s, 3H). **^{13}C NMR** (101 MHz, $CDCl_3$) δ 157.6, 151.2, 146.0, 144.6, 141.5, 131.7, 130.9, 130.2, 129.7, 129.1, 128.7, 124.5, 124.2, 120.7, 120.4, 111.4, 100.2, 55.7. **HR-MS** (ESI): calculated for $C_{22}H_{16}BrN_3O_3Na$ ($[M+Na]^+$): 472.0267, 474.0248 observed : 472.0281, 474.0263.

Synthesis of 3-(2-methoxyphenyl)-1-(4-nitrophenyl)-4,5-diphenyl-1H-pyrazole (5d)

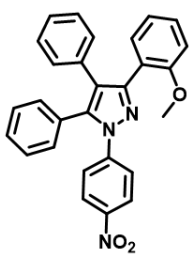

Compound **5d** was prepared following a procedure similar to that used for **1b**. The quantities involved are as follows: 4-bromo-3-(2-methoxyphenyl)-1-(4-nitrophenyl)-5-phenyl-1H-pyrazole **(5e)** (1.55 g,

3.70 mmol, 1.0 eq), $Pd(PPh_3)_4$ (0.13 g, 0.11 mmol, 0.035 eq), phenylboronic acid (0.58 g, 4.81 mmol, 1.3 eq), Sodium carbonate (1.17 g, 11.10 mmol, 3.0 eq). The product **(5d)** was purified using silica gel column chromatography (*n*-hexane/EtOAc (96:4)). Yield: 1.52 g (92%). **^{1}H NMR** (400 MHz, $CDCl_3$) δ 8.14 (d, *J* = 8.0 Hz, 2H), 7.57 (d, *J* = 8.0 Hz, 1H), 7.48 (d, *J* = 8.0 Hz, 2H), 7.42 – 7.26 (m, 4H), 7.17 (d, *J* = 8.0 Hz, 2H), 7.15 – 7.08 (m, 3H), 7.05 (t, *J* = 7.4 Hz, 1H), 6.97 – 6.89 (m, 2H), 6.81 (d, *J* = 8.0 Hz, 1H), 3.25 (s, 3H). **^{13}C NMR** (101 MHz, $CDCl_3$) δ 157.0, 150.7, 145.7, 144.9, 140.4, 133.2, 131.5, 130.6, 130.2, 129.8, 129.1, 129.0, 129.0, 127.9, 126.4, 124.7, 124.4, 121.9, 120.9, 115.4, 111.3, 54.9. **HR-MS** (ESI): calculated for $C_{28}H_{22}N_3O_3$ ($[M+H]^+$): 448.1661, observed : 448.1631.

Synthesis of 4-(3-(2-methoxyphenyl)-4,5-diphenyl-1H-pyrazol-1-yl)aniline (5c)

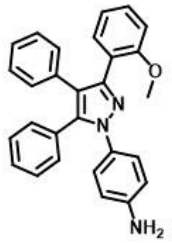

Compound **5c** was prepared following a procedure similar to that used for **2c**. The quantities involved are as follows: 3-(2-Methoxyphenyl)-1-(4-nitrophenyl)-4,5-diphenyl-1H-pyrazole **(5d)** (5.60 g, 12.6 mmol, 1.0 eq), hydrazine hydrate (6.2 mL, 126.00 mmol, 10.0 eq), and Pd/C (0.13 g, 1.26 mmol, 0.1 eq). The product **(5c)** was purified using silica gel column chromatography (*n*-hexane/EtOAc (70:30)). Yield: 5.05 g (96%). **^{1}H NMR** (400 MHz, $CDCl_3$) δ 7.57 (d, *J* = 8.0 Hz, 1H), 7.31 (td, *J* = 7.9, 1.8 Hz, 2H), 7.25 – 7.19 (m, 3H), 7.16 – 7.07 (m, 7H), 7.00 (td, *J* = 7.5, 1.1 Hz, 1H), 6.96 – 6.91 (m, 2H), 6.78 (d, *J* = 7.3 Hz, 2H), 3.22 (s, 3H). **^{13}C NMR** (101 MHz, $CDCl_3$) δ 157.0, 148.1, 145.6, 139.9, 134.5, 131.8, 131.5, 130.7, 130.5, 129.5, 129.2, 128.2, 127.9, 127.7, 126.8, 125.8, 122.9, 121.2, 120.8, 114.9, 111.1, 54.8. **HR-MS** (ESI): calculated for $C_{28}H_{24}N_3O$ ($[M+H]^+$): 418.1914, observed : 418.1931.

Synthesis of 4-(3-(2-methoxyphenyl)-4,5-diphenyl-1H-pyrazol-1-yl)-N,N-dimethylaniline (5b): 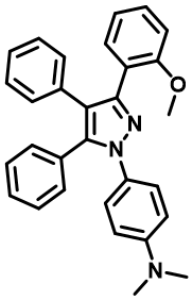 Compound **5b** was prepared following a procedure similar to that used for **2b**. The quantities involved are as follows: 4-(3-(2-Methoxyphenyl)-4,5-diphenyl-1H-pyrazol-1-yl)aniline **(5c)** (1.90 g, 4.56 mmol, 1.0 eq), sodium cyanoborohydride (1.4 g, 21.96 mmol, 4.8 eq), 37% formaldehyde solution (5.6 mL, 68.43 mmol, 15.0 eq) and acetic acid (0.52 mL, 9.12 mmol, 2.0 eq). The product was purified using silica gel column chromatography (*n*-hexane/EtOAc/CH_2Cl_2 (80:10:10)). Yield: 1.83 g (90 %). **^{1}H NMR** (400 MHz, $CDCl_3$) δ 7.64 (d, *J* = 8.0 Hz, 1H), 7.34 (t, *J* = 8.0 Hz, 1H), 7.29 – 7.22 (m, 3H), 7.24 – 7.12 (m, 7H), 7.04 (t, *J* = 8.0 Hz, 1H), 7.01 – 6.92 (m, 2H), 6.81 (d, *J* = 8.0 Hz, 1H), 6.64 – 6.66 (m, 2H), 3.24 (s, 3H), 2.96 (s, 6H). **^{13}C NMR** (101 MHz, $CDCl_3$) δ 157.0, 149.5, 148.0, 139.9, 134.7, 131.9, 130.8, 130.7, 129.8, 129.4, 129.2, 128.2, 127.8, 127.7, 126.4, 125.7, 123.1, 121.2, 120.8, 112.1, 111.2, 54.8, 40.6. **HR-MS** (ESI): calculated for $C_{30}H_{28}N_3O$ ($[M+H]^+$): 446.2227, observed : 446.2252.

Synthesis of 2-(1-(4-(dimethylamino)phenyl)-4,5-diphenyl-1H-pyrazol-3-yl)phenol (5a): 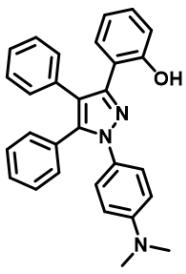 Compound **5a** was prepared following a procedure similar to that used for **1a**. The quantities involved are as follows: Compound **5b** (1.00 g, 2.24 mmol, 1.0 eq) and BBr_3 (1.06 mL, 11.2 mmol, 5.0 eq). The product **(5a)** was purified using silica gel column chromatography (*n*-hexane/EtOAc (94:06)). Crystallisation was done using CH_2Cl_2/*n*-hexane. Yield: 0.88 g (92 %). **^{1}H NMR** (400 MHz, $CDCl_3$) δ = 11.09 (s, 1H), 7.30 – 7.29 (m, 3H), 7.22 – 7.12 (m, 8H), 7.06 – 7.03 (m, 4H), 6.65 – 6.55 (m,

3H), 2.97 (s, 6H). **^{13}C NMR** (101 MHz, $CDCl_3$) δ = 156.5, 149.7, 147.4, 141.5, 135.3, 133.5, 131.1, 130.5, 129.6, 129.0, 128.7, 128.6, 128.2, 127.2, 126.0, 120.2, 118.7, 117.4, 117.1, 116.9, 111.9, 40.5. HR-MS (ESI): calculated for $C_{29}H_{26}N_3O$ ($[M+H]^+$): 432.2070, observed: 432.2076.

Synthesis of complex 5: Compound **5** was prepared following a procedure similar

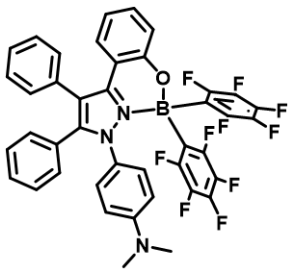

to that used for **1**. The quantities involved are as follows: Compound **5a** (0.30 g, 0.69 mmol, 1.0 eq) and tris(pentafluorophenyl)borane (0.39 g, 0.76 mmol, 1.2 eq). Crystallisation was done using CH_2Cl_2/*n*-hexane. Yield: 0.34 g (63 %). **^{1}H NMR** (400 MHz, $CDCl_3$) δ = 7.42 – 7.31 (m, 5H), 7.30 – 7.10 (m, 4H), 7.09 – 7.03 (m, 2H), 7.02 – 6.94 (m, 2H), 6.93 – 6.83 (m, 2H), 6.60 (t, *J* = 8.0 Hz, 1H), 6.24 (d, *J* = 8.0 Hz, 2H), 2.87 (s, 6H). **^{13}C NMR** (101 MHz, $CDCl_3$) δ = 155.6, 150.9, 148.1 (d, *J* = 245.43 Hz), 147.3, 142.3, 142.2 (d, *J* = 233.31), 137.0 (d, *J* = 250.48), 132.2, 131.0, 130.7, 130.5, 129.5, 129.1, 128.5, 128.4, 126.7, 126.6, 123.1, 119.7, 118.7, 115.3, 111.4, 40.3. **^{19}F NMR** (376 MHz, $CDCl_3$) δ = -132.53 (bs, 4F, Pf), -157.63 (t, 2F, Pf), -164.42 (s, 4F, Pf). **^{11}B NMR** (128 MHz, $CDCl_3$) δ = -0.77. **HR-MS** (ESI): calculated for $C_{41}H_{25}BF_{10}N_3O$ ($[M+H]^+$): 776.1967, observed : 776.2001. Anal. Calcd for $C_{41}H_{24}BF_{10}N_3O$: C, 63.50; H, 3.12, N, 5.42. Found: C, 64.02; H, 3.27, N, 5.82.

Synthesis of 4-(3-(2-methoxyphenyl)-4,5-diphenyl-1H-pyrazol-1-yl)-N,N-diphenylaniline (6b): Compound **6b** was prepared following a procedure similar to that used for **3b**. 4-(3-(2-Methoxyphenyl)-4,5-diphenyl-1*H*-pyrazol-1-yl)aniline **(5c)** (5.20 g, 12.47 mmol, 1.0 eq), iodobenzene (4.20 mL, 37.27 mmol, 3.0 eq),

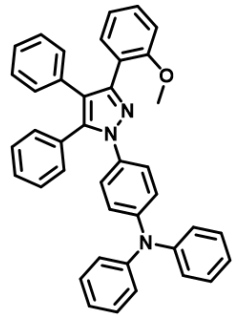

copper iodide (0.14 g, 0.74 mmol, 0.02 eq), 1,10-phenanthroline monohydrate (0.15 g , 0.74 mmol, 0.02 eq), and potassium *tert*-butoxide (4.20 g, 37.27 mmol, 3.0 eq). The product **(6b)** was purified using silica gel column chromatography (*n*-hexane/EtOAc/CH_2Cl_2 (80:10:10)). Yield: 6.09 g (86 %). **^{1}H NMR** (400 MHz, $CDCl_3$) δ 7.65 (d, *J* = 8.0 Hz, 1H), 7.36 (t, *J* = 7.8 Hz, 1H), 7.29 (d, *J* = 6.2 Hz, 7H), 7.21 – 7.17 (m, 4H), 7.15 – 7.09 (m, 8H), 7.08 – 7.03 (m, 2H), 7.02 – 6.96 (m, 4H), 6.82 (d, *J* = 8.2 Hz, 1H), 3.25 (s, 3H). **^{13}C NMR** (101 MHz, $CDCl_3$) δ 157.0, 148.7, 147.6, 146.8, 139.5, 134.4, 134.4, 131.9, 130.7, 130.5, 129.6, 129.4, 129.2, 128.3, 128.2, 127.8, 126.4, 125.9, 124.6, 123.2, 122.8, 121.7, 120.8, 117.4, 111.2, 54.8. **HR-MS** (ESI): calculated for $C_{40}H_{32}N_3O$ ($[M+H]^+$): 570.2540, observed : 570.2564.

Synthesis of 2-(1-(4-(diphenylamino)phenyl)-4,5-diphenyl-1H-pyrazol-3-yl)phenol (6a): Compound **6a** was prepared following a procedure similar to that used for **1a**. The quantities involved are as follows: Compound **6b** (1.50 g, 2.63 mmol, 1.0 eq), BBr_3 (1.25 mL, 13.18 mmol, 5.0 eq). The product **(6a)** was purified using silica gel column chromatography (*n*-hexane/EtOAc (94:06)). Crystallisation was done using CH_2Cl_2/*n*-hexane. Yield: 1.0 g (69 %). **^{1}H NMR** (400 MHz, $CDCl_3$) δ = 11.01 (s, 1H, -OH), 7.30 – 7.18 (m, 12H), 7.16 – 7.01 (m, 13H), 6.99 (d, *J* = 8.0 Hz, 2H), 6.60 (t, *J* = 8.0 Hz, 1H). **^{13}C NMR** (101 MHz, $CDCl_3$) δ = 156.4, 147.8, 147.3, 147.3, 141.6, 133.2, 132.5, 131.0, 130.4, 129.5, 129.4, 129.2, 128.6, 128.5, 128.3, 128.3, 127.4, 125.7, 124.9, 123.6, 122.6,

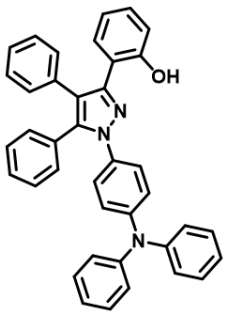

120.7, 118.8, 117.1, 116.7. **HR-MS** (ESI): calculated for $C_{39}H_{30}N_3O$ ($[M+H]^+$): 556.2389, observed : 556.2392.

Synthesis of complex 6: Compound **6** was prepared following a procedure similar

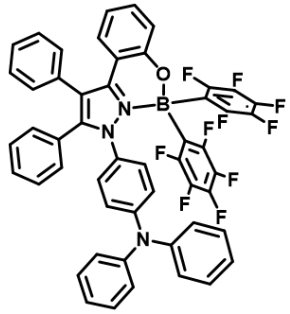

to that used for **1**. The quantities involved are as follows: Compound **6a** (0.30 g, 0.54 mmol, 1.0 eq) and tris(pentafluorophenyl)borane (0.33 g, 0.64 mmol, 1.2 eq) Crystallisation was done using $CHCl_3$/*n*-hexane. Yield: 0.25 g (52 %), **^{1}H NMR** (400 MHz, $CDCl_3$) δ = 7.40 – 7.35 (m, 3H), 7.36 – 7.28 (m, 7H), 7.22 – 7.16 (m, 3H), 7.15 – 7.09 (m, 2H), 7.05 – 6.95 (m, 8H), 6.81 (d, *J* = 8.0 Hz, 2H), 6.64 – 6.58 (m, 1H), 6.54 (d, *J*=8.0, 2H). **^{13}C NMR** (101 MHz, $CDCl_3$) δ = 155.5, 149.4, 148.3 (d, *J* = 282.8 Hz) 147.3, 146.1, 142.3, 140.0 (d, *J* = 274.72 Hz), 139.8, 137.2 (d, *J* = 226.24 Hz) 133.0, 132.3, 130.9, 130.5, 129.9, 129.6, 129.1, 128.9, 128.6, 129.5, 128.4, 127.3, 126.7, 126.2, 125.2, 124.7, 119.7, 119.7, 118.9, 118.7. **^{19}F NMR** (376 MHz, $CDCl_3$) δ = -134.27 (bs, 4F, Pf), -156.85 (t, 2F, Pf), -163.79 (t, 4F, Pf). **^{11}B NMR** (128 MHz, $CDCl_3$) δ = -0.85. **HR-MS** (ESI): calculated for $C_{51}H_{29}BF_{10}N_3O$ ($[M+H]^+$): 900.2358, observed : 900.2347. Anal. Calcd for $C_{51}H_{28}BF_{10}N_3O$: C, 68.09; H, 3.14, N, 4.67. Found: C, 67.89; H, 3.32, N, 4.27.

3.5 References

1. Andreopoulou, A. K.; Gioti, M.; Kallitsis, J. K. In *Organic Light-emitting Diodes Based on Solution-Processable Organic Materials*, Wiley-VCH Verlag GmbH & Co. KGaA: 2019; p 413.

2. Ha, J. M.; Hur, S. H.; Pathak, A.; Jeong, J.-E.; Woo, H. Y. *NPG Asia Mater.* **2021,** *13*, 53.

3. Mooney, M.; Crep, C.; Rondeau-Gagne, S. *ACS Appl. Electron. Mater.* **2022,** *4*, 5652-5663.

4. Chen, M.-C.; Chen, D.-G.; Chou, P.-T. *ChemPlusChem* **2021,** *86*, 11-27.

5. Kagatikar, S.; Sunil, D. *J. Mater. Sci.* **2022,** *57*, 105-139.

6. Kim, H. J.; Yasuda, T. *Adv. Opt. Mater.* **2022,** *10*, 2201714.

7. Luo, W.; Tan, Y.; Gui, Y.; Yan, D.; Wang, D.; Tang, B. Z. *Molecules* **2022,** *27*, 3914.

8. Biswas, A.; Bakthavatsalam, R.; Bahadur, V.; Biswas, C.; Mali, B. P.; Raavi, S. S. K.; Gonnade, R. G.; Kundu, J. *J. Mater. Chem. C* **2021,** *9*, 4351-4358.

9. Kashida, J.; Shoji, Y.; Ikabata, Y.; Taka, H.; Sakai, H.; Hasobe, T.; Nakai, H.; Fukushima, T. *Angew. Chem., Int. Ed.* **2021,** *60*, 23812-23818.

10. Zhang, C.; Zhang, M.; Zheng, W.; Wei, J.; Wang, S.; Huang, P.; Cheng, X.; Dai, T.; Chen, Z.; Chen, X. *Nano Res.* **2022,** *15*, 179-185.

11. Nakazato, T.; Shinokubo, H.; Miyake, Y. *Chem. Commun.* **2021,** *57*, 327-330.

12. Song, S.; Zhang, P.; Liu, H.; Zhu, X.; Feng, X.; Zhao, Z.; Tang, B. Z. *Dyes Pigm.* **2021,** *196*, 109776.

13. Wu, Z.; Dinkelbach, F.; Kerner, F.; Friedrich, A.; Ji, L.; Stepanenko, V.; Wuerthner, F.; Marian, C. M.; Marder, T. B. *Chem. - Eur. J.* **2022,** *28*, e202200525.

14. Qin, Y.-y.; Xu, W.-j.; Hu, C.-y.; Liu, S.-j.; Zhao, Q. *Chin. J. Inorg. Chem.* **2017,** *33*, 1705-1721.

15. Oda, S.; Shimizu, T.; Katayama, T.; Yoshikawa, H.; Hatakeyama, T. *Org. Lett.* **2019,** *21*, 1770-1773.

16. Yang, K.; Song, Q. *Acc. Chem. Res.* **2021,** *54*, 2298-2312.

17. Murali, A. C.; Nayak, P.; Venkatasubbaiah, K. *Dalton Trans.* **2022,** *51*, 5751-5771.

18. Mukundam, V.; Kumar, A.; Dhanunjayarao, K.; Ravi, A.; Peruncheralathan, S.; Venkatasubbaiah, K. *Polym. Chem.* **2015,** *6*, 7764-7770.

19. Mukundam, V.; Dhanunjayarao, K.; Samal, S.; Venkatasubbaiah, K. *Asian J. Org. Chem.* **2017,** *6*, 1054-1062.

20. Zhang, P.; Liu, W.; Niu, G.; Xiao, H.; Wang, M.; Ge, J.; Wu, J.; Zhang, H.; Li, Y.; Wang, P. *J. Org. Chem.* **2017,** *82*, 3456-3462.

21. Bonacorso, H. G.; Calheiro, T. P.; Acunha, T. V.; Iglesias, B. A.; Franceschini, S. Z.; Ketzer, A.; Meyer, A. R.; Nogara, P. A.; Rocha, J. B. T.; Zanatta, N.; Martins, M. A. P. *Dyes Pigm.* **2019,** *161*, 396-402.

22. Cetin, A. *Mini-Rev. Org. Chem.* **2021,** *18*, 93-109.

23. Li, X.; Yu, Y.; Tu, Z. Pyrazole Scaffold Synthesis, Functionalization, and Applications in Alzheimer's Disease and Parkinson's Disease Treatment (2011–2020) *Molecules* [Online], 2021.

24. Karati, D.; Mahadik, K. R.; Kumar, D. *Med. Chem.* **2022,** *18*, 1060-1072.

25. Ardevines, S.; Marques-Lopez, E.; Herrera, R. P. *Curr. Med. Chem.* **2023,** *30*, 1145-1174.

26. Catalan, J.; Fabero, F.; Claramunt, R. M.; Santa Maria, M. D.; Foces-Foces, M. d. l. C.; Hernandez Cano, F.; Martinez-Ripoll, M.; Elguero, J.; Sastre, R. *J. Am. Chem. Soc.* **1992,** *114*, 5039.

27. Tyagi, P.; Singh, U. P. *Curr. Bioact. Compd.* **2009,** *5*, 296-320.

28. Kuwata, S.; Ikariya, T. *Chem. - Eur. J.* **2011,** *17*, 3542-3556.

29. Mamidala, R.; Samser, S.; Sharma, N.; Lourderaj, U.; Venkatasubbaiah, K. *Organometallics* **2017,** *36*, 3343-3351.

30. Zhao, S.; Wu, J.; Chen, W. *J. Organomet. Chem.* **2017,** *848*, 249-280.

31. Ardiansah, B. *Asian J. Pharm. Clin. Res* **2018,** *11*, 88-94.

32. Katarzyna, M.; Anna, S.; Zielinska-Blizniewska, H.; Ireneusz, M. *Mini-Rev. Med. Chem.* **2018,** *18*, 1373-1381.

33. Tabassum, K.; Ekta, P.; Kavitkumar, P. *Mini-Rev. Org. Chem.* **2018,** *15*, 459-475.

34. Xu, J.-X.; Wu, X.-F. *J. Org. Chem.* **2019,** *84*, 9907-9912.

35. Karati, D.; Mahadik, K. R.; Trivedi, P.; Kumar, D. *Med. Chem.* **2022,** *18*, 1044-1059.

36. Mor, S.; Khatri, M.; Punia, R.; Sindhu, S. *Mini-Rev. Med. Chem.* **2022,** *22*, 115-163.

37. Biswal, P.; Siva Subramani, M.; Samser, S.; Chandrasekhar, V.; Venkatasubbaiah, K. *J. Org. Chem. 10.1021/acs.joc.2c00653* **2022**.

38. Sa, S.; Sahoo, A.; Mukherjee, S.; Perumal, A.; Venkatasubbaiah, K. *Dyes Pigm.* **2022,** *206*, 110585.

39. Mukundam, V.; Sa, S.; Kumari, A.; Teja Ponduru, T.; Das, R.; Venkatasubbaiah, K. *Chem. - Asian J.* **2022,** *17*, e202200291.

40. Sa, S.; Mukundam, V.; Kumari, A.; Das, R.; Venkatasubbaiah, K. *Dalton Trans.* **2021,** *50*, 6204-6212.

41. Mukundam, V.; Sa, S.; Kumari, A.; Das, R.; Venkatasubbaiah, K. *J. Mater. Chem. C* **2019,** *7*, 12725-12737.

42. Kumar, S. V.; Yadav, S. K.; Raghava, B.; Saraiah, B.; Ila, H.; Rangappa, K. S.; Hazra, A. *J. Org. Chem.* **2013,** *78*, 4960-4973.

43. Dhanunjayarao, K.; Mukundam, V.; Ramesh, M.; Venkatasubbaiah, K. *Eur. J. Inorg. Chem.* **2014,** *2014*, 539-545.

44. Mukundam, V.; Dhanunjayarao, K.; Chuang, C.-N.; Kang, D.-Y.; Leung, M.-k.; Hsieh, K.-H.; Venkatasubbaiah, K. *Dalton Trans.* **2015,** *44*, 10228-10236.

45. Dhanunjayarao, K.; Mukundam, V.; Ranga Naidu Chinta, R. V.; Venkatasubbaiah, K. *J. Organomet. Chem.* **2018,** *865*, 234-238.

46. Chinta, R. V. R. N.; Aradhyula, B. P. R.; Murali, A. C.; Venkatasubbaiah, K. *J. Organomet. Chem.* **2019,** *891*, 20-27.

47. Dhanunjayarao, K.; Mukundam, V.; Venkatasubbaiah, K. *Inorg. Chem.* **2016,** *55*, 11153-11159.

48. Yugandar, S.; Konda, S.; Ila, H. *Org. Lett.* **2017,** *19*, 1512-1515.

CHAPTER 4

Poly(indazaboles) a new class of optical materials analogues of poly(pyrazaboles)

4.1 Introduction

There is considerable contemporary interest in the design and synthesis of tetra-coordinated boron compounds.[1-12] Among the different tetra-coordinated boron compounds, N,N-chelated boron compounds have attracted substantial attention owing to their excellent photophysical properties.[8] Much effort has been devoted in the design and synthesis of novel boron dyes with N,N-chelating motif. The pyrazaboles are a class of N,N-chelated boron heterocycles has emerged as prominent materials for applications in the field of liquid crystals, π-conducting and as luminescent materials.[13] Several examples of pyrazaboles with different substitutions have been reported to tailor the properties.[14-20] For instance, Chujo and co-workers reported polymers that contain pyrazaboles in the main-chain and studied their photophysical properties,[21-23] more recently, Wagner and Jäkle groups elegantly shown the synthesis of rigid-rod redox-active pyrazaboles.[24, 25] However, in comparison with pyrazaboles, indazaboles analogues of pyrazaboles have received far less attention. In spite of the added rich chemistry of indazoles, the indazaboles has not been studied to a greater extent. Moreover, the polymer chemistry of indazaboles in not explored yet. Herein, we report the design, synthesis, characterization and photophysical properties of model indazaboles and the corresponding polymers.

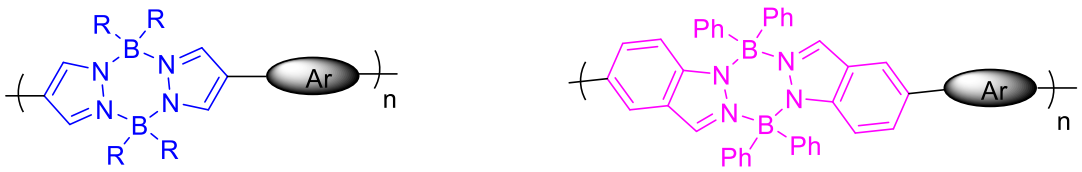

reported not reported

Figure 4.1: Chem-draw structure of poly(pyrazabole) and poly(indazabole)

4.2 Results and discussion

4.2.1 Synthesis and characterization

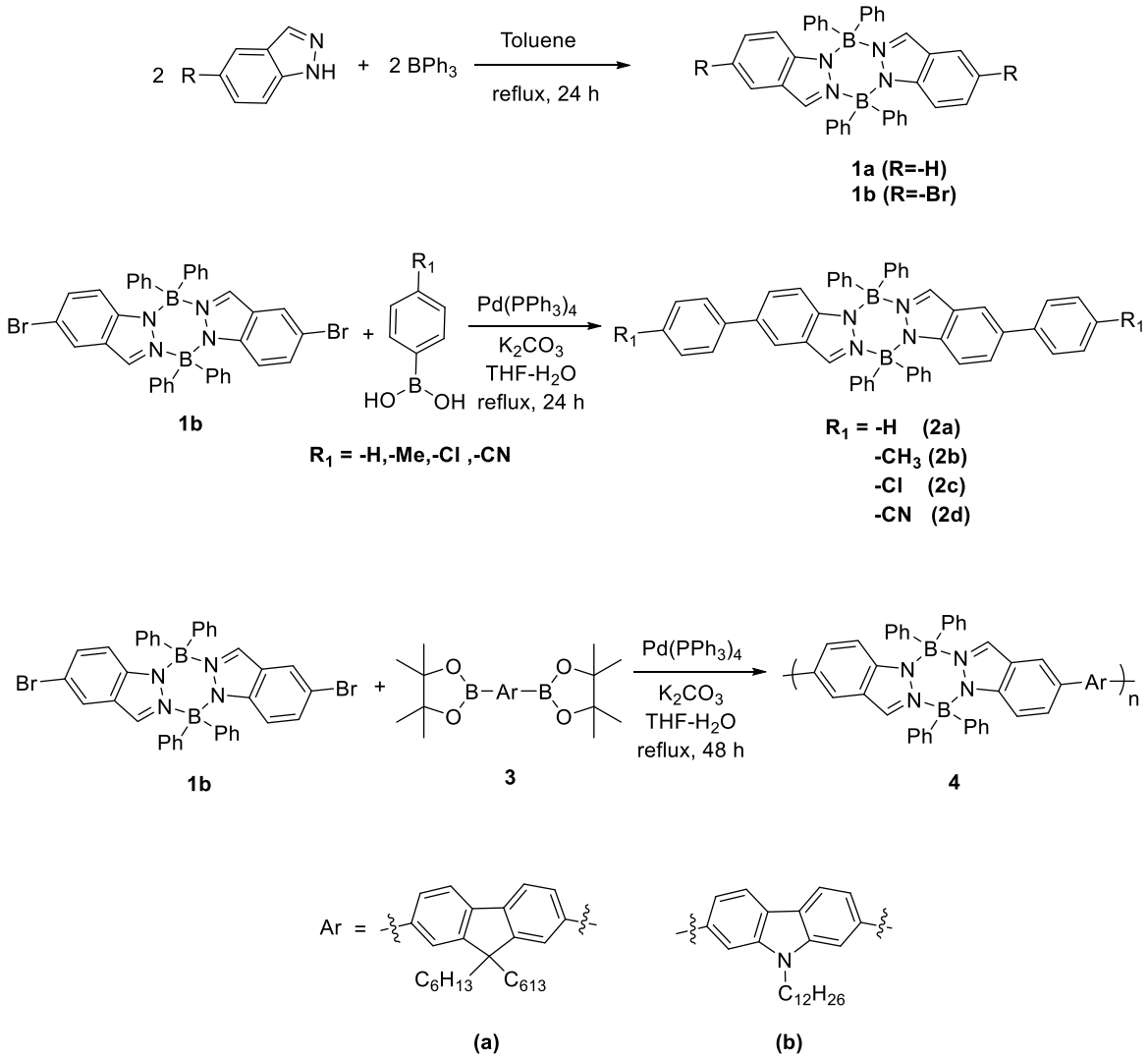

Scheme 4.1: Synthetic routes for indazaboles (**1a-1b** and **2a-2d**), poly(indazaboles) (**4a-4b**).

The indazabole precursor **1b** and model compound **1a** were synthesized by refluxing 5-bromo-1-H indazole/1-H indazole with triphenylborane as shown in **Scheme 4.1.** The feasibility of functionalization of **1b** was confirmed by performing Suzuki-coupling reaction using different boronic acids (**2a-2d**). All the synthesized precursor (**1b**), and model compounds (**1a**, and **2a-2d**) were characterized using multi-nuclear NMR and HRMS. The absence of indazole -NH proton (10.88 ppm) in the ^{1}H-NMR spectrum of **1** confirms the formation of boron fused ring system. The tetra-coordinated nature of precursor **1** and **2a-2d** were confirmed by the ^{11}B-NMR spectroscopy (1.84 ppm for **1a**;

1.98 ppm for **1b**; 1.81 ppm for **2a**; 1.41 ppm for **2b**; 0.84 ppm for **2c**; and 4.81 ppm for **2d**). The desired polymers (**4a** and **4b**) were synthesized by the cross-coupling of precursor **1b** with aryl diboronic ester (monomers **3a** and **3b**) under Suzuki coupling reaction conditions (Scheme **4.1**). The polymers were soluble in tetrahydrofuran solvent and purified by reprecipitation from hexane and methanol solutions. The synthesized polymers (**4a** and **4b**) were characterized using ^{1}H-NMR, ^{13}C-NMR, and ^{11}B-NMR spectroscopy. The NMR spectra of polymers **4a** and **4b** are consistent with the proposed structure. Further, the molecular weight of the polymers **4a** and **4b** were studied by gel-permeation chromatography (GPC). GPC analysis in THF gave M_w = 56600 (PDI = 1.67) for **4a** and M_w = 102400 (PDI = 1.97) for **4b**.

X-Ray diffraction structural analysis

To realize the confirmation of the indazaborole, single crystals of precursor **1b** and functionalized compound **2b** were grown by the slow evaporation of MeOH/CH_2Cl_2. Both **1b** and **2b** crystallize in triclinic P-1 space group. In both instance, we observed dimeric structures with central six-membered ring B_2N_4 having benzo rings oriented in the opposite directions. The molecular structure of **1b** and **2b** consists of five fused rings with a boat conformation. The boron atoms are in a distorted-tetrahedral environment and deviate from the six membered plane defined by B_2N_4 (0.403 Å and 0.363 Å for **1b**; 0.375 Å and 0.406 Å for **2b**). The bond distances and bond angles around the boron atoms are comparable with N-N chelated boron fused pyrazabole molecules reported in the literaure.[15, 16, 18, 26, 27] Two of the phenyl rings attached to the opposite boron atoms stacked in a face-to-face manner with a distance of 3.744 (2) and 3.647(2) and in **1b** and **2b** respectively.

Table 4.1. Bond length **(Å)**, bond angle **(degree)** measurement data for compound **1b and 2b**.

	1b	**2b**
N1-B1	1.580 (4)	1.579 (3)
N4-B1	1.577 (4)	1.589 (4)
N2-B2	1.589 (4)	1.584 (4)
N3-B2	1.597 (4)	1.579 (3)
C1-B1	1.613 (4)	1.606 (4)
C2-B1	1.610 (4)	1.617 (4)
C3-B2	1.617 (4)	1.619 (4)
C4-B2	1.614 (4)	1.619 (4)
N1-B1-N4	103.7 (2)	104.03 (19)
N1-B1-C1	108.0 (2)	110.7 (2)
C1-B1-C2	114.7 (2)	114.3 (2)
C2-B1-N4	110.4 (2)	110.6 (2)
N2-B2-N3	104.5 (2)	103.47 (19)
N2-B2-C3	107.5 (2)	107.1 (2)
C3-B2-C4	115.2 (2)	114.0 (2)
C4-B2-N3	109.2 (2)	109.7 (2)
Deviation of boron atom (B1 and B2) from $N_1N_2N_3N_4B1B2$ plane (Å)	0.403, 0.363	0.378, 0.406

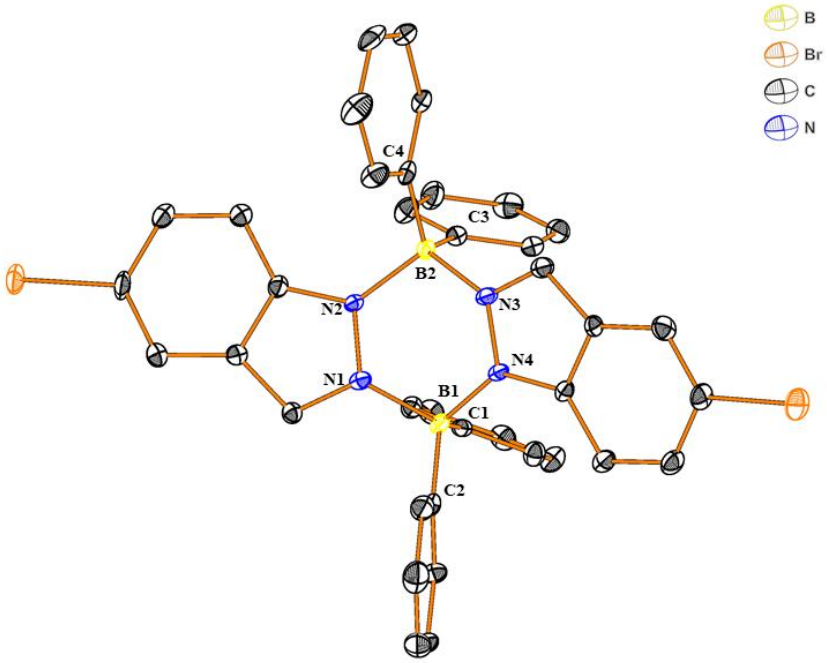

Figure 4.2: Molecualr structure of compound **1b** with thermal ellipsoid at the 50% probability level (Hydrogen atoms are omitted for clarity).

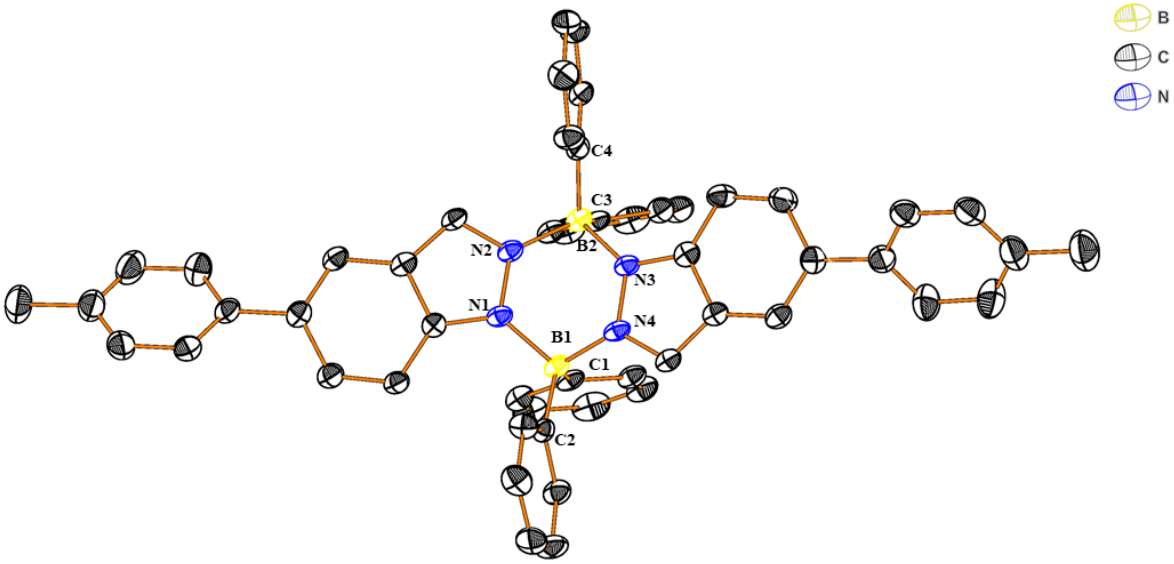

Figure 4.3. Molecular structure of boron compound **2b** with thermal ellipsoid at the 50% probability level (Hydrogen atoms are omitted for clarity).

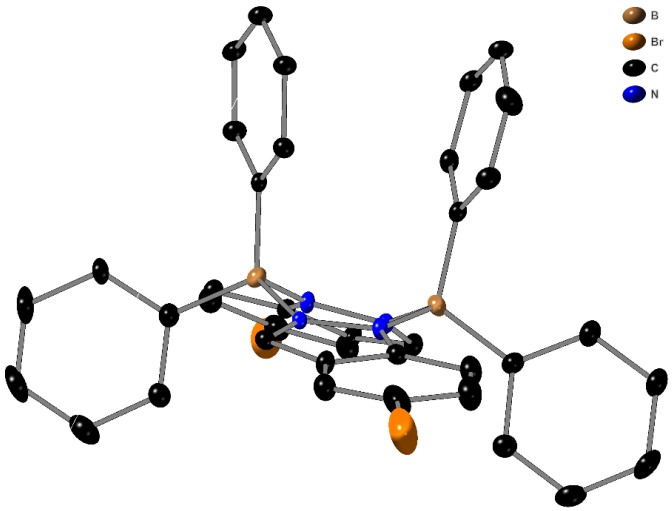

Figure 4.4. Molecular structure of compound **1b** in boat form with thermal ellipsoid at the 50% probability level (Hydrogen atoms are omitted for clarity).

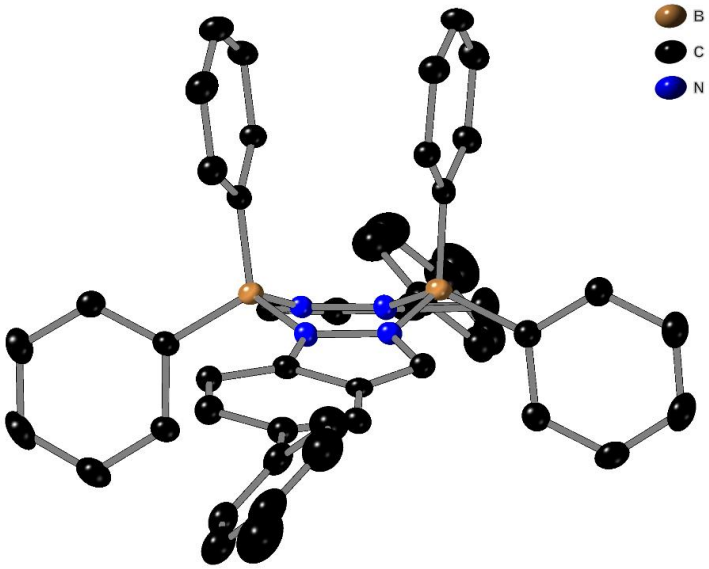

Figure 4.5: Molecular structure of compound **2b** in boat form with thermal ellipsoid at the 50% probability level (Hydrogen atoms are omitted for clarity).

Table 4.2. Crystal data and structure refinement for compound 1b and 2b.

	1b	**2b**
Empirical formula	$C_{38}H_{28}B_2Br_2N_4$	$C_{52}H_{42}B_2N_4$
Formula weight	722.08	744.51
Temperature/K	100.00(15)	100.00(10)
Crystal system	triclinic	triclinic
Space group	P-1	P-1
a/Å	12.0865(3)	9.5235(4)

b/Å	12.6993(4)	15.5702(5)
c/Å	12.8343(5)	16.1292(7)
α/°	119.427(4)	96.263(3)
β/°	95.982(3)	106.699(4)
γ/°	97.327(2)	101.562(3)
Volume/$Å^3$	1669.72(11)	2208.64(16)
Z	2	2
$\rho_{calc}g/cm^3$	1.436	1.120
μ/mm^{-1}	2.461	0.065
F(000)	728.0	784.0
Crystal size/mm^3	0.10 × 0.12 × 0.14	0.08 × 0.06 × 0.05
Radiation	MoKα (λ = 0.71073)	MoKα (λ = 0.71073)
2Θ range for data collection/°	6.502 to 61.35	6.558 to 60.814
Index ranges	-17 ≤ h ≤ 16, -17 ≤ k ≤ 18, -16 ≤ l ≤ 16	-12 ≤ h ≤ 12, -20 ≤ k ≤ 20, -22 ≤ l ≤ 22
Reflections collected	30983	50568
Independent reflections	8172 [R_{int} = 0.0499, R_{sigma} = 0.0413]	10796 [R_{int} = 0.0983, R_{sigma} = 0.0830]
Data/restraints/parameters	8172/0/415	10796/0/525
Goodness-of-fit on F^2	1.033	1.038
Final R indexes [I>=2σ (I)]	R_1 = 0.0531, wR_2 = 0.1357	R_1 = 0.0791, wR_2 = 0.1992
Final R indexes [all data]	R_1 = 0.0686, wR_2 = 0.1423	R_1 = 0.1168, wR_2 = 0.2159
Largest diff. peak/hole / e $Å^{-3}$	2.30/-0.69	0.42/-0.33

4.2.2 Photophysical properties

The optical properties of the model compounds **1a,** and **2a-2d** were analysed by UV-Vis absorption and fluorescence spectroscopy in three different solvents (toluene, tetrahydrofuran-THF, and acetonitrile) of different polarity. However, the optical properties of polymers were recorded in only THF owing to their solubility constraint. The data pertaining to the optical properties is presented in the **Table 4.3** and **Figure 4.6.**

Table 4.3. Photophysical data of compounds **1a, 2a-2d, 4a** and **4b** at 298K

Compounds	**Solvent**	**λ_{abs}[a] /nm (ε x 10^4/M^{-1} cm^{-1})**	**λ_{ems}[b] (nm)**	**Stokes Shift (cm^{-1})**	**ϕ_F[c,d] (%)**	**τ (ns)**
1a	Toluene	294 (1.48)	364	6541	35.3	
	THF	293 (1.43)	360	6352	21.6, 11.2[d]	1.6
	ACN	292 (1.38)	363	6698	22.1	
2a	Toluene	313 (0.54)	367	4701	28.5	
	THF	312 (1.05)	367	4804	25.6, 4.7 [d]	3.9
	ACN	311 (0.11)	364	4682	15.2	
2b	Toluene	314 (0.77)	372	4966	29.3	
	THF	313 (1.22)	373	5139	28.6, 2.7 [d]	4.1
	ACN	314 (0.13)	380	5532	20.0	
2c	Toluene	313 (1.60)	368	4775	30.6	
	THF	313 (1.28)	369	4848	23.5, 9.8 [d]	2.8
	ACN	314 (0.18)	376	5252	19.0	
2d	Toluene	303 (2.97)	364	5531	56.2	
	THF	303 (3.71)	362	5379	54.6, 1.6 [d]	3.6
	ACN	301 (1.32)	363	5674	41.1	
4a	THF	335 (5.38)	399	4788	69.2, 0.2 [d]	1.3
4b	THF	335 (4.48)	404	5098	56.0, 1.3 [d]	2.8

[a]Absorption maximum (concentration = 4.0 x 10^{-5} M), [b]Excited at λ_{max}, [c]Absolute quantum yield using integrating sphere module, [d]Solid state quantum yield using integrating sphere module.

All the model compounds **1a,** and **2a-2d,** exhibit absorption maxima at ca. 293-313 nm with a molar absorption coefficient ranging between 10500 to 37100 $M^{-1}cm^{-1}$ in THF. Compound **1a** exhibit blue shifted absorption in THF compared to **2a-2d** due to the increased conjugation present in the later. A slight blue shift observed in THF for compound **2d** compared to **2a-2c** owing to the strong electron withdrawing nature of –CN present in **2d**. Both the polymers (**4a** and **4b**) exhibit intense absorption maxima at 335 nm with a molar absorption coefficient of 53800 $M^{-1}cm^{-1}$ and 44800 $M^{-1}cm^{-1}$ for **4a** and

4b respectively. The pronounced red shift (~30 nm) observed in the polymers **4a** and **4b**, due to the extension of π-conjugation through the backbone. The steady state emission of model compounds **1a**, **2a-2d** and polymers **4a** and **4b** were recorded by exciting at their absorption maxima and the results are presented in **Table 4.3** and **Figure 4.6.** Model compounds **1a** and **2a-2d** exhibit emission maxima ranged from 360 nm to 373 nm in THF and also does not show any appreciable solvatochromism. Among the π-extended model compounds studied (**2a-2d**), **2d** showed blue shifted emission (362 nm) with larger Stokes shift (5379 cm^{-1}) and highest quantum yield (54.6) in THF, which can be attributed to the presence of -CN present in the moiety. Model compounds **1a** and **2a-2d** and polymers **4a** and **4b** showed single exponential decay with lifetimes ranging between 1.3 ns to 4.1 ns in THF solution.

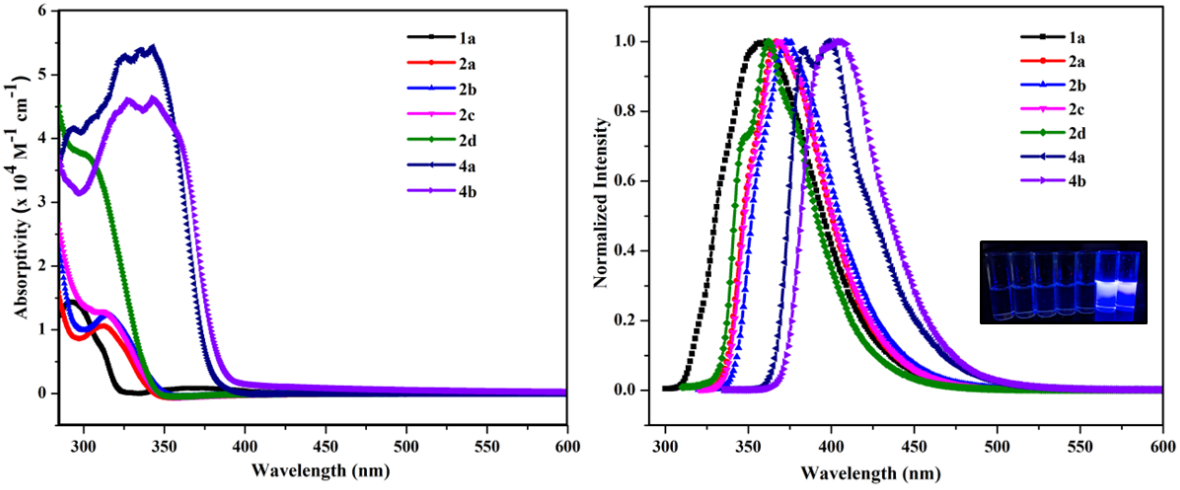

Figure 4.6: Absorption spectra of compounds **1a, 2a-2d, 4a** and **4b** (Left) and normalized emission spectra of compounds **1a, 2a-2d, 4a** and **4b** (Right) in THF ($4.0x10^{-5}$ M concentration). Inset (Right): photograph of compounds **1a, 2a-2d, 4a** and **4b** in THF under a hand-held UV lamp at 365 nm

4.2.3 DFT studies

To understand the photophysical and electronic properties of polymers, density functional theory (DFT) and time-dependent-DFT (TD-DFT) calculations of the model compounds

1a and **2a-2d** were performed using the B3LYP/6-31G(d). The highest occupied molecular orbitals (HOMO) in **1a** and **2d** mainly localized on face-to-face stacked phenyl rings attached to the boron atoms, in case of **2a** and **2b** they are localized on face-to-face stacked phenyl rings attached to the boron atoms, both indazole moieties along with extended phenyl rings, where as in case of **2c** they are localized on face-to-face stacked phenyl rings attached to the boron atoms, partly both indazole moieties. Except **2d,** the lowest unoccupied molecular orbitals (LUMO) of **1a** and **2a-2c** are localized on both indazole moieties, where as in case of **2d** the LUMO got extended to –CN and cyanophenyl aromatic moiety. On examination of the HOMO and LUMO energy levels for **1a** and **2a-2d** reveals that the later have the low energy band gap owing to the increased conjugation. The electron withdrawing nature of –CN in **2d** is responsible for the lowered LUMO energy level and low energy band gap observed in comparison to **2a-2c,** consistent with the blue shift observed for compound **2d.**

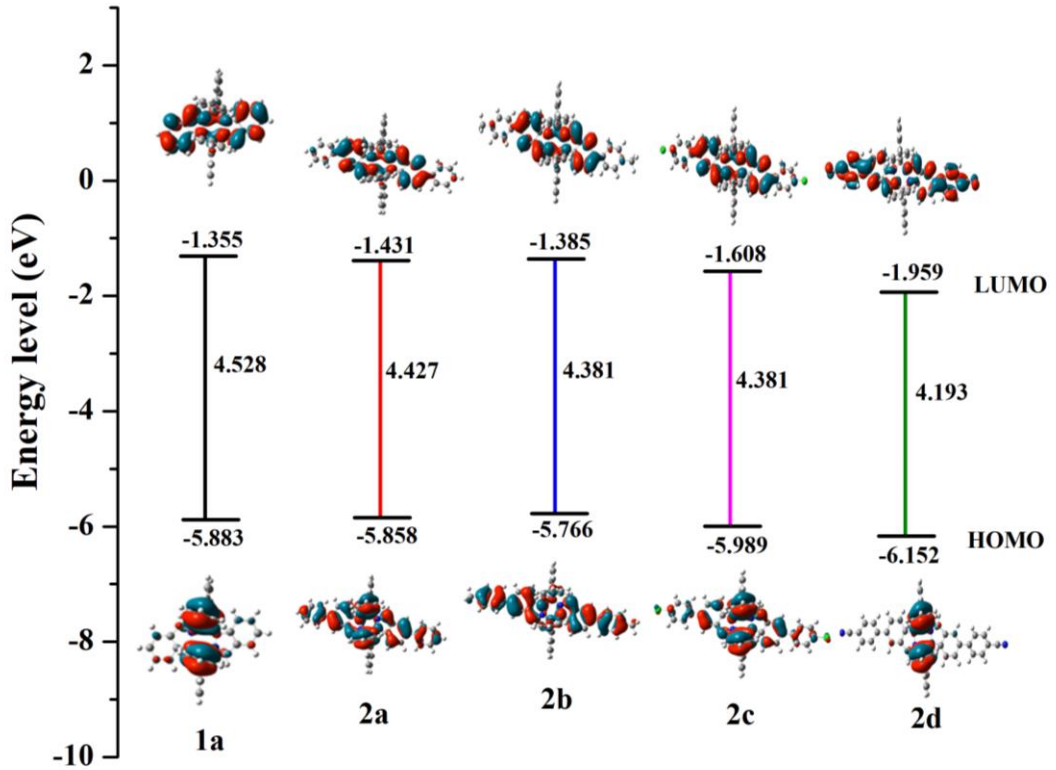

Figure 4.7: Calculated HOMOs and LUMOs of compounds **1a, 2a-2d** with their 3D representation

4.2.4 Thermal Studies

Thermal properties of the synthesized poly(indazaboles) **4a** and **4b** were analysed by thermogravimetric analysis (TGA). The TGA curve of the polymers suggest that they are thermally stable upto 300 °C.

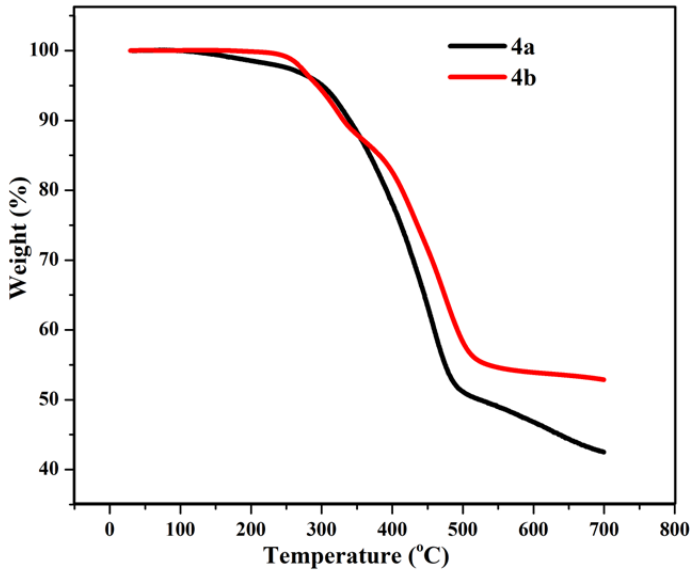

Figure 4.8: TGA graph of polymers (**4a** and **4b**)

4.3 CONCLUSION

In summary, we have synthesized new tetra-coordinated boron compounds that were fused by indazole moieties. Furthermore, the indazabole main chain polymers **4a** and **4b** were synthesized by Suzuki coupling reaction. From the X-ray analysis, it was realized that the indazabole's adopt a boat conformation having benzo rings oriented in the opposite direction. The optical properties reveal that the polymers exhibited high absorption coefficient and strong emission over the model compounds.

4.4 Experimental section

4.4.1 General information

All the reactions were carried out under N_2 atmosphere using standard glove box, Schlenk line and vacuum line techniques. Solvents and other general reagents were purified according to standard procedures. All the reactions were monitored by thin layer chromatography. Nuclear magnetic resonance spectra were recorded on a 400 MHz Fourier transform NMR spectrometer (JEOL or Bruker) with $CDCl_3$ as a solvent. ^{11}B and ^{19}F NMR spectra were externally referenced to $BF_3.Et_2O$ in $CDCl_3$ (δ=0 ppm) and α,α,α-trifluoro toluene in $CDCl_3$ (δ=-63.73 ppm), respectively. Chemical shifts are reported in δ ppm (parts per million) using residual solvent protons as the internal standard (δ 7.26 for $CDCl_3$ in ^1H NMR, δ 77.16 for $CDCl_3$ in ^{13}C NMR). Coupling constants are reported as J values in hertz (Hz). Splitting patterns are designated as s(singlet), d(doublet), t(triplet), q(quartet), dd(doublet of doublet), dt(doublet of triplet), m(multiplet) and br(broad). HRMS were recorded using Waters XEVO G2-XS QTOF mass spectrometer. Elemental analyses were performed in a Euro Vector EA 3000 CHNS analyzer. UV – Visible spectra were recorded on Agilent Technologies Cary 60 UV/Visible spectrometer. Fluorescence spectra and quantum yield were measured using Edinburgh specrofluorimeter instrument FS5. For the measurement of absolute quantum yield, the concentration of the boron compounds was such as to give an absorbance of around 0.1 at excitation wavelength. Absolute total quantum yields were measured using an integrating sphere (Edinburgh instrument FS5) mounted in SC-30 compartment of the spectrofluorimeter, The time-resolved fluorescence studies, a time-correlated single-photon counting (TCSPC) spectrometer (Edinburgh, OB920) has been used with a laser of 330 nm as a source of excitation and an MCP photomultiplier (Hamamatsu R3809U-50) is used as a detector. In order to check the laser profile, a water:ludox (4:1) solution

has been used. Using water:ludox (4:1) solution, the instrument response function (IRF) has been obtained. A Rigaku Super Nova fine-focused dual diffractometer, fitted with a PILATUS200K, was utilised to gather single crystal X-ray diffraction data using MoKα radiation (λ = 0.71073). The structures were solved using Olex2 and the ShelXS structure solution program using Direct Methods. The ShelXL refinement tool was then used to refine the structures using Least Squares minimization. Anisotropic displacement coefficients were utilised in the refinement of all non-hydrogen atoms. The H atoms were placed at calculated positions and were refined as riding atoms. 9,9-dihexyl-9H-fluorene, 2,7-dibromo-9,9-dihexyl-9H-fluorene, 4,4'-dibromo-2-nitro-1,1'-biphenyl, 2,7-dibromocarbazole, compound **3a,** compound **3b** were synthesized by adopting literature reported methods.[28-32]

4.4.2 Synthetic procedure and spectral characterization

Synthesis of compound 1a:

Inside the glove box, 1H-indazole (0.2 g, 1.694 mmol) and BPh_3 (0.61 g, 2.541 mmol) were added to a pressure tube followed by the addition of toluene (10 mL). The reaction mixture was refluxed for 24 h at 110 ^oC. After removing the solvent, the residue was sonicated in hexane until a white precipitate appears. The resultant white precipitate was collected by filtration. Yield: 0.25 g, (26%). **^{1}H NMR** (400 MHz, $CDCl_3$) δ 8.06 (s, 2H), 7.76 – 7.71 (m, 2H), 7.21 – 7.11 (m, 4H), 7.11 – 7.03 (m, 4H), 6.99 (t, *J* = 7.4 Hz, 8H), 6.85 (dd, *J* = 7.6, 1.5 Hz, 8H), 6.67 – 6.59 (m, 2H). **^{13}C NMR** (101 MHz, $CDCl_3$) δ 144.6, 133.6, 132.7, 128.7, 127.3, 126.7, 122.5, 121.6, 121.5, 115.3. **^{11}B NMR** (128 MHz, $CDCl_3$) δ 1.84. **HR-MS** (TOF MS ASAP+): calculated for $C_{38}H_{30}B_2N_4$ ($[M]^+$): 564.2651, observed : 564.2596.

Synthesis of compound 1b:

Compound **1b** was prepared following a protocol similar to that used for compound **1a**. The quantities involved are as follows: bromo-indazole (0.30 g, 1.52 mmol) and BPh_3 (0.55 g, 2.28 mmol) were added to a pressure tube followed by the addition of toluene (10 mL). Yield: 0.27 g, (25%). **^{1}H NMR** (400 MHz, $CDCl_3$) δ 8.04 – 7.99 (m, 2H), 7.91-7.86 (m, 2H), 7.24-7.18 (m, 2H), 7.11-7.04 (m, 4H), 6.99 (m, 8H), 6.84 – 6.75 (m, 8H), 6.47 (m, 2H). **^{13}C NMR** (101 MHz, $CDCl_3$) δ 145.0, 133.4, 132.3, 131.9, 127.5, 127.0, 123.7, 122.9, 116.8, 116.1. **^{11}B NMR** (128 MHz, $CDCl_3$) δ 1.98. **HR-MS** (TOF MS ASAP+): calculated for $C_{38}H_{28}B_2Br_2N_4$ ($[M]^+$): 722.0828, observed : 722.0829.

General procedure for synthesis of compounds 2a-2d:

A 100 mL two neck RB was charged with compound **1b** (1.0 mmol), boronic acid (2.2 mmol), K_2CO_3 (10.0 mmol) and $Pd(PPh_3)_4$ (0.05 mmol) was refluxed in THF (20 mL) and H_2O (8 mL) under nitrogen for 24 h. After the reaction was completed, the reaction was cooled to room temperature. The resultant mixture was poured into CH_2Cl_2 and water, extracted with CH_2Cl_2 (100 mL) thrice and dried with anhydrous sodium sulfate, filtered, and then concentrated under vacuum. The obtained organic compound was purified using silica gel column chromatography n-hexane/EtOAc.

Synthesis of compound 2a:

The quantities involved are as follows: Compound **1b** (0.5 g, 0.692 mmol), phenyl boronic acid (0.25 g, 2.076 mmol), K_2CO_3 (0.97 g, 7.058 mmol) and $Pd(PPh_3)_4$ (0.019 g, 0.0399 mmol). The obtained organic compound was purified using silica gel column chromatography (n-hexane/EtOAc (50:50). Yield: 0.38 g, (77%). **^{1}H NMR** (400 MHz, $CDCl_3$) δ 8.13 (s, 2H), 7.90 (s, 2H), 7.57-7.53 (m, 4H), 7.48 – 7.38 (m, 8H), 7.39 – 7.31 (m, 2H), 7.11 – 7.05 (m, 4H), 7.04 (s, 2H), 7.02 (s, 4H), 7.00 (s, 2H), 6.92 – 6.87 (m,

6H), 6.68 (d, *J* = 8.0 Hz, 2H). **^{13}C NMR** (101 MHz, $CDCl_3$) δ 145.8, 144.0, 140.7, 136.0, 133.6, 133.0, 129.3, 129.0, 127.4, 127.3, 126.8, 122.2, 119.0, 115.6. **^{11}B NMR** (128 MHz, $CDCl_3$) δ 1.81. **HR-MS** (ESI): calculated for $C_{50}H_{38}B_2N_4$ ($[M+Na]^+$): 739.3175, observed : 739.3190.

Synthesis of compound 2b:

The quantities involved are as follows: Compound **1b** (0.25 g, 0.346 mmol), 4-methylphenyl boronic acid (0.14 g, 1.038 mmol), K_2CO_3 (0.48 g, 3.529 mmol) and $Pd(PPh_3)_4$ (0.019 g, 0.0173 mmol). The obtained organic compound was purified using silica gel column chromatography (n-hexane/EtOAc (20:80). Yield: 0.24 g, (94%). **^{1}H NMR** (400 MHz, $CDCl_3$) δ 8.11 (s, 2H), 7.88 (s, 2H), 7.45 (d, *J* = 8.0 Hz, 4H), 7.41 (dd, *J* = 9.2, 1.8 Hz, 2H), 7.25 (s, 2H), 7.23 (s, 2H), 7.14 – 7.01 (m, 4H), 7.02 (t, *J* = 7.4 Hz, 8H), 6.94 – 6.86 (m, 8H), 6.67 (d, *J* = 8.0 Hz, 2H), 2.39 (s, 6H). **^{13}C NMR** (101 MHz, $CDCl_3$) δ 145.9, 143.9, 137.8, 135.9, 133.6, 132.9, 129.7, 129.2, 127.3, 127.1, 126.8, 122.2, 118.6, 115.5, 21.2. **^{11}B NMR** (128 MHz, $CDCl_3$) δ 1.41. **HR-MS** (TOF MS ASAP+): calculated for $C_{52}H_{42}B_2N_4$ ($[M]^+$): 744.3590, observed : 744.3624.

Synthesis of compound 2c:

The quantities involved are as follows: Compound **1b** (0.5 g, 0.692 mmol), 4-chlorophenyl boronic acid (0.32 g, 2.076 mmol), K_2CO_3 (0.97 g, 7.058 mmol) and $Pd(PPh_3)_4$ (0.04 g, 0.0346 mmol). The obtained organic compound was purified using silica gel column chromatography (n-hexane/EtOAc (10:90). Yield: 0.44 g, (82%). **^{1}H NMR** (400 MHz, $CDCl_3$) δ 8.13 (s, 2H), 7.88 (s, 2H), 7.49 (s, 2H), 7.47 (s, 2H), 7.42 – 7.36 (m, 6H), 7.13 – 7.06 (m, 4H), 7.02 (t, *J* = 7.3 Hz, 8H), 6.94 – 6.84 (m, 8H), 6.68 (d, *J* = 8.0 Hz, 2H). **^{13}C NMR** (101 MHz, $CDCl_3$) δ 145.6, 144.0, 139.1, 134.8, 133.5, 133.1, 129.1, 128.9, 128.5, 127.4, 126.9, 122.1, 119.1, 115.7. **^{11}B NMR** (128 MHz, $CDCl_3$) δ

0.84. **HR-MS** (TOF MS ASAP+): calculated for $C_{50}H_{36}B_2Cl_2N_4$ ($[M]^+$): 784.2498, observed : 784.2464.

Synthesis of compound 2d:

The quantities involved are as follows: Compound **1b** (0.5 g, 0.692 mmol), 4-cyanophenyl boronic acid (0.3 g, 2.076 mmol), K_2CO_3 (0.97 g, 7.058 mmol) and $Pd(PPh_3)_4$ (0.04 g, 0.0346 mmol). The obtained organic compound was purified using silica gel column chromatography (DCM/MeOH (95:5). Yield: 0.15 g, (28%). **^{1}H NMR** (400 MHz, $CDCl_3$) δ 8.18 (s, 2H), 7.95 (s, 2H), 7.72 (d, *J* = 8.0 Hz, 4H), 7.65 (d, *J* = 8.0 Hz, 4H), 7.40 (dd, *J* = 9.2, 1.8 Hz, 2H), 7.10 (t, *J* = 7.3 Hz, 4H), 7.02 (t, *J* = 7.4 Hz, 8H), 6.88 (d, *J* = 6.7 Hz, 8H), 6.71 (d, *J* = 9.2 Hz, 2H). **^{13}C NMR** (101 MHz, $CDCl_3$) δ 145.4, 145.1, 144.3, 134.0, 133.5, 132.8, 128.6, 127.8, 127.5, 127.0, 122.1, 120.1, 118.9, 116.1, 111.1. ^{11}B NMR (128 MHz, $CDCl_3$) δ 4.81. **HR-MS** (ESI): calculated for $C_{52}H_{36}B_2N_6$ ($[M+Na]^+$): 789.3096, observed : 789.3080.

Synthesis of polymer 4a:

A 100mL two necked RB was charged with compound **1b** (0.50g, 0.69 mmol), 2,2'-(9,9-dihexyl-9H-fluorene-2,7-diyl)bis(4,4,5,5-tetramethyl-1,3,2-dioxaborolane) (**3a**) (0.30g, 0.69 mmol), K_2CO_3 (0.97 g, 7.03 mmol), $Pd(PPh_3)_4$ (0.019 g, 0.0346 mmol) in degassed THF (20 ml) and H_2O (8 mL) were added and refluxed under nitrogen for 48 h. After cooling to room temperature, the volatiles were removed under reduced pressure, the insoluble solid materials was filtered and washed with water. The solid material thus obtained was dissolved in small amount of THF (~ 2 mL) . Precipitation of the product was achieved by slow addition of the THF solution into a vigorously stirred hexane (250 mL) solution. The precipitation was repeated one more time with hexane and once with methanol. The solid thus collected was dried under vacuum to obtain the polymer **4a** as a

white solid. Yield: 0.45g, (79%). Mn = 33700, Mw/Mn = 1.67. **^{1}H NMR** (400 MHz, $CDCl_3$) δ 8.16 (s, 2H), 8.00 (s, 2H), 7.85 – 7.67 (m, 3H), 7.59 – 7.50 (m, 5H), 7.13 – 7.09 (m, 4H), 7.08 – 7.01 (m, 7H), 6.99 – 6.90 (m, 7H), 6.80 – 6.87 (m, 2H), 1.99 (s, 4H), 1.69 – 1.57 (m, 4H), 1.40 (s, 4H), 1.26 (m, 2H), 1.14 – 0.95 (m, 15H), 0.91 – 0.81 (m, 3H), 0.73 (m, 7H), 0.62 (s, 4H). **^{11}B NMR** (128 MHz, $CDCl_3$) δ -1.98.

Synthesis of polymer 4b:

Polymer 4b was prepared following a procedure similar to that used for polymer **4a.** The quantities involved are as follows: compound **1b** (0.5g, 0.692 mmol) and 9-dodecyl-2,7-bis(4,4,5,5-tetramethyl-1,3,2-dioxaborolan-2-yl)-9H-carbazole (**3b**) (0.40g, 0.681 mmol), K_2CO_3 (0.97 g, 7.028 mmol) and $Pd(PPh_3)_4$ (0.019 g, 0.0346 mmol). Yield: 0.14 g, (23%). Mn = 56600, Mw/Mn = 1.97. **^{1}H NMR** (400 MHz, $CDCl_3$) δ 8.21 – 8.09 (m, 6H), 8.05 (s, 3H), 7.65 – 7.34 (m, 10H), 7.17 – 6.67 (m, 40H), 4.34 (s, 2H), 1.90 (s, 3H), 1.59 (s, 6H), 1.42 (m, 4H), 1.22 (s, 26H), 0.86 (m, 5H). **^{11}B NMR** (128 MHz, $CDCl_3$) δ -2.77.

4.5 References

1. Suresh, D.; Gomes, P. T. In *Advances in luminescent tetracoordinate organoboron compounds*, John Wiley & Sons, Inc.: 2014; p 485.

2. Qin, Y.-y.; Xu, W.-j.; Hu, C.-y.; Liu, S.-j.; Zhao, Q. *Wuji Huaxue Xuebao* **2017,** *33*, 1705-1721.

3. DeRosa, C. A.; Fraser, C. L. In *Tetracoordinate Boron Materials for Biological Imaging*, John Wiley & Sons, Inc.: 2018; p 111.

4. Mellerup, S. K.; Wang, S. *Trends Chem.* **2019,** *1*, 77-89.

5. Oda, S.; Shimizu, T.; Katayama, T.; Yoshikawa, H.; Hatakeyama, T. *Org. Lett.* **2019,** *21*, 1770-1773.

6. Nakazato, T.; Shinokubo, H.; Miyake, Y. *Chem. Commun. (Cambridge, U. K.)* **2021,** *57*, 327-330.

7. Yang, T.; Tang, N.; Wan, Q.; Yin, S.-F.; Qiu, R. *Molecules* **2021,** *26*, 1401.

8. Murali, A. C.; Nayak, P.; Venkatasubbaiah, K. *Dalton Trans.* **2022,** *51*, 5751-5771.

9. Nayak, P.; Murali, A. C.; Pal, P. K.; Priyakumar, U. D.; Chandrasekhar, V.; Venkatasubbaiah, K. *Inorg. Chem.* **2022,** *61*, 14511-14516.

10. Shi, J.; Ran, Z.; Peng, F. *Dyes Pigm.* **2022,** *204*, 110383.

11. Tanaka, K.; Gon, M.; Ito, S.; Ochi, J.; Chujo, Y. *Coord. Chem. Rev.* **2022,** *472*, 214779.

12. Murali, A. C.; Nayak, P.; Nayak, S.; Das, S.; Senanayak, S. P.; Venkatasubbaiah, K. *Angew. Chem., Int. Ed.* **2023,** *62*, e202216871.

13. Nieto, C. I.; Sanz, D.; Claramunt, R. M.; Alkorta, I.; Elguero, J. *Coord. Chem. Rev.* **2022,** *473*, 214812.

14. Jadhav, T.; Maragani, R.; Misra, R.; Sreeramulu, V.; Rao, D. N.; Mobin, S. M. *Dalton Trans.* **2013,** *42*, 4340-4342.

15. Misra, R.; Jadhav, T.; Mobin, S. M. *Dalton Trans.* **2013,** *42*, 16614-16620.

16. Misra, R.; Jadhav, T.; Mobin, S. M. *Dalton Trans.* **2014,** *43*, 2013-2022.

17. Jadhav, T.; Dhokale, B.; patil, Y.; Misra, R. *RSC Adv.* **2015,** *5*, 68187-68191.

18. Misra, R.; Jadhav, T.; Dhokale, B.; Mobin, S. M. *Dalton Trans.* **2015,** *44*, 16052-16060.

19. Patil, Y.; Jadhav, T.; Dhokale, B.; Butenschön, H.; Misra, R. *ChemistrySelect* **2017,** *2*, 415-420.

20. Patil, Y.; Misra, R. *J. Organomet. Chem.* **2017,** *840*, 23-29.

21. Matsumoto, F.; Chujo, Y. *Macromolecules* **2003,** *36*, 5516-5519.

22. Matsumoto, F.; Nagata, Y.; Chujo, Y. *Polym. Bull.* **2005,** *53*, 155-160.

23. Matsumoto, F.; Chujo, Y. **2006,** *78*, 1407-1411.

24. Dörr, J.; Alahmadi, A. F.; Henkelmann, M.; Bolte, M.; Lerner, H.-W.; Wagner, M.; Jäkle, F. *Can. J. Chem.* **2022,** *101*, 140-145.

25. Jäkle, F. *Chem. Rev.* **2010,** *110*, 3985-4022.

26. Cavero, E.; Giménez, R.; Uriel, S.; Beltrán, E.; Serrano, J. L.; Alkorta, I.; Elguero, J. *Cryst. Growth Des.* **2008,** *8*, 838-847.

27. Dąbrowski, M.; Serwatowski, J.; Zachara, J.; Rufińska, A. *J. Organomet. Chem.* **2000,** *613*, 93-98.

28. Chen, D.-H.; Lin, L.; Sheng, T.-L.; Wen, Y.-H.; Hu, S.-M.; Fu, R.-B.; Zhuo, C.; Li, H.-R.; Wu, X.-T. *CrystEngComm* **2017,** *19*, 2632-2643.

29. Li, Z.; Wang, J.; Huang, H.; Liu, Y.; Yun, Y.; Cheng, Z.; Liu, S.; Ding, Z.; Zhao, B.; Huang, W. *New J. Chem.* **2019,** *43*, 13775-13782.

30. Vanga, M.; Sa, S.; Kumari, A.; Murali, A. C.; Nayak, P.; Das, R.; Venkatasubbaiah, K. *Dalton Trans.* **2020,** *49*, 7737-7746.

31. Peng, Q.; Liu, X.; Qin, Y.; Zhou, D.; Xu, J. *J. Polym. Sci., Part A: Polym. Chem.* **2011,** *49*, 4458-4467.

32. Qiu, C.; Liu, X.; Cheng, C.; Gong, Y.; Xiong, W.; Guo, Y.; Wang, C.; Zhao, J.; Che, Y. *Anal. Chem.* **2019,** *91*, 6408-6412.

SUMMARY

CHAPTER 2

CHAPTER 2A

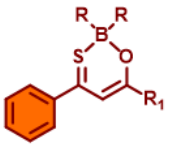

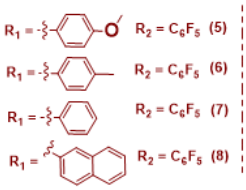

- ✓ Synthesis
- ✓ Optical properties
- ✓ Electrochemical studies
- ✓ DFT studies

CHAPTER 2B

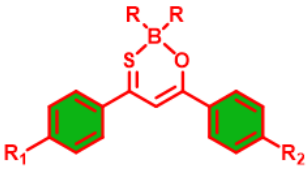

R_1 = OMe R_2 = OMe (10)
R_1 = OMe R_2 = NMe_2 (11)
R_1 = NMe_2 R_2 = NPh_2 (12)
R_1 = NPh_2 R_2 = NPh_2 (13)
R = C_6F_5

- ✓ Synthesis
- ✓ Optical properties
- ✓ Electrochemical studies
- ✓ Charge transport properties
- ✓ Sensing studies

CHAPTER 2C

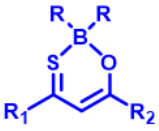

R_1 = TPE R_2 = TPE (1)
R_1 = TPE R_2 = NMe_2 (2)
R_1 = NMe_2 R_2 = TPE (3)
R_1 = NMe_2 R_2 = NMe_2 (4)
R = C_6F_5

- ✓ Synthesis
- ✓ Optical properties
- ✓ AIE studies
- ✓ Electrochemical studies
- ✓ Cyanide ion sensing
- ✓ NLO properties

CHAPTER 2D

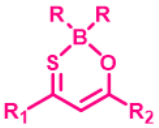

R_1 = CAR R_2 = OMe (4a)
R_1 = OMe R_2 = CAR (4b)
R_1 = CAR R_2 = CAR (4c)
R = C_6F_5

- ✓ Synthesis
- ✓ Optical properties
- ✓ Electrochemical studies
- ✓ DFT studies

CHAPTER 3

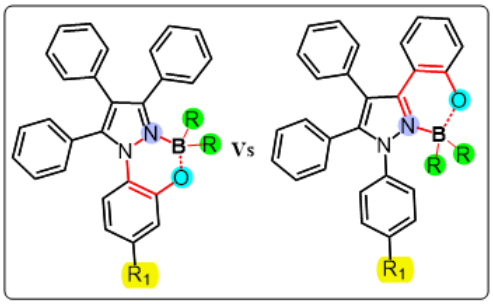

- ✓ Synthesis
- ✓ Optical properties
- ✓ AIE studies
- ✓ Picric acid sensing

CHAPTER 4

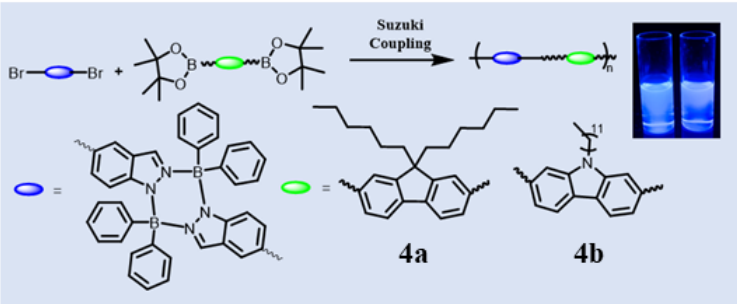

- ✓ Synthesis
- ✓ Optical properties
- ✓ Thermal properties